UNIVERSITY OF SOUTHAMPTON

Faculty of Medicine

School of Medicine

Developmental Origins of Health & Disease

Bone and Joint Research Group

Skeletal stem cell isolation and differentiation: Interdisciplinary strategies for skeletal tissue engineering

By

Peter D Mitchell

Thesis for the degree of Doctor of Philosophy

November 2011

Supervisors: Professor Richard OC Oreffo and Professor Hywel Morgan

ABSTRACT

UNIVERSITY OF SOUTHAMPTON

FACULTY OF MEDICINE, HEALTH AND LIFE SCIENCES,

SCHOOL OF MEDICINE

Doctor of Philosophy

SKELETAL STEM CELL ISOLATION AND DIFFERENTIATION: INTERDISCIPLINARY

STRATEGIES FOR SKELETAL TISSUE ENGINEERING

By Peter D Mitchell

Stem cell based tissue engineering is viewed as a promising approach for orthopaedic reparative medicine and the application of microfluidic techniques for isolation and characterisation of individual skeletal stem cells is considered a potential source of cells for regenerative medicine. The studies described in this thesis aim to develop original techniques for isolation and characterisation of mesenchymal stem cells and to examine their possible uses in skeletal tissue engineering. These studies developed novel microfluidic technology using dielectrophoretic ring traps and sorting gates for isolation and recovery of specific cells according to immunofluorescent intensity. To date, the devices outlined in this work are limited by the small number of cells that can be isolated, but are capable of recovering established and primary cell populations with 100% purity for specific markers such as STRO-1, while also displaying potential for on-chip analysis and culture due to the ability to precisely control the device's microenvironment. This study has also investigated 28 day organotypic culture of 3D fetal femur-derived cell pellets at an air-liquid interface. It was demonstrated that addition of serum, ascorbate, dexamethasone and BMP-2 resulted in mimicry of *in vivo* femur development, while addition of ascorbate and TGF-β3 resulted in a cartilaginous phenotype, thus offering potential models for both cartilage and early bone development. Analysis of pellets demonstrated that significant pellet diameter at day 1 (greater than 0.8mm) is crucial for maintaining reproducible results in osteogenic and chondrogenic conditions. Furthermore, addition of BMP-2 to fetal femur-derived cells cultured in chemically defined media induced formation of a novel cobblestone cell morphology. Characterisation of the cobblestone cells demonstrated a primitive adipogenic phenotype as indicated by the lack of endothelial and haematopoietic marker expression including CD146, TIE2, CD34, and CD105 and upregulation of mesenchymal differentiation markers, ubiquitous expression of PPARγ and retention of lipid. Overall these studies have offered a novel approach to stem cell isolation for characterisation and have furthered the knowledge of fetal femur-derived cell and their potential as an alternative cell source for skeletal tissue engineering.

CONTENTS

LIST OF FIGURES AND TABLES

DECLARATION OF AUTHORSHIP

I, Peter Mitchell, declare that the thesis entitled:

SKELETAL STEM CELL ISOLATION AND DIFFERENTIATION: INTERDISCIPLINARY STRATEGIES FOR SKELETAL TISSUE ENGINEERING

and the work presented in it are my own and have been generated by me as the result of my own original research. I confirm that:

- this work was done wholly or mainly while in candidature for a research degree at this University;
- where any part of this thesis has previously been submitted for a degree or any other qualification at this University or any other institution, this has been clearly stated;
- where I have consulted the published work of others, this is always clearly attributed;
- where I have quoted from the work of others, the source is always given. With the exception of such quotations, this thesis is entirely my own work;
- I have acknowledged all main sources of help;
- where the thesis is based on work done by myself jointly with others, I have made clear exactly what was done by others and what I have contributed myself;
- parts of this work have been published as:

Thomas, R.S.W.*, **Mitchell, P.D**.*, Oreffo, R.O.C., & Morgan, H. 2010. "Trapping single human osteoblast-like cells from a heterogeneous population using a dielectrophoretic microfluidic device." *Biomicrofluidics*, 4, (2) (*Joint first author).

Gothard, D., Tare, R.S., **Mitchell, P.D**., Dawson, J.I., & Oreffo, R.O.C. 2011. "In search of the skeletal stem cell: isolation and separation strategies at the macro/micro scale for skeletal regeneration." *Lab on a Chip*, 11, 1206-1220.

Signed:

Date: 21st November 2011

ACKNOWLEDGEMENTS

LIST OF ABBREVIATIONS

3D	Three-dimensional
α-MEM	Minimum essential medium, alpha Eagle's modification
μ-TAS	Micro-total analysis system
A/S	Alcian blue/Sirius red
AC	Alternating current
ACI	Autologous chondrocyte implantation
AEC	3-amino-9-ethyl-carbazole
AER	Apical ectodermal ridge
ALP	Alkaline phosphatase
ANOVA	Analysis of variance
BMP	Bone morphogenetic protein
BMU	Basic multicellular units
BSA	Bovine serum albumin
BSP	Bone sialoprotein
CDM	Chemically defined medium
cDNA	Complementary DNA
CFDA	Carboxyfluorescein diacetate
CFU-F	Colony forming unit-fibroblastic
CMFDA	5-chloromethyl-fluorescein diacetate
CTG	Cell Tracker Green
DAPI	4',6-diamidino-2-phenylindole
DEP	Dielectrophoresis
dH$_2$O	Distilled water
DMEM	Dulbecco's modified Eagle's medium
DNA	Deoxyribonucleic acid
dNTPs	Deoxynucleotide triphosphates
DPX	Dibutyl phthalate xylene
ECM	Extra cellular matrix
EDTA	Ethylenediamine tetra-acetic acid
EIS	Electrochemical impedance spectroscopy
ES	Embryonic stem (cell)
FABP	Fatty-acid binding protein
FACS	Fluorescence-activated cell sorting
FCS	Foetal calf serum
FFDC	Fetal femur-derived cells
FGF	Fibroblast growth factor
GAG	Glycosaminoglycan
GAPDH	Glyceraldehyde-3-phosphate dehydrogenase
GDF	Growth & differentiation factor
GFP	Green fluorescent protein
GH	Growth hormone
HA	Hyaluronan

hBMSC	Human bone marrow stromal cell
HOX	Homeobox (genes)
IGF	Insulin-like growth factor
IHH	Indian hedgehog
IL	Interleukin
IMDM	Iscove's modified Dulbecco's medium
iPSC	Induced pluripotent stem cell
ITS	Insulin, transferrin, selenium
LDM	Laser dissection microscopy
LoaC	Lab on a chip
MACS	Magnetic-activated cell separation
MMP	Matrix metalloproteinase
MSC	Mesenchymal stem cell
NCP	Non-collagenous protein
OA	Osteoarthritis
OCN	Osteocalcin
OPG	Osteoprotegerin
OPN	Osteopontin
ONN	Osteonectin
p0	Passage zero
PBS	Phosphate buffered saline
PDGF	Platelet-derived growth factor
PEG	Poly(ethylene glycol)
PFA	Paraformaldehyde
PPAR-γ	Peroxisome proliferation-activated receptor-γ
PTHrP	Parathyroid hormone-related peptide
RANK	Receptor activator of nuclear factor kappa-B
RNA	Ribonucleic acid
RT-PCR	Reverse transcriptase-polymerase chain reaction
RUNX2	Runt-related transcription factor 2
SH-3	Src (sarcoma) homology 3
SHH	Sonic hedgehog
SOX	Sry (sex reversal Y-related) high mobility group box protein
TE	Tris-EDTA
TGF	Transforming growth factor
UPW	Ultra pure water
VEGF	Vascular endothelial growth factor
VWF	Von Willebrand factor
WNT	Wingless integration
WPC	Weeks post conception

CHAPTER 1

INTRODUCTION

1.1. Overview

As the population continues to rise and life-expectancy increases, there is an urgent socio-economic and clinical challenge to develop strategies for the repair of cartilage and bone lost as a consequence of trauma, disease or natural degeneration. In the US alone, approximately 6.8 million bone fractures occur per year, with 5-10% requiring bone augmentation (data from American Academy of Orthopaedic Surgeons), whilst current technologies for the repair of cartilage defects rarely succeed in restoring full, long-lasting function (reviewed in Tare et al. 2010). Stem cell based tissue engineering is viewed as a promising approach for orthopaedic reparative medicine and the application of microfluidic techniques for isolation and characterisation of individual skeletal stem cells is considered a potential source for regenerative medicine, specifically in treating skeletal disorders such as osteoporosis and osteoarthritis. The aim of these studies is to further characterise both adult and fetal-derived mesenchymal/skeletal cells and to examine their possible uses in skeletal tissue engineering.

1.2. Cartilage

Cartilage is a specialised, dense connective tissue composed of a collagenous extracellular matrix and chondrocytes embedded in a non-collagenous mix of proteoglycans, matrix proteins and water known as ground substance (Aigner & Stove 2003). The main roles of cartilage are to provide structure, cushion joints and support other tissues whilst displaying enhanced flexibility and greater elasticity than bone. Cartilage lacks blood vessels and is therefore dependent on nutrient diffusion through the extracellular matrix (Bhosale & Richardson 2008). There are three major types of cartilage, separated according to the structure and appearance of the tissue; these types are hyaline, elastic and fibrous (Figure 1.1).

Hyaline cartilage is the most common type of cartilage in the human body; covering the surface of bone at synovial joints, protecting the bone from wear (also known as articular cartilage). Hyaline cartilage is also found as a support structure in trachea, at the ventral ends of ribs attaching them to the sternum and in the developing foetus, where it acts as the template for bone formation (Shea & Miller 2005). Hyaline cartilage matrix is composed predominantly of Type II collagen.

Elastic cartilage shows greater elasticity than other types of cartilage due the presence of elastin fibres within its extracellular matrix in addition to collagen and is found in areas of the body that require elastic but robust support such as the outer ear and the larynx (Stockwell 1979).

Fibrous cartilage contains large bundles of collagen fibres interspersed with chondrocytes surrounded by loose fibrils. Fibrous cartilage is found in areas that require large amounts of tensile strength such as where ligaments and tendons attach to bone and the intervertebral discs (Shea & Miller 2005). Fibrous cartilage is the only cartilage type that contains Type I collagen.
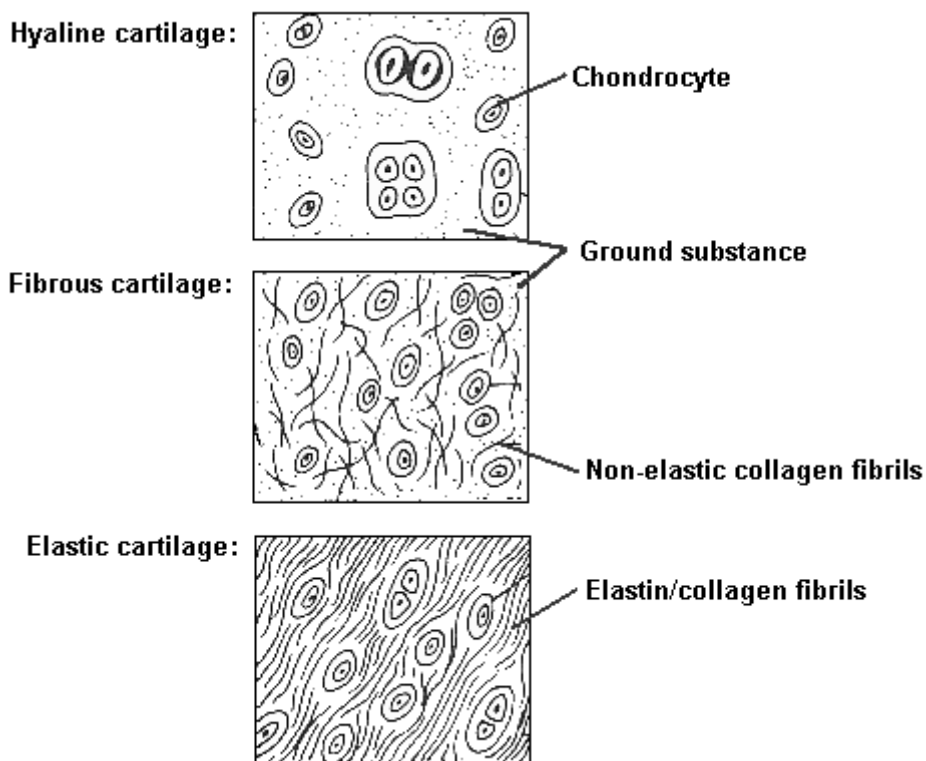
Figure 1.1. The structure of the three types of cartilage (Adapted from www.botany.uwc.ac.za/sci_ed).

1.2.1. Structure and composition of articular cartilage

Articular cartilage is found at free-moving diarthroidal/synovial joints where the cartilage prevents bone abrasion and protects the joint against compressive forces and other stress (Figure 1.2). A typical diarthroidal joint consists of two adjoining, cartilage-covered bones surrounded by a synovial capsule, the inner of which is covered in a synovial membrane that produces synovial fluid to fill the joint and provide lubrication for the bone surfaces.
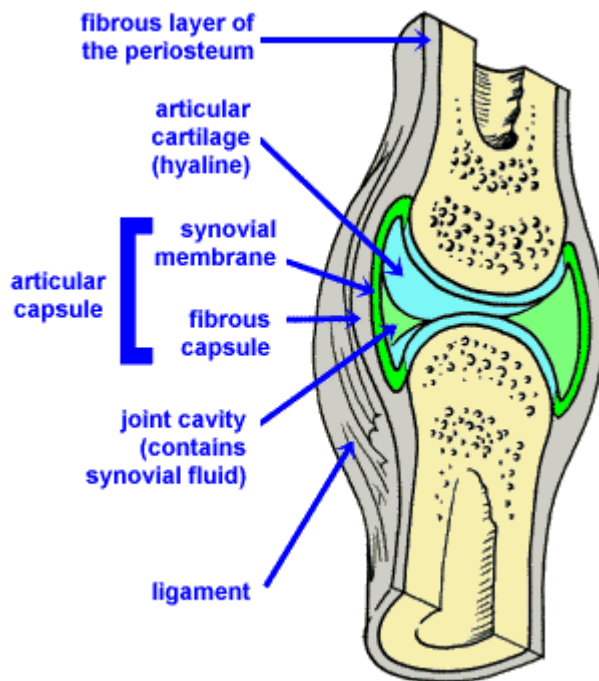
Figure 1.2. A schematic diagram of a diarthroidal joint showing the synovial capsule and articular cartilage. (Adapted from www.zoology.ubc.ca).

Articular cartilage is made up entirely of hyaline cartilage and as such, is composed of chondrocytes embedded in a collagen and proteoglycan rich extracellular matrix. The extracellular matrix of articular cartilage is 70-80% water containing metabolites and ions. It is this fluid that provides the cartilage with its ability to tolerate compressive forces. Type II collagen makes up approximately 50-90% of the dry weight of articular cartilage and provides tensile strength to the tissue (Muir 1995).

Articular cartilage is divided into 4 distinct regions, known as the superficial, transitional, middle and calcified zones (Figure 1.3). Each of these zones is further divided into three distinct regions: the pericellular region and territorial region, which

facilitate chondrocyte-Extra Cellular Matrix (ECM) binding and support; and the interterritorial region, which facilitates the mechanical and structural properties of the cartilage (Temenoff & Mikos 2000).

- Superficial zone: The thinnest part of the cartilage, consisting of a sheet of collagen fibres covering the joint surrounded by a sheet of flattened chondrocytes. This zone has high tensile strength imparted from a high concentration of collagen, fibronectin and water. Contains less proteoglycan than other zones
- Transitional zone: As the name suggests, acts as a transition from the superficial zone to the middle zone. Possesses spherical chondrocytes containing organelles such as Golgi apparatus, endoplasmic reticulum and mitochondria. The transitional zone has a higher concentration of proteoglycan, less collagen, but larger collagen fibrils than the superficial zone.
- Middle zone: Most often the largest zone, contains the largest collagen fibrils and the most proteoglycan. Chondrocytes are spherical, arranged in columns at a 90° angle to the bone, contain large numbers of synthesising organelles and are highly active.
- Calcified zone: Acts as a transition phase from cartilage to subchondral bone. Contains small spherical chondrocytes often completely surrounded by calcified ECM.

(Temenoff & Mikos 2000)
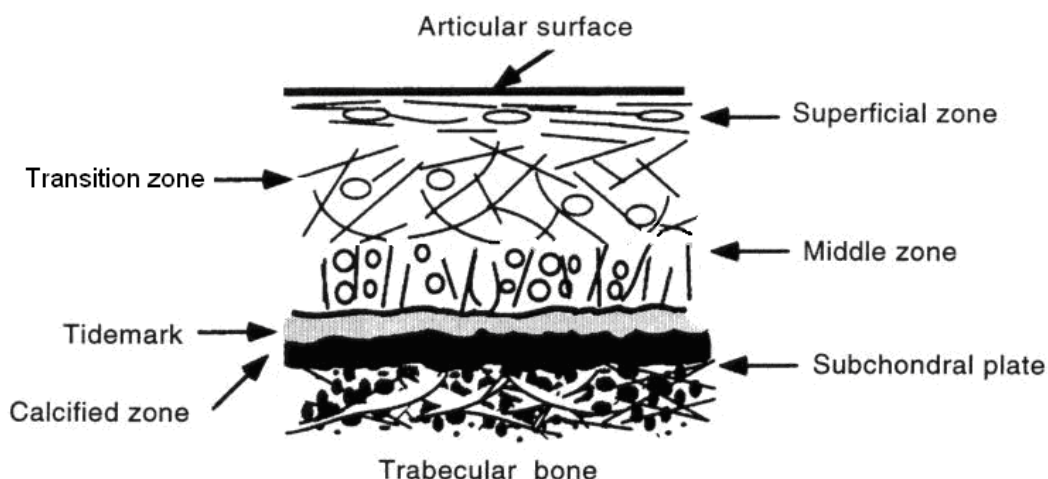
Figure 1.3. Graphical representation showing the different zones of cartilage (Adapted from Cohen et al. 1998).

1.2.2. Chondrocytes

Chondrocytes are embedded within the extracellular matrix of cartilage in small cavities known as lacunae. These cells make up approximately 10% of the total weight of articular cartilage and are fundamental for the generation and maintenance of the extracellular matrix of cartilage through production and/or degradation of important matrix proteins (Cohen et al. 1998). The avascular nature of cartilage creates an atmosphere with very low levels of oxygen and nutrients; chondrocytes are adapted to survive these conditions through efficient use of anaerobic metabolism. The avascular conditions in cartilage may limit the number of cells that can be sustained within the extracellular matrix, predisposing an individual to degenerative diseases such as osteoarthritis (OA) (Muir 1995). The majority of chondrocytes have a spherical appearance except for those found at the periphery of cartilage, which have a flattened, disc-like shape (Stockwell 1979).

1.2.3. Collagen

Collagen proteins (also known as tropocollagen) are long extracellular proteins with a right-handed helical structure, composed of three coiled polypeptide subunits held together and stabilised by hydrogen bonds; two α1-chains and an α2-chain. Each of these subunits has a left-handed helical structure as a consequence of the tripeptide sequences Glycine-Proline-X and Glycine-X-Hydroxyproline, where X can be any amino acid (Lodish et al. 2007). Tropocollagen proteins are synthesised as inactive precursors which become active upon cleavage of N- and C-terminal propeptide extensions by procollagen proteinases. Upon activation, tropocollagens will spontaneously assemble into semi-crystalline collagen microfibrils, which will in turn aggregate to form fibrils and fibres (Hulmes 2002) (Figure 1.4).

The extracellular matrix of articular cartilage is composed mainly of Type II collagen fibrils (~80%) interwoven into a mesh that provides tensile strength and contains proteoglycans such as aggrecan, fibronectin and chondronectin (Aigner & Stove 2003). Articular collagen also contains types VI, IX, X and XI, albeit in much smaller quantities than Type II. Type VI collagen is found in the extracellular matrix of most tissues where it forms a microfibril network that is thought to mediate interaction between chondrocytes and their surrounding matrix (Aigner & Stove 2003). Type IX collagen is found on the surface of Type II fibrils and stabilises the 3D structure of Type II collagen by cross-linking with other Type IX molecules (Eyre 2002). Type X

collagen is only found within hypertrophic chondrocytes and plays a role in regulating matrix mineralisation during endochondral bone formation (Shen 2005). Type XI collagen is found in articular cartilage copolymerised with Type II collagen and is thought to cross-link fibrils of the collagen 3D structure and also restrict and therefore regulate the growth of collagen Type II fibrils (Eyre 2002).
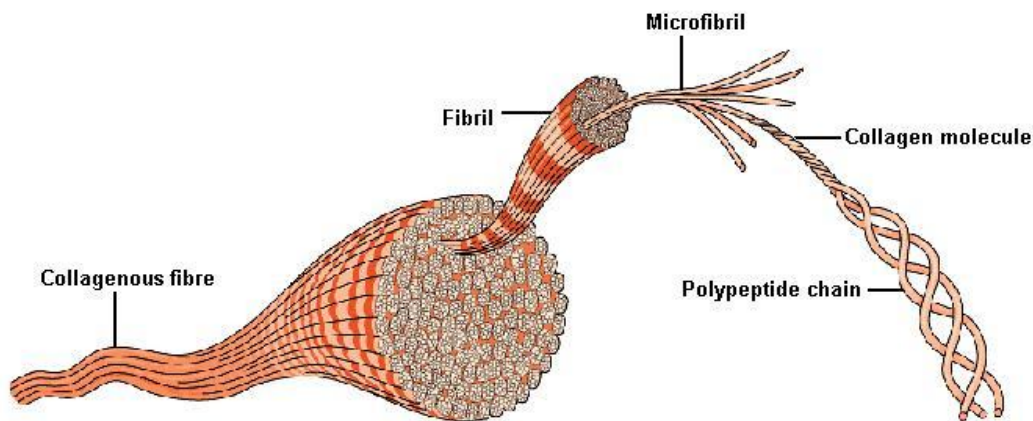
Figure 1.4. Collagen structure (http://fig.cox.miami.edu).

1.2.4. Proteoglycans and other non-collagenous proteins

Proteoglycans are a type of glycoprotein containing large numbers of glycosaminoglycan (GAG) chains attached to a core protein. Glycosaminoglycans are composed of a repeating disaccharide formed into a long unbranched polysaccharide and have a high negative charge (Reece et al. 2010). Proteoglycans are a diverse group of proteins and can be found throughout the body carrying out many different biochemical functions. The high negative charge from the GAGs causes a constant negative charge and imparts hydrophilic properties on the articular cartilage causing a swelling pressure as water is attracted to the joint (Iozzo 1998). This swelling pressure exerts a tensile stress on the collagen network and it is the balance between the swelling pressure and restricting tensile force that imparts the load-bearing ability of the cartilage (Cohen et al. 1998). Proteoglycans are categorised according to their types of GAG chains, their size and their localisation within the body.

The major proteoglycan in articular cartilage is Aggrecan. Aggrecan forms complexes with hyaluronan (HA) and link protein, a small, 40-48 kDa glycoprotein, to produce multimolecular aggregates that are trapped by the collagen network, creating a strong, fibre-reinforced matrix (Figure 1.5). It is due to the presence of these aggregates that the cartilage retains a high negative charge and in turn, a high level of hydration, providing structural support and nutrient and solute transport to the cartilage (Watanabe et al. 1998).
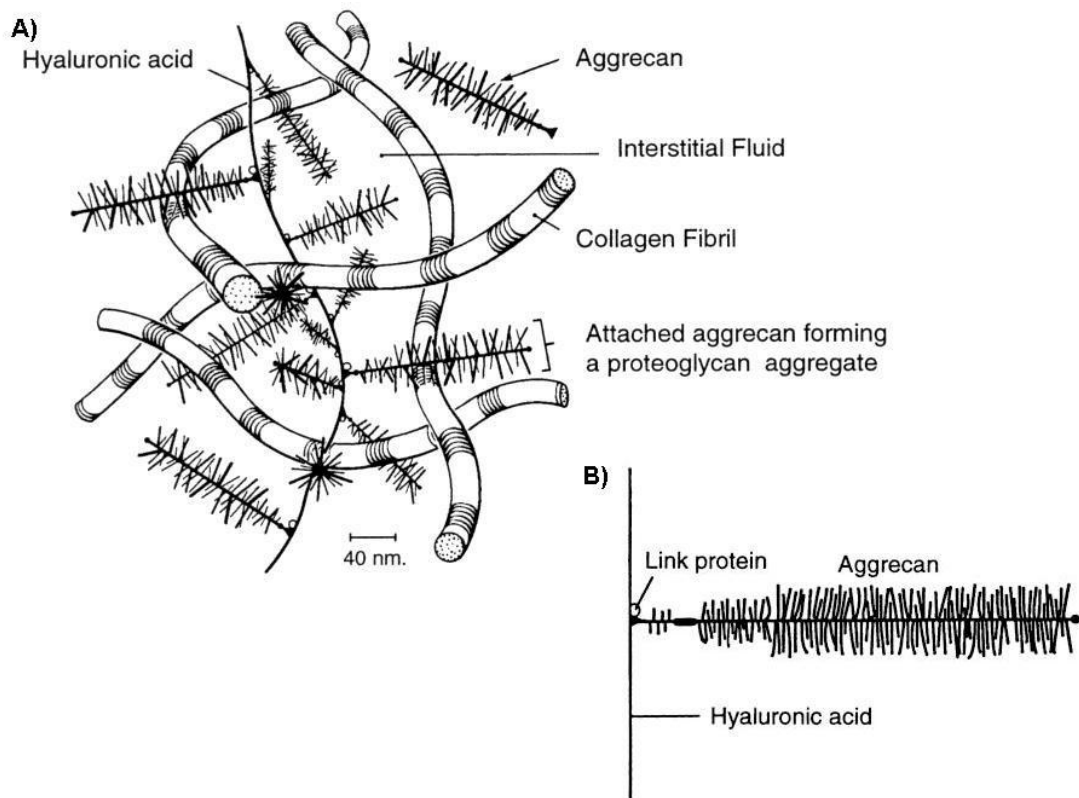
Figure 1.5. (A) A graphic representation showing how the collagen network traps proteoglycan aggregate to form a fibre-reinforced composite. (B) The binding of aggrecan to hyaluronic acid is stabilised by link protein (Cohen et al. 1998).

Hyaluronic acid (HA), also known as hyaluronan or hyaluronate, is a glucosaminoglycan composed of alternating repeats of N-acetylglucosamine (GlcNAc) and glucuronic acid (GlcUA). HA is found in most parts of the body, and is predominant in soft connective tissues and their surroundings such as the synovial fluid in articular joints (Reed et al. 1988;Fraser et al. 1997). Several different functions have been described for HA, these include: a structural and water-balancing role in the ECM

of cartilage via its interaction with aggrecan and the regulation of plasma protein distribution and transport via the steric interactions of HA networks (Laurent & Fraser 1992;Fraser et al. 1997). Hyaluronan also acts to bind aggregates to the cell surface of chondrocytes by interacting with the cell surface receptor, CD44, a transmembrane glycoprotein involved in cell adhesion, ECM regulation and many other functions (Knudson & Knudson 2001).

In addition to aggrecan, many smaller proteoglycans can be found within articular joint cartilage, such as decorin, biglycan and fibromodulin (Figure 1.6). These are much shorter and contain less GAG chains than aggrecan and tend to play roles in cell function and matrix organisation rather than affecting the physical properties of the cartilage (Temenoff & Mikos 2000).
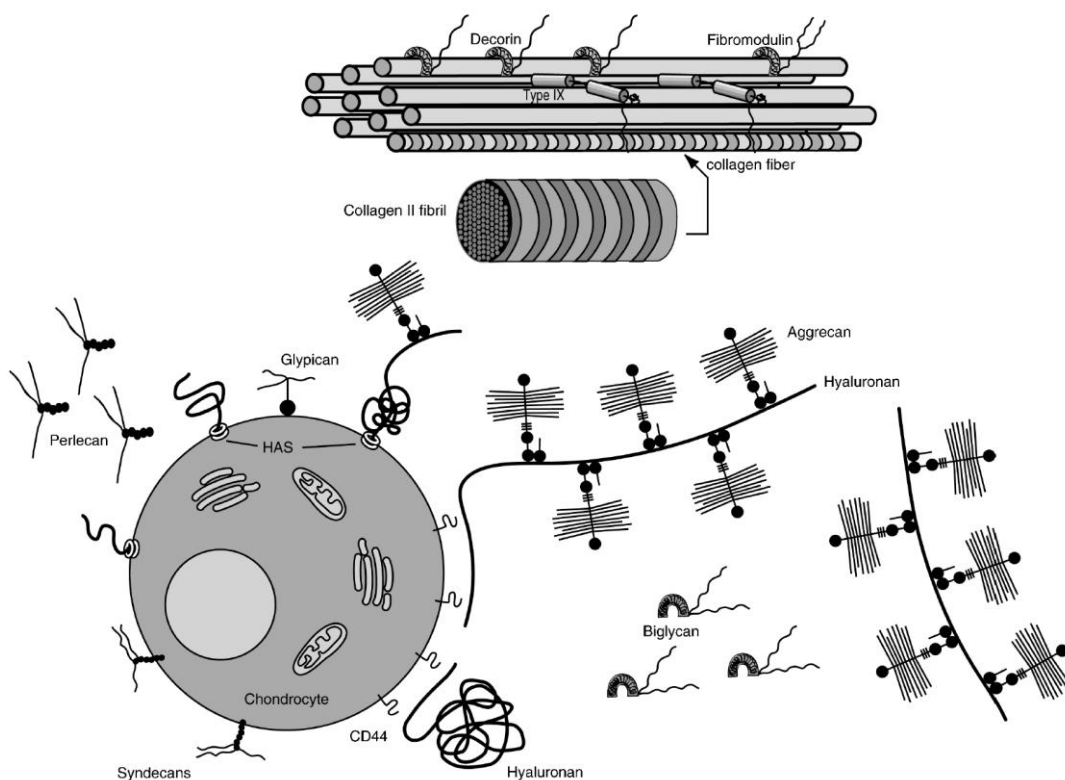
Figure 1.6. Overview of the proteoglycans and other non-collagenous proteins present in cartilage (Knudson & Knudson 2001).

1.3. Skeletogenesis

1.3.1. Chondrogenesis and development of the cartilage anlagen:

Chondrogenesis is the first phase of skeletal development, characterised by the formation of cartilage and leading to the formation of true bone through endochondral ossification. During the development of the human embryo, skeletal growth begins with the formation of limb buds from the lateral plate mesoderm at around 4 weeks gestation (Goldring et al. 2006). Formation and development of the embryonic limb skeleton is regulated by two signalling centres; the apical ectodermal ridge (AER), which directs the proximal-distal growth of the limb, and the zone of polarizing activity, which directs the anterior-posterior growth of the limb (Olsen et al. 2000).

Skeletogenesis begins with the recruitment of mesenchymal cells to sites of chondrogenesis, where they undergo proliferation and pre-cartilage condensation. Condensation involves the recruited mesenchymal precursor cells adhering to each other to form clusters that become the cartilage anlagen template for bone formation (Delise et al. 2000). This process is dependent on cell-cell/cell-matrix communication and interaction via adhesion molecules and gap junctions, as well as secreted factors such as members of the TGF-β family (Hall & Miyake 1995). The cells surrounding the condensations eventually become elongated and form dense perichondrium, important for growth and repair of the cartilage (Delise et al. 2000).

Pre-condensation mesenchymal cells secrete hyaluronan- and collagen Type I -rich ECM that prevents cell-cell adhesion but facilitates cell migration and recruitment. Versican, a large chondroitinsulphate proteoglycan interacts with hyaluronan to maintain the structure of the ECM and act as an anti-adhesive via tenascin-mediated binding to cell adhesion molecules (Matsumoto et al. 2006). As cells are recruited to the site of limb formation and condensation is initiated, the cells begin to produce hyaluronidase that breaks down the ECM and allows the cells to adhere and interact (Tuan 2004). Cell-cell adhesion during condensation is facilitated by the cell adhesion molecules, neural cell adhesion molecule (N-CAM), neural cadherin (N-cadherin) CD44 and syndecan-3 (Knudson & Knudson 2001). During the initiation of condensation, the TGF-β family member, Activin, upregulates the ECM glycoprotein, fibronectin, this binds with syndecan to downregulate N-CAM, setting the boundaries of the condensation (Goldring et al. 2006).

Control of limb development and chondrogenesis is patterned by a number of genes working in coordination along the 3 axes of the limb to ensure correct development. To date, key gene pathways identified are the fibroblast growth factor (FGF), hedgehog, bone morphogenetic protein (BMP), homeobox (HOX) and WNT pathways (Zhu et al. 2010). WNT signals produced early in development induce expression of FGFs, which then act via positive feedback loops to upregulate both WNT and FGF (Goldring et al. 2006). FGFs are essential for limb bud initiation and outgrowth (Tickle & Munsterberg 2001). Transcription factors belonging to the HOX family play an important role in regulating the expression of FGF, BMP, Sonic hedgehog (SHH) and proliferation of cells located in condensations (Delise et al. 2000). SHH does not play a role in limb growth, but is important for patterning the early limb. BMPs are required for the development of polarity within the developing embryo and in limiting the expansion of the limb bud (Chen et al. 2004). BMPs interact with BMP receptors (BMPRs) on cell surfaces to initiate differentiation and maturation of prechondrocytes cells into terminally differentiated chondrocytes at specific pre-patterned sites (Zhu et al. 2010). At this stage, sex determining region Y-box (*SOX*) genes, specifically *SOX9*, *SOX5* and *SOX6*, are upregulated by BMP signalling and are required for expression of cartilage specific ECM components such as Type II, IX and XI collagen, link protein and aggrecan (Lefebvre et al. 2001).

1.3.2. Chondrocyte hypertrophy and endochondral ossification

Endochondral ossification is the process whereby long bones are developed by replacing the cartilage anlagen with bone. Upregulation of growth hormone (GH) within the embryo leads to proliferation of cells within condensations via the actions of insulin-like growth factors (IGFs), WNTs, BMPs and Indian hedgehog (IHH), leading to expansion and elongation of the collagen anlagen and an increase in the deposition of ECM (Mackie et al. 2008). Cells in the centre of the cartilage then undergo terminal differentiation and hypertrophy, characterised by an increase in their fluid content by almost 20 times, removal of the cell cycle and production of alkaline phosphatase and a unique collagen; type X (Goldring et al. 2006). Hypertrophy of these cells is regulated by a feedback loop between FGF, parathyroid hormone-related peptide (PTHrP), and IHH (Delise et al. 2000). Upregulation of thyroid hormone (T3) upregulates FGF

expression, which inhibits the PTHrP-binding activity of IHH. PTHrP then binds to, and inhibits SOX9, allowing hypertrophy of the cell (Figure 1.7) (Mackie et al. 2008).
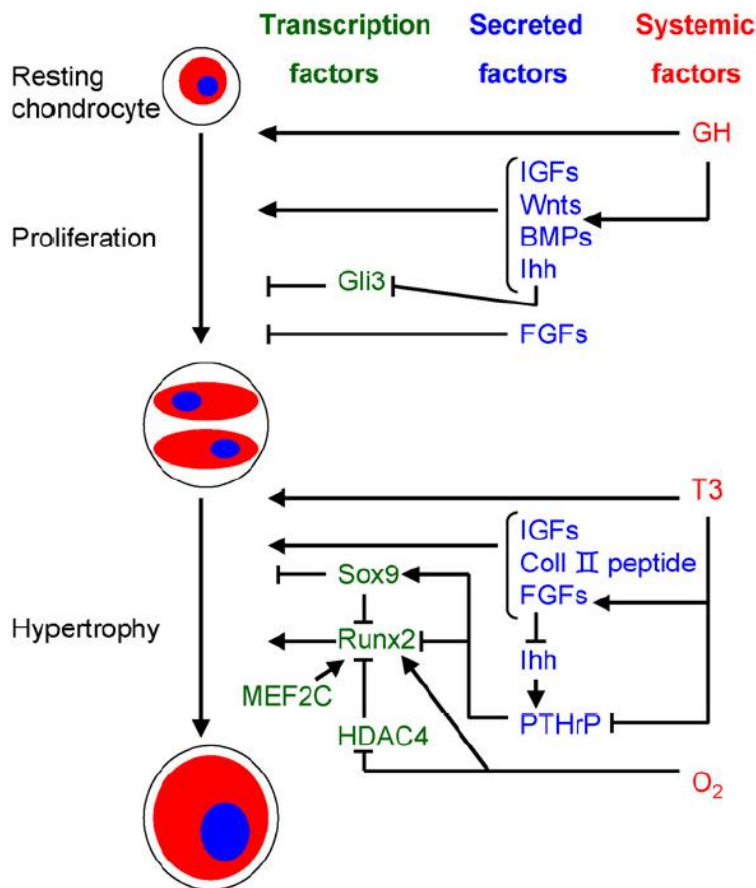
Figure 1.7. Overview of the regulation of chondrocyte proliferation and differentiation (Mackie et al. 2008).

Hypertrophic chondrocytes produce angiogenic factors such as vascular endothelial growth factor (VEGF) that stimulate the development of blood vessels throughout the perichondrium and hypertrophic zone. Osteoblasts, osteoclasts and haematopoietic cells enter the cartilage anlagen via these blood vessels and form primary ossification centres (Mackie et al. 2008). Hypertrophic cells within these centres undergo apoptosis and the type X collagen-rich ECM is degraded as osteoblasts begin to replace the cartilage with trabecular bone, forming bone marrow. The perichondrium surrounding the primary ossification centres is converted into a collar of compact bone by osteoblasts. Vascularisation of the cartilage epiphysis leads to the formation of secondary ossification centres at the ends of the cartilage. The areas of cartilage remaining are the

growth plates, located between the primary and secondary ossification centres and the articular epiphyseal growth cartilage, located between the epiphysis of the cartilage and the secondary growth plates. These areas undergo repeated sequences of endochondral ossification that results in the longitudinal growth and expansion of the bone (Figure 1.8) (Olsen et al. 2000;Mackie et al. 2008).
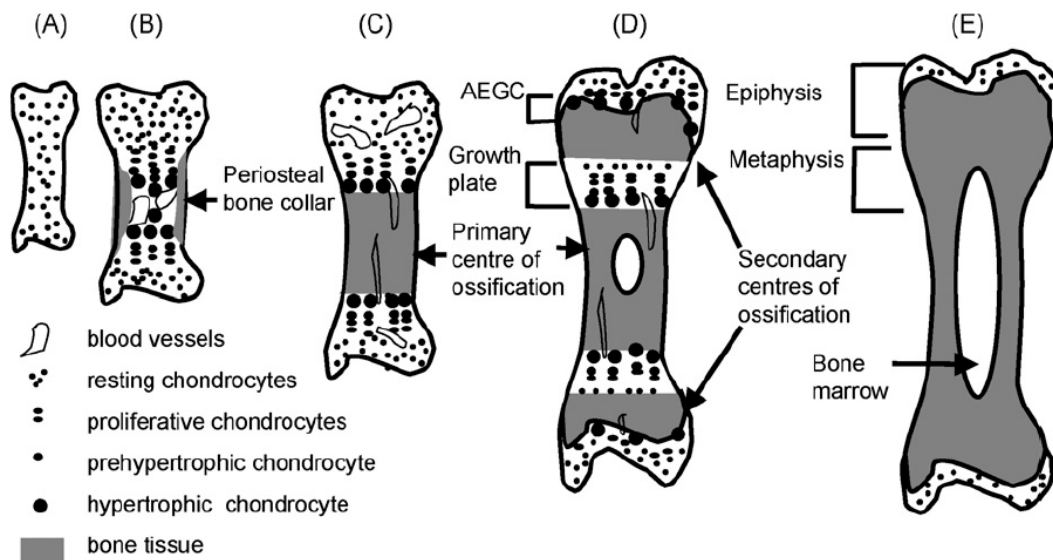
Figure 1.8. The process of endochondral ossification. (A) formation of the cartilage anlagen; (B) chondrocyte hypertrophy and vascularisation initiates the formation of the bone tissue; (C) invasion of blood vessels into the epiphysis of the cartilage anlagen establishes the primary centre of ossification; (D) secondary centres of ossification form at the epiphysis of the cartilage; (E) fusion of the primary and secondary centres of ossification due to expansion and ossification of the growth plates. At this stage, all cartilage anlagen has been converted to bone, only the permanent articular cartilage remains (Mackie et al. 2008).

1.3.3. Intramembranous ossification

Intramembranous ossification occurs in fibrous tissue and involves the direct formation of compact bone with no cartilage anlagen via differentiation of groups of mesenchymal stem cells into osteoblasts (Gilbert 2000) (Figure 1.9). These groups of differentiated cells produce Type I collagen-rich ECM which undergoes calcification to form immature woven bone; eventually replaced with mature bone. Many of the osteoblasts become trapped in the secreted ECM and develop into osteocytes. This type of bone

14

growth is important for repair of damaged bone and during development and growth of bones such as the calvarial bones (Choi et al. 2005).
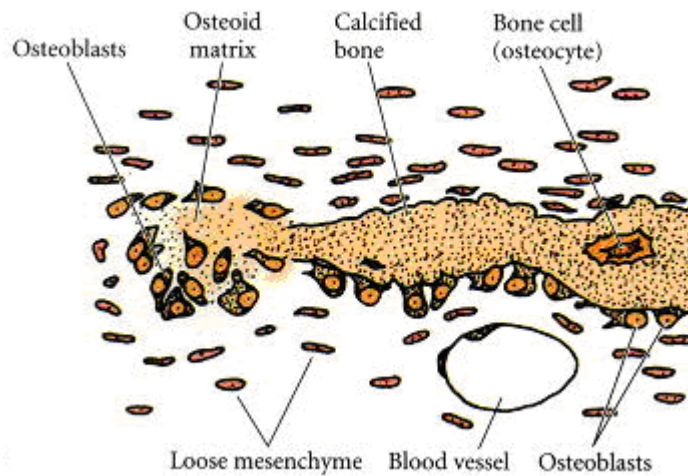
Figure 1.9. Schematic diagram of intramembranous ossification. Mesenchymal cells aggregate to produce groups of osteoblasts, which deposit ECM that undergoes calcification. These osteoblasts become arrayed along the calcified region of the matrix and continue to produce new bone. Osteoblasts that are trapped within the bone matrix become osteocytes (Gilbert 2000).

1.4. Bone

As the major component of the skeleton, bone is the key structural connective tissue of the human body. The primary function of bone is to provide support and centres of movement for the body and protect the various organs of the body. Bone is also the focal point for haematopoiesis (the production of blood cells), regulation of homeostasis, and storage of minerals. The majority of bone is composed of mineralised osseous tissue, this tissue is a hard and yet lightweight composite of calcium hydroxyapatite, which has an extremely high compressive strength. In addition, bone contains a variety of other tissues embedded within its calcified matrix, these include: marrow, nerves, blood vessels and cartilage (Reece et al. 2010).

1.4.1. Bone Structure

Three types of bone structure exist: woven bone, compact or cortical bone and trabecular or cancellous bone (Figure 1.10). Compact and cancellous bone are known as lamellar bone due to their highly organised, layered structures. Woven bone is immature bone with a disorganized structure found during formation of new bone in embryonic development and injury repair; it is eventually replaced by slower-forming lamellar bone (Downey & Siegel 2006). Compact bone is the dense outer layer of bone mainly found on long bones and makes up roughly 80% of the bone in the skeleton. It is composed of large numbers of cylindrical structures called Haversian systems. These systems are made up of a Haversian canal, which encloses blood vessels and nerve cells, surrounded by concentric layers of bone tissue (Buckwalter et al. 1996). Trabecular bone is a network of rod- and plate-like components that give it a spongy, porous structure. This makes the bone lighter and allows room for blood vessels and marrow. Trabecular bone is enclosed in layers of compact bone to provide compressive strength (Downey & Siegel 2006).
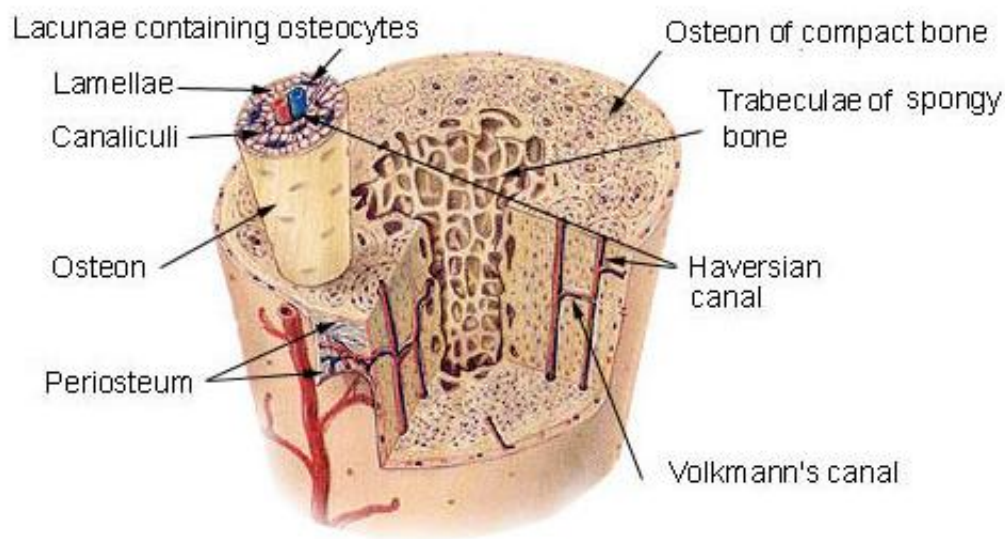
Figure 1.10. Diagram showing the structure of compact and trabecular bone. The Haversian systems are also illustrated (http://training.seer.cancer.gov).

1.4.2. Bone Composition

Bone is composed of varying levels of bone mineral, organic and inorganic matrix, water and lipids, according to the age, health, and anatomical location of the bone.

1.4.2.1. Bone mineral/Inorganic matrix

Bone mineral is composed of calcium hydroxyapatite [$Ca_{10}(PO_4)_6(OH)_2$], a rigid, crystalline structure which provides strength to bone, allowing it to resist compressive forces. This substance makes up the majority of bone weight and volume.

1.4.2.2. Organic matrix

This substance is composed of glycoproteins and collagen fibres, about 90% of which is Type I collagen. Type I collagen is found in bone, tendon, skin and a variety of other soft tissues. It is a long fibrous protein composed of two identical α-1 chains and an α-2 chain (Gelse et al. 2003) and is essential for providing the tensile strength of bone. Type I collagen is produced by osteoblasts and is deposited in layers onto mature bone; this gives the collagen an orientated, cross-linked lamellar structure which provides the bone with its tremendous strength (Shea & Miller 2005). In addition to Type I collagen, there are approximately two hundred non-collagenous proteins (NCPs) found within the organic matrix of bone (Weiner & Wagner 1998), these include osteonectin, Osteocalcin, Osteopontin and bone sialoprotein.

- Osteonectin (ONN) is a glycoprotein that selectively binds to both Type I collagen and hydroxyapatite. When bound to Type I collagen, the resulting complex catalyses the binding of mineral apatite crystals with free calcium ion, acting as a regulator of bone extracellular matrix production and mediates interactions between the extracellular matrix and cells (Termine et al. 1981). In addition, osteonectin also controls cell behaviour by modifying signalling at specific transmembrane receptors and plays a role in osteoblast cell survival (Delany et al. 2007).

- Osteocalcin (OCN) is secreted by osteoblasts and is one of the major NCPs, representing 1-2% of the protein in bone. In bone Osteocalcin binds hydroxyapatite crystals with high affinity and inhibits hydroxyapatite crystal formation, down-regulating bone growth. In addition Osteocalcin also acts as a chemoattractant that recruits osteoblasts and osteoclasts to specific points in the bone for remodelling (Huang et al. 2005). Due to the secretion of Osteocalcin by osteoblasts, Osteocalcin is often used as a biochemical marker of osteogenesis.

- Osteopontin (OPN), also known as bone sialoprotein I, is an adhesive glycophosphoprotein synthesised by a large number of cells including osteoblasts and osteocytes. Osteopontin has a regulatory effect on bone homeostasis; it inhibits mineral deposition by binding to hydroxyapatite and inhibiting crystal growth and Osteopontin promotes differentiation of osteoclasts and enhances their activity in bone resorption (Standal et al. 2004).

- Bone sialoprotein (BSP) is a heavily sulphated, phosphorylated and glycosylated protein produced by osteoblasts that mediates cell attachment to extracellular matrices via an arginine-glycine-aspartate (RGD) motif. BSP promotes bone resorption by controlling the attachment and activation of osteoclasts to mineralised bone surfaces. BSP also has a high binding affinity for apatite, and is believed to be involved in the formation of hydroxyapatite crystals (Huang et al. 2005).

1.4.3. Bone cells

1.4.3.1. Osteoblasts

Osteoblasts are small, mononuclear cells responsible for bone formation. They are derived from mesenchymal precursors and are considered to be mature bone cells. Osteoblasts are found on narrow regions of newly formed, un-mineralised organic matrix. Osteoblasts produce osteoid; a protein matrix primarily composed of Type I collagen, which mineralises to become new bone tissue (Ducy et al. 2000). Osteoblasts also produce alkaline phosphatase, a hydrolase enzyme that dephosphorylates proteins and other molecules. Alkaline phosphatase has been shown to be an important marker of osteogenesis and may be involved in mineral deposition and crystallisation, however, the exact function of this substance on bone has yet to be determined (Shea & Miller 2005). In addition to their function in bone formation, osteoblasts also play roles in osteoclast regulation and bone resorption via the OPG/RANK/RANKL system (Boyle et al. 2003). Preosteoblastic cells express RANKL, which binds to RANK on preosteoclast cells, initiating differentiation and activation of osteoclasts, resulting in bone resorption, while the cytokine receptor osteoprotegerin (OPG) regulates the activity of osteoclasts by blocking the effect of RANKL (Khosla 2001). The regulation of osteoclast development by preosteoblastic/stromal cells ensures that the processes of bone resorption and formation are tightly coupled. Osteoblasts also produce hormones such as IL-6, which induce bone resorption on its own and with other bone-resorbing agents (Ishimi et al. 1990).

18

1.4.3.2. Osteoclasts

These cells act opposite osteoblasts and are responsible for the resorption of mineralised bone. Osteoclasts are haematopoietic cells derived from the fusion of mononuclear cells from the monocyte and macrophage lineage to create large, multinucleated cells (Roodman 1999). Bone resorption is carried out at the 'ruffled border', a specialised, highly invaginated membrane found on osteoclasts that releases acid and enzymes to degrade the bone matrix and the resorption area, which breaks down bone proteins using proteolytic enzymes (Teitelbaum 2007). Bone formation and resorption is a continuous process in constant equilibrium that helps to prevent and heal bone damage. Damage to this equilibrium can result in orthopaedic disease.

1.4.3.3. Osteocytes

These cells are formed from osteoblasts that become trapped within bone during its formation. They occupy spaces known as lacunae. Osteocytes are able to transport nutrients and communicate with other osteocytes, osteoblasts and bone lining cells via small channels in the bone known as canaliculi (Noble & Reeve 2000). The osteocyte is believed to have many roles within the bone; it acts as a mechanical receptor that regulates bone remodelling and repair in adaptation to load and also maintains mineral homeostasis through the canalicular system (Bonewald 2011).

1.4.3.4. Bone lining cells

These are long, flat, inactivated osteoblasts that comprise the majority of the inactive surfaces of bone. They regulate the passage of calcium in and out of the bone and also play a role in the regulation of nutrient transport and initiation of osteoclast resorption of bone by facilitating transport of osteoclasts to the bone interior (Shea & Miller 2005).

1.4.4. Bone remodelling

During bone growth, alteration of the bone shape and size is known as modelling. Remodelling refers to the natural turnover of existing bone tissue without affecting the shape or density of the bone. This process is constant and proceeds rapidly during growth. Bone remodelling is a two-part process, involving the resorption of old bone by active osteoclasts and replacement with new bone produced by osteoblasts.

Bone remodelling is carried out by small groups of cells known as basic multicellular units (BMUs) that ensure that at least 20% of trabecular bone undergoes remodelling at any time (Jilka 2003). Bone remodelling is a complex process, regulated by multiple factors, including the OPG/RANKL/RANK system. Regulation of bone resorption has yet to be fully characterised, but is thought to respond to damage caused by physical stress and osteocyte death (Lee et al. 2002). Regulation of remodelling occurs at the paracrine or autocrine level as demonstrated by the fact that BMUs occur both geographically and chronologically separate from each other (Henriksen et al. 2009). Remodelling is separated into phases: osteoclast activation, resorption of bone, osteoblast activation, formation/calcification of new bone and the resting phase (Lee et al. 2002) (Figure 1.11). At the activation of remodelling, haematopoietic osteoclast progenitors are recruited to the bone and undergo proliferation and differentiation into mature osteoclasts (Hadjidakis & Androulakis 2006). Osteoblasts lining the bone surface produce matrix metalloproteinases (MMPs) that degrade the unmineralised osteoid on the surface of the bone, allowing osteoclasts to access the exposed mineralised surface and begin the resorption phase (Hill 1998). During resorption, osteoclasts adhere to the exposed mineralised surface and form a ruffled border that secretes acid and proteolytic enzymes. The secreted acid acts to demineralise the extracellular matrix of the bone, while the proteolytic enzymes degrade the organic components (Schindeler et al. 2008). Degradation of bone releases growth factors such as TGF-β, insulin-like growth factors (IGFs) I and II and platelet derived growth factor (PDGF) that stimulate the proliferation and differentiation of osteoblast progenitors, which in turn initiate the formation of new bone matrix at the sites of resorption (Mundy 1999). After erosion of the bone is complete osteoclasts undergo apoptosis, terminating the resorption phase and allowing formation of osteoid in the degraded area (Henriksen et al. 2009). The osteoid then undergoes the process of mineralisation, taking approximately 124-168 days to fill in the resorption cavity with new calcified bone (Hill

20

1998). The process of bone resorption is important in calcium homeostasis as it releases the calcium stored in bone into the circulation.
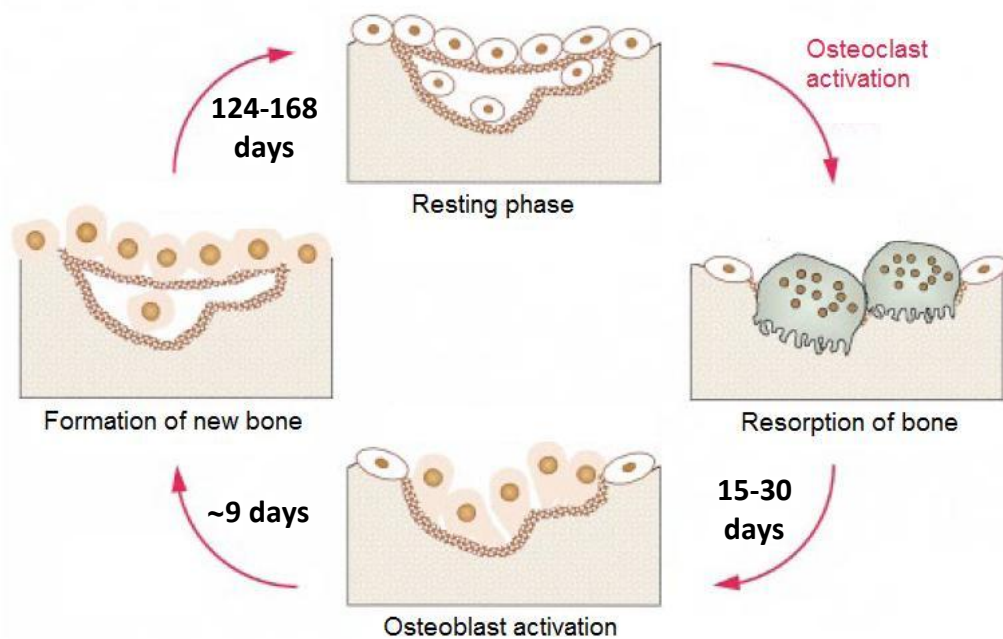
Figure 1.11. The phases of bone remodelling (Adapted from Hill 1998).

1.5. Injury and repair

1.5.1. Bone

Typically, bone injury occurs in the form of a fracture or break caused by pressure being exerted on the bone greater than its tensile strength. Bone fractures vary in their severity, from complete fractures, where the bone is completely broken into 2 or more pieces, to microfractures, tiny fractures in the bone that often occur under tensile stress and do not affect the stability of the whole bone. Microfractures and other small breaks are normally repaired by the normal process of bone remodelling, which removes the damaged part of the bone and replaces it with new calcified tissue. Larger fractures are healed by endochondral ossification. Fracture healing is separated into the reactive, reparative and remodelling phases (Mckibbin 1978). The reactive phase occurs shortly after a fracture is made and begins when blood fills the cavity to form a haematoma at the site of injury (Figure 1.12 A). The inflammatory response results in the recruitment of macrophages, monocytes, neutrophils, lymphocytes, osteoclasts and fibroblasts to the site of injury, resulting in the removal of cell debris, stimulation of vascular invasion and recruitment of mesenchymal cells (Carano & Filvaroff 2003). This whole process

results in the formation of granular tissue around the wound. Various growth factors and cytokines are essential for the inflammatory and reparative responses to bone injury, including IL-1, IL-6, TGF-βs, BMPs, FGFs, IGFs and PDGF (Lieberman & Friedlaender 2005). Mesenchymal stem cells either originating in the damaged tissue or recruited by the inflammatory response begin to differentiate into cells such as fibroblasts, osteoblasts and chondroblasts. Chondrogenesis occurs within the granular tissue around the fracture site resulting in the formation of hyaline cartilage, known as the soft callus (Figure 1.12 B), while woven bone is formed at the border of the callus by intramembranous ossification (Mckibbin 1978). The cartilage of the soft callus then experiences angiogenic invasion and undergoes conversion to woven bone by endochondral ossification, resulting in a hard callus that connects the two ends of the fracture (Figure 1.12 C) (Lieberman & Friedlaender 2005). Finally, remodelling replaces the woven bone with lamellar bone and returns the bone to its original shape and strength (Figure 1.12 D). Bone repair takes approximately 3-6 months for adequate strength to return, depending on the type and severity of bone fracture, age and health of the individual.
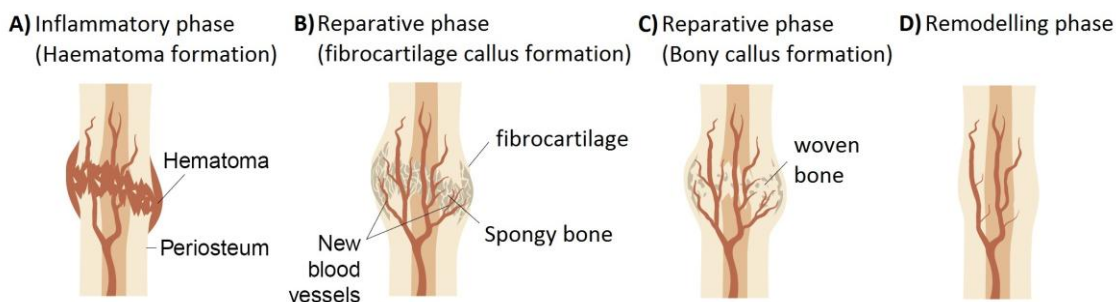
Figure 1.12. The stages of bone repair (Adapted from Carano & Filvaroff 2003).

1.5.2 Cartilage

Cartilage injury occurs in 3 main forms: disruption of the cartilage matrix, partial thickness defects and full thickness defects (Figure 1.13). Matrix disruption is often caused by trauma to an articular joint, causing damage to the cartilage ECM and the cells contained within. Matrix disruption can heal over time provided the injury is not severe, as remaining chondrocytes upregulate their matrix synthesis to repair the ECM (Temenoff & Mikos 2000). The term partial thickness defect is used to describe damage to the surface of the cartilage, whilst a full thickness defect concerns damage to the

22

entire cartilage, up to and including the subchondral bone. Following creation of a partial thickness defect, local chondrocytes begin to proliferate and fill the injured area. However, for unknown reasons the chondrocytes stop proliferating before the damage is fully healed, leaving the defect only partially repaired (Redman et al. 2005). Full thickness defects can undergo spontaneous repair through the production of fibrous cartilage clot. This clot is sufficient to allow progenitor cells to migrate from the bone marrow to the site of injury and replace the damaged tissue with a hybrid of hyaline and fibrous cartilage. This tissue is weak compared to true hyaline cartilage and degrades over time, leading to further injury (Redman et al. 2005). As partial thickness defects do not extend to the subchondral bone, there is no migration of progenitor cells to the site of injury and therefore no wound healing takes place.
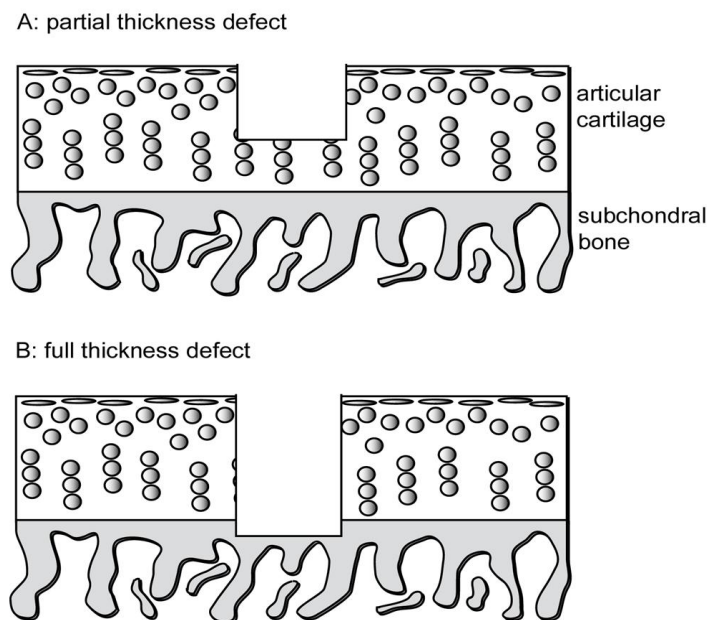
Figure 1.13. Illustration of partial and full thickness defects (Redman et al. 2005).

Chondrocytes maintain the structure of cartilage by sensing and compensating for any changes in the matrix. However, as cartilage is avascular it has limited access to the important nutrients, ECM components and wound healing factors found within the blood. Chondrocytes have a low metabolic activity and undergo very little proliferation as the cells are not required in large numbers to maintain the ECM-rich tissue (Temenoff & Mikos 2000). Furthermore, chondrocytes are embedded within lacunae, preventing their migration to sites of injury. Due to these limitations, once injured, articular cartilage regularly demonstrates insufficient capacity to heal fully, often

leading to defects of the articular joints, causing joint dysfunction, pain and in some cases, development of osteoarthritis. In addition to trauma, several diseases and disorders exist that lead to damage of cartilage, including osteoarthritis, rheumatoid arthritis and osteochondritis dissecans. Osteoarthritis is caused by articular cartilage being worn down in joints continually exposed to high stress, resulting in loss of cartilage and creation of bone-on-bone joints, causing joint dysfunction and severe pain when moved. Rheumatoid arthritis is classified by an autoimmune disorder involving the degradation of bone and cartilage in the joints due to attack from the immune system. Osteochondritis dissecans is where a piece of bone or cartilage becomes loose in the joint, and can lead to destruction of articular cartilage through friction (Emmerson et al. 2007).

1.6. Regenerative medicine

Regenerative medicine refers to the use of artificial organs, specially-grown tissues or cells, specific gene or protein therapy, laboratory-made pharmaceutical compounds, or combinations of these approaches for treatment of injuries and disease. The idea of using cells to cure human diseases has been a key area of research since Paul Niehans first practised "cellular therapy" in 1931 by injecting various cell types into individuals to act as cures and replace damaged cells (reviewed in Togel et al. 2007). The use of cells for therapeutics is highly beneficial due to their plasticity and ability to influence multiple disorders at once, both locally and systematically via the release of various factors. Furthermore, integration of cells into damaged tissues offers a rapid method of healing against a variety of injuries. Introduction of foreign tissue into a patient is coupled with the risk that the body will treat the transplanted tissue as an invading pathogen and produce an immune response leading to rejection of the tissue. To produce a sufficient number of a patient's own cells for transplant, most attention has been focused on the use of multipotential cells such as embryonic stem cells, somatic stem cells and mesenchymal stem cells.

1.6.1. Current treatment and therapies

1.6.1.1. Cartilage defects

The exact frequency of articular cartilage injury is not known due to the difficulty of diagnosis and lack of awareness regarding the symptoms. However, evidence from surgery has shown that roughly 66% of knee injuries undergoing surgery showed damage to cartilage (Curl et al. 1997). Most defects of the articular cartilage lack the capacity to spontaneously heal, resulting in a need for medical intervention. Most repair techniques are concerned with replacement of damaged cartilage with a substance that can mimic the actions of natural articular cartilage or aid healing of existing cartilage.

1.6.1.2. Bone marrow stimulation using arthroscopic techniques

Abrasion arthroplasty: This technique is where, during arthroscopic surgery, all damaged articular cartilage is removed from the site of damage using an automated burr, right down to the subchondral bone. The consequent bleeding and formation of a haematoma is thought to allow the influx of mesenchymal progenitor cells into the site, leading to natural autonomous fibrocartilage repair (Johnson 2001). Arthroscopic surgery differs from open surgery in that incisions are made only for the arthroscope and the surgical instruments, reducing the risk of damage to connective tissue surrounding sites of injury.

Microfracture: Similar to abrasion arthroplasty as it aims to induce autonomous repair by stimulating the bodies healing process, this method is an improvement as it avoids damage or removal of layers of the subchondral bone. The microfracture procedure was designed for patients with trauma-induced lesions of the knee that have progressed to full-thickness chondral defects (Steadman et al. 2001). Injured cartilage is removed down to the stable, undamaged mineralised cartilage, which is then carefully removed to prevent damage to the subchondral bone. Perforations are then made in the exposed bone between 3 to 4mm apart to induce bleeding whilst maintaining bone integrity. These perforations allow the release of blood, mesenchymal stem cells and healing factors from the bone marrow, inducing the formation of a haematoma that provides perfect conditions for new tissue formation (Kasper & Mandelbaum 2006).

The clinical success of these arthroscopic methods is unpredictable, varying from full, but temporary healing of the wound to no lasting remedial effect. Reasons for these inconsistencies may include the variable and flexible nature of the repair tissue formed and the age and activity levels of the patient (Redman et al. 2005).

1.6.1.3. Soft Tissue Grafts

Periosteal/perichondreal grafts: The membrane lining the outer surface of bones, known as the periosteum, is a dense connective tissue containing an outer layer of fibroblasts (fibrous layer) and an inner layer of progenitor cells (cambial layer) with chondrogenic and osteogenic potential (De Bari et al. 2006). Transplantation of periosteum grafts into full thickness defects have been performed by implanting the graft into defects with the cambial layer facing the articular surface. Despite production of a hyaline-like tissue being reported, periosteal grafts demonstrate a high rate of failure and the little repair observed may be due to mesenchymal stem cell release from the subchondral bone rather than the effects of the graft (Meyerkort et al. 2010). Grafts utilising the perichodrium (the layer of connective tissue which surrounds the cartilage of developing bone) have also been tested and have shown similar results to that of periosteum grafts (Homminga et al. 1990). However, perichodrium is harder to attain and less available than periosteum and is therefore used with less frequency.

Osteochondral transplantation: Full thickness cartilage defects can also be repaired by inserting grafts of existing osteocartilage taken from a less weight bearing region of a joint (autografts) or from other individuals (allografts). This method is limited by the amount of cartilage available but has been shown to cause a decrease in pain in 70% of patients (Temenoff & Mikos 2000).

1.6.1.4. Autologous Chondrocyte Implantation (ACI)

Autologous chondrocyte implantation involves the introduction of a patient's own chondrocytes to the site of a wound to promote cartilage healing and requires the removal of a healthy biopsy of non-load bearing cartilage from the patient (Brittberg et al. 1994) (Figure 1.14). The extracted tissue is digested to release the chondrocytes, which are then expanded in culture conditions. When the cell population has reached a sufficient size, the chondrocytes are suspended in culture medium and implanted into a debrided cartilage defect, covered with a periosteal graft and sealed with fibrin glue.
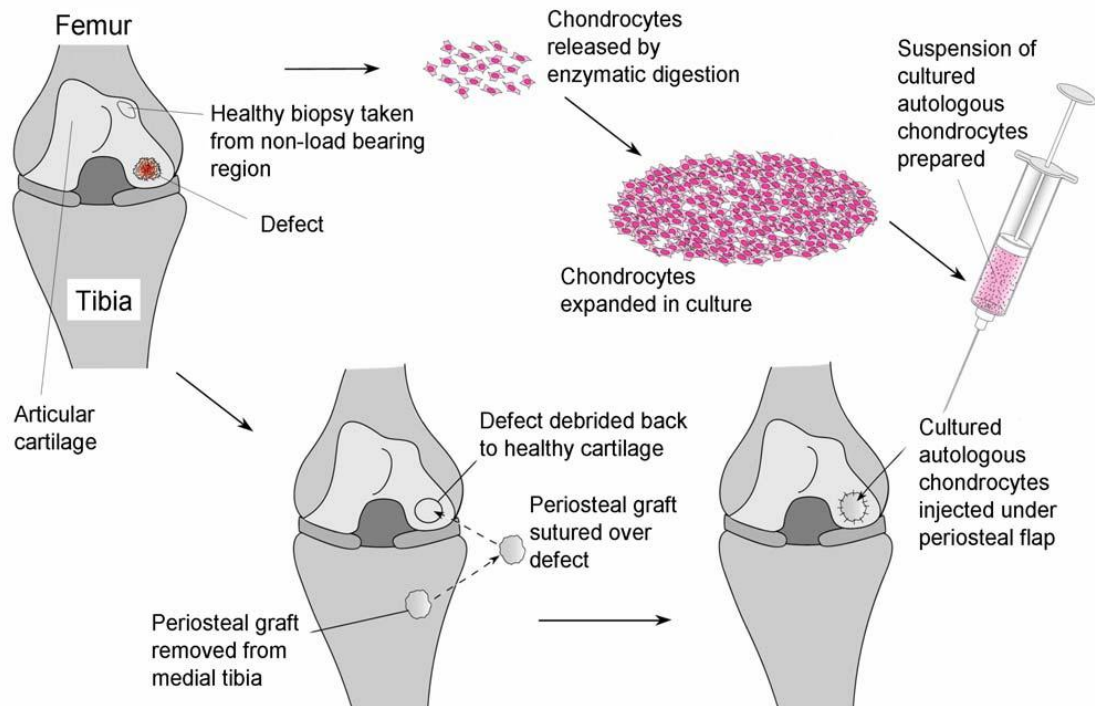
Figure 1.14. Diagram showing the processes involved in autologous cartilage implantation (Redman et al. 2005).

Clinical results from use of this procedure have proved varied but have showed an overall increase in mobility and decrease in pain in around 75-90% of patients (Brittberg et al. 2003), depending on the type and complexity of the cartilage defect, with the best results being found when used for healing the femoral condyle cartilage (Temenoff & Mikos 2000). Despite its success, there are many areas of ACI that cast doubt on its effectiveness. Firstly, a number of questions have risen regarding the effect on the extracted chondrocytes when expanded *in vitro*, such as dedifferentiation of the chondrocytes into precursor cells or modification of cell surface proteins. Secondly, there is no unequivocal evidence that the implanted chondrocytes are responsible for the repair and structural integrity of new cartilage during ACI-mediated repair as there are potentially three different sources of cells that could be responsible for the repair of cartilage, these are the implanted chondrocytes, precursor cells from the periosteal graft or mesenchymal stem cells from the subchondral bone marrow (Redman et al. 2005).

1.7. Tissue Engineering

As technology has improved, a new alternative to tissue grafting and ACI has evolved in the form of tissue engineering. Put simply, tissue engineering involves the development of biological substitutes for the repair or replacement of damaged tissues, and is therefore deemed a highly attractive approach to skeletal tissue repair, specifically with regards to cartilage. For tissue engineering to be successful it requires, typically, the spatially and temporally coordinated application of multiple separate but equally important factors. The first of these is a patient-derived population of cells such as chondrocytes, osteoblasts or mesenchymal stem cells that can be expanded in culture. Secondly an extracellular matrix or scaffold is required to provide structure and support for the cells and define the shape of the new tissue. Specific tissue-inducing growth factors such as BMP-2 for bone or TGF-β3 for cartilage are required to induce the correct phenotype from the cells (Langer & Vacanti 1993). In some circumstances cells can also be manipulated and prepared for tissue engineering using genetic transfection to select certain desirable traits. Mechanical stimuli such as compression/pressure, fluid flow and tissue shear/deformation also act as key factors in the development and maintenance of load-bearing tissues such as bone and articular cartilage. Mechanical stimulation via compression or fluid-flow induced shear have been shown to affect cell viability, differentiation and proliferation and induce biosynthesis of extracellular matrix in both cartilage and bone tissue samples (Lee et al. 2006;Sandino et al. 2008). The effects of pressure and shear stress on skeletal tissue development have been examined by mechanically stretching, twisting or compressing tissue samples in culture, while the effects of fluid flow have been examined using techniques such as spinner flasks, rotating-wall bioreactors, and perfusion culture systems that create fluid flow around cell constructs (Lee et al. 2006;Yeatts & Fisher 2011). According to (Hutmacher 2000), the tissue engineering process can be identified into six phases: (1) Manufacture of a biocompatible scaffold; (2) seeding of an appropriate cell line onto the scaffold in a static culture; (3) expansion of tissue in dynamic culture conditions such as a spinner flask; (4) development of matured tissue under physiological conditions such as in a bioreactor; (5) surgical transplantation into the patient and finally; (6) assimilation and remodelling of the transplant *in vivo* (Hutmacher 2000). Each of these phases requires large amounts of research to ensure appropriate integration.

28

1.7.1. Scaffolds

The use of biocompatible porous scaffolds that can support adherent cultured cells is critical for anchoring the cells within the wound, providing a template for new tissue growth and maintaining the cell's differentiated state (as monolayer-cultured cells will dedifferentiate such as in the case of chondrocytes, where monolayer-cultured populations produce Type I collagen instead of Type II, preventing the formation of hyaline cartilage). Ideally, scaffolds should be manufactured using materials that closely mimic the environment found within the targeted tissue, that do not produce an immunological response, are non-toxic and would be designed so that the bioresorption or erosion of the scaffold matched the production rate of new tissue to enable the most efficient recovery (Lanza et al. 2007). A variety of materials are currently used in scaffold production, including naturally derived polymers such as collagens and FDA approved synthetic polymers such as poly(ethylene glycol) (PEG) and poly(L-lactic acid) (PLLA). Other polymers are under investigation and have yet to be FDA approved, such as poly(lactic acid-co-lysine), which is designed to promote the differentiation and proliferation of specific cell types (Panetta et al., 2009). Naturally derived biomaterials, particularly collagens, are favoured as scaffolds for bone and cartilage repair as they can be found within the normal structure of the tissues. Due to this, collagen scaffolds allow efficient attachment of cells and are recognised and remodelled by enzymes released during the production of new tissue, providing space for its expansion (reviewed in Glowacki & Mizuno 2008). Clinical testing of natural scaffolds using Type I and III collagen (known as matrix-induced autologous chondrocyte implantation (MACI™)) has shown hyaline-cartilage formation and partial restoration of the articular surface and is a more effective method than microfracture (Redman et al. 2005). Testing of a hyaluronan-based scaffold known as Hyalograft C has met with success and has shown 96.7% of repair tissue was hyaline cartilage and 87% of patients showed normal or nearly-normal function of the knee after 17 months (Pavesio et al. 2003). Issues with use of natural biomaterials include the difficulty to produce large amounts of the polymers and fears over the presence of pathogens within the materials, highlighting the need for development of a cheap and easily producible synthetic polymer that replicates the conditions of the natural tissue. Use of FDA-approved synthetic materials such as poly(glycolic acid) (PGA) and PLLA show attachment and proliferation of cells at a level only slightly less than that of collagen scaffolds (Suh & Matthew 2000). In a recent study, chondrocytes cultured on a

poly(vinyl alcohol) (PVA) and poly(caprolactone) (PCL) scaffold that mimics the ECM present in cartilage, demonstrated retention of the chondrocyte phenotype and enhanced secretion of extracellular matrix components in comparison to chondrocytes cultured on a natural polymer composed of gelatin-albumin (Mohan & Nair 2010). Despite their advances over some existing treatments, the use of scaffolds still has many areas that require improvement such as the continued need for surgery to implant the scaffold and problems with the adhesion of synthetic grafts with existing tissue within a wound. As an alternative to fibrous scaffolds, hydrogels can be manufactured from both natural and synthetic polymers and show great potential for tissue engineering, as they can mimic the structural and functional characteristics of natural extracellular matrices, can be injected into a wound to form a matrix in-situ (Nicodemus & Bryant 2008). Hydrogels have demonstrated support of growth and differentiation of many tissues types, including cartilage, bone and fat (Pound et al. 2006;Tan et al. 2009;Brandl et al. 2010).

1.7.2. Tissue-inducing signals

In order to be applied to damaged tissue, it is crucial that a cell population is exposed to the correct conditions to form the required phenotype. In this sense, inductive substances such as growth factors play a vital role. The addition of an appropriate growth factor during tissue engineering can induce the differentiation of cells into a specific lineage or can enhance the production of tissue-specific factors such as ECM from the cells. Growth factors are naturally-produced polypeptides with the ability to promote cell growth, proliferation, differentiation and maturation. Certain growth factors such as those from the transforming growth factor-β (TGF-β) superfamily play fundamental roles in the formation of bone and cartilage.

1.7.2.1. Transforming growth factor-β (TGF-β) superfamily

Members of the TGF-β superfamily have been shown to play a role in both bone and cartilage development (Frenkel et al. 2000). The TGF-β superfamily includes five isoforms of TGF-β (TGF-β1-5), bone morphogenetic proteins (BMPs), inhibins, Activins, müllerian inhibiting substance and many other growth factors, all of which have similar primary amino acid sequences and form dimeric molecules (Massague 1990). TGF-β members are produced in an inactive form and are activated by extreme pH or proteolytic cleavage of a latency-associated peptide (LAP) (Grimaud et al. 2002).

30

TGF-β1-3 are highly expressed during bone and cartilage development, remodelling and during wound healing. TGF-β1 plays an important role promoting migration, proliferation and differentiation of preosteoblast cells and in the production of matrix proteins (Tang et al. 2009). However, it inhibits later stages of differentiation, which is instead regulated by BMPs and other TGF-β superfamily members (Janssens et al. 2005). TGF-β1 is also present in cartilage from the precartilaginous stage through to the mature and mineralising stages and has been shown to promote chondrogenesis in a variety of cell types, including embryonic mesenchymal stem cells, periosteum-derived cells and early chondrocytes (Kato 1992). TGF-β2 and TGF-β3 also act in bone formation and repair by inducing osteoblast development and the formation of pre-bone cartilage (Linkhart et al. 1996;Janssens et al. 2005). TGF-β2 and TGF-β3 rapidly induce differentiation of bone marrow-derived mesenchymal stem cells into chondrocytes by preventing hypertrophy, regulating growth and stimulating production of cartilage-specific matrix including fibromodulin, aggrecan, decorin, Type II collagen (Barry et al. 2001). TGF-β1 has also been shown to induce chondrogenesis in bone marrow-derived mesenchymal stem cells but to a lesser extent than that of TGF-β2 and -β3 (Barry et al. 2001).

1.7.2.2. Bone morphogenetic proteins
Bone morphogenetic proteins (BMPs) are multifunctional polypeptides belonging to the TGF-β superfamily that were first described as promoters of bone formation by Marshall Urist in 1965 (reviewed in Marcus et al. 2007) and subsequently cloned by John Wozney and colleagues, enabling their use in tissue engineering (Wozney et al. 1988). BMPs act as proliferation and differentiation stimuli for many tissues and have been shown to induce cartilage and bone formation both *in vivo* and *in vitro* (Akino et al. 2003;Noel et al. 2003). Around 30 different BMPs have been identified to date, with BMP-2, 3, 4, 5, 6, 7, and 8 comprising the human family members, all of which signal through serine/threonine kinase receptors comprising a heterodimer of various Type I and Type II isoforms (Chen et al. 2004). An eighth molecule; BMP-1, also shows bone and cartilage-inducing properties via activation of TGF-β family members such as BMP-2 and BMP-4, but is structurally different and not classed as part of the TGF-β superfamily (Hopkins et al. 2007). BMPs, specifically BMP-2 and BMP-7, have been used in various clinical trials for skeletal repair and have produced some very promising results. A previous trial known as the BMP-2 evaluation in surgery for tibial trauma

(BESTT) treated 450 tibial fracture patients with either recombinant human BMP-2 or the standard fracture treatment (control group). It was found that significantly more patients had faster wound-healing and lower risk of failure or need for intervention when treated with BMP-2 (Govender et al. 2002).

1.7.3. Cell therapy in tissue engineering

1.7.3.1. Embryonic stem (ES) cells

Stem cells are defined by their ability to differentiate into more than one cell type and their ability to maintain a consistent population, maintaining cell division indefinitely (known as self-renewal) (Taylor et al. 2001). Embryonic stem cells are extracted from the inner cell mass of the blastocyst during early stage embryonic development (Figure 1.15). These cells are pluripotent, meaning they are able to differentiate into all cell types derived from the three primary germ layers: ectoderm, endoderm, and mesoderm (Evans & Kaufman 1981). Human ES cells were first isolated by Thomson and colleagues in 1998 (Thomson et al. 1998). When no differentiation stimulus is present, such as when grown *in vitro*, ES cells maintain pluripotency through proliferation, allowing cultures to be maintained indefinitely (Pera et al. 2000). To maintain an undifferentiated state in culture, ES cells require the presence of specific conditions such as feeder cells, chemically defined medium or cytokines such as FGF-2 (Biswas & Hutchins 2007). Despite their potential for producing cures to a large number of diseases and disorders, the use of human embryonic stem cells is beset by problems such as ethical issues and tissue rejection problems (Pera et al. 2000;Outka 2002;Takahashi & Yamanaka 2006). The first clinical trial using human ES cells for treatment of patients is currently being performed by the Geron corporation, with the aim to induce recovery of feeling and movement in patients with spinal cord injuries.
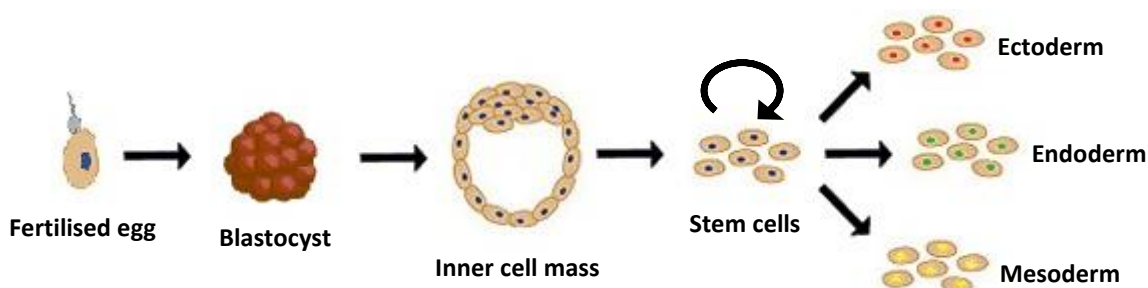
Figure 1.15. The development of embryonic stem cells.

1.7.3.2. Induced pluripotent stem cells

Induced pluripotent stem cells (iPSCs) are pluripotent stem cells typically derived via the introduction of stem cell-related genes into non-pluripotent cells by retroviral transfection. Takahashi and Yamanaka first generated iPSCs in 2006 by introducing the stem cell factors *Oct-3/4*, *Sox2*, *c-myc* and *Klf4* into mice fibroblasts (Takahashi & Yamanaka 2006). Since then, iPSCs have been established from human somatic cells using a variety of stem cell factors, including OCT-3/4; SOX2; NANOG; LIN28; C-MYC and KLF-4 (Takahashi et al. 2007;Yu et al. 2007;Zaehres et al. 2010). Human iPSCs demonstrate growth properties, morphology, stem cell surface and genetic markers, epigenetic status of stem cell-specific genes, and telomerase activity similar to that found in human ES cells, whilst also demonstrating the ability to differentiate into all three germ layers (Takahashi et al. 2007). Use of retroviral transfection poses risks of random genetic modification and creation of cancerous cells, eliciting a need for alternative methods for insertion of the inducing factors. Such alternatives include use of non-integrating adenoviruses (Stadtfeld et al. 2008) and delivery of protein forms of pluripotency-inducing factors (Zhou et al. 2009;Cho et al. 2010).

1.7.3.3. Somatic (adult) stem cells and progenitor cells

Adult stem cells are derived from adult tissues. This process removes any ethical controversy regarding their use as isolating a population of somatic stem cells does not require destruction of an embryo. Adult stem cells are present in most tissues, such as neural (Gage 2000), epidermal (Watt et al. 2006), hepatic (Alison & Sarraf 1998) and mesenchymal tissues (Caplan 1991). Somatic stem cells are often termed progenitor cells, as they define the intermediate stage between a pluripotent stem cell and the differentiated cell. Due to the confusion regarding the nomenclature of these cells the definition of these cells often varies. When compared to ES cells, somatic stem cells have a reduced ability to self-renew and are only multipotent as they are already partially specialised; only able to differentiate into cell types found in the organ from which they are derived.

1.7.3.4. Human bone marrow stromal cells (hBMSCs) and the mesenchymal stem cell

Bone marrow contains two different types of stem cells; the haemopoietic stem cells (HSCs), which give rise to red blood cells, white blood cells and platelets; and the multipotent mesenchymal cells, which were termed as "mesenchymal stem cells (MSCs)" or "human bone marrow stromal cells (hBMSCs)" by Friedenstein and collegues (Togel et al. 2007). There is currently no unequivocal evidence for the existence of MSCs *in vivo* (Baksh et al. 2004), and knowledge of the location and distribution of MSCs in organisms is scant (Bianco et al. 2001). Despite this, the existence of MSCs is generally accepted, as populations of hBMSCs have demonstrated the ability to differentiate into osteoblasts, adipocytes, chondrocytes, myocytes, neurons and hepatocytes (Pittenger et al. 2000;Sanchez-Ramos et al. 2000;Baksh et al. 2004) (Figure 1.16). MSCs are considered an ideal candidate for use in therapeutic medicine as they are multipotent, versatile, easy to grow and can be used for transduction of therapeutic genes into a host. Since the realisation that MSCs could be used for regenerative therapy of many different tissues, many scientific papers have been released detailing the regulation of MSC differentiation and the plasticity of MSCs. However, distinct boundaries between MSCs and progenitor cells have yet to be defined due to the heterogeneous populations often produced by MSCs in culture (Bianco et al. 2001). Therefore very little is known about the phenotypic characteristics of these cells as the "true" MSC has yet to be isolated and characterised. To fully characterise the true MSC, it is necessary to carry out physiological, genetic and biochemical studies at the single-cell scale to obtain significant data.

Due to the uncharacterised nature of differences between true MSC and later, more defined stages such as progenitor cells, nomenclature for hBMSCs varies greatly from paper to paper. Examples of terms coined to date include mesenchymal stem cells, stromal precursor cells, skeletal stem cells, bone marrow stromal cells, osteogenic stem cells and marrow stromal fibroblastic cells (Oreffo et al. 2005). A paper backed by the International Society for Cellular Therapy, produced by Horwitz and colleagues, attempted to clarify the nomenclature for hBMSCs. It was suggested that fibroblastic-like plastic adherent cells should be termed multipotent mesenchymal stromal cells, and that only cells demonstrating true stem cell properties be termed mesenchymal stem cells (Horwitz et al. 2005). Currently, populations of cells with the ability to differentiate into skeletal tissues are often termed as skeletal stem cells.
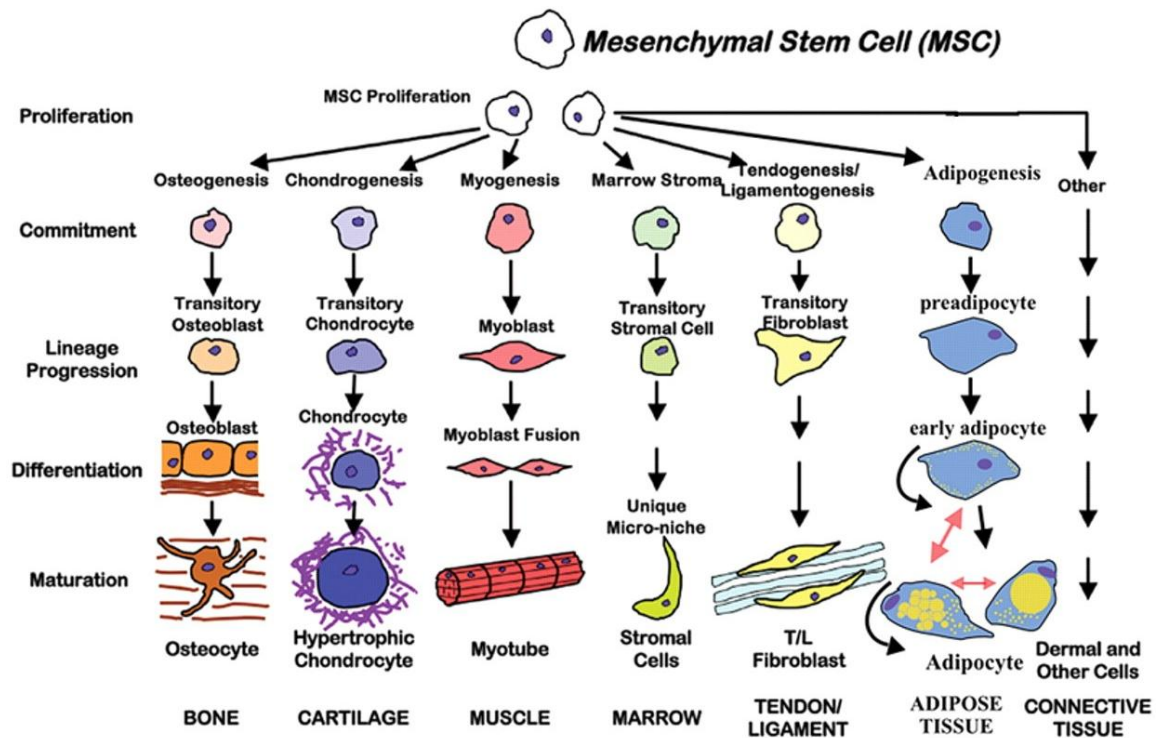
Figure 1.16. The connective tissue family (Bonfield 2010). MSCs have the ability to differentiate into many different types of cell.

Isolation of MSCs from bone marrow extracts is simplified by the fact that MSCs and the progenitor cells will adhere to tissue grade plastic when cultured while haemopoietic cells will not. The standard method used to identify MSCs is the colony forming unit-fibroblastic (CFU-F) assay, which produces clonogenic, fibroblast-like populations (Friedenstein et al. 1970), although these populations maintain heterogenity and many cells are not multipotent (Gronthos et al. 2003;Bianco et al. 2008) In order to further isolate specific cells stage-specific markers are required. However, due to the lack of knowledge surrounding the biochemical and phenotypic structure of these cells and the sharing of common features with other cells, both epithelial and endothelial (Baksh et al. 2004); very few MSC-specific markers have been identified to date and none of these have been accepted as a definitive marker for the MSC phenotype, thus requiring use of multiple markers to enrich MSC populations (Baksh et al. 2004). Characterisation of the MSC cell surface has been carried out by fluorescence activated cell sorting (FACS, Figure 1.17 A) (Radbruch 1999) and the similar technique, magnetic activated cell sorting (MACS, Figure 1.17 B) (Miltenyi et al. 1990). Current markers known to enrich for MSCs include the absence of haematopoietic and endothelial markers (CD45, CD34, CD11b and glycophorin A) and the presence of STRO-1, CD29, CD44, CD49a,

CD63 [HOP-26], CD73 [SH-3/SH-4], CD90, CD105 [SH-2], CD106, CD146 and CD166 [SB-10] (Gronthos et al. 1994;Pittenger et al. 1999;Minguell et al. 2001;Stewart et al. 2003;Jones et al. 2006). Table 1.1 displays a list of many surface markers used to characterise hBMSCs in the attempt to determine the phenotype of the MSC. Gronthos and colleagues have demonstrated that STRO-1$^+$ hBMSCs contained the CFU-F cells, giving rise to fibroblast, fat, muscle and bone cells, confirming the presence of the osteoprogenitor cell and therefore, potentially, the MSC in the STRO-1$^+$ population (Gronthos et al. 1994). To date, the epitope of STRO-1 remains unknown.
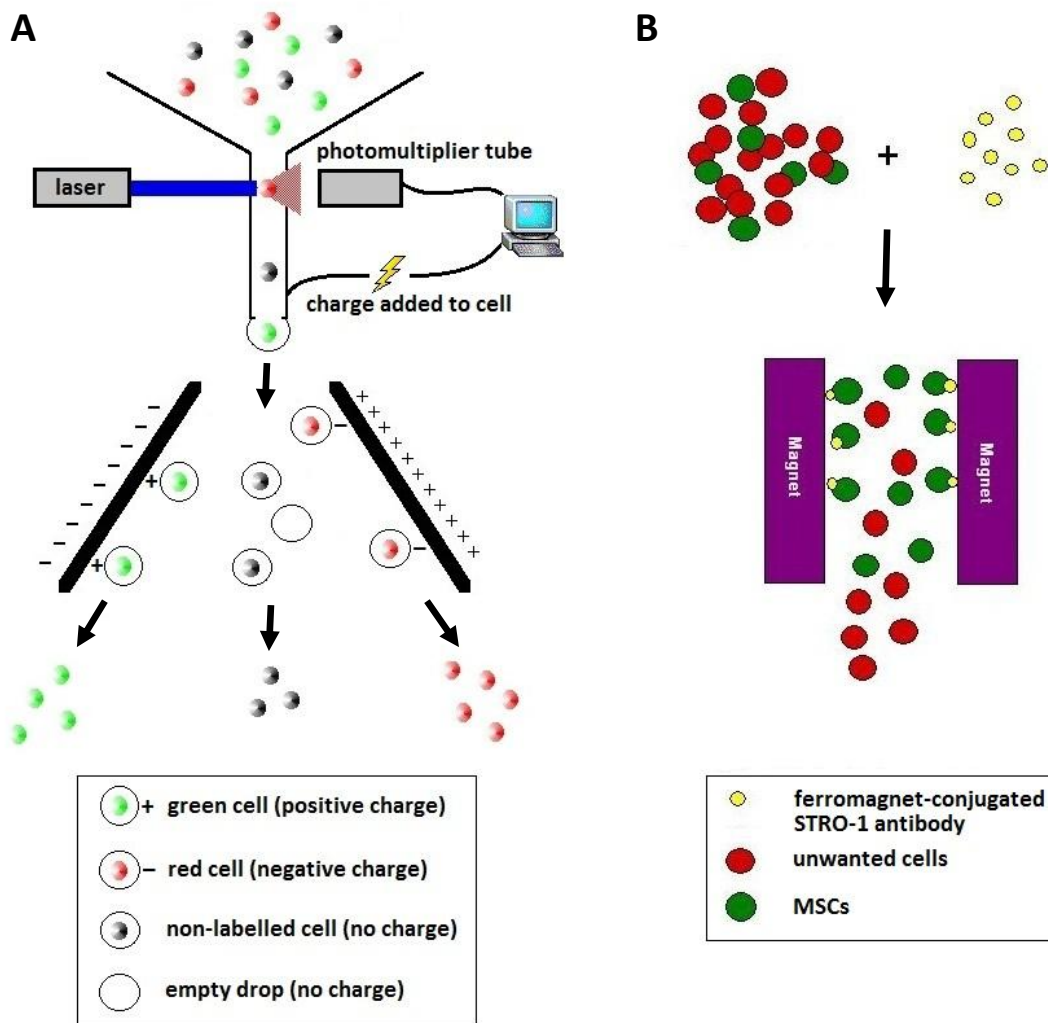
Figure 1.17. Graphic illustration of cell isolation using FACS (A) and MACS (B).

Category	Surface marker	Expression
Adhesion molecules	ALCAM (CD166)	+
	ICAM-1 (CD54)	+
	ICAM-2 (CD102)	+
	ICAM-3 (CD50)	±
	L-Selectin (CD62L)	+
	E-Selectin (CD62E)	-
	VCAM (CD106)	+
	Hyaluronate-R (CD44)	+
Growth factor receptors	Interleukin 1-R (CD121)	+
	Interleukin 2-R (CD25)	-
	Interleukin 3-R (CD123)	+
	Transferrin-R (CD71)	+
	C-kit-R (CD117)	±
	granulocyte colony-stimulating factor-R (CD114)	-
	Platelet-derived growth factor-R	±
	Epidermal growth factor-R	±
Haematopoietic markers	CD1a	-
	Integrin, alpha M (CD11b)	-
	CD14	-
	CD34	-
	Protein tyrosine phosphatase, receptor type, C (CD45)	-
	Prominin 1 (CD133)	-
Endothelial markers	PECAM (CD31)	±
	Von Willebrand factor	-
	Endoglin (CD105)	+
	Melanoma cell adhesion molecule (CD146)	+
Integrins	Integrin, α1,2,3,5 (CD49a,b,c,e)	+
	Integrin, α4 (CD49d)	-
	Integrin, β1 (CD29)	+
	Integrin, β4 (CD104)	+
Intracellular markers	Vimentin	+
	Laminin	+
Stemness markers	OCT-4	-
	Nanog	-
Co-stimulatory molecules	B7-1 (CD80)	-
	B7-2 (CD86)	-
	CD40	-
Other markers	Thy-1 (CD90)	±
	5'-nucleotidase (SH-3/SH-4, CD73)	+
	STRO-1	+
	Low-Affinity Nerve Growth Factor Receptor (CD271)	±

Table 1.1. Phenotypic characterisation of hBMSCs. Key: +, routinely expressed in all studies; ±, variably expressed; -, no expression. (Pittenger et al. 1999;Deans & Moseley 2000;Minguell et al. 2001;Devine 2002;Sorrentino et al. 2008;Uccelli et al. 2008;Zhang et al. 2009).

1.7.3.5. Fetal and extraembryonic tissue-derived cells

Recently, cells derived from fetal tissues, cord blood and extraembryonic tissues have emerged as an alternative to both ES and adult stem cell use and are currently undergoing intensive investigation. These cells are attractive for use in regenerative medicine due to their avoidance of invasive isolation procedures, primitive phenotype, non-tumorigenic nature and high expansion potential (Abdulrazzak et al. 2010). While use of extraembryonic tissues has few ethical issues, the isolation of cells from an aborted fetus is still subject to public unease.

Umbilical cord blood (UCB) is a rich source of haematopoietic stem cells and progenitor cells. UCB-derived cells have demonstrated ability to generate cells with characteristics of MSCs in multiple studies (Erices et al. 2000). In a study by Musina and colleagues, mononuclear cells isolated from the UCB displayed morphology and expression of surface markers similar to that of both adipose and skin-derived MSCs, while also demonstrating the ability to undergo both osteogenic and adipogenic differentiation (Musina et al. 2007). UCB cells have also demonstrated ability to differentiate into hepatocyte-like cells (Hong et al. 2005) and chondrocytes (Choi et al. 2008). Despite their potential, UCB extracts have been shown to have extremely low counts of MSCs and a reduced proliferation rate and opinions are divided as to whether the UCB can be regarded as a source of MSCs as effective isolation of MSCs from both term and preterm UCB has been varied (Bieback et al. 2004).

Cells isolated from the placenta and umbilical cord connective tissue are considered as acceptable alternative sources of large numbers of MSC-like cells. Placenta and umbilical cord matrix cells have demonstrated similarity to bone marrow-derived MSC populations in both morphology, cell surface marker expression and differentiative capacity (Barlow et al. 2008;Zeddou et al. 2010).

Cells derived from fetal blood, femur, liver and amniotic fluid have also demonstrated multipotentcy and expression of many MSC markers including CD29, CD44, CD73, CD105 (Campagnoli et al. 2001;Soncini et al. 2007).

1.8. Microfluidic cell isolation

The use of analytical science in areas with only minute quantities available, such as proteomics, genetics and cell analysis, has led to an ever decreasing amount of reagents being used. Handling such small volumes in modern laboratory equipment is difficult, therefore many novel, micro-scale techniques and devices have arisen, giving rise to the Lab-on-a-chip (LoaC) system. Early integration of mechanical, electrical and thermal elements into silicon chips led to the idea of producing LoaC devices incorporating all the components necessary to perform a specific analysis, known as micro-total-analysis-systems (μ-TAS) (Jakeway et al. 2000). These systems have provided many benefits and new methods to a variety of research areas including detection and analysis of bacteria, viruses and cancers (Arora et al. 2010). LoaCs are cheaper to produce than normal laboratory equipment and use very low volumes of reagents; therefore they can be used at much lower running costs and for analysis of rare substances and cell types (Manaresi et al. 2003). LoaCs are also able to integrate multiple analytical devices and can be adapted for portable devices. The majority of LoaC research has been focused on increasing the efficiency of DNA amplification and detection, fluid motion and other analytical functions, with many devices now commercially available (Mark et al. 2010). However, in recent years there has been an increase in development of LoaC systems able to manipulate and analyse cells using a variety of different techniques.

Two types of microfluidic cell separation exist: contact and non-contact. Contact techniques mainly consist of chemical trapping, where a chemical attached to the chip is used to detect a certain molecule within the fluid flow, and hydrodynamic trapping, which utilises mechanical obstacles to sieve an object from a fluid suspension (Johann 2006). Contact methods are generally avoided when attempting to isolate individual cells or populations, as contact-free immobilisation prevents damage to, or interference with the cells that could lead to false data from samples. A variety of non-contact microfluidic cell separation techniques exist, using mechanisms including optical trapping, acoustics, magnetic forces and dielectrophoresis.

1.8.1. Dielectrophoresis (DEP)

In a uniform electric field an uncharged particle will polarise and form a dipole, but due to the force on the particle being equal and opposite, the particle will not move. DEP is the phenomenon whereby particles exposed to non-uniform electric fields experience a net force directed towards locations with either increasing or decreasing field intensity. The strength of the force is dependent on a variety of factors including the particles' dielectric properties, determined by the physical properties of the particle such as the size and shape and the interior structure; the medium; and the frequency of the electric field (Pohl 1978). By varying the frequency of the electric field, it is therefore possible to non-invasively distinguish between different cells and particles. Furthermore, DEP is effective on all particles, both charged and uncharged. DEP has been developed for use in a variety of applications including separation, manipulation, trapping and characterisation of particles. DEP utilises the interaction force between a non-uniform electric field and the induced dipole of a particle. When a dielectric particle is suspended in an electric field, it will polarise. If the electric field is uniform, then the attraction between the dipolar charges and the electric field is equal and opposite and there is no net movement of the particle unless it carries its own net charge (Hughes 2002) (Figure 1.18).
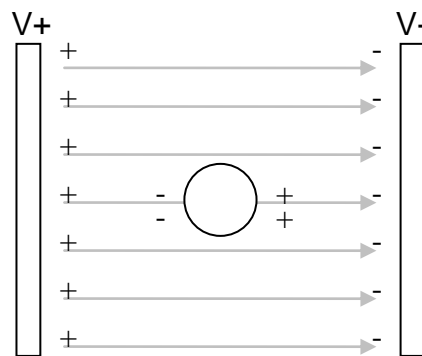
Figure 1.18. Diagram showing the lack of net movement of a dielectric particle when placed in a uniform electric field.

If the electric field is non-uniform then the attractive forces on either side of the particle will be different, resulting in a net force on the particle. The particle will move in the direction of greatest electric field gradient, independent of the polarity of the electric field. The DEP force is dictated by the relationship between the polarisability of the particle and the suspending medium.

40

DEP is classified into two types: positive and negative DEP (Figure 1.19). Which of these forces a particle experiences is dependent on its permittivity relative to its surrounding medium. When the permittivity of the medium is less than that of the particles' then the net-force causes it to move towards the increasing field gradient. This is known as positive DEP (pDEP). However, in negative DEP (nDEP), the permittivity of the medium is greater than the particles, causing the particle to be repelled from areas of high electric energy (Medoro et al. 2007).
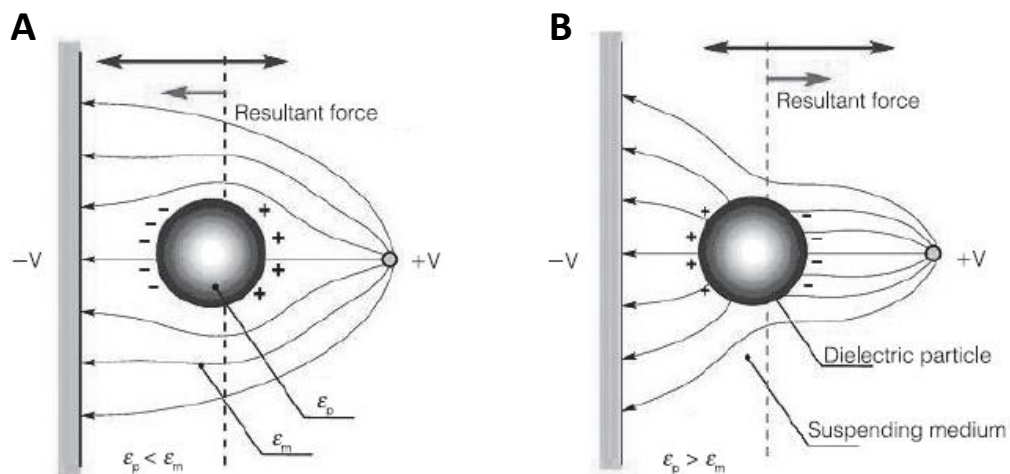
Figure 1.19. Negative (A) and positive (B) dielectrophoresis on a homogenous sphere (Medoro et al. 2007).

1.8.2. Dielectrophoresis-specific LoaCs

Dielectrophoretic separation and manipulation of cells has been greatly improved by the development and introduction of microelectronic devices. The majority of microfluidic chips involved in DEP use a conducting material such as gold patterned onto an insulating substrate such as glass. The patterning is usually performed by photolithography (Hughes 2002). The majority of work on DEP-specific LoaCs has been undertaken with the aim of creating cell detectors for medical use, for example in the detection of cancer (Cheng et al. 1998). Devices with the ability to separate different cell types have been previously demonstrated, such as the isolation of CD34+ haematopoietic stem cells from bone marrow and blood by Talary and collegues (Talary et al. 1995), highlighting the potential for using DEP-specific LoaCs to isolate specific MSC populations such as those expressing STRO-1.

New techniques using DEP have provided analytical science with a number of ways to isolate single cells from a population. Many different types of DEP single-cell traps currently exist, these include pDEP ring-dot, nDEP octopoles and nDEP cages (Rosenthal & Voldman 2005).

Positive DEP is a useful technique for patterning cells onto a substrate as this requires only a simple electrical setup. Although pDEP can be used effectively without significant loss of cell viability, it has been shown to cause considerable damage to cells due to field disruption by the regions of high electrical field to which the cells are drawn. Prolonged exposure to these regions can create instability in the transmembrane voltage of a cell, causing lysis and cell death. In addition, in order to create the appropriate environment for pDEP, a media with low ionic content is needed; this can be detrimental to the health of the cells, leading to decrease in viability (Thomas 2006).

Negative DEP has many advantages over pDEP, notably the ability to suspend particles above a surface for non-contact isolation of single cells, especially important for studying adherent cells. Technological advancements in the production of electrodes with micro-sized features have led to an increase in the availability of DEP. Different electrode designs have been designed for DEP, each providing different properties for particle manipulation, for example, the quadrupole electrode uses four electrodes to immobilise and levitate a single particle via negative DEP and offers a method to separate specific cells for characterisation (Voldman et al. 2003) (Figure 1.20). The introduction of octopole electrode designs into DEP (Schnelle et al. 1993) allowed the creation of nDEP cages. In this layout, electrodes are placed on both the top and bottom surfaces of a trap; the fields produced are able isolate a single cell in the middle of a flow channel, allowing single-cell isolation from a flow of cells (Manaresi et al. 2003). More recent techniques have looked at using computer-run recognition programs to selectively trap specific cells such as those expressing certain levels of fluorescence (Thomas 2006).
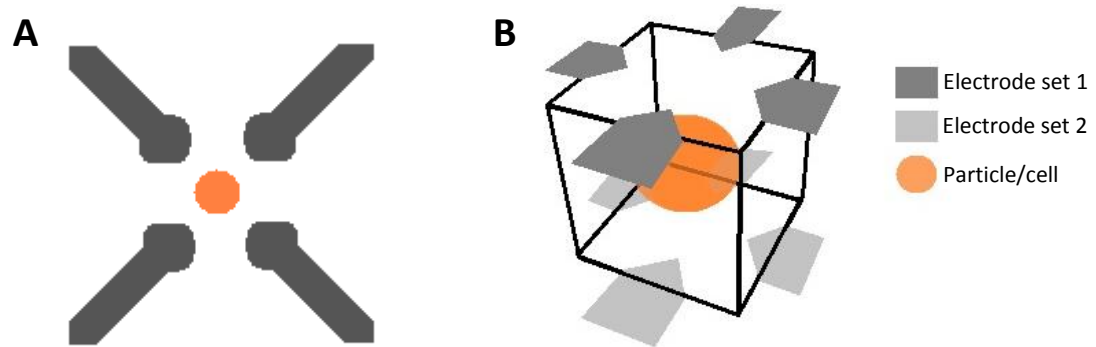
Figure 1.20. Basic representations of quadropole (A) and octopole (B) DEP electrodes.

The introduction of new technologies such as complementary metal–oxide–semiconductor (CMOS) chips have enabled the development of matrices of DEP electrodes (Manaresi et al. 2003), in this method, each of the 102,400 electrode elements on the chip contain an integrated transistor, allowing each element to be addressed separately. Using groups of these electrodes it is possible to create nDEP cages, allowing high throughput single cell trapping. However, use of CMOS fabrication is currently expensive and time-consuming and therefore may not be suitable for disposable devices.

1.8.3. Cellular reactions to dielectrophoretic manipulation

One drawback of using DEP for cell manipulation and isolation is the application of strong AC fields to cell populations. These fields can induce joule heating of buffer in the vicinity of the electrodes, potentially damaging cellular protein and DNA crucial for survival and fitness. Furthermore, the fields can alter the electrical potential of the cell membrane, stimulating destabilisation and potential cell lysis (Menachery & Pethig 2005). A crucial study carried out by Steffen Archer and colleagues (Archer et al. 1999) showed that under controlled conditions, DEP can be used to manipulate the cells with no permanent effect. However, it was shown that cells exposed to DEP showed unknown differential gene expression compared to those not exposed to DEP, lasting more than 30 minutes after exposure. Use of high frequency AC fields in the Megahertz range has been shown to produce fewer problems with disruption of the transmembrane potential and use of miniature electrodes has improved heat dissipation (Glasser & Fuhr 1998).

1.8.4. Mechanisms of detection for cell trapping

1.8.4.1. Optical detection

The majority of methods for trapping and manipulation of cells require manual activation. This is not suitable for high throughput assays and therefore it has become apparent that automated systems are required. Optical observance of cells by microscopy is an established technique with much of the equipment readily available, making this an obvious method for automated detection of specific cells in a microfluidic chip. This method uses a microscope-mounted camera to send images to a computer using rule-based algorithms to identify and trap particles according to specific characteristics such as colour or shape (Thomas 2007). One way of simplifying the software-based recognition of cells is to use fluorescent labelling. By using immunogenic labelling for specific membrane-bound antigens it is possible to ensure that fluorescence is expressed by a specific cell type, for example, fluorescent labelling of MSCs expressing STRO-1. Labelling of cells with a combination of different fluorescently labelled antibodies can be used to further isolate specific cell types.

One disadvantage of optical detection is the requirement for optical devices such as microscopes which are often bulky and require complex setup, making them inappropriate for LoaC systems. However, integration of optical detection into an LoaC system is possible (Manaresi et al. 2003) and is an area for future research and development.

1.8.5. Microfluidic analysis of single cells

1.8.5.1. Electrorotation

As described by Pohl (Pohl 1978), when a dielectric particle is suspended in a fluid, the interaction between a non-uniform field and the induced dipole can generate a torque on the particle, causing it to rotate. It is thus possible to use quadrupole electrodes to produce and control the rotation of a particle by subjecting it to a rotating electrical field (Arnold & Zimmermann 1982). The speed at which a particle rotates is related to the dielectric properties of the particle, the suspending medium and the electric field, as such, by knowing the properties of the medium and electric field, electrorotation can be used to measure the electrical properties of cells (Fuhr et al. 1985).

It has been demonstrated that electrorotation provides a very sensitive method for determining the physiological state of cells and their sensitivity to chemicals and other agents (Arnold & Zimmermann 1988).

1.8.5.2. Impedance spectroscopy

Most current analysis techniques involve labelling of cells using antibody-bound substrates e.g. FACS, MACS. Dielectric analysis of cells, also known as electrochemical impedance spectroscopy (EIS), offers a label-free method analysis and can be carried out on-chip (Gawad et al. 2001;Gawad et al. 2004). Impedance spectroscopy measures the electrochemical impedance of the cell. The cell is placed between a set of AC electrodes between which current and voltage are measured to determine the base electrical impedance. The presence of a cell between the electrodes causes distortion of the electrical field, altering the impedance of the system and allowing the impedance and in turn, the electrical properties of the cell to be determined (Figure 1.21). EIS is carried out over a variety of frequency ranges and can provide data on the structural features of a cell according to their affects on overall impedance (Gawad et al. 2001).
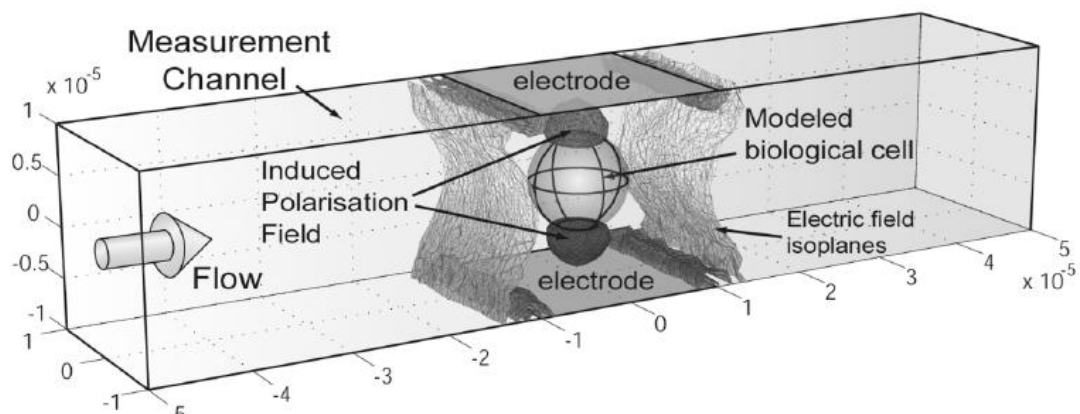
Figure 1.21. Impedance spectroscopy of a single cell (Gawad et al. 2004).

1.9. Aims and Objectives

The aim of this thesis was to further the understanding of both adult and fetal mesenchymal stem cells and the mechanisms regulating their stem cell state and their differentiation towards bone and cartilage tissues. To achieve this goal, this thesis set out to develop novel microfluidic-based technologies for the isolation and characterisation of mesenchymal stem cells. In addition, this thesis has examined a subpopulation of fetal femur-derived cells expressing a novel cobblestone phenotype and has assessed the potential of a novel 3D organotypic system for modelling skeletogenesis using fetal-derived cells.

Objectives:

- To isolate, culture and characterise a novel cobblestone phenotype Induced by use of chemically defined media on human fetal femur cell populations.
- To determine the viability of fetal femur-derived cells in organotypic pellet culture and assess the effects of osteogenic and chondrogenic stimulatory factors on organotypic culture and their ability to promote formation of cartilage- or bone-like tissue *in vitro.*
- To develop novel dielectrophoresis-based microfluidic devices (in collaboration with the Electronics and Computer Sciences department, University of Southampton) for the isolation of specific subpopulations of cells.
- To demonstrate the purity, viability and growth of cells isolated using microfluidic devices in culture and characterise recovered populations.

CHAPTER 2

METHODS

2.1. Materials and reagents

All tissue culture, histological reagents and biochemical reagents were obtained from Sigma-Aldrich Ltd. unless otherwise indicated, including α-MEM (minimum essential medium, α-modification, M0644), phosphate buffered saline (PBS, P4417), foetal calf serum (FCS, 8K3381), trypsin-EDTA (ethylenediamine tetra-acetic acid, T4174), bovine serum albumin (BSA, A3294), Tris-EDTA (Tris-hydrochloric acid EDTA, T9285), alkaline buffer solution (A9226), alkaline phosphatase assay kit with Sigma 104® phosphatase substrate (104-0) and AP standard (104-1), Naphthol AS-MX Phosphate 0.25% (855) and Fast Violet B Salts (F1631). PicoGreen® dsDNA quantification reagent (P7589), Cell tracker green™ CMFDA (C7025) Vybrant® CFDA SE cell tracer kit (V12883) and Vybrant® DiD (V-22887)/DiO (V-22886) were all purchased from Invitrogen UK. Alcian blue 8GX (343291G) and Sirius red F3B (341492F) were purchased from VWR International. Anti-Type I collagen antibody (rabbit anti-human polyclonal, LF67) was purchased from Dr Larry Fisher (NIH, Bethesda, USA). Sources for all other primary antibodies can be found in Table 2.1. Relevant secondary antibodies and ExtrAvidin Peroxidase (E2886) were purchased from Sigma-Aldrich. Human recombinant transforming growth factor-β3 (TGF-β3, PHG9305) was purchased from Invitrogen. Recombinant BMP-2 was sourced as part of a collaboration with Professor Walter Sebald, University of Wurzburg, Germany. Molecular biology reagents were purchased from Invitrogen Life Technologies, UK, including TRIzol solution (15596-018), Superscript™ first-strand synthesis system (11904-018), SuperScript™ III Reverse Transcriptase (18080-044) and Power SYBR Green PCR master mix (4367659). Molecular biology reagents were also purchased from Promega UK Ltd., including RNase-free DNase (M6101) and dNTPs (deoxynucleotide triphosphates, U1511). DNA-free RNA Kit (R1013) was procured from Zymo Research Corporation (http://www.zymoresearch.com). First strand primers for RT-PCR were ordered from Sigma-Genosys, UK and are listed in Table 2.2.

2.2. Tissue Culture

2.2.1. Human bone marrow preparation and stromal cell culture

Bone marrow samples were obtained from haematologically normal patients undergoing routine total hip replacement surgery (Figure 2.1 A). Only waste tissue was used, with approval from the Southampton & South West Hampshire Local Research Ethics

Committee (LREC 194-99). Marrow stromal cells were obtained as previously described (Oreffo et al. 1998). Marrow samples were washed vigorously in α-MEM up to 4 times (Figure 2.1 B) and the resulting suspension was centrifuged at 1100rpm for 4 minutes at 4°C. The pellet was resuspended and run through a 70μm filter to remove large debris. Remaining cells were plated to culture flasks at appropriate densities. Cultures were PBS washed and media changed after one week to remove non-adherent cells and red blood cells. Cells were cultured in α-MEM containing 10% FCS at 37°C with 5% CO_2 and passaged at confluence for maintenance or use in experiments (Figure 2.1 C). A list of samples used in these studies can be found in Appendix 1.

Figure 2.1. Isolation of human adult bone marrow stromal cells (hBMSCs) from bone marrow aspirants. (A) Marrow sample after collection; (B) Marrow aspirant after repeated media washes; (C) tissue cultured hBMSCs. Scale bar: 100μm.

2.2.2. STRO-1$^+$ immunoselection of adult stromal cells

Magnetically activated cell separation (MACS) was used to isolate the STRO-1$^+$ population from adult marrow cells as described (Howard et al. 2002). Following bone marrow preparation, lymphoprep solution was added to the cell solution to remove red blood cells via centrifugation. The remaining cells were resuspended in blocking solution (PBS containing 5% FCS and 1% BSA) and incubated in the presence of STRO-1 antibody hybridomas for 1 hour. The solution was washed with MACS buffer (PBS containing 1% BSA) and incubated with MACS anti-IgM beads for 45 minutes. The cell suspension was passed through a MACS column located next to a magnet to remove the STRO-1$^-$ fraction. After two further washes, the magnet was removed and MACS buffer was passed through the column to produce the STRO-1$^+$ fraction, which was cultured in α-MEM containing 10% FCS at 37°C with 5% CO_2

2.2.3. Isolation and culture of fetal femur-derived cells

Human fetal tissue was obtained with informed and written consent from terminations of pregnancy according to guidelines issued by the Polkinghorne Report and ethical approval from the Southampton & South West Hampshire Local Research Ethics Committee (LREC 296100). Fetal femurs at 7-12 weeks post conception were isolated from the fetus by Prof Neil Hanley and Prof David Wilson, Human Genetics Division, University of Southampton. Femurs were dissected in sterile PBS to remove surrounding skeletal muscle (Figure 2.2). Femurs were plated into T25 flasks overnight in 2ml α-MEM containing collagenase B. The cell solution was passed through a 70µm filter to remove debris, spun down and resuspended in α-MEM containing 10% FCS. Cells were maintained at 37°C with 5% CO_2. Fetal age was determined by measuring fetal foot length and described as weeks post conception (WPC). A list of fetal samples used in these studies can be found in Appendix 1.
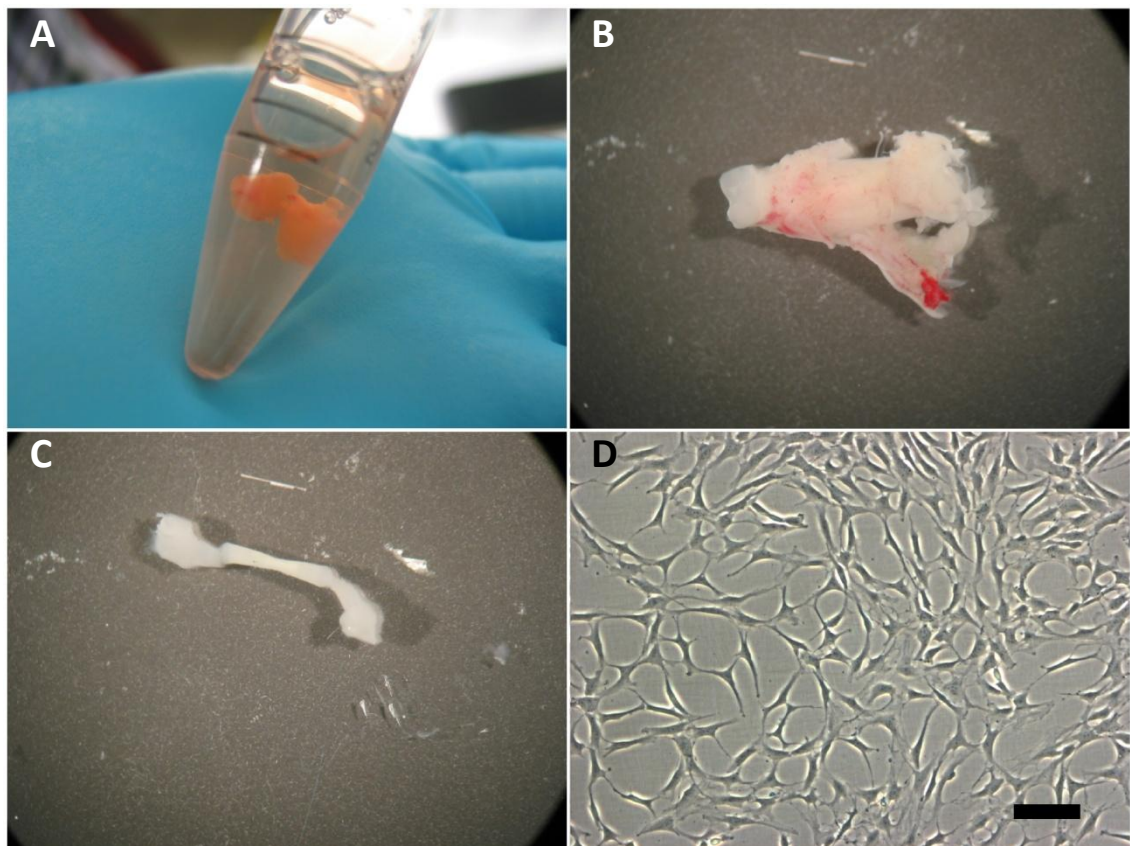
Figure 2.2. Femur isolation pictures. (A) on collection; (B) before processing; (C) after processing; (D) explanted fetal cells in culture. Scale bar: 100µm.

2.2.4. Culture of established cell lines

Immortalised human MG-63 cells, a line derived from an osteosarcoma (ATCC, CRL-1427) were cultured as monolayer cultures in DMEM plus 10% FCS. Cells were maintained at 37°C with 5% CO_2 and passaged at confluence for maintenance or use in experiments.

2.2.5. Differentiation media

2.2.5.1. Osteogenic conditions

To promote osteogenesis, cells were cultured in appropriate culture media (DMEM for established cell lines, α-MEM for primary cell lines) containing 10% serum plus 100μM ascorbic acid 2-phosphate, 10nM dexamethasone and 150ng/ml BMP-2.

2.2.5.2. Chondrogenic conditions

To promote chondrogenesis, cells were cultured in appropriate media containing no FCS, supplemented with 100μM ascorbic acid 2-phosphate, 10nM dexamethasone, 10μl/ml 100x ITS solution and 10ng/ml TGF-β3.

2.2.5.3. Adipogenic conditions

Confluent cell cultures were treated with appropriate media containing 10% serum, 1μM dexamethasone, 10μg/ml 100x ITS solution (insulin - transferrin - sodium selenite solution), 0.5mM 3-isobutyl-1-methylxanthine (IBMX) and 100 μM indomethacin.

2.2.6. Cell passage

Monolayer cells were rinsed with PBS to remove excess medium and cell debris and incubated with 1X trypsin at 37°C for 5-10 minutes to allow breakdown of adhesion proteins. Media plus FCS was added to the resulting cell solution to deactivate the trypsin and the suspension was centrifuged at 1100rpm for 4 minutes. The supernatant was discarded and cells resuspended in culture media for use in further culture.

2.3. Histological analysis

2.3.1. Viability assays

2.3.1.1. Live/dead staining

Cell viability was examined using Cell Tracker Green™ CMFDA (5-chloromethylfluorescein diacetate), which labels metabolically active cells green and ethidium homodimer-1, which labels necrotic or damaged cells red. 10μl DMSO was added to 50μg of cell tracker green and added to 5ml media along with 25μg ethidium homodimer. This solution was added to cell cultures for a 1 hour incubation at 37°C. The media was removed and fresh culture media was added for 1 hour to remove any residual dye. Samples were rinsed in PBS and fixed in 90% ethanol for 15 minutes before being re-immersed in PBS for visualisation.

2.3.1.2. Long-term assays

For long term viability assays the Vybrant® CFDA SE cell tracer kit (carboxyfluorescein diacetate, succinimidyl ester) was used. For most uses, the cells were stained whilst in suspension to aid uniform labelling. Cells were centrifuged at 1100rpm for 4 minutes to obtain a cell pellet and the supernatant was removed. 500μg of Vybrant CFDA was dissolved in 90μl DMSO and added to prewarmed PBS, which was added to the cells. The suspension was incubated at 37°C for 30 minutes, centrifuged and resuspended in fresh prewarmed culture media for a further 30 minutes to ensure complete activation of the fluorescent probe. The cells were washed once more in culture media before being cultured.

2.3.2. Sample preparation

Samples were fixed using 90% ethanol or 4% paraformaldehyde in PBS (15 minutes incubation in ethanol or overnight for PFA). Monolayer cultures were washed and resuspended in PBS at 4°C until ready for staining. 3D cultures (fetal femurs, cell pellets) were processed through graded alcohols after fixation (90%, 100% for 30 minutes each), cleared in chloroform (50% chloroform/ethanol, 100% chloroform twice, for 30 minutes each), soaked in paraffin wax at 60°C for at least 30 minutes to allow the sample to become saturated with wax, embedded in wax blocks for sectioning. Sectioning was performed on a Microm 330 microtome at 7μm and sections were transferred to pre-heated glass slides for staining. In preparation for staining, paraffin

sections were incubated in 2 histoclear solutions for 7 minutes each to remove the wax, and rehydrated by 2 minute incubations in 100% methanol (twice), 90% methanol and 50% methanol before being submerged in a cold water bath for 10 minutes.

2.3.3. Alcian blue/Sirius red staining

Weigert's haematoxylin was added to rehydrated samples for 10 minutes to stain the cell nuclei, followed by a water and acid alcohol (20ml hydrochloric acid in 2 litres 50% methanol) rinse to remove excess stain. Samples were immersed in 0.5% Alcian blue 8GX for 10 minutes to stain for proteoglycans, followed by a water rinse. Sections were placed in 1% molybdophosphoric acid for 20 minutes to prepare the samples, followed by a 1 hour incubation in 0.1% Sirius red F3B to stain for collagen. Slides were rinsed thoroughly with water and dehydrated in reverse graded methanols back in to histoclear before mounting in dibutyl phthalate xylene (DPX; Sigma 317616).

2.3.4. Immunocytochemistry

Rehydrated samples were incubated with 3% H_2O_2 for 5 minutes to quench endogenous peroxidase activity and blocked with 1% bovine serum albumin (BSA) in PBS for 30 minutes. Positive slides were drained and incubated with the primary antibody overnight at 4°C (diluted in 1% BSA in PBS). Following incubation, residual antibodies were removed from sections by rinsing in water and incubating the sections in wash buffer (0.1% tween in PBS) for 5 minutes. Biotin-conjugated secondary antibody was diluted in 1% BSA in PBS (1:100) and incubated with sections for 1 to 2 hours at room temperature. Sections were rinsed and incubated for a further 30 minutes in ExtrAvidin peroxidase solution at room temperature (1:50 dilution in 1% BSA in PBS) (Sigma, E2886). Antibody binding was developed using 3-amino-9-ethyl-carbazole (AEC, Sigma A5754) in acetate buffer containing H_2O_2, to yield a reddish-brown reaction product. Slides were counterstained in Light Green or Alcian Blue for 1 minute, rinsed in water and mounted with crystal mount. Negative controls either lacked treatment with the relevant primary antibodies or were incubated with suitable isotype controls. No staining was expected to be observed in negative controls.

2.3.5. Immunofluorescent staining

Samples were prepared for staining following the same protocol as used for immunocytochemistry. After overnight incubation with the primary antibody (Table 2.1), the relevant Alexafluor 594-conjugated secondary antibody (Invitrogen) was diluted in 1% BSA in PBS (1:100) and added to slides for a further 1 to 2 hour incubation at room temperature. Samples were washed and incubated for 5 minutes with DAPI solution diluted in PBS (1:100), washed in running water and mounted in Fluromount (Sigma F4680). Examples of positive and negative controls can be found in Appendix 2.

Samples fixed in PFA required permeabilisation and antigen retrieval when staining for some antibodies, such as those for internal or nuclear markers. Ethanol-fixed samples did not require permeabilisation or antigen retrieval due to the non-crosslinking nature of the fixative. Antigen retrieval was performed prior to blocking by treating rehydrated slides with 0.01M citrate buffer in a microwave for 5 minutes. Permeabilisation was performed by adding 0.1% tween to the normal PBS + 1% BSA blocking buffer and incubating for 30 minutes prior to addition of the primary antibody.

Target	Host	Isotype	Clonality	Dilution	Source	Positive control	Secondary antibody
OCT-4	Mouse	IgG2b	Mono	1:100	Santa Cruz, SC-5279	ES cells	Goat anti-mouse IgG
SOX2	Rabbit	IgG	Poly	1:1000	Millipore, AB5603	ES cells	Goat anti-rabbit IgG
KI-67	Rabbit	IgG	Poly	1:200	Abcam, ab15580	Proliferating culture	Goat anti-rabbit IgG
Type I col.	Rabbit	IgG	Poly	1:1000	Dr Larry Fisher, NIH	Fetal femur	Goat anti-rabbit IgG
Type II col.	Rabbit	IgG	Poly	1:500	Calbiochem, 234187	Fetal femur	Goat anti-rabbit IgG
SOX9	Rabbit	IgG	Poly	1:100	Millipore, AB5535	Fetal femur	Goat anti-rabbit IgG
Osteopontin	Rabbit	IgG	Poly	1:100	Genetex, GTX28448	Fetal femur	Goat anti-rabbit IgG
Osteocalcin	Mouse	IgG2a	Mono	1:100	Genetex, GTX13418	Fetal femur	Goat anti-mouse IgG
PPARγ	Mouse	IgG1	Mono	1:500	Millipore, MAB3872	Marrow fat layer	Goat anti-mouse IgG
FABP4	Rabbit	IgG	Poly	1:200	Abcam, ab13979	Marrow fat layer	Goat anti-rabbit IgG
CD34	Mouse	IgG1	Mono	N/A	Genetex, GTX73657	Fetal umbilical cord	Goat anti-mouse IgG
CD105	Mouse	IgG	Mono	1:100	BD Biosciences, 611314	HUVEC	Goat anti-mouse IgG
CD146	Mouse	IgG1	Mono	1:100	BD Biosciences, 550314	HUVEC	Goat anti-mouse IgG
TIE-2	Rabbit	IgG	Poly	1:100	Santa Cruz, SC-324	HUVEC	Goat anti-rabbit IgG
VWF	Rabbit	IgG	Poly	N/A	Dako, A0082	HUVEC	Goat anti-rabbit IgG
STRO-1	Mouse	IgM	Mono	N/A	In house	HK cells	Goat anti-mouse IgM

Table 2.1. List of antibodies used during immunohistological analysis. Key: Mono; Monoclonal; Poly, Polycolonal; ES cells, Embryonic Stem cells; HUVEC; Human Umbilical Vein Endothelial Cells; HK cells; Human Kidney cells

2.3.6. Alkaline phosphatase staining

Samples were rinsed in PBS, fixed in 90% ethanol for 15 minutes and rinsed again in PBS. Naphthol AS-MX Phosphate (4% v/v) and Fast Violet B salt (0.024% w/v) were mixed in water following a modified Sigma-Aldrich protocol, applied to fixed samples and incubated until the stain turned a red-purple colour. The reaction was terminated by adding distilled water.

2.3.7. Oil red O staining

Samples were rinsed in PBS, fixed in Baker's formal calcium (4% formaldehyde plus calcium chloride), rinsed with 60% isopropanol and incubated in double-filtered Oil Red O solution for 15 minutes. The reaction was terminated by adding distilled water.

2.4. Biochemical analysis

2.4.1. Preparation

Samples were fixed in 90% ethanol, air dried and treated with 0.05% TRITON-X100 to induce cell lysis. Samples were taken through at least 3 freeze/thaw cycles with repeated distruption of the cells via scraping or sonication. Samples were kept at -20°C until used in biochemical assays.

2.4.2. PicoGreen® dsDNA quantification

10μl of lysed cell solution was added to 90μl Tris-EDTA buffer and 100μl of diluted PicoGreen® solution in Tris-EDTA buffer (1:200) per well in a black 96-well cyto-fluor plate. Plates were read using a BioTek FLx-800 96-well plate reader at 480nm excitation and 520nm emission. Results were expressed as ng/ml DNA.

2.4.3. Quantification of alkaline phosphatase activity

10μl cell lysate was added to 90μl 2-amino-2-methyl-1-propanol buffer containing 100mM p-nitrophenolphosphate (pNPP) per well in a clear 96-well plate. The samples were incubated at 37°C and timed until a colour change occurred, at which point the reaction was stopped using 100μl of sodium hydroxide (NaOH). Plates were read on a BioTek ELx-800 colourimetric plate reader at 410nm absorbance. Results were expressed as nmol pNPP/hr, whilst specific alkaline phosphatase activity (derived by comparing the total DNA with alkaline phosphatase expression) was expressed as nmol pNPP/ng DNA/hr.

2.5. Molecular analysis

2.5.1. TRIzol RNA extraction

Cell samples were washed thoroughly with PBS and placed on ice. 1 to 2 TRIzol reagent (Invitrogen, 15596-018) were added and the samples were broken down by cell scraping (Simms et al. 1993). The resulting solution was transferred to a molecular grade eppendorf and either stored at -80°C until needed or used immediately. To isolate the RNA from the extracted samples, 200µl chloroform was added, mixed by vortex and spun at 13000rpm for 15 minutes to separate the organic phenol layer from the inorganic aqueous layer containing the RNA. The aqueous phase was transferred to a fresh eppendorf and precipitated with 600µl isopropanol overnight at -20°C. The samples were centrifuged to provide an RNA pellet, washed with 75% ethanol, air dried and resuspended in ultra pure water at 65°C. Samples could be kept at -80°C until needed or used immediately.

2.5.2. RNA cleanup

RNA samples were purified using the Zymo DNA-free RNA kit. Samples were digested with DNase I for 15 minutes at 37°C, mixed with RNA binding buffer and run through RNA collection columns. The columns were treated with wash buffer to remove any remaining DNA or protein. To recover purified RNA, columns were treated with ultra pure water at 65°C, centrifuged and the eluate collected into fresh eppendorfs.

2.5.3. cDNA synthesis

cDNA was produced using the SuperScript© first-strand synthesis system (Invitrogen, 11904-018). Purified RNA was incubated at 65°C for 5 minutes with free dNTPs and Oligo(dT) primers to begin cDNA synthesis, followed by a 50 minute incubation at 42°C with Reverse Transcriptase II, RNase OUT recombinat RNase Inhibitor, 10x RT buffer, 25mM $MgCl_2$ and 0.1M DTT to produce full cDNA strands. The reaction was terminated by a 15 minute incubation at 70°C. cDNA samples could be stored at -20°C until needed for PCR.

2.5.4. Quantitative RT-PCR

Real-time PCR was performed using SYBR Green PCR master mix (Applied Biosystems). 96-well PCR plates were loaded with master mix, forward and reverse

primers for specific genes (Table 2.2) and cDNA and loaded in to an Applied Biosystems real-time PCR system and run with a dissociation stage. Data was analysed using the delta – delta Ct (crossover threshold) method. Ct values for genes of interest were compared with those for housekeeping genes (*GAPDH*) to provide relative expression.

Gene	Primer sequences	Amplicon size
Human *RUNX2* (NM_001024630, NM_001015051)	F: 5' gta gat gga cct cgg gaa cc 3' R: 5' gag gcg gtc aga gaa caa ac 3'	78 bp
Human *ALP* (NM_000478)	F: 5' gga act cct gac cct tga cc 3' R: 5' tcc tgt tca gct cgt act gc 3'	86 bp
Human *COL1A1* (NM_ 000088)	F: 5' gag tgc tgt ccc gtc tgc 3' R: 5' ttt ctt ggt cgg tgg gtg 3'	52 bp
Human Osteocalcin (NM_199173)	F: 5' ggc agc gag gta gtg aag ag 3' R: 5' ctc aca cac ctc cct cct g 3'	102 bp
Human *SOX9* (NM_000346)	F: 5' ccc ttc aac ctc cca cac ta 3' R: 5' tgg tgg tcg tgt agt cg ta 3'	74 bp
Human *COL2A1* (NM_001844, NM_033150)	F: 5' cct ggt ccc cct ggt ctt gg 3' R: 5' cat caa atc ctc cag cca tc 3'	58 bp

Table 2.2. List of primers used for RT-PCR.

2.5.5. RNA amplification and the RT^2 Prolifer™ PCR array system

For analysis of gene expression in small samples, RNA was amplified and qPCR performed using the RT^2 PCR array system. RNA extraction and clean up was performed using the Arcturus® PicoPure® isolation kit (Applied Biosystems, KIT0204). RNA was amplified for 2 rounds according to the manufacturer's instructions, using the Arcturus® RiboAmp® HS PLUS kit (Applied Biosystems, KIT0525) that amplifies total RNA up to 1,000,000-fold. cDNA first strand synthesis was performed using the RT^2 first strand kit (SABiosciences, C-03). Synthesised cDNA was combined with ready-to-use RT^2 SYBR Green/ROX qPCR Master Mix (SABiosciences, PA-012) and aliquoted onto the pre-dispensed plate containing the relevant RT^2 PCR array primer set (Mesenchymal stem cell PCR array, SABiosciences, PAHS-082).

2.6. Microfluidics

2.6.1. Cell tracking for microfluidics

To aid in identification of cells during microfluidic isolation and separation of cell types, Vybrant™ labelling solutions (carbocyanine) were used that fluoresced under green and red wavelengths. Vybrant DiD (red) was used to stain negative cell populations and DiO (green) was used to stain positive populations (Table 2.3). Vybrant labelling solution was added to dissociated cells suspended in PBS pre-warmed to 37°C (1:200 dilution) and incubated at 37°C for 7 minutes. Cell were washed twice with PBS to remove any excess dye and resuspended in the relevant buffer for microfluidic manipulation. Greater than 90% of cells expressed fluorescence in all stains and cells were found to retain cell viability and demonstrate proliferation at normal rates, as well as maintaining fluorescence for at least 3 days (Figure 2.3).

Tracer	Catalog #	Abs (nm)	Em (nm)
DiO (green)	V-22886	484	501
DiD (red)	V-22887	644	665

Table 2.3. The different Vybrant cell tracers and their absorbance/emission spectra.
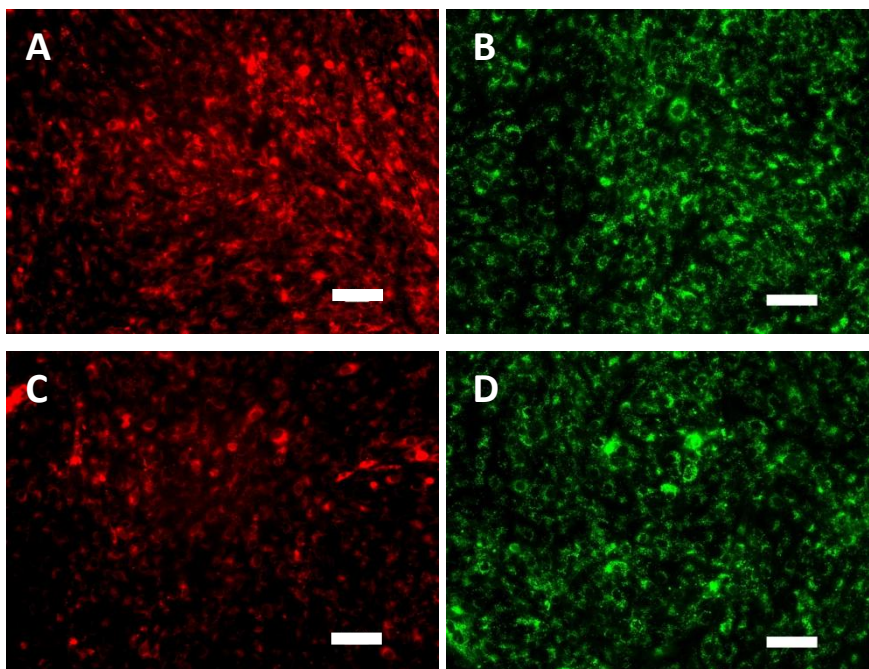
Figure 2.3. Captured images of fluorescently stained MG-63 cells. Vybrant DiD red 3 days after staining (A) and after passage (C). Vybrant DiO green after staining (B) and after passage (D). Scale bars: 100μm.

60

2.7. Image capture and analysis

Sample images were captured using a Zeiss Axiovert 200 inverted microscope and Zeiss Axiovision software version 4.7. Light microscopy images were captured using an Axiocam HR camera, whilst fluorescent images were captured using an Axiocam MR.

2.8. Statistics

Statistical analysis was carried out using the Student's t-test or One-way Analysis of Variance (ANOVA) with Tukey-Kramer multiple comparisons post-test using the statistics software integrated into GraphPad Prism and InStat software. Values were expressed as mean ± standard deviation. All experiments were performed using at least 3 separate populations unless otherwise stated. Results for each population were performed in triplicate unless otherwise stated. Values for $p \leq 0.05$ were considered significant.

CHAPTER 3

CHARACTERISATION OF A NOVEL COBBLESTONE

PHENOTYPE OBSERVED IN FETAL FEMUR-DERIVED

CELL POPULATIONS CULTURED IN CHEMICALLY

DEFINED MEDIA

3.1. Introduction

Tissue engineering requires the coordinated application of a number of important factors including a suitable population of cells, an extracellular matrix or scaffold to provide structure and support for the cells and to define the shape of the new tissue and specific tissue-inducing growth factors to induce the correct phenotype from the cells (Langer & Vacanti 1993). It is essential that the cells selected for use in tissue regeneration are capable of producing the correct tissues when inserted into a patient and it is critical to identify and isolate skeletal stem cell and progenitor cell populations for bone and cartilage restoration. One potential source of skeletal cells to have undergone recent study are fetal-femur derived cells.

Fetal femur-derived cells (FFDCs) are typically isolated from femurs 7 to 12 weeks post-conception. Younger femurs are characterised by a primitive chondrogenic phenotype, with older femurs expressing the first stages of endochondral ossification and vascularisation. To date, very few studies have been carried out to determine the multipotential and self-renewal properties of FFDCs. However, it has been shown that fetal cells can be differentiated along both osteogenic and chondrogenic lineages by the addition specific growth factors (Mirmalek-Sani et al. 2006), establishing the multipotency of the cells. It has been hypothesised that FFDCs may express similar levels of multipotency as the MSCs and may provide a new alternative cell line for tissue regeneration (Montjovent et al. 2004). A recent study by Zhang and colleagues, demonstrated that FFDCs have a greater osteogenic potential than adult MSCs and express many markers in common with adult-derived MSCs, including STRO-1, CD73, CD105, CD44, CD90 and CD106, but were also found to express the ES cell markers Nanog and OCT-4. Furthermore, approximately 50% of fetal MSCs were found to express STRO-1 in any given population, while only 10% of cells expressed STRO-1 in adult MSC populations (Zhang et al. 2009).

Tissue culture typically utilises fetal calf serum (FCS) to provide nutrients and growth factors that benefit growth and expansion. The complete composition of FCS is unknown and different batches may contain considerably different factors and nutrients, preventing determination of any specific effect of the FCS on cell processes (Ulloa-Montoya et al. 2005). Use of chemically defined media (CDM) removes any variability

introduced by FCS, allowing improved modelling of cellular growth and differentiation on exposure to specific stimulatory factors. One particular serum-free CDM developed by Johansson and Wiles (Johansson & Wiles 1995) was able to maintain human embryonic stem cells in a undifferentiated, proliferative state when supplemented with Activin A and FGF2 (Vallier et al. 2005).

Previous work by Mirmalek-Sani et al, demonstrated that culture of fetal femur cells in Activin A/FGF2 supplemented CDM resulted in the establishment of undifferentiated, proliferative populations that demonstrated downregulation of differentiation-inducing genes (Mirmalek-Sani et al. 2009). Unusually, addition of bone morphogenetic protein-2 (BMP-2) to CDM-treated cultures resulted in the development of a novel cobblestone-like phenotype. Cells expressing a cobblestone morphology have previously been observed in many different tissues, including epithelial (Davis et al. 1995;Kaushik et al. 2008), endothelial (Deschaseaux et al. 2007;Kirton & Xu 2010) and haematopoietic tissues (de Haan & Ploemacher 2001), but not in mesenchymal tissues.

Activins are members of the TGF-β superfamily and have a wide variety of roles in cell maintenance and differentiation. Activin-A is required to maintain pluripotency and self-renewal by inducing the expression of both Nodal and FGF-2 (Xiao et al. 2006). Self-renewal of stem cells is dependent on activation of the Activin/Nodal/Smad2,3 pathway along with suppression of the BMP/GDF/Smad5 pathway involved in cell differentiation (Vallier et al. 2009). FGF-2 is a member of the FGF family, involved in cell division and proliferation. It has been demonstrated that FGF-2 is necessary for self-renewal and maintenance of pluripotency in stem cells by acting as a competence factor for the Nodal pathway (Vallier et al. 2005).

This study set out to further characterize the fetal femur-cell phenotype, with specific regard to that of the novel cobblestone cells resulting from treatment with CDM and BMP-2. Heterogeneous CDM-treated populations were subjected to histological and microarray analysis, while use of laser-dissection techniques enabled isolation of pure populations of cobblestone cells for further microarray analysis.

66

3.2. Methods

Where not detailed below, methods for FFDC culture and differentiation can be found in Chapter 2 (Sections 2.2.3, 2.2.5 and 2.2.6). Techniques used for histological analysis of monolayer culture and fetal femurs included Alcian blue/Sirius red staining, Alkaline phosphatase staining, Oil Red O staining, immunohistochemistry and immunofluorescent staining (see Section 2.3). Biochemical analysis was also performed to determine the specific activity of Alkaline phosphatase (see Section 2.4). Analysis of FFDC monolayer culture was performed by quantitative RT-PCR (see Section 2.5)

3.2.1. Formation of cobblestone cells

Freshly isolated fetal cell cultures (passage 0) were established in basal medium for 24-48 hours, washed with PBS and media changed to chemically defined media (CDM) containing 10ng/ml Activin A and 12ng/ml FGF-2 to retain cells in an undifferentiated state (Vallier et al. 2005). CDM was composed of 50% IMDM (Invitrogen, 21980-032), 50% F-12 nutrient mixture (Invitrogen, 31765-027), supplemented with 5mg/ml BSA, Lipid 100X at 1% concentration (Invitrogen, 11905-031), 450μM monothioglycerol (Sigma, M6145), 7μg/ml insulin (Roche, 1376497) and 15μg/ml transferrin (Roche, 652202) (Johansson & Wiles 1995). Media changes were carried out every other day for a total of 3 times then the media was substituted for CDM plus 150ng/ml BMP-2 for at least another 3 media changes. At this stage, large numbers of cells expressing cobblestone morphology were usually present in the culture.

3.2.2. Laser dissection microscopy (LDM)

Cells were cultured and differentiated on membrane slides or Lumox™ dishes for laser dissection (Carl Zeiss Ltd.) (Figure 3.1). Membrane slides used for culture of cells for laser dissection were non-tissue culture treated and provided non-sterile, requiring sterilisation before use. Use of ethanol or other fluid sterilisation techniques affected the membrane coating of the slides, therefore gamma irradiation was used to sterilise the slides without damaging the membrane. Lumox™ dishes and inserts were tissue culture treated and specifically designed with an ultra-thin (25μm), gas-permeable bases that allowed laser dissection. Laser dissection of samples was carried out using a PALM CombiSystem (Carl Zeiss Ltd.) (Figure 3.2). Isolation of samples was performed via positive selection (for membrane slides) or negative selection (Lumox™ dishes).

3.2.2.1. Positive selection

This cell capture method was classed as positive selection as isolation of cells was performed by laser cutting around the desired cells and using the laser to "lift" the samples into the lid of an Eppendorf tube. Cells could then be transferred to a new culture dish or used directly for analysis. Isolation of cells by this method was beneficial as it offered minimal risk of contamination of the isolated cells.

3.2.2.2. Negative selection

This method was only available for cells cultured on a tissue culture treated membrane insert placed in a lumox™-based dish. Laser dissection was used to cut the insert membrane around desired cells, but not to lift them from the dish. The insert was then removed, leaving only the selected cells present on the dish.
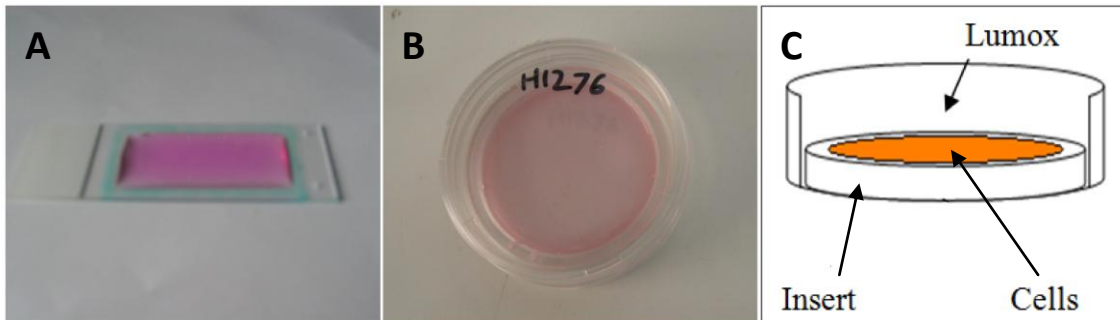
Figure 3.1. Images of different culture surfaces for laser dissection microscope. Membrane-coated slides during culture are demonstrated in (A). The Lumox™ culture dishes are shown in culture in (B) and in schematic form in (C).
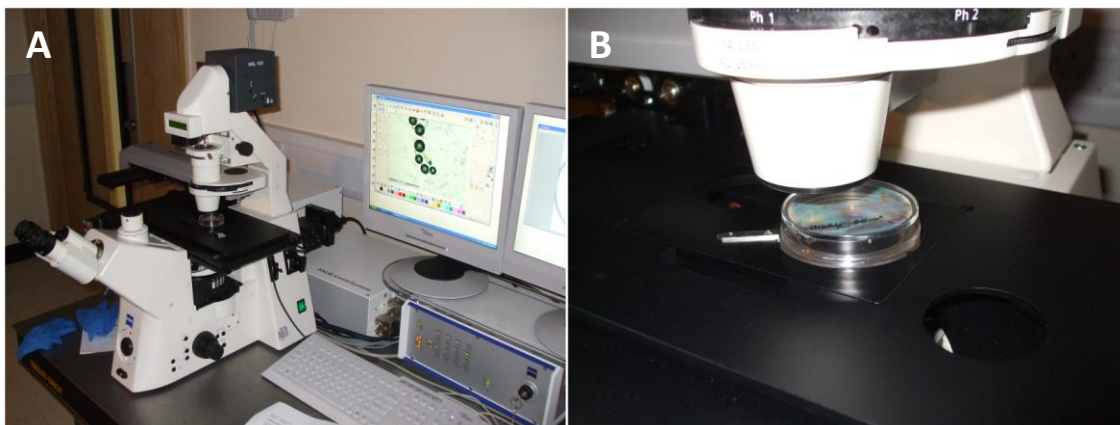
Figure 3.2. PALM CombiSystem setup (A) and a Lumox™ dish in place, ready for laser dissection (B).

3.2.3. Molecular analysis of cobblestone cells

Characterisation of cobblestone populations was performed using the RT² Profiler™ PCR Array for mesenchymal stem cell markers. Populations of cells were grown in αMEM + FCS, CDM + Activin A/FGF2 and CDM + BMP-2 until approximately 90% confluence. Only populations expressing strong cobblestone phenotypes after CDM + BMP-2 treatment were chosen for analysis. To determine the effects of the different media conditions on the cells, molecular results were compared between the different conditions to allow observation of gene up-regulation and down-regulation. Results for different conditions were compared by calculating the fold change between normalised gene expression in the control and test samples. These values were then converted to fold-regulation to present the fold-change results in a biologically meaningful way. Only genes with values greater than two fold up-regulation or down-regulation were considered relevant. Some genes with relatively high (> 30) average threshold cycles in both control and test samples were excluded as their relative expression level was low, while all genes with an average threshold cycle greater than the 35 in both samples were viewed difficult to interpret as the relative expression level was negligible.

3.2.3.1. Analysis of LDM-isolated cobblestone cells

Due to the low numbers of recovered cells, extracted RNA was subjected to two rounds of RNA amplification using the RiboAmp kit from Molecular devices. Amplification of the RNA provided sufficient quantities to allow analysis using the RT² Profiler™ PCR Array for mesenchymal stem cell markers from SABiosciences. The amplification process is known to cause reduction in RNA sequence length, which can lead to bias towards certain nucleic acid sequences (Croner et al. 2009), therefore microarray results from isolated cobblestone populations could not be directly compared to those of the non-isolated populations. Instead, the trends in gene expression were analysed. Only genes with a Ct less than 25 are shown. Genes were normalised against *GAPDH* (set as 1) to show relative expression levels. Despite the known risk of bias in amplified samples, amplification is a random process, therefore the use of multiple samples to provide n ≥ 3, reduced the risk of interpreting false signals. Due to this, only those genes demonstrating similar results in all separate populations were considered relevant.

3.3. Results

3.3.1. Histological analysis of human fetal femurs

Fetal femurs at 7-12 weeks post conception (Figure 3.3 A) were comprised of a cartilaginous anlage with an emergent bone collar that increased in size with age of the femur. Both the epiphysis and diaphysis of the fetal femurs expressed a strong chondrogenic phenotype evidenced by the presence of nucleated cells embedded within lacunae of a proteoglycan-rich matrix. However, in comparison to the diaphysis (Figure 3.3 B), the epiphysis consisted of a more densely populated region of nucleated cells with less defined lacunae (Figure 3.3 C). Determination of SOX9 expression established that the nucleated cells were indeed chondrocytes (Figure 3.3 H). Sirius red staining highlighted collagen-deposition in the emergent bone collar and along the edges of the diaphysis (Figure 3.3 B) and in modest quantities in the epiphysis of femurs from more developed samples. The presence of alkaline phosphatase (ALP) (Figure 3.3 D) Type I collagen (Figure 3.3 E), Type II collagen (Figure 3.3 F), Osteopontin (Figure 3.3 G) and low levels of Osteocalcin (Figure 3.3 I) at the sites of collagen deposition confirmed the presence of chondrocyte hypertrophy and the emergent bone collar. Analysis of the fetal femur by immunofluorescence was limited due to autofluorescence of the fetal femur. When explanted, FFDCs expressed a fibroblast-like morphology (Figure 3.3 J).
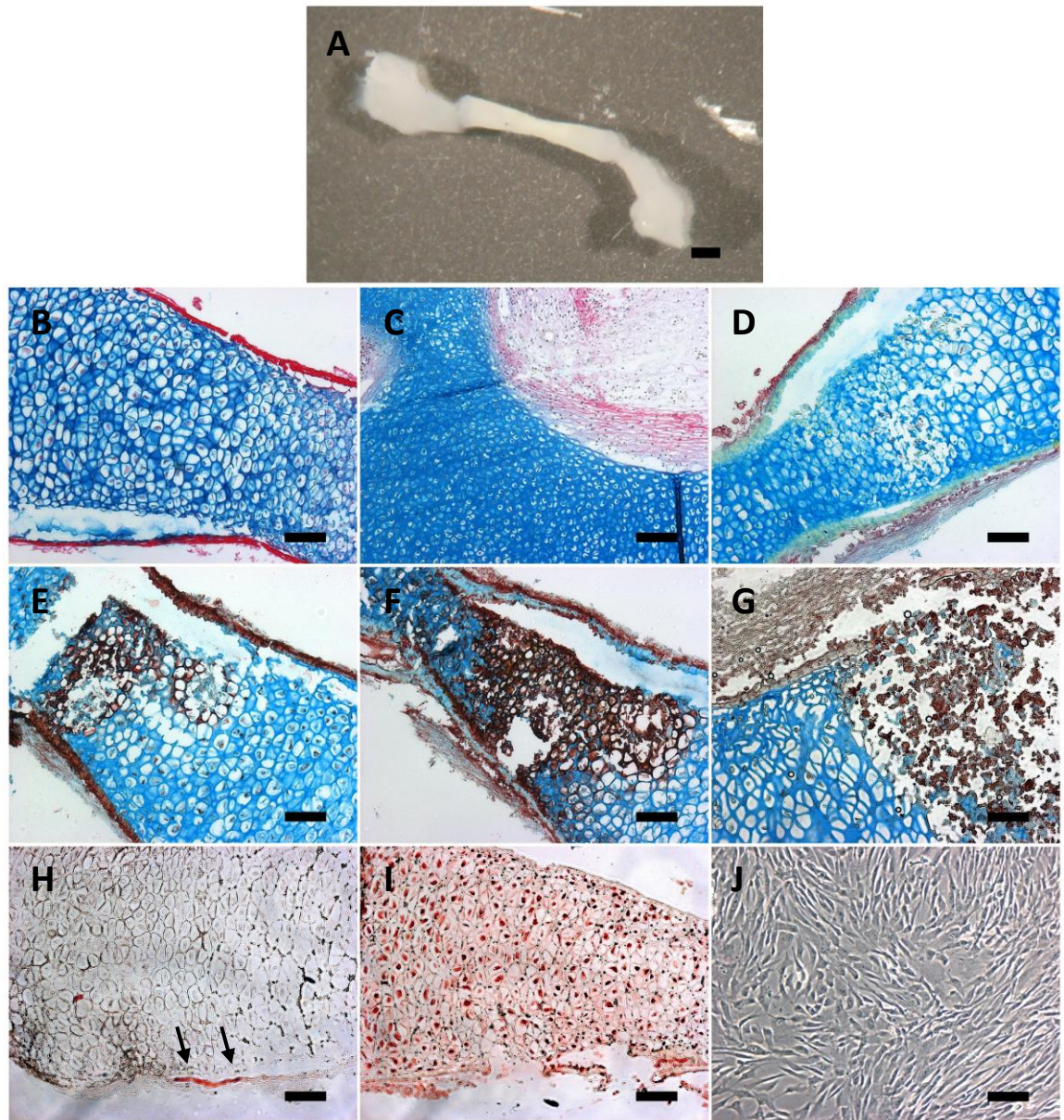
Figure 3.3. Analysis of fetal femur by histology. (A) fetal femur before dissection, (B) Alcian blue (proteoglycan) and Sirius red (collagen) staining of diaphysis, (C) Alcian blue and Sirius red staining of epiphysis, (D) ALP staining, (E) Type I collagen staining, (F) Type II collagen staining, (G) Osteopontin staining, (H) Osteocalcin staining (highlighted by arrows), (I) SOX9 staining, (J) explanted fetal cells in culture. Scale bar for (A) is 1mm, scale bars for (B-J) are 100μM.

3.3.2. Characterisation of fetal femur-derived cells

When grown in monolayer culture in basal conditions, collagenase-extracted FFDCs expressed large amounts of extracellular matrix rich in both Type I and Type II collagen fibres (Figure 3.4 A,D). The majority of explanted FFDCs demonstrated some level of SOX9 expression, with approximately half the population demonstrating strong expression (Figure 3.4 G), confirming that the chondrogenic phenotype was maintained in culture, while low levels of alkaline phosphatase suggested some early osteogenic activity (Figures 3.5 A,E & 3.6). Negligible Osteocalcin was observed in basal conditions.

3.3.2.1. Osteogenic differentiation of FFDCs

Addition of the osteogenic-inducing factors dexamethasone and ascorbate-2-phosphate resulted in increased expression of Type I collagen (Figure 3.4 B), while Type II collagen expression was equivalent to that observed in basal cultures (Figure 3.4 E). SOX9 expression demonstrated little difference to that observed in basal culture (Figure 3.4 H) and samples treated with osteogenic media demonstrated significantly higher (p < 0.001) ALP activity in samples treated with osteogenic media than in basal (Figure 3.5 B,F & 3.6), suggesting differentiation of cells towards the osteogenic lineage. Osteogenic cultures further treated with the TGF-β superfamily growth factor, BMP-2 were found to express lower levels of ALP than those without BMP-2 (Figure 3.5 C,G & 3.6). Negligible Osteocalcin was observed in osteogenically treated cultures, confirming that no late stage osteogenic differentiation had yet occurred. RT-PCR analysis demonstrated that *ALP* expression was enhanced in samples treated with osteogenic media, with basal samples expressing almost 10 fold less *ALP* mRNA than osteogenic cultures (Figure 3.7 A). Two other osteogenic markers; Osteocalcin and *RUNX2* were also demonstrated to be expressed at significantly higher levels in osteogenic cultures than in basal (Figure 3.7 B, D), although the differences were not as substantial as those seen in *ALP*, with osteogenic cultures only expressing approximately 3 fold more *RUNX2* than basal. The difference between basal and osteogenic cultures was least significant for Osteocalcin. Type I collagen expression in osteogenic culture was found to be approximately double that of basal cultures (Figure 3.7 C). Unusually, RT-PCR for *SOX9* revealed expression of the gene to be highest in osteogenic cultures rather than chondrogenic, with levels of *SOX9* approximately 2

times greater in osteogenic conditions than in basal (Figure 3.7 E). Upregulation of *ALP, RUNX2* and Osteocalcin RNA expression, combined with the expression of osteogenic markers suggested differentiation of the cells towards an early osteogenic phenotype. The higher levels of *SOX9* RNA expression indicates increased profileration of chondrocytes, while increased *RUNX2* expression in FFDCs treated with osteogenic media was suggestive of an upregulation of hypertrophy of the chondrocyte progenitor population, further indicating a shift towards the osteogenic lineage.

3.3.2.2. Chondrogenic differentiation of FFDCs

Cultures treated with chondrogenic media maintained modest Type I collagen expression similar to that of basal and osteogenic conditions (Figure 3.4 C), but were found to express higher levels of chondrogenic marker, Type II collagen (Figure 3.4 F). SOX9 staining demonstrated equivocal expression to that observed in basally grown FFDCs (Figure 3.4 I). Samples treated with chondrogenic media displayed negligible ALP expression and produced biochemical values for ALP below the baseline (Figure 3.5 D,H & 3.6), demonstrating the lack of osteogenic differentiation in these cultures. Negligible Osteocalcin expression was observed in chondrogenic cultures. RT-PCR analysis of FFDCs in chondrogenic culture demonstrated significantly reduced *ALP* expression in comparison to basal culture (Figure 3.7 A), while Osteocalcin and *RUNX2* exhibited minimal difference in expression when compared to basal cultures, suggesting that neither culture condition induced osteogenic differentiation (Figure 3.7 B, D). Type I collagen expression in chondrogenic culture was found to be equivalent to that seen in osteogenic culture, with both expressing approximately double that of basal cultures (Figure 3.7 C). Chondrogenic cultures expressed significantly less *SOX9* RNA than basal culture (Figure 3.7 E). The negligible expression of osteogenic markers such as *ALP, RUNX2* and Osteocalcin, combined with the small increase in Type II collagen expression suggested a chondrogenic potential for FFDCs treated with chondrogenic media. However, it was clear that the culture of cells in monolayer culture was not suitable for inducing a chondrogenic phenotype as negligible changes were seen in SOX9 staining and *SOX9* RNA expression was downregulated.

3.3.2.3. Adipogenic differentiation of FFDCs

When treated with adipogenic media, fetal femur-derived cell populations displayed clear adipogenic differentiation after only 12 days. Cells were found to display the characteristic lipid-globule phenotype of adipocytes, evidenced by oil red O staining (Figure 3.8 A,B), as well as expressing the adipogenic markers, PPARγ (Figure 3.8 C) and FABP-4 (Figure 3.8 D).
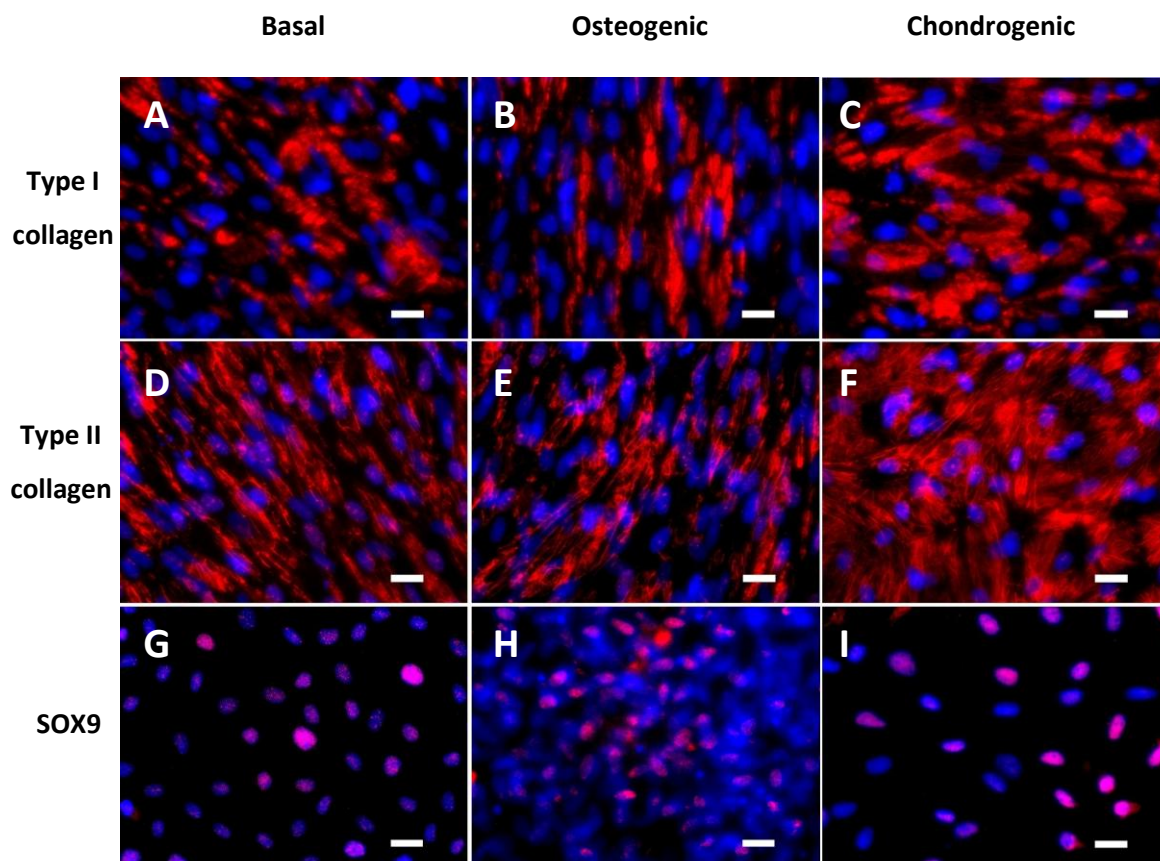
Figure 3.4. Histological analysis of FFDCs after 7 days in basal (left column), osteogenic (middle column) or chondrogenic media (right column). Type I collagen (A-C) Type II collagen (D-F), SOX9 (G-I). Scale bars are 20μm.
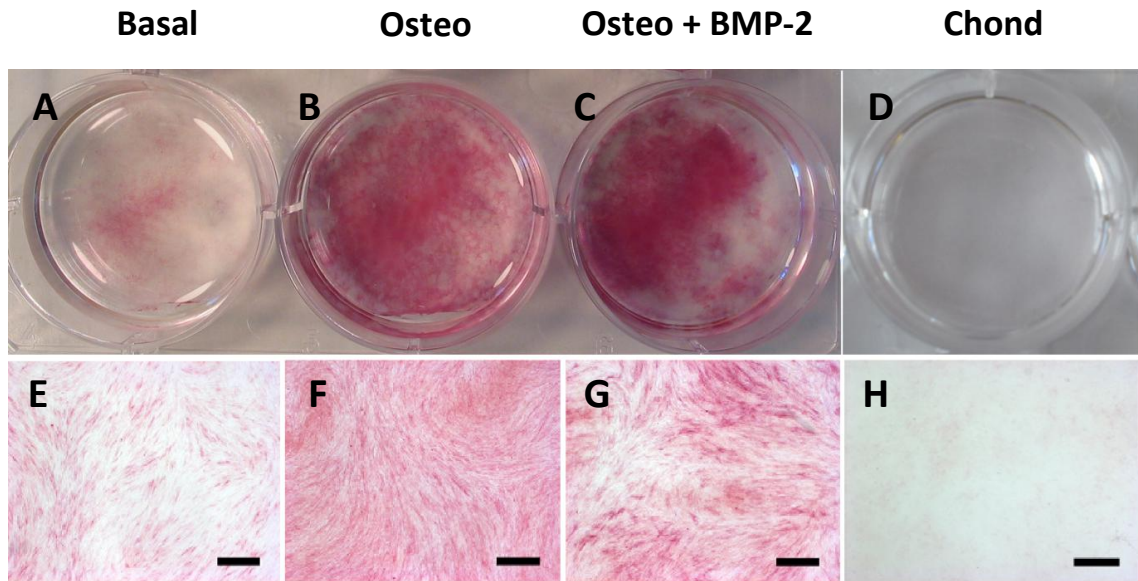
Figure 3.5. Alkaline phosphatase staining of fetal cells after 7 days in culture in basal (A,E), osteogenic (B,F), osteogenic plus BMP-2 (C,G) and chondrogenic media (D,H). Scale bars for E-H are 500µm.
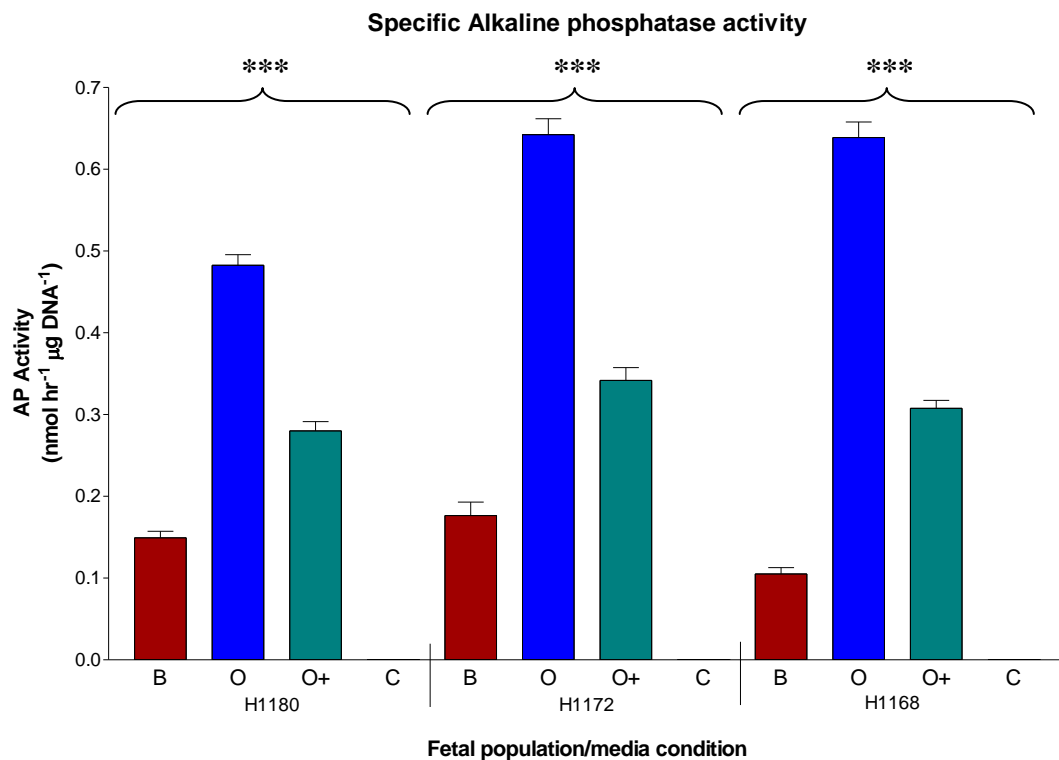
Figure 3.6. Biochemical analysis of alkaline phosphatase expression in fetal culture at day 7. Key: B, Basal; O, Osteogenic; O+, Osteogenic + BMP-2; C, Chondrogenic. Values are expressed as mean ± SD, n=6. *** p < 0.001.
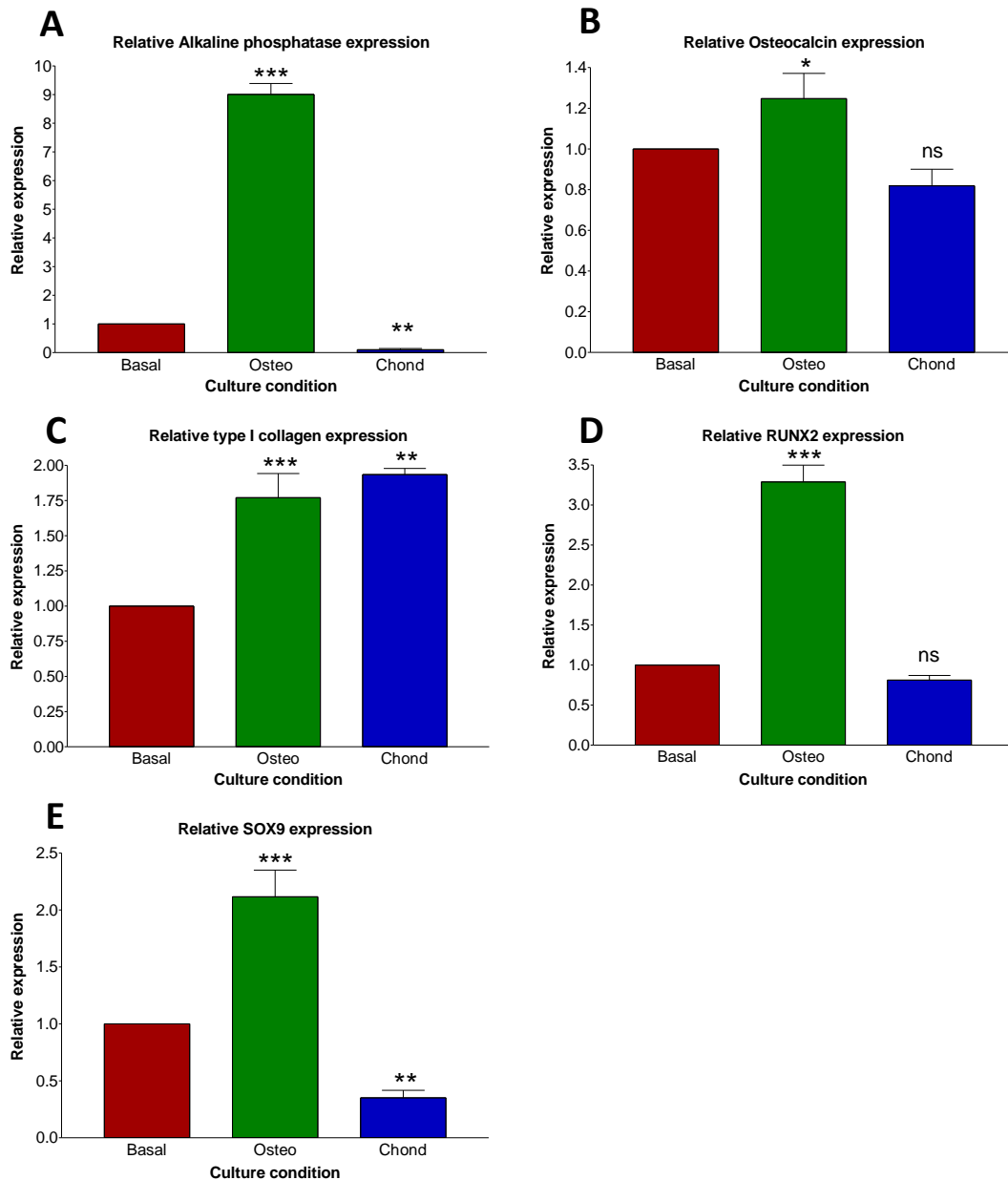
Figure 3.7. Molecular analysis of fetal femur cells when treated with basal, osteogenic or chondrogenic media for 7 days. Relative expression is shown for the osteogenic markers alkaline phosphatase (A), Osteocalcin (B), Type I collagen (C), the late chondrogenic/early osteogenic marker *RUNX2* (D) and the chondrogenic markers *SOX9* (E). Values are expressed as mean ± SD, n=3. Statistical significance of increase/decrease compared to basal conditions shown as: ns = non significant,* = p<0.05, ** = p<0.01, *** = p < 0.001.
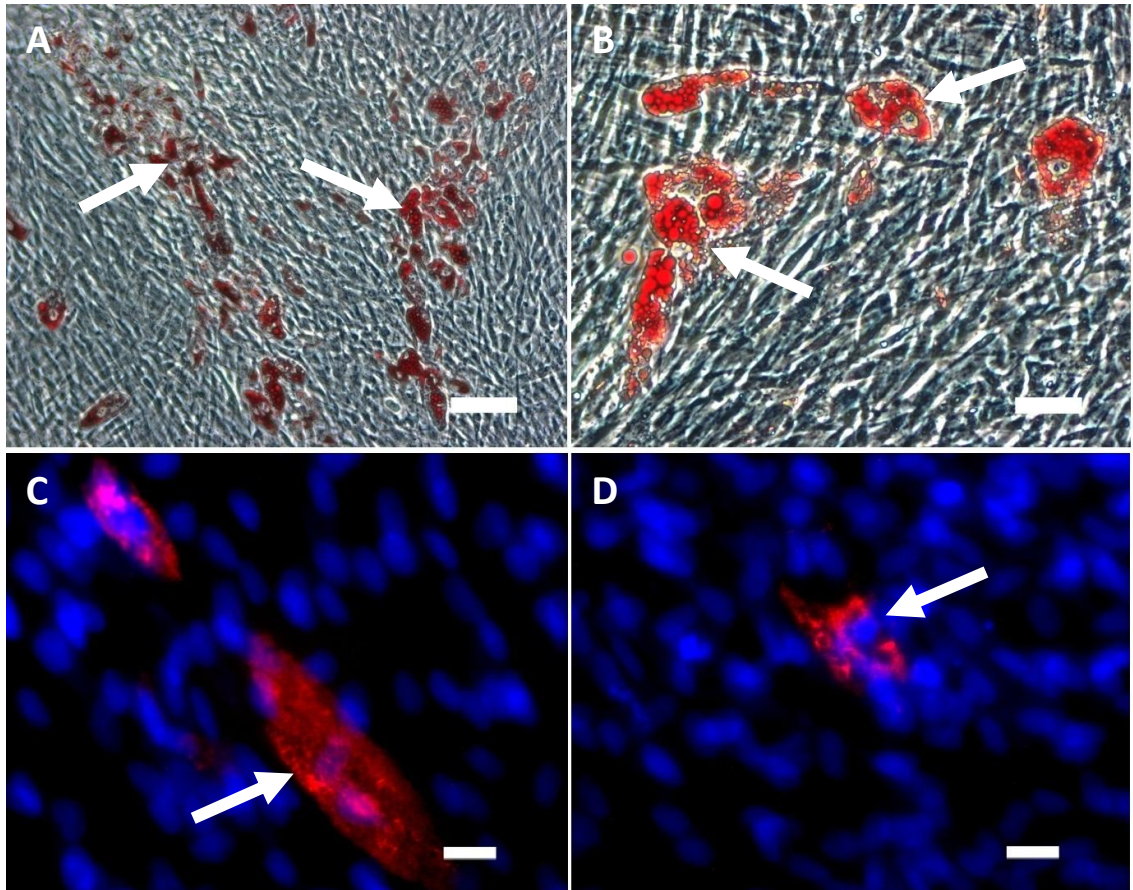
Figure 3.8. Histological analysis of adipogenic treated fetal femur cultures for Oil red O staining (A, B), PPARγ (C) and FABP4 (D). Figures C and D are stained with the nuclear dye, DAPI (blue), and the fluorescent antibody-bound Alexafluor 594 (red). The large numbers of nuclei highlighted by DAPI are due to the high level of confluence of adipogenic cultures. The arrows highlight adipocytes. Scale bars are 100µm (A); 50µm (B) and 20µm (C & D).

3.3.3. Induction of the cobblestone phenotype

Culture of FFDCs in CDM containing Activin A and FGF-2 resulted in cells able to maintain a fibroblastic, undifferentiated, proliferative state (Figure 3.9 B). After 6 days in CDM plus Activin A and FGF-2, the media was substituted for CDM plus 150ng/ml BMP-2 in an attempt to induce osteogenic differentiation. Upon addition of BMP-2, fetal cells began expressing a cobblestone-like morphology characterised by cells becoming rounded and expressing what appeared to be lipid globules (Figure 3.9 C). The cobblestone phenotype was found to be more pronounced in confluent patches of cell growth. After 6 days in CDM plus BMP-2, approximately 60-70% of the population of fetal femur cells expressed the cobblestone phenotype, with the remaining cells maintaining a fibroblastic phenotype. Cobblestone cells were only observed in large numbers in non-passaged samples (p0); with passaged, trypsinised samples showing negligible cobblestone differentiation (Figure 3.9 D). It was also noted that small numbers of cells expressed a cobblestone-like phenotype at passage 0 in some, but not all, populations of FFDCs before the addition of CDM (Figure 3.9 E). Expression of the cobblestone-like cells was maintained alongside the proliferative, fibroblastic cells after addition of CDM + Activin A/FGF2 (Figure 3.9 F). Upon addition of BMP-2 to the populations, the majority of cells, both fibroblastic and cobblestone-like were observed to differentiate into cobblestone cells. Long-term culture of cells in αMEM + FCS (Figure 3.10 A) or in αMEM + FCS + BMP-2 (Figure 3.10 B) resulted in an exclusively fibroblastic cell population and loss of cobblestone-like cells and addition of CDM + BMP-2 directly to populations treated long-term with only αMEM + FCS%, resulted in negligible formation of the established cobblestone phenotype. Populations treated short-term with αMEM + FCS% but not CDM + Activin A/FGF2 maintained the pre-cobblestone phenotype and established populations of cobblestone cells when treated with CDM + BMP-2, albeit in less numbers than in those cultures pre-treated with CDM + Activin A/FGF2 (Figure 3.10 C). Furthermore, cobblestone cells induced in non pre-treated populations were centred around areas containing the pre-cobblestone cells found in non CDM + BMP-2 treated samples (Figure 3.9 E,F). Cultures of FFDCs treated with vascular endothelial growth factor (VEGF), together with CDM + BMP-2, demonstrated expression of cobblestone cells similar to populations treated with CDM + BMP-2 only (Figure 3.10 D).

78
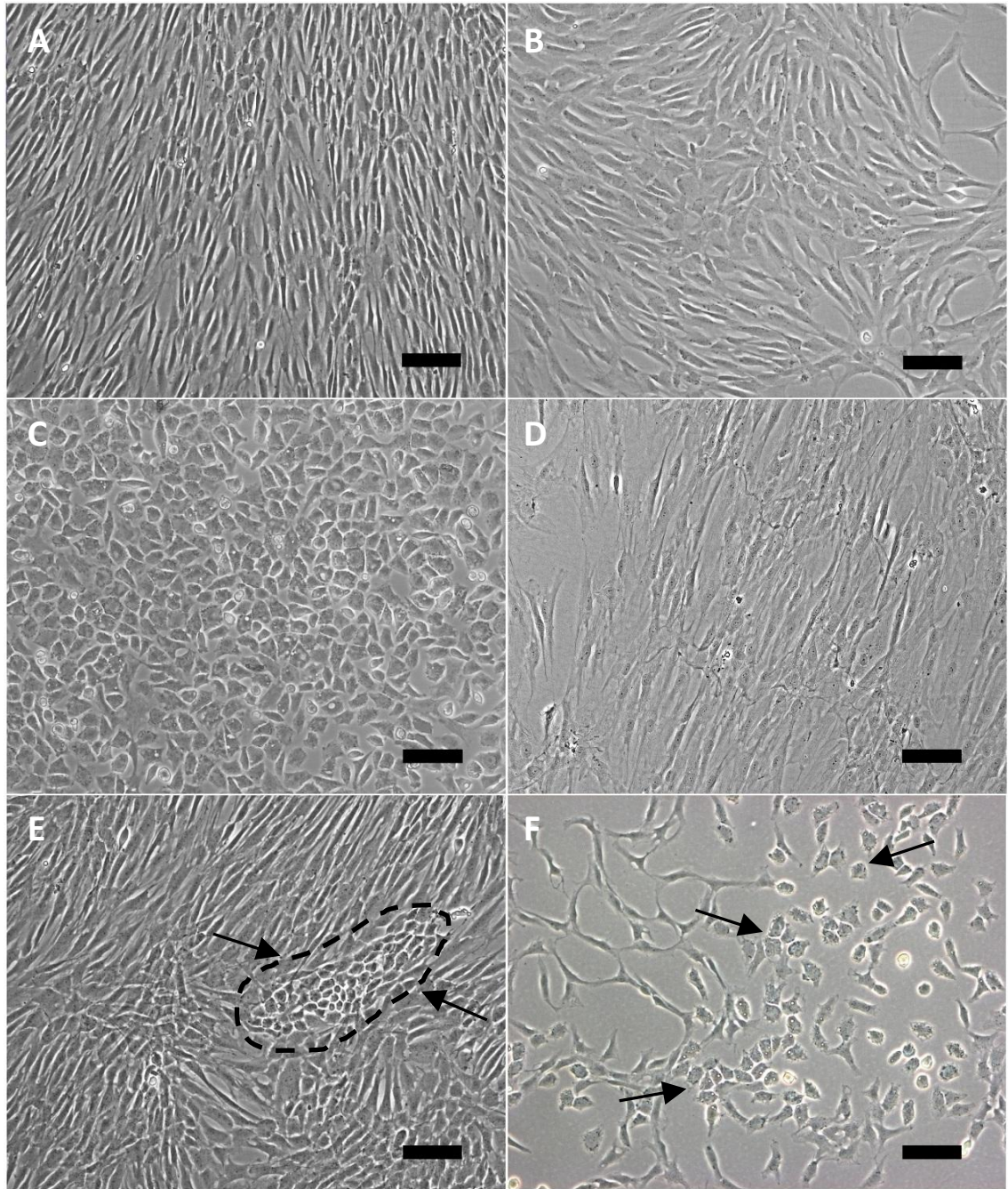
Figure 3.9. Images of fetal femur cells grown in αMEM + 10% FCS (A), CDM + Activin A/FGF2 (B) and CDM + BMP-2 (C) at passage 0. Passage 0 cells expressing a clear cobblestone phenotype can be seen in samples treated with CDM + BMP-2 but not in those at passage 1 or greater (D). In some populations of fetal cells, small numbers of cells expressing a cobblestone-like phenotype were observed in both αMEM + 10% FCS (E) and CDM + Activin A/FGF2 (F) treated populations, demonstrating the presence of the cobblestone phenotype or it's precursor in the heterogeneous fetal femur cell population (highlighted by arrows). Scale bars are 100μm.
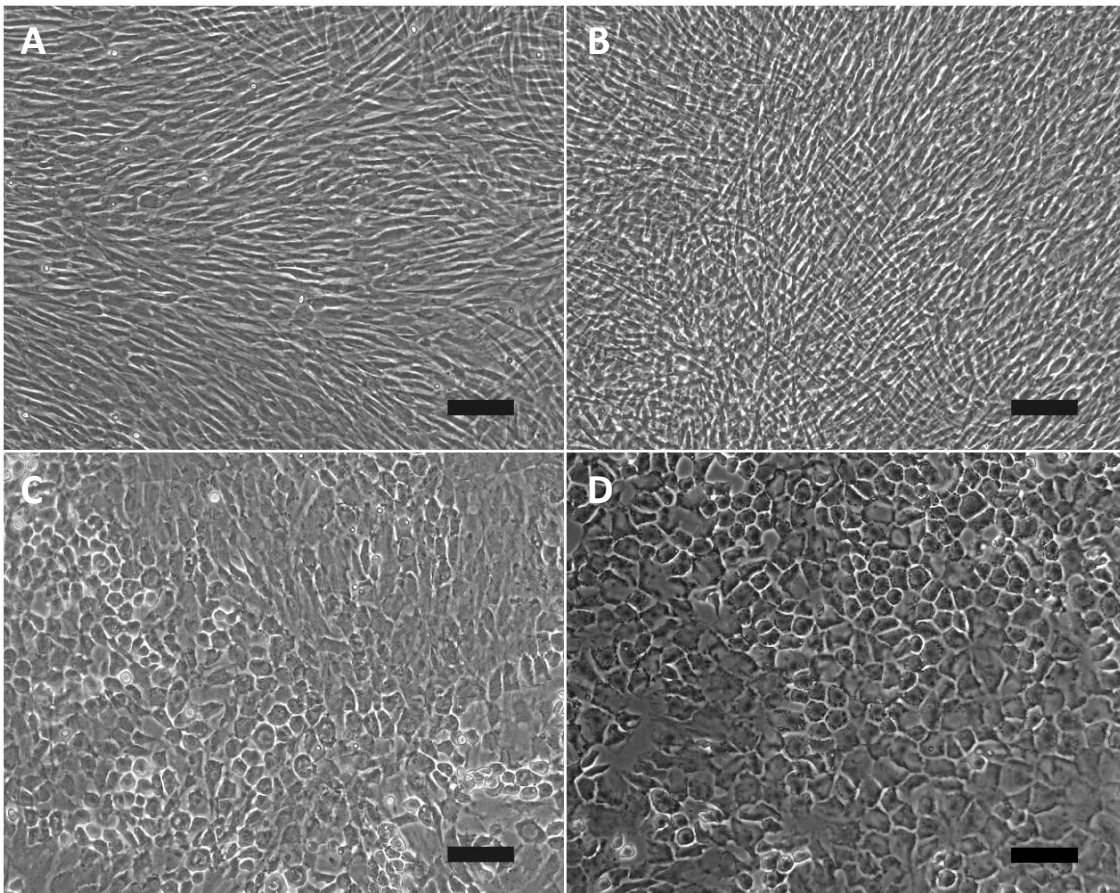
Figure 3.10. Fetal cell populations treated with αMEM + 10% FCS (A), αMEM + 10% FCS + BMP-2 (B), CDM + BMP-2 with no CDM + Activin A/FGF2 pre-treat (C) and CDM + BMP-2 + VEGF (D). Addition of BMP-2 to fetal cells without CDM media failed to produce the cobblestone phenotype. However, addition of CDM + BMP-2 media to a population of fetal femur cells not pre-treated with CDM + Activin A/FGF2 induced cobblestone formation, albeit in less numbers than in those pre-treated with CDM + Activin A/FGF2. Scale bars are 100μm.

3.3.4. Histological characterisation of heterogeneous cobblestone cell populations

To determine the phenotype of the cobblestone cells, populations of cells were treated with αMEM + FCS, CDM + Activin A/FGF2 and CDM + BMP-2 and stained for a variety of mesenchymal and endothelial cell markers, a summary of which can be found in Table 3.1. The skeletal stem cell marker STRO-1 was expressed in varying levels in αMEM treated cells, from approximately 10-30%, highlighting the expected heterogeneity of the population for this marker (Figure 3.11 A). In cells treated with CDM + Activin A/FGF2 the majority of fibroblastic cells (approximately 80-90%) strongly expressed STRO-1 (Figure 3.11 B). In CDM + BMP-2 cultures, the majority of fibroblastic cells continued to strongly express STRO-1, whilst cobblestone cells expressed STRO-1 across the cell membrane albeit at a lower intensity than observed in fibroblastic cells (Figure 3.11 C). Staining for the proliferation marker KI-67 was carried out to determine if the cobblestone phenotype was capable of proliferation or had undergone terminal differentiation. αMEM and CDM + Activin A/FGF2 treated cells maintained a strong expression of KI-67 provided that the cells were subconfluent, highlighting the proliferative ability of the fibroblastic cells (Figure 3.11 D, E). The majority of cobblestone cells were found to be negative for KI-67, especially in areas of cell confluence; with a small number of cobblestone cells and the majority of fibroblastic cells in CDM + BMP-2 cultures maintaining some expression (Figure 3.11 F). Expression of the stem cell marker SOX2 was demonstrated in all three culture conditions, with both fibroblastic and cobblestone cells expressing the protein (Figure 3.11 G-I). The expression of SOX2 was found to be offset from the nucleus in some cells, but was attributed to the fixation of the cells causing delocalisation of the protein. The stem cell marker OCT4 was also assessed and found to be negative in all cultures (Figure 3.11 J-L).
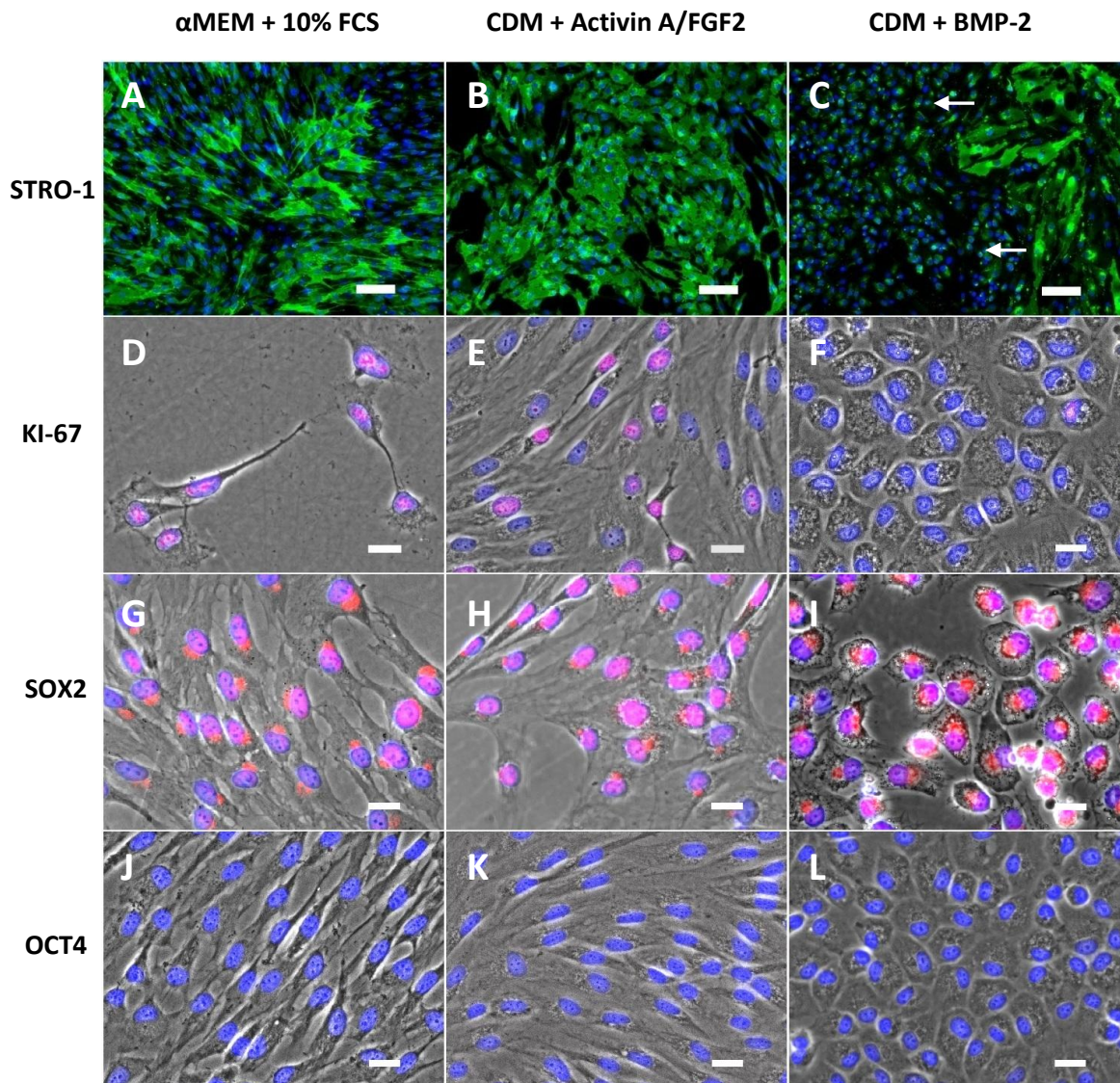
Figure 3.11. Histological analysis for stem cell and cell cycle markers. STRO-1 (A-C), Ki-67 (D-F), SOX2 (G-I) and OCT4 (J-L) are shown. Arrows highlight patches of cobblestone cells in CDM + BMP-2. Green/red fluorescent staining represents the expression of the specific marker, while blue staining represents cell nuclei. Except for images A-C, stains are set against brightfield images to allow visualisation of cell morphology. Scale bars are 100µm (A-C) and 20µm (D-L).

Analysis of the osteogenic marker, Type I collagen, showed strong expression in fibroblastic cells in all three culture conditions (Figure 3.12 A-C), whilst cobblestone cells exhibited negligible expression of the matrix collagen (Figure 3.12 C, highlighted by arrows). Type II collagen staining of cobblestone populations showed ubiquitous expression in all cultures, with the protein present both on fibroblastic and cobblestone cells in equivalent concentration (Figure 3.12 D-F). The early chondrogenic marker, SOX9, was expressed in both fibroblastic and cobblestone cells in all conditions, but was found to be expressed in greater intensity in cobblestone cells (Figure 3.12 G-I).
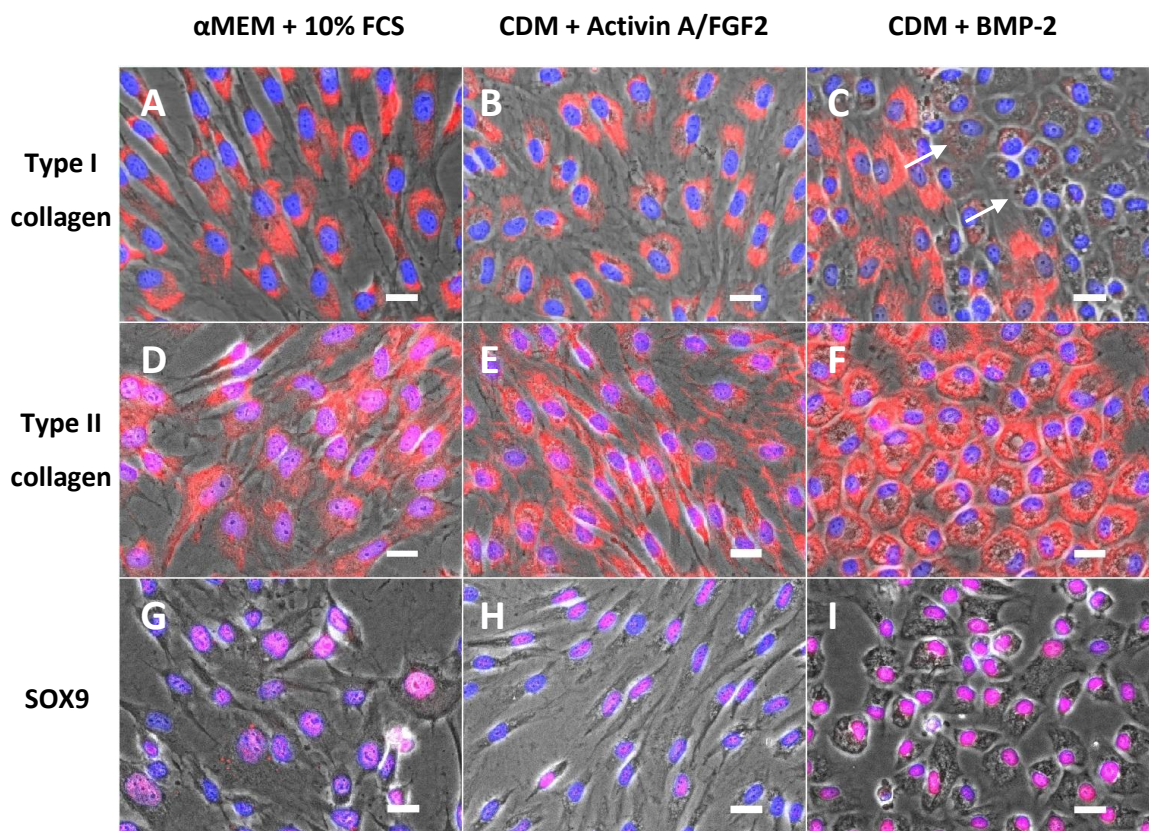
Figure 3.12. Histological analysis for the osteogenic and chondrogenic markers; Type I collagen (A-C), Type II collagen (D-F) and SOX9 (G-I). Arrows highlight patches of cobblestone cells in CDM + BMP-2 images where fibroblastic cells are present. Red fluorescent staining represents the expression of the specific marker, while blue staining represents cell nuclei. Stains are set against brightfield images to allow visualisation of cell morphology. Scale bars are 20μm.

Observation of potential lipid globules in cells expressing the cobblestone phenotype suggested an adipogenic phenotype. Oil red O staining for lipid vacuoles revealed that fibroblastic cells in all conditions contained no lipid (Figure 3.13 A, B), while the majority of cobblestone cells were shown to contain lipid globules in a ring around the edge of the cells (Figure 3.13 C). Expression of the adipogenic markers PPARγ and FABP4 was negative in fibroblastic cells (Figure 3.13 D, E, G, H). Cobblestone cells were found to ubquitously express PPARγ but not FABP4 (Figure 3.13 F, I). Less than 1% of cobblestone cells expressed FABP4.
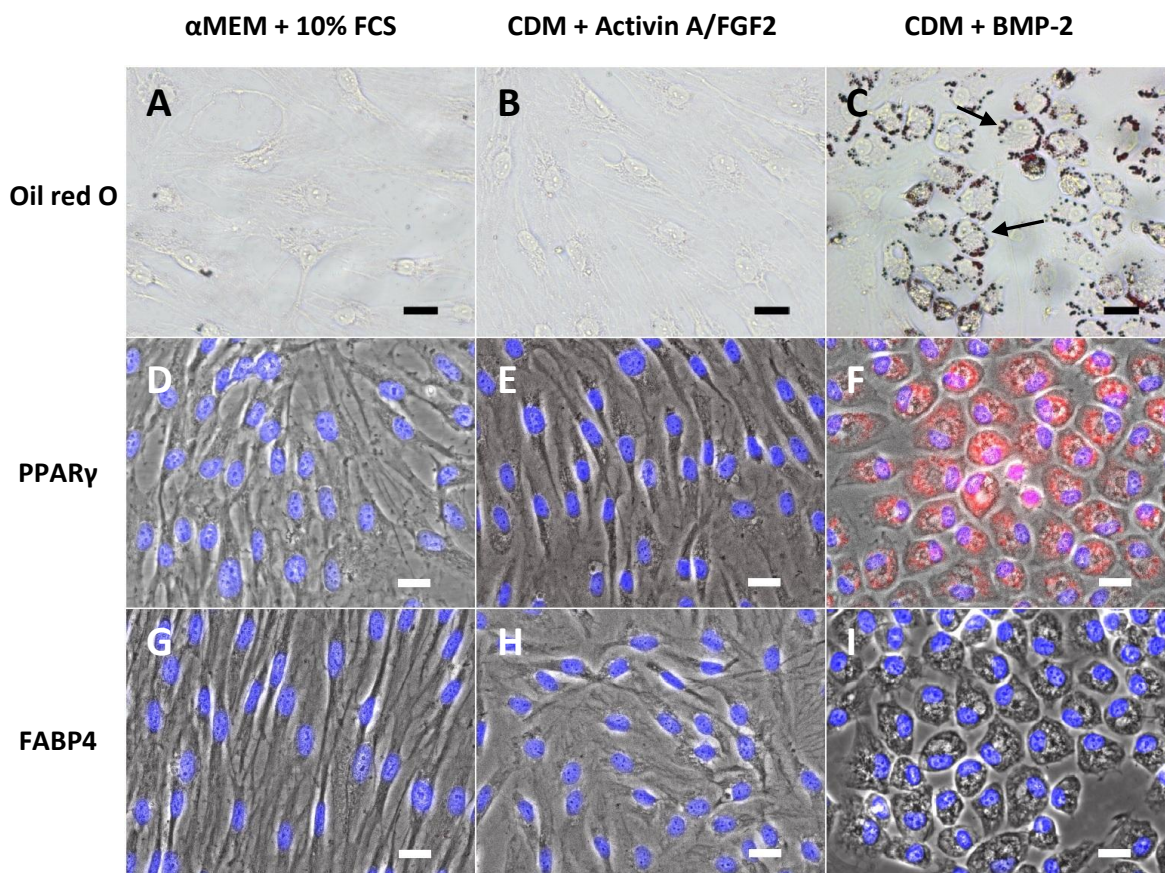
Figure 3.13. Histological analysis of adipogenic markers. Oil red O staining for lipid vacuoles (A-C), PPARγ (D-F) and FABP4 (G-I). Arrows highlight patches of cobblestone cells in CDM + BMP-2 images where some fibroblastic cells are present. For Figures D-I, red fluorescent staining represents the expression of the specific marker, while blue staining represents cell nuclei. Stains are set against brightfield images to allow visualisation of cell morphology. Scale bars are 20µm.

Staining for the endothelial marker, CD146 (MCAM) and the haematopoietic marker, CD34, was negligible in all 3 culture conditions (Figure 3.14 A-C, M-O). Positive control staining of HUVEC cells demonstrated that the antibodies were effective, confirming the negative expression. The vascular endothelial receptor for angiopoietin, TIE-2, was present at minimal levels in αMEM + FCS populations (Figure 3.14 D). Addition of CDM + Activin A/FGF2 induced an increase in TIE-2 expression, with many cells expressing the receptor (Figure 3.14 E). After addition of CDM + BMP-2, TIE-2 expression was inhibited in cobblestone cells, with only a few fibroblastic and early-cobblestone cells maintaining expression of the marker (Figure 3.14 F).

Von Willebrand's factor (VWF) was present in all three media conditions (Figure 3.14 G-I) and was expressed predominantly in the extracellular matrix and on the surface of a minority of fibroblastic cells. Cobblestone cells lacked expression of vWF. The endothelial marker CD105 (endoglin) was expressed at low levels in αMEM + FCS and CDM + Activin A/FGF2 populations and at negligible levels in cobblestone populations (Figure 3.14 J-L).
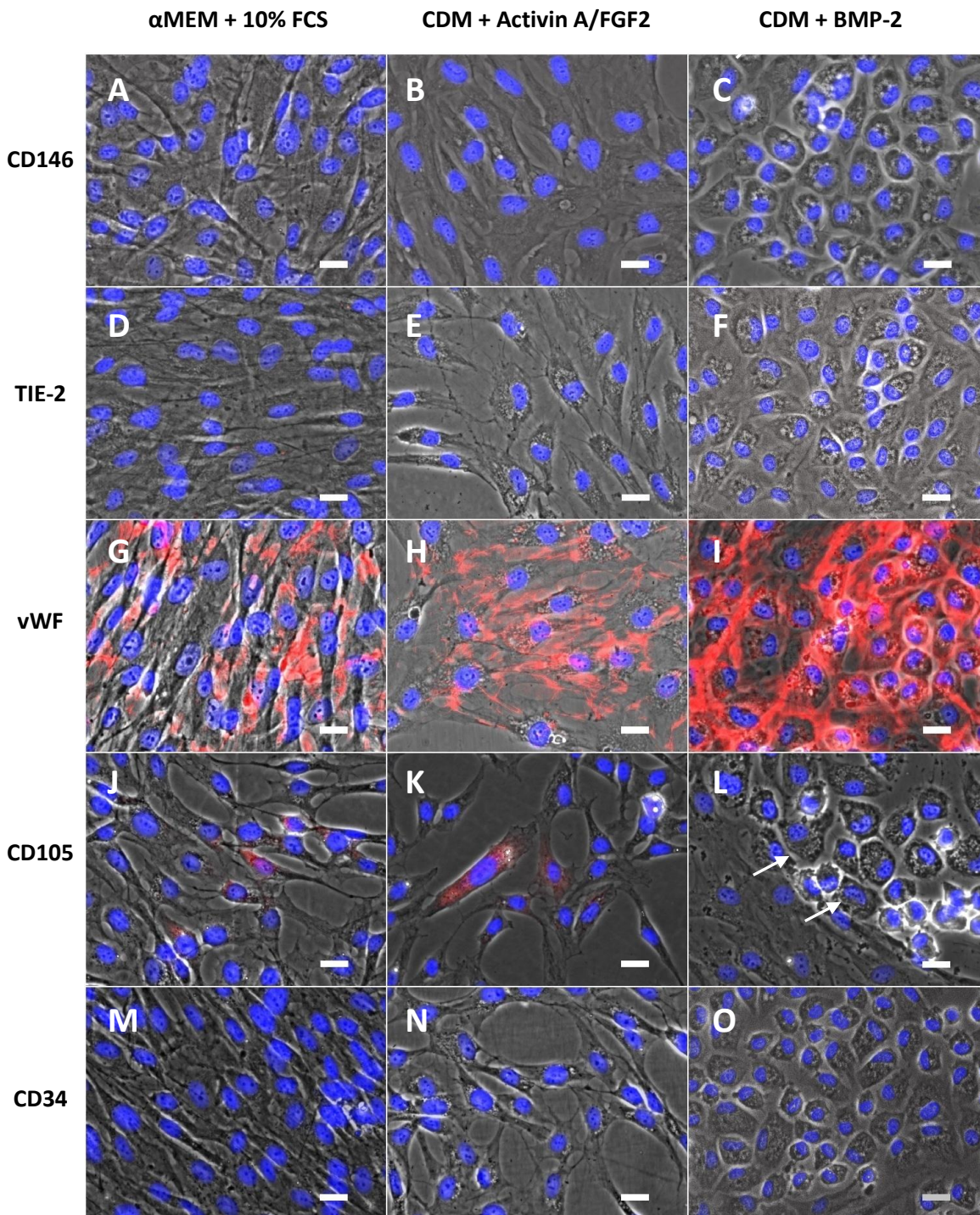
Figure 3.14. Histological analysis of endothelial cell markers CD146 (A-C), TIE2 (D-F), VWF (G-I) and CD105 (J-L) and the haematopoeitic marker CD34 (M-O). Red fluorescent staining represents the expression of the specific marker, while blue staining represents cell nuclei. Stains are set against brightfield images to allow visualisation of cell morphology. Scale bars are 20µm.

Histological analysis of alkaline phosphatase levels (Figure 3.15) demonstrated that in fetal cell populations treated with CDM plus Activin A and FGF-2, negligible alkaline phosphatase was expressed, in contrast with the normal fetal cell phenotype under normal culture medium, which expressed low levels of alkaline phosphatase. Addition of CDM plus BMP-2 to the cell culture restored some alkaline phosphatase expression, although this was not sufficient to restore the phenotype seen in normal culture. Furthermore, the staining was only observed in cells expressing a fibroblastic phenotype. Biochemical analysis of fetal cells cultured in CDM plus Activin A and FGF-2 and in CDM plus BMP-2 showed insignificant differences between the values for alkaline phosphatase expression in treated samples and the background levels.
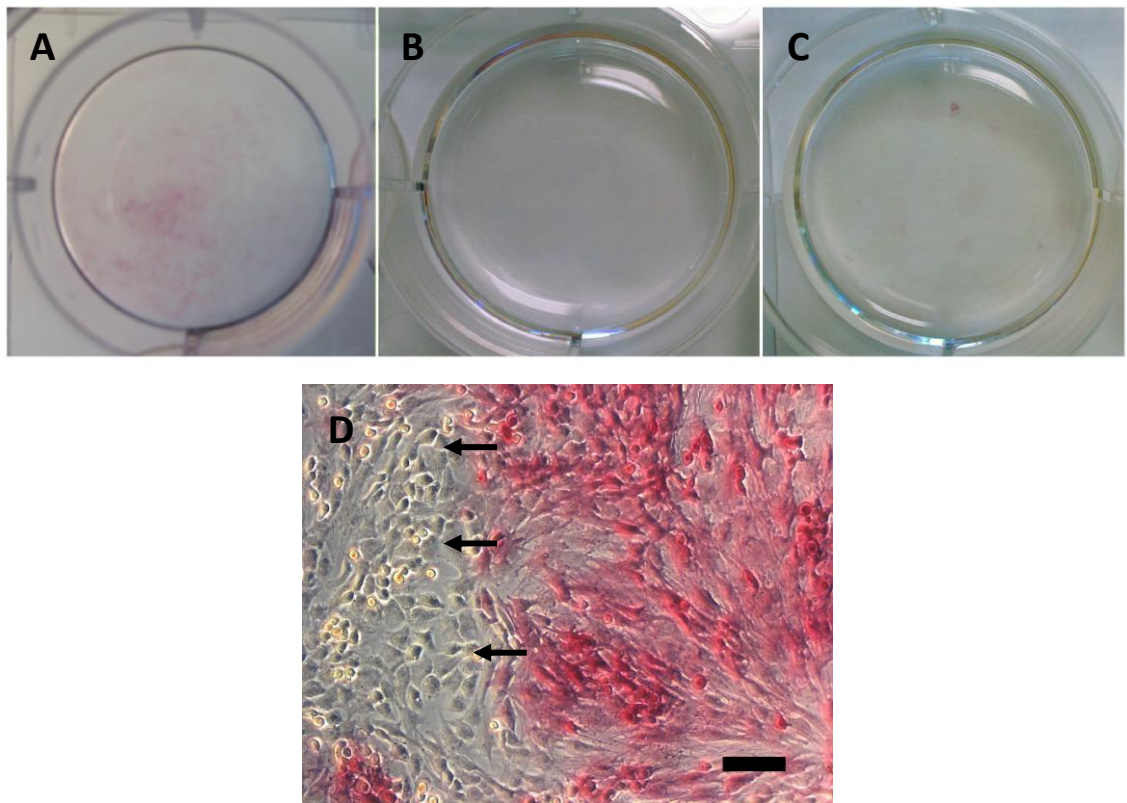
Figure 3.15. Alkaline phosphatase staining of CDM treated cultures. αMEM treated wells expressed low levels of ALP (A), while populations cultured in CDM + Activin A/FGF2 expressed negligible ALP (B). In CDM + BMP-2 populations, minor alkaline phosphatase expression was observed in some fibroblastic cells but was absent in cobblestone cells (C, D). Arrows highlight areas of cobblestone formation. Scale bar is 100µm.

3.3.5. Summary of cell marker expression in fetal cells

Marker	Tissue/function	Marker expression		
		Untreated	CDM + A/FGF2	Cobblestone cells
KI-67	Proliferation	++	++	-
SOX2	Stem cells	++	++	++
OCT4	Stem cells	-	-	-
STRO-1	MSCs	++	++	++
Type I collagen	Osteogenesis	++	++	-
Alkaline phosphatase	Osteogenesis	+	-	-
Type II collagen	Chondrogenesis	++	++	++
SOX9	Chondrogenesis	+	+	++
Oil red O	Adipogenesis	-	-	++
PPARγ	Adipogenesis	-	-	++
FABP4	Adipogenesis	-	-	-
CD146	Endothelial cells	-	-	-
CD105	Endothelial cells	+ (low)	+ (low)	-
TIE2	Endothelial cells	-	-	-
VWF	Endothelial cells	++	++	++
CD34	Haematopoietic cells	-	-	-

Table 3.1. Summary of cell marker expression in FFDCs at passage 0 (untreated), in CDM + Activin A/FGF2 treated FFDCs (CDM + A/FGF2) and in fetal femur-derived cobblestone cells. Antibody efficacy was confirmed via positive controls. Key: ++ = strong ubiquitous staining; + = some staining; - = negligible/absent staining.

3.3.6. Molecular characterisation of heterogeneous cobblestone cell populations

Comparison of CDM + Activin A/FGF2 to αMEM + FCS treated cells demonstrated significant differences in expression of 18 genes, 12 of which were up-regulated and 6 down-regulated (Figure 3.16, Table 3.2). Populations treated with CDM + Activin A/FGF2 demonstrated an increased expression of a variety of stem cell markers including; *FGF2, PROM-1, ZFP42, FZD9, FUT1* and *MMP2*. A number of genes involved in mesenchymal tissue development, including *SOX9, BMP2, BMP4, BMP7, GDF7* and *GDF15* were also upregulated, while genes involved in haematopoietic, neuronal and endothelial cell differentiation, including *BDNF, JAG1, LIF, PTPRC* and *HGF* demonstrated significant down-regulation. The osteogenic promoter, *RUNX2*, was also downregulated.

Addition of CDM + BMP-2 to populations pre-treated with CDM + Activin A/FGF2, induced up-regulation of 6 genes and down-regulation of 15 genes, unique to the CDM + BMP-2 populations (Figure 3.17, Table 3.3). Addition of BMP-2 induced up-regulation of genes including the epidermal and epithelial growth factor, *EGF*; the growth factor, *IGF1*; the skeletogenic promoters, *BMP-2* and *SOX9*; the neurogenic stem cell marker, *NES*; and the endothelial marker, *VWF*. The stem cell marker *FZD9* also demonstrated upregulation.

Addition of CDM + BMP-2 to proliferative cultures resulted in down-regulation of genes thought to maintain pluripotency and self-renewal, including *FUT1, PROM1, LIF* and *FGF10*, as well as other suspected stem cell-related markers such as *VCAM1, NT5E, THY1* and *HGF*. Downregulation was also observed in genes involved in skeletal development (*BMP4, GDF5, GDF6, GDF7* and *SMURF2*), and other tissues including endothelial, epithelial, haematopoietic and immunogenic (*BDNF, CSF2, ICAM1* and *IL6*). Other genes exhibiting downregulation included *ANPEP* and *TNF*.
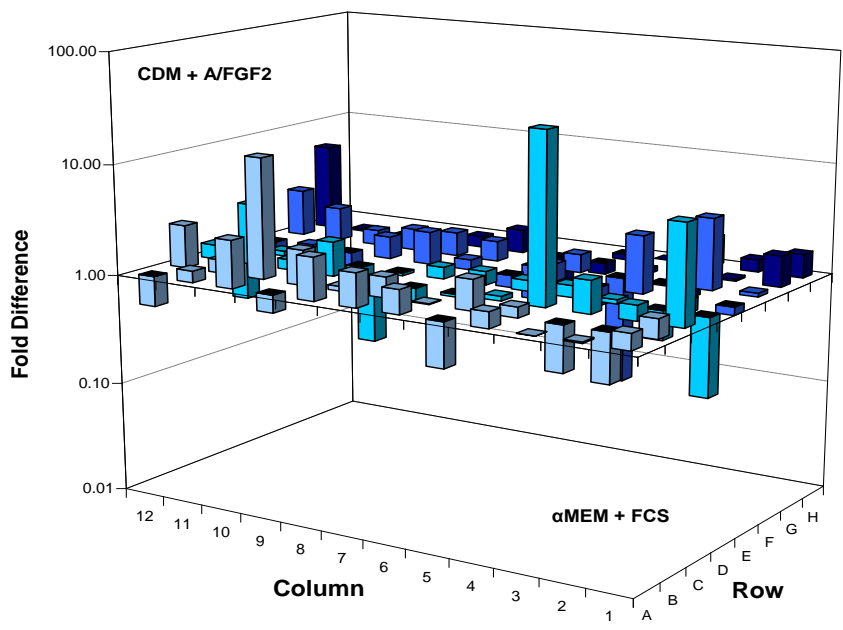
Figure 3.16. Comparison of αMEM + FCS and CDM + Activin A/FGF2 populations analysed using the RT² Profiler™ PCR Array for mesenchymal stem cell markers. Columns with a value greater than 1 demonstrate genes only upregulated by addition of CDM + A/FGF2, while columns less than 1 demonstrate down-regulated of genes. n=3.

UP-REGULATED		DOWN-REGULATED	
SYMBOL	GENE NAME	SYMBOL	GENE NAME
BMP-2	bone morphogenetic protein 2	BDNF	brain-derived neurotrophic factor
BMP4	bone morphogenetic protein 4	HGF	hepatocyte growth factor
BMP7	bone morphogenetic protein 7	JAG1	jagged 1
FGF2	fibroblast growth factor 2	LIF	leukemia inhibitory factor
FUT1	fucosyltransferase 1	PTPRC	protein tyrosine phosphatase receptor type C
FZD9	frizzled homolog 9	RUNX2	runt-related transcription factor 2
GDF15	growth differentiation factor 15		
GDF7	growth differentiation factor 7		
MMP2	matrix metallopeptidase 2		
PROM1	prominin 1		
SOX9	SRY (sex determining region Y)-box 9		
ZFP42	zinc finger protein 42 homolog		

Table 3.2. List of genes affected by addition of CDM + Activin A/FGF2 to αMEM + FCS treated cells.
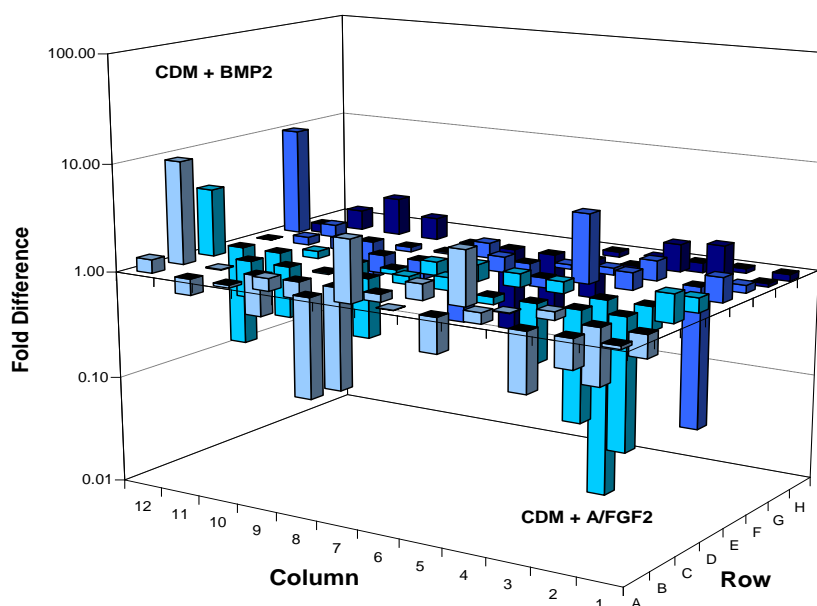
Figure 3.17. Comparison of CDM + Activin A/FGF2 and CDM + BMP-2 populations analysed using the RT² Profiler™ PCR Array for mesenchymal stem cell markers. Columns with a value greater than 1 demonstrate genes only upregulated by addition of CDM + BMP-2, while columns less than 1 demonstrate downregulated of genes. n=3.

UP-REGULATED		DOWN-REGULATED	
SYMBOL	GENE NAME	SYMBOL	GENE NAME
BMP-2	bone morphogenetic protein 2	ANPEP	alanyl (membrane) aminopeptidase
EGF	epidermal growth factor	BDNF	brain-derived neurotrophic factor
FZD9	frizzled homolog 9	BMP4	bone morphogenetic protein 4
IGF1	insulin-like growth factor 1	CSF2	colony stimulating factor 2
NES	nestin	FGF10	fibroblast growth factor 10
SOX9	SRY (sex determining region Y)-box 9	FUT1	fucosyltransferase 1
VWF	von Willebrand factor	GDF5	growth differentiation factor 5
		GDF6	growth differentiation factor 6
		GDF7	growth differentiation factor 7
		HGF	hepatocyte growth factor
		ICAM1	intercellular adhesion molecule 1
		IL6	interleukin 6
		LIF	leukemia inhibitory factor
		NT5E	5'-nucleotidase, ecto
		PROM1	prominin 1
		SMURF2	SMAD specific E3 ubiquitin protein ligase 2
		THY1	Thy-1 cell surface antigen
		TNF	tumor necrosis factor
		VCAM1	vascular cell adhesion molecule 1

Table 3.3. List of genes affected by addition of CDM + BMP-2 to CDM + Activin A/FGF2 treated cells.

3.3.7. Isolation of pure cobblestone cell populations

Further molecular characterisation of FFDC-derived cobblestone cells required the isolation of the cobblestone phenotype from heterogeneous populations. Using laser dissection microscopy it was possible to isolate cobblestone cells from heterogeneous populations for culture and analysis (Figure 3.18 A). Populations of fibroblastic cells isolated and recovered from heterogeneous CDM + BMP-2 populations demonstrated readherance and proliferation when seeded onto tissue culture plastic and grown in CDM + Activin A/FGF2 media (Figure 3.18 B, D). Furthermore, addition of CDM + BMP-2 to isolated fibroblast cells resulted in the recovery of the cobblestone phenotype. In samples where cobblestone cells were isolated, recovered cells were viable and would readhere to tissue culture plastic but failed to proliferate when treated with CDM + BMP-2 media (Figure 3.18 C).
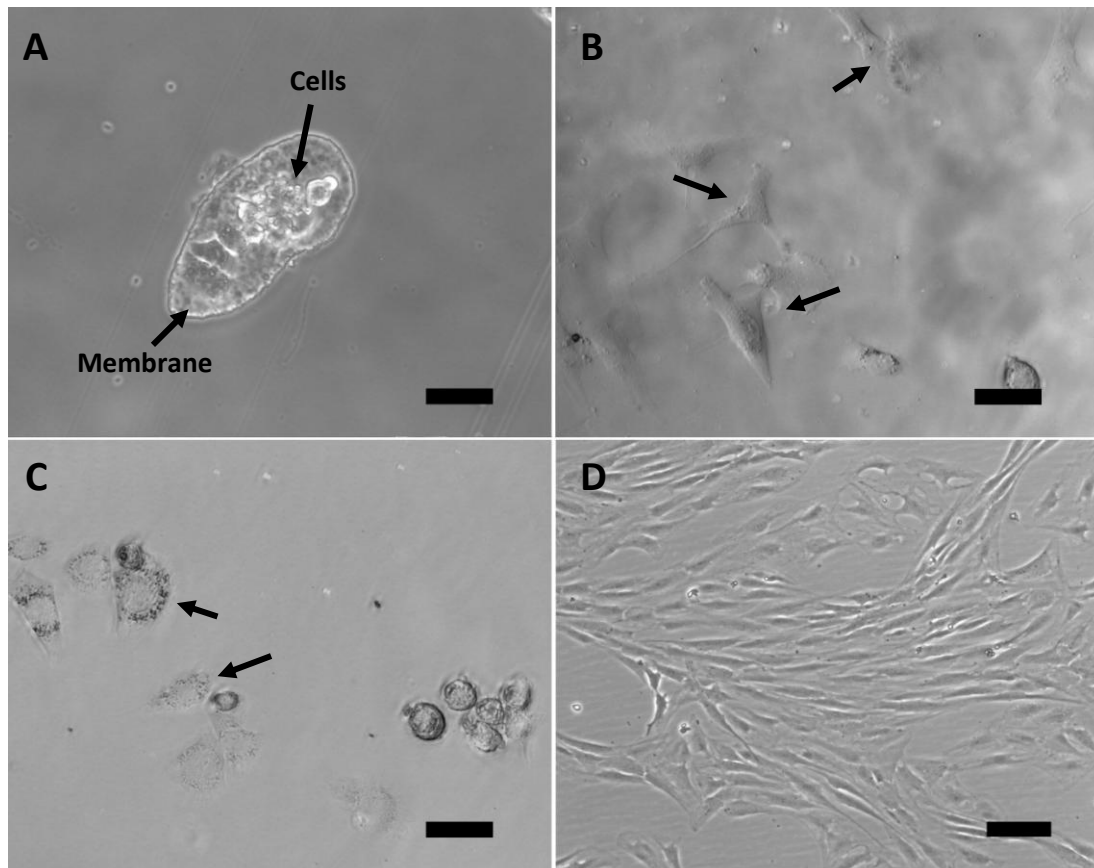
Figure 3.18. Phase contrast images of cobblestone cells isolated using laser dissection microscopy. 15 minutes post dissection, cells can still be seen attached to dissected Lumox™ membrane (A). At 3 days post dissection, cells from both fibroblastic (B) and cobblestone isolations (C) can be seen adhered (highlighted by arrows). Isolated fibroblastic cells demonstrated proliferation after 2 weeks culture in CDM + Activin A/FGF2 (D). Scale bars are 50µm (A-C) and 100µm (D), n=4 populations.

3.3.8. Molecular characterisation of isolated cobblestone cells

The number of cobblestone cells isolated per population varied from approximately 50-300 cells depending on the availability of cobblestone cells. Trizol extraction performed on isolated populations resulted in minimal recovery of RNA due to the low number of cells. This prevented characterisation of the cells via RT-qPCR as the levels of cDNA produced were too small to provide reliable results (see Appendix 3).

Analysis of amplified RNA from isolated cobblestone populations demonstrated expression of a variety of genes present in stem cell maintenance and differentiation (Table 3.4). Genes expressed during adipogenesis (*PPARγ*) and skeletogenesis (*TGFβ3, GDF15, SMAD4, CASP3, ANXA5* and *MITF*) were found expressed alongside stem cell

markers (*FGF2, ALCAM* and *GTF3A*) and stem cell differentiation-inducing genes (*NUDT6, HDAC1*). Other genes demonstrating high levels of expression included the integrin genes, *ITGA6, ITGAV* and *ITGB1*; the solute carrier family member, *SLC17A5*; GPI transamidase component, *PIGS*; transcriptional regulator, *HAT1*; cytoskeletal modulator, *RHOA* and the mesenchymal marker, *VIM*. Comparison of the gene profiles demonstrated that all genes highly expressed (Ct ≤ 25) by dissected cobblestone cells, except for *PPARG* and *MITF*, were also highly expressed in non-dissected heterogeneous populations (see Appendix 3 for list of genes highly expressed in heterogeneous populations).

FUNCTION	SYMBOL	GENE NAME
MSC markers	*ALCAM*	activated leukocyte cell adhesion molecule
	VCAM1	vascular cell adhesion molecule 1
	NT5E	5'-nucleotidase, ecto
	ITGB1	integrin, beta 1
	GTF3A	general transcription factor IIIA
Proliferation	*FGF2*	fibroblast growth factor 2
	NUDT6	nudix (nucleoside diphosphate linked moiety X)-type motif 6
Adipogenesis	*PPARG*	peroxisome proliferator-activated receptor gamma
Skeletogenesis	*ANXA5*	annexin A5
	CASP3	caspase 3, apoptosis-related cysteine peptidase
	GDF15	growth differentiation factor 15
	MITF	microphthalmia-associated transcription factor
	SMAD4	SMAD family member 4
	TGFB3	transforming growth factor, beta 3
Integrins	*ITGA6*	integrin, alpha 6
	ITGAV	integrin, alpha V
Gene expression	*HAT1*	histone acetyltransferase 1
	HDAC1	histone deacetylase 1
Other genes related to the MSC	*PIGS*	phosphatidylinositol glycan anchor biosynthesis, class S
	RHOA	ras homolog gene family, member A
	SLC17A5	solute carrier family 17 (anion/sugar transporter), member 5
	VIM	vimentin

Table 3.4. List of genes highly expressed in microarray analysis of isolated cobblestone populations. Shaded genes are not highly expressed in heterogeneous CDM + BMP-2 populations. Only genes that have a Ct less than 25 are shown. n=4 populations.

94

3.4. Discussion

Previous studies have demonstrated the multipotency and phenotype of FFDCs and their potential as an alternative source of skeletal stem cells for use in tissue engineering (Montjovent et al. 2004;Mirmalek-Sani et al. 2006). This study has re-examined the characteristics of whole fetal femurs and their explanted cells at 7 to 12 weeks post conception and has furthered previous analysis of the phenotypes induced in FFDC populations by the addition of chemically defined media.

Fetal femurs used in this study were predominantly composed of a cartilage anlage bordered by emergent bone collar, and explanted cells expressed a predominantly fibroblastic morphology, matching the phenotype previously reported (Mirmalek-Sani et al. 2006). Due to the presence of both cartilage anlage and perichondrium/periosteum, it is still unknown if the majority of cells cultured from fetal femur digests are early chondrocytes (cartilage anlage) or fibroblastic/mesenchymal stem cells (perichondrium). Cultures of explanted FFDCs were positive for the mesenchymal stem cell markers; CD105 (low expression) and STRO-1, while also demonstrating expression of the skeletal markers ALP and SOX9, confirming the mesenchymal phenotype of the cells. The adipogenic markers, PPARγ and FABP4 were negligible, confirming the lack of adipogenic cells in fetal femur digests. FFDCs were negative for CD146, TIE-2 and CD34, indicating the absence of cells belonging to the endothelial or haematopoietic lineages. While the endothelial marker, CD146, has been recently recognised as a potential marker for MSCs isolated from a variety of fetal and adult tissues (Covas et al. 2008), it has not yet been confirmed in fetal femur-derived populations. While FFDCs lacked expression of the CD146 and TIE-2, the endothelial marker vWF was expressed in a small number of cells and the extracellular matrix, inferring the presence of a minority of cells with some subendothelial characteristics. The strong expression of vWF in the ECM of FFDC cultures is likely due to the secreted protein's ability to interact with Type I collagen (Sharapova et al. 2009). Considering the marker expression demonstrated by FFDCs, as well as the fact that chondrocytes are expected to be the most frequent cell type present in fetal femurs due to their cartilage-rich phenotype, it is likely that the majority of cells cultured from fetal femur digests are early chondrocyte/chondroprogenitor and mesenchymal progenitor populations, while a minority of cells expressed subendothelial characteristics. Previous

studies into the expression of STRO-1 in populations of FFDCs have resulted in varied results, ranging from 3% of cells to 50% of cells expressing STRO-1 (Mirmalek-Sani et al. 2006;Zhang et al. 2009). While exact values for STRO-1 have not been calculated using FACS, in this study, direct comparison between FFDC and hBMSC populations enabled observation that expression of STRO-1 in FFDC populations was repeatedly higher than in adult marrow-derived cell populations, suggestive of a population of mesenchymal precursor cells in fetal femur digests. In the few studies that exist, data on expression of ES cell markers in FFDC populations is contradictory, with some studies demonstrating the presence of both NANOG and OCT-4 in FFDCs (Guillot et al. 2007;Zhang et al. 2009) and others demonstrating lack of expression of NANOG and OCT-4 (Mirmalek-Sani et al. 2006). While this study found no expression of OCT-4 in FFDCs, ubiquitous expression of SOX2, another ES cell marker essential for maintenance of self-renewal were observed. The lack of OCT-4 expression may be an artefact of culture in monolayer conditions before fixation and staining. This data, combined with the presence of stem cell markers in other fetal tissues, indicate the presence of early developmental cells within the fetal femurs or the maintenance of stem cell-like characteristics throughout fetal femur-derived populations.

FFDCs demonstrated the ability to form both osteogenic and adipogenic tissues in monolayer culture, confirming the multipotency of FFDCs and other fetal tissue-derived cells as shown by previously published data (Campagnoli et al. 2001;Mirmalek-Sani et al. 2006;Zhang et al. 2009). Expression of high levels of both Type I and Type II collagen in all cultures was noted as a side effect of monolayer culture, demonstrating a significant effect of monolayer culture on the phenotype of cells. Failure to produce homogeneous cartilage-like populations, evidenced by high levels of the osteogenic marker Type I collagen and poor expression of the chondrogenic marker SOX9, further demonstrated that while monolayer culture is useful for expansion of isolated cells, it is ineffective for facilitating total differentiation of cells. The multipotency of FFDC populations suggests that the cells were predominately composed of early skeletal progenitor cells, which despite exhibiting chondrocyte characteristics, maintained the ability to differentiate into multiple mesenchymal tissues when treated with the relevant inducing factors. Alternatively, monolayer culture of differentiated cells such as chondrocytes is known to induce dedifferentiation towards a more fibroblastic

96

phenotype (Goessler et al. 2005), thus FFDC cultures may exhibit multipotency due to dedifferentiation of early chondrocytes towards an early skeletal progenitor that maintains multipotentcy. Addition of the osteogenic inducer, BMP-2, to fetal populations treated with osteogenic media resulted in significantly reduced alkaline phosphatase activity, substantiating the data previously described by Mirmalek-Sani et al. (2006).

Studies have demonstrated the use of chemically defined media (CDM) on embryonic stem cells to maintain an undifferentiated and proliferative population of viable cells (Johansson & Wiles 1995;Vallier et al. 2005). A study performed by Mirmalek-Sani et al. demonstrated induction of undifferentiated and proliferative populations of FFDCs when cultured in monolayer conditions with CDM supplemented with Activin A and FGF2. Furthermore, treatment of these proliferative populations with BMP-2 resulted in the establishment of a novel cobblestone cell morphology (Mirmalek-Sani et al. 2009). This study confirms that treatment of FFDC populations with CDM + Activin A/FGF2 results in transformation of the heterogeneous cell populations towards a more homogeneous, undifferentiated mesenchymal progenitor phenotype and presents evidence that CDM + BMP-2 induced cobblestone cells are the result of a BMP-2-induced primitive adipogenic phenotype.

FFDCs cultured in CDM + Activin A/FGF2 demonstrated up-regulation of the *FGF2* and *ZFP42* genes involved in maintaining stem cell properties by promoting cell renewal and suppressing differentiation (Raman et al. 2006), alongside up-regulation of the WNT signalling receptor and mesenchymal stem cell marker, *FZD9* (Battula et al. 2008); *FUT1*, a gene strongly expressed by hESCs (Satomaa et al. 2009); and *MMP2*, a gene strongly expressed in MSCs and involved in stem cell migration (Lapidot et al. 2005;Ries et al. 2007). Expression of these genes indicates that the addition of Activin A and FGF2 promotes dedifferentiation of the cells towards an undifferentiated, proliferative stem cell-like phenotype, similar to a previous study by Battula and co-workers, where adult mesenchymal stem cell populations cultured in a chemically defined media supplemented with FGF2 demonstrated upregulation of *FZD9* and other stem cell markers including *NANOG* and *OCT-4*, as well as demonstrating multipotency (Battula et al. 2007). Downregulation of various genes involved in the promotion of

endothelial, epithelial and haematopoietic tissue differentiation, including *HGF* (You & McDonald 2008); *PTPRC* (CD45) (Shivtiel et al. 2008) and *BDNF* (Wang et al. 2008), combined with upregulation of genes involved in mesenchymal differentiation and development, such as *SOX9, BMP2, BMP4, BMP7, GDF7* and *GDF15*, indicated that the undifferentiated, proliferative populations produced by addition of Activin A and FGF2 were dedifferentiating towards a more homogeneous population of mesenchymal progenitors. Cells treated with CDM + Activin A/FGF2 also demonstrated strong expression of the MSC marker STRO-1 in the majority of cells, further indicating a multipotent and proliferative mesenchymal state.

Down-regulation of stem cell-related genes such as *FUT1, PROM-1* (a gene thought to maintain pluripotency by suppressing differentiation (Bauer et al. 2008)), *LIF* (a cytokine that maintains cells in a stem cell state (Jiang et al. 2002;Metcalf 2003)) and *HGF* (involved in stem cell migration (Forte et al. 2006)) in CDM + BMP-2 treated cultures, combined with the strong expression in LDM-isolated cobblestone cells of the anti-proliferative FGF2-antisense gene, *NUDT6* and *HDAC1*, a gene responsible for cell fate determination during stem cell differentiation, alluded that the majority of cells were in the process of differentiation away from a stem cell phenotype towards a terminal differentiation. Loss of expression of *VCAM1* (CD106), *NT5E* (CD73) and *THY1* (CD90), markers for MSC cells (see Section 1.7.3.4), further corroborated BMP-2-induced loss of the proliferative, self-renewing phenotype. However, strong expression of the stem cell/MSC markers *ALCAM* and *FGF2* in LDM-isolated cobblestone populations indicate that cobblestone cells maintain some stem-cell characteristics. Cobblestone cells were observed to lack expression of the proliferation marker KI-67 and cobblestone cells isolated with laser dissection demonstrated readherence to tissue culture plastic but failure to proliferate, further indicating the cobblestone phenotype to be a terminal differentiation. The expression of KI-67 in CDM + BMP-2-treated fibroblastic cells and a small number of cobblestone cells suggested that the small number of cobblestone cells expressing KI-67 were early cobblestone cells that had yet to reach terminal differentiation.

FFDC cobblestone cells lack endothelial and haematopoietic marker expression but demonstrate lipid retention and strong expression of the adipogenic marker, PPARγ, as well as retention of other mesenchymal cell markers, including STRO-1, Type II

collagen and SOX9. Furthermore, populations of cobblestone cells isolated by laser dissection strongly express the adipogenic gene *PPARγ*, indicating that the cobblestone cells have an adipogenic phenotype. Poor FABP4 expression and limited numbers of lipid vacuoles observed in cobblestone cells is suggestive of a primitive adipogenic phenotype. The adipogenic hypothesis was furthered by the fact that insulin and BMP-2, both found in cobblestone-inducing media, are known to induce adipogenic differentiation in mesenchymal precursor cells (Kang et al. 2009) and cultures of preadipocyte cells such as 3T3-L1 demonstrate morphology similar to that of the FFDC-derived cobblestone cells (Guo et al. 2004;Bohm et al. 2008). Expression of SOX9 and Type II collagen in the cobblestone cells was not unexpected due to the inherent chondrogenic nature of FFDCs and the cartilage-inducing properties of BMP-2 (Pan et al. 2008). The presence of the osteogenic markers ALP and Type I collagen in the fibroblastic cells but not in the cobblestone cells observed in CDM + BMP-2 cultures indicates that addition of BMP-2 to FFDCs treated with CDM may induce both early osteogenic (fibroblastic) and adipogenic (cobblestone) differentiation, explaining the presence of both a fibroblastic and cobblestone phenotype as BMP-2 is known to induce both osteogenic and adipogenic differentiation (Mikami et al. 2011).

The cobblestone phenotype induced by culture in CDM + BMP-2 was found to be more pronounced in confluent patches of cell growth, suggesting that some attributes of the phenotype may be due to the spatial environment. The presence of cobblestone-like precursors in FFDC cultures shortly after digest indicates the presence of cobblestone precursors in fetal femur digests. However, while the pre-cobblestone cells demonstrate the ability to form cobblestone cells when treated with CDM + BMP-2, prior addition of CDM + Activin A/FGF2 resulted in significantly increased cobblestone cell formation, suggesting that cobblestone cells required a proliferative, undifferentiated precursor. The inability of FFDCs cultured for long periods of time in αMEM + FCS% to form cobblestone cells, even with addition of CDM + Activin A/FGF2 and CDM + BMP-2, indicated a culture-induced differentiation of cells towards a phenotype unable to form cobblestone cells.

Previous studies have demonstrated that cells with a cobblestone morphology are present in both early trophoectodermal and endodermal (Talbot et al. 2000), endothelial

(Deschaseaux et al. 2007;Kirton & Xu 2010) and epithelial cells (Davis et al. 1995;Kaushik et al. 2008). Mesenchymal stem cells have been shown to possess the ability to differentiate into endothelial cells *in vitro* when grown in low serum culture (Oswald et al. 2004), provoking the original hypothesis that the FFDC-derived cobblestone cells were expressing endothelial characteristics despite their strong mesenchymal phenotype. FFDC-derived cobblestone cells demonstrated upregulation of RNA expression for the epidermal and epithelial growth factor, *EGF* and the endothelial marker *VWF*, suggestive of an endodermal-derived cell lineage. However, FFDC-derived cobblestone cells demonstrated a lack of staining for the endothelial markers CD146, vWF and TIE-2, indicating that the cells did not belong to the endothelial lineage. Expression of vWF in the ECM and some fibroblastic cells in FFDCs treated CDM + BMP-2, suggested the maintained expression of a subpopulation of fibroblastic cells with subendothelial characteristics. Cobblestone-like cells have also been previously observed in haematopoietic tissues in the cobblestone-area forming assay, used to establish colonies of haematopoietic stem and progenitor cells (de Haan & Ploemacher 2001). However, the lack of expression of the haematopoietic marker, CD34 and the perivascular marker, CD146 in FFDC cobblestone cells suggests a non-haematopoietic lineage (Shi & Gronthos 2003).

In conclusion, this study has demonstrated that fetal femur-derived cell populations are multipotent and are predominantly composed of early chondrocytes and other skeletal precursors, with some cells with subendothelial characteristics also present. The addition of CDM supplemented with Activin A and FGF2 resulted in the shifting of cells towards a more homogeneous population of proliferative and undifferentiated mesenchymal precursor cells, while addition of CDM supplemented with BMP-2 induced formation of cobblestone cells with a primitive adipogenic phenotype. The arrest of adipogenic differentiation at the preadipocyte stage may be accounted for by the lack of late adipogenic inducers in the chemically defined media, therefore, future work to determine whether the cobblestone cells are able to differentiate into mature adipocytes could be performed with the addition of adipogenic supplements such as high glucose content, dexamethasone, isobutylmethylxanthine (IBMX) and indomethacin. Furthermore, bovine endodermal cells derived from the inner cell mass of 7 to 8 day blastocysts have been observed growing as tight knit colonies with

100

cobblestone morphology and expression of numerous lipid vacuoles in the cells (Talbot et al., 2000), thus expressing a similar morphology to that of the cobblestone cells induced in CDM + BMP-2 treated FFDC populations. Therefore, analysis of FFDC cobblestone cells for markers of endoderm and trophoblast populations would enable definition of whether FFDC-derived cobblestone cells have characteristics of non-mesenchymal lineages or are truly adipogenic. Finally, the lack of comparability between amplified and non-amplified RNA samples hindered the analysis of isolated cobblestone cells. While amplification was chosen as the optimal route for analysis of gene expression due to funding and time constraints, future work using alternative methods for single cell molecular analysis, such as microfluidic diagnostic chips, would enable a clearer image of the genetic makeup of laser dissected cells.

The majority of studies utilising FFDCs, have focused on the isolation of fetal MSCs and characterisation of their phenotype in comparison to adult MSCs. These studies have confirmed that fetal femur-derived cells offer a potential alternative to adult hBMSCs as a source of MSCs with greater stem-like characterisitics. Investigation of the growth and differentiation potential of FFDCs in common tissue engineering protocols, such as 3D pellet culture or bioreactor culture, is required before these cells can be deemed suitable for use in tissue regeneration. The following chapter (Chapter 4) describes the utilisation of FFDCs in a 3D pellet culture model and investigates the phenotypes derived from growth in osteogenic and chondrogenic conditions over 28 days.

CHAPTER 4

DEVELOPMENT OF A NOVEL 3D ORGANOTYPIC AIR-LIQUID INTERFACE MODEL FOR SKELETOGENESIS USING FETAL FEMUR-DERIVED CELL POPULATIONS

4.1. Introduction

As previously described in Section 1.7, stem cell based tissue engineering is viewed as a promising approach for orthopaedic reparative medicine, involving the development of biological substitutes for the repair or replacement of damaged tissues.

Expansion of skeletal cell populations for tissue modelling or tissue engineering can be performed using *in vivo* or *ex vivo* culturing techniques. *In vivo* expansion is unrivalled as a model for tissue growth as it maintains the biological and physiological interactions native to skeletal tissue. However, *in vivo* culture is restricted due to cost, ethical concerns and a constrained ability to examine the characteristics of tissues. As such, current models for developing and testing the effects of new skeletal tissue engineering techniques *in vivo* are limited. Propagation of mammalian tissue has mainly been focused on culture of specific, purified populations of cells *in vitro*. *In vitro* culture offers ease of manipulation and scalability, enabling generation of large amounts of tissue at relatively low cost. Current and emerging methods of *in vitro* culture have potential in various aspects of tissue engineering. Monolayer cell culture facilitates large-scale expansion of cells but lacks the physiological interactions, as well as the nutritional and hormonal conditions to closely replicate growth *in vivo,* compromising the efficacy of these cultures as models for skeletal tissues. While techniques such as bioreactor-based tissue engineering enable cell culture in a strictly controlled dynamic microenvironment (Ellis et al. 2005;Yeatts & Fisher 2011).

The term "organotypic culture" is used to describe methods of *in vitro* culture that allow multiple cell types to interact and affect each other in similar conditions to those found *in vivo*. A common method for organotypic culture is the growth and differentiation of cells at an air-liquid interface (ALI). In this method, explanted cells or whole tissues are cultured on a semiporous membrane and fed by medium underneath the membrane (Stoppini et al. 1991;Freshney 2005) (Figure 4.1). Since its first use by Gahwiler and co-workers for the culture of hippocampal slices (Gahwiler 1981), ALI culture has been modified for use with many other tissue types including skin (Parenteau 1992;Stark et al. 2004), fat (Sonoda 2008), heart (Habeler 2009) and many more. All of these cultures have been found to provide an adequate *in vitro* mimicry of *in vivo* conditions, allowing for long-term histological and physiological studies. The aim of the work presented in

this chapter was to examine the potential of skeletal cell-based organotypic ALI culture as a novel *in vitro* model for skeletogenesis, whilst also presenting a possible *in vitro* method for testing new tissue engineering techniques.
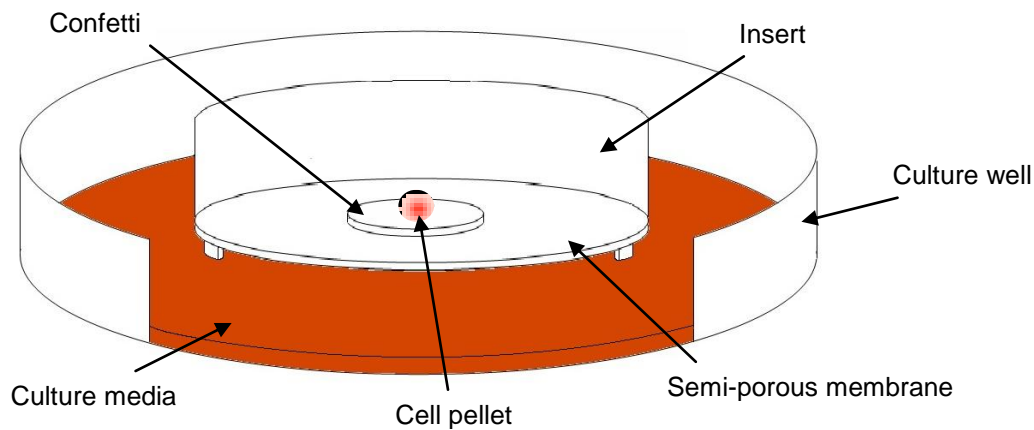
Figure 4.1. Schematic representation of cell pellet organotypic ALI culture. Cell pellets are cultured on a semi-porous membrane that provides an air-liquid interface. Semi-porous confetti is used to allow facile manipulation of pellets without disrupting their 3D structure.

4.2. Materials and methods

4.2.1. Organotypic ALI culture

The organotypic ALI culture protocol was modified from an existing protocol used by Capsant Neurotechnologies Ltd. (see Figure 4.2). Cell pellets were formed from collagenase IV treated monolayer cultures of FFDCs by aliquoting trypsinised cell solutions at $3x10^5$ cells per ml and centrifuging at 400g for 10 minutes. For viability assays, Vybrant® CFDA SE cell tracer (see Section 2.3.1.2) was added after trypsinisation. After formation of pellets by centrifugation, samples were left for a minimum of 2 days at 37°C with 5% CO_2 to allow cell-cell interactions to occur. Pellets were then transferred to pre-prepared 6-well plates containing 30mm diameter Millicell-CM inserts (Fisher, FDR-541-020X) and 6mm diameter, 0.45µm pore size PTFE membrane confetti (Biocell Interface) and the appropriate culture/differentiation media added. Cultures were run up to 28 days, after which pellet cores would begin to undergo necrosis.
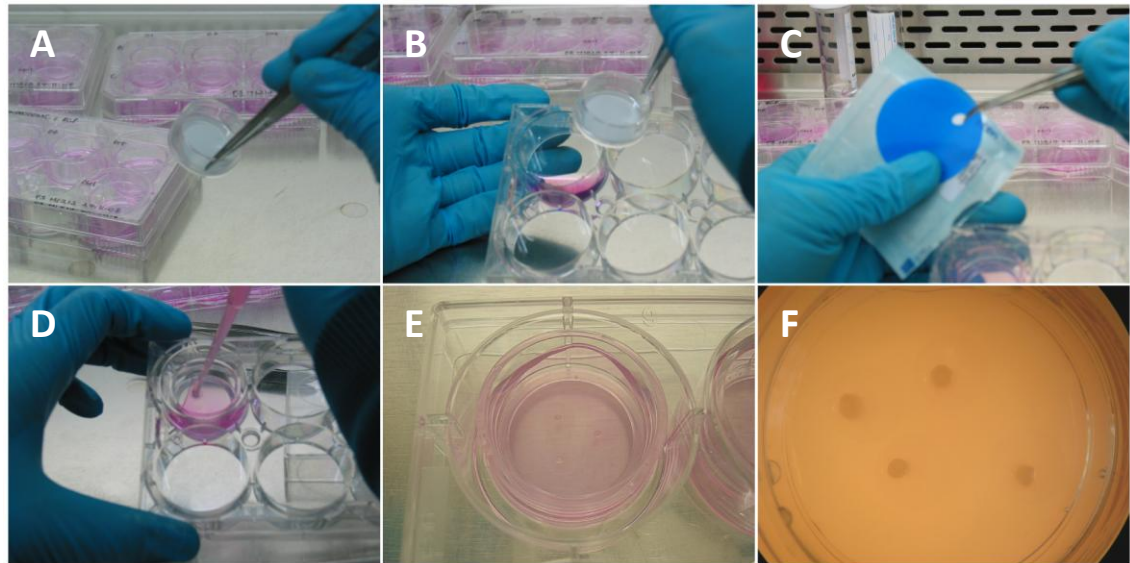
Figure 4.2. Five-step setup of organotypic ALI culture. (A) media added to 6 well plates; (B) Addition of Millicell inserts; (C) confetti added to the insert surface; (D) pellets placed onto the confetti surface; (E) a complete organotypic ALI culture well; (F) organotypic fetal cell pellets *in situ.*

4.2.2. Issues with pellet culture

Performing biochemical and molecular analysis on organotypic pellets provided a significant problem due to the pellets not degrading. This resulted in very little protein, DNA and RNA being released from the samples. This problem was solved by modifying the protocol to include sonication stages as well as vigorous "mashing" of the pellets using a pipette tip.

4.2.3. Differentiation media

To promote osteogenesis, cells were cultured in appropriate α-MEM containing 10% serum plus 100μM ascorbic acid 2-phosphate, 10nM dexamethasone and 150ng/ml BMP-2. To promote chondrogenesis, cells were cultured in α-MEM containing no FCS, supplemented with 100μM ascorbic acid 2-phosphate, 10nM dexamethasone, 10μl/ml 100x ITS solution and 10ng/ml TGF-β3. Control cell pellets were cultured in basal conditions (α-MEM containing 10% FCS only). Media compositions designated as follows:

   i.   Basal: αMEM + 10% serum

   ii.   Osteogenic: αMEM + 10% serum + ascorbate + dexamethasone + BMP-2

   iii.   Chondrogenic: αMEM + ascorbate + dexamethasone + ITS solution + TGF-β3

4.2.4. Histological and biochemical analysis

3D pellet samples were fixed, processed, embedded in paraffin wax and sectioned for histological analysis (Section 2.3.2). Techniques used for histological analysis included Alcian blue/Sirius red staining, Alkaline phosphatase staining and immunofluorescent staining (see Section 2.3). Biochemical analysis was performed to determine the specific activity of Alkaline phosphatase in 3D organotypic pellets (see Section 2.4).

4.2.5. RNA extraction and molecular analysis

Extraction of RNA from pellets provided only small amounts of RNA sample for use in cDNA production and RT-PCR due to the size of the pellets (small) and in later stages, large amounts of matrix. Molecular analysis showed a large degree of variance between the six different fetal cell populations used (see table 4.1). As a consequence, it was required that each population be analysed separately and the trends between basal, osteogenic and chondrogenic conditions be compared rather than group all samples together. Molecular analysis was used to determine the expression of SOX9, Type II collagen, RUNX2, alkaline phosphatase, Type I collagen and Osteocalcin. Results for each population were performed in triplicate.

4.2.5.1. Chomczynski and Sacchi high-recovery method for pellet cultures

Total RNA was extracted using a protocol modified from (Chomczynski and Sacchi 1987). Pellets were washed in PBS then transferred to a molecular grade eppendorf containing 600μl of solution D for pellet degradation (guanidinium thiocyanate, 0.75M (tri)sodium citrate, sarkosyl and 2-mercaptoethanol dissolved in ultra pure water). Pellets were incubated in this solution at 4°C for 1 hour then gently sonicated to disrupt any remaining pellets. RNA was isolated by incubating the degraded samples at 4°C for 15 minutes with 60μl 2M sodium acetate and 600μl phenol/chloroform/iso-amyl-alcohol (25:24:1), then centrifuged at 13000rpm for 20 minutes at 4°C to separate the organic phenol layer from the inorganic aqueous layer containing the RNA. The inorganic layer was then transferred to a fresh eppendorf and the RNA precipitated with isopropanol overnight at -20°C. Following precipitation, the samples were centrifuged to provide an RNA pellet, washed with 75% ethanol, air dried, then resuspended in ultra pure water at 65°C. Samples could then be kept at -80°C until needed or used immediately.

RNA samples were purified using the Zymo DNA-free RNA kit (Section 2.5.2) and cDNA was produced using the Invitrogen SuperScript© first-strand synthesis system (Section 2.5.3). Real-time PCR was performed using SYBR Green PCR master mix (Applied Biosystems). Primer sequences for genes are shown in Table 2.2 (Section 2.5.4).

FFDC population	Femur length (mm)
A	5.5
B	5.5
C	3.0
D	7.0
E	8.0
F	7.0

Table 4.1. List of fetal femur samples utilised in molecular analysis of organotypic ALI culture.

4.3. Results

4.3.1. Pilot study

To determine the effectiveness of the organotypic protocol, FFDCs were stained with Vybrant cell tracer and aggregated in cell pellets or alginate capsules (alginate samples provided by Dr Jodie Babister, University of Southampton. See Appendix 4 for protocol). Samples were kept in organotypic ALI culture under basal media for up to 21 days. At day 1, both fetal cell pellets and alginate capsules maintained their structure (Figure 4.3 A, B). After 21 days of culture, alginate capsules were found to degrade and lose their structure (Figure 4.3 C), making it difficult to handle the samples and analyse the effects of the culture. Fetal cell pellets demonstrated cell growth and increased pellet diameter after 21 days in organotypic ALI culture (Figure 4.3 D). Both pellet and alginate 3D structures maintained cell viability up to 21 days in culture (Figure 4.3 E, F).

Alcian blue and Sirius red staining of samples at day 21 provided clear insights into the effectiveness of organotypic ALI culture. The majority of capsules were found to stain strongly for proteoglycan (blue) with small patches of collagen (red), however the stained areas, particularly those positive for Sirius red show no structural similarities to proteoglycan or collagen and were an artefact of the alginate capsule (Figure 4.4. A), this was confirmed by comparing the results with positive controls showing proteoglycan and collagen matrix production (Figure 4.4. C). Fetal pellets were found to produce a defined proteoglycan core bordered by collagen (Figure 4.4. B).
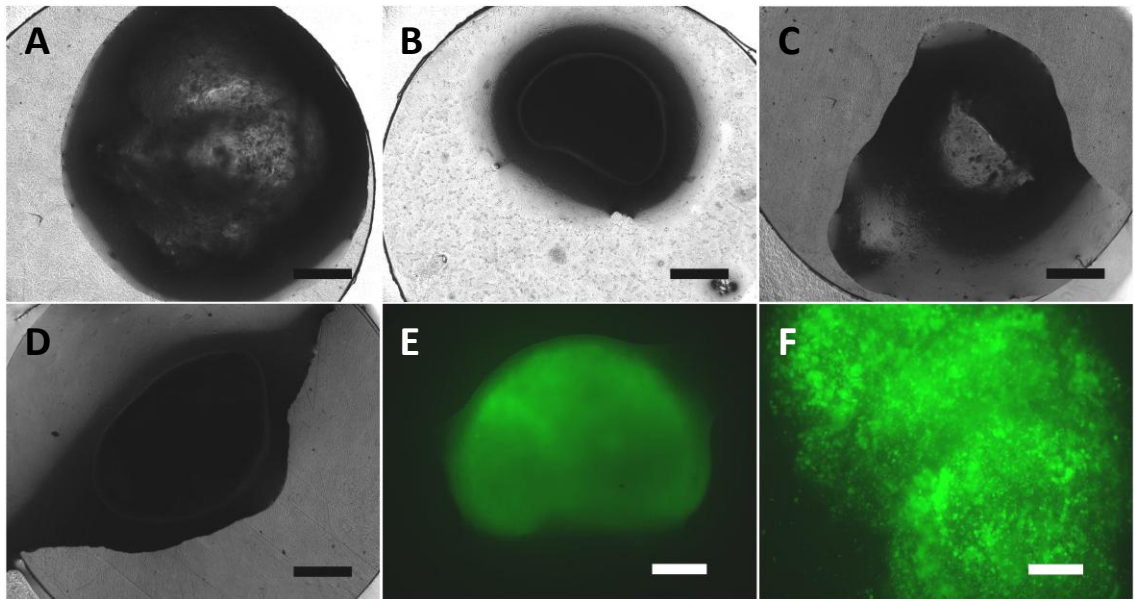
Figure 4.3. Photographs of fetal femur-derived cell samples on confetti supports *in situ*. At day 1, alginate capsules (A) and pellets (B) retained their 3D structure. By day 21 fetal cell alginate structures were found to collapse (C) while fetal pellets retained their structure and expanded in culture (D). Vybrant staining showed cells were viable at day 21 in fetal pellets (E) and alginate capsules (F). Scale bars are 500μm.
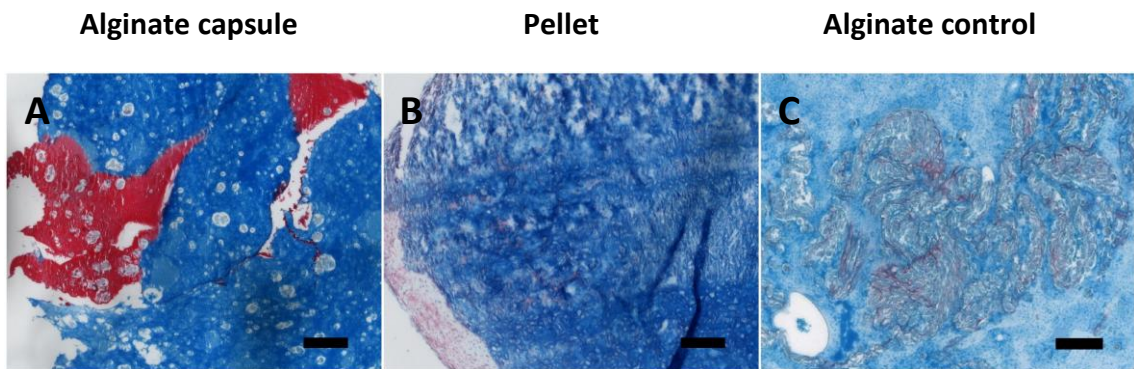
Figure 4.4. Alcian blue and Sirius red staining of FFDC alginate capsules (A) and pellets (B) at day 21 in organotypic ALI culture. A positive control for proteoglycan and collagen production in alginate capsules is shown in (C) (sample courtesy of Dr Jodie Babister, University of Southampton). Scale bars are 100μm.

4.3.2. Differentiation within organotypic pellets

Following confirmation of cell viability in organotypic ALI culture, fetal pellets were set up and grown in skeletogenic culture for up to 21 days under basal, osteogenic (ascorbate and dexamethasone) and chondrogenic (ascorbate, dexamethasone, ITS and TGF-β3) media (see Section 4.2.3).

Samples were analysed at days 1, 7, 14 and 21 for proteoglycan and collagen expression by Alcian blue/Sirius red histochemistry. Pellets at day 1 in all culture conditions stained predominantly light blue with negligible proteoglycan or collagen (Figure 4.5 A). However, in some pellets, large aggregates of collagen carried over from monolayer culture were observed. At day 21, pellets treated with basal media showed a small core of proteoglycan bordered by collagen (Figure 4.5 B), whilst pellets under osteogenic media expressed a similar phenotype but with a larger proteoglycan content, small amounts of collagen throughout the pellet and at the pellet edges (Figure 4.5 C). In contrast, chondrogenic treated pellets expressed a proteoglycan core surrounded by significant amounts of collagen and samples were observed to draw in the confetti around the pellet (Figure 4.5 D). Collagen expression was noted to be highest at sites of pellet-confetti adhesion.

After analysis of the initial results, the assay was extended to 28 days to determine if a more defined phenotype could be established with longer culture. Furthermore, due to the lack of definitive osteogenic differentiation, BMP-2 was added to the osteogenic culture conditions due to its bone-inducing role *in vivo*.
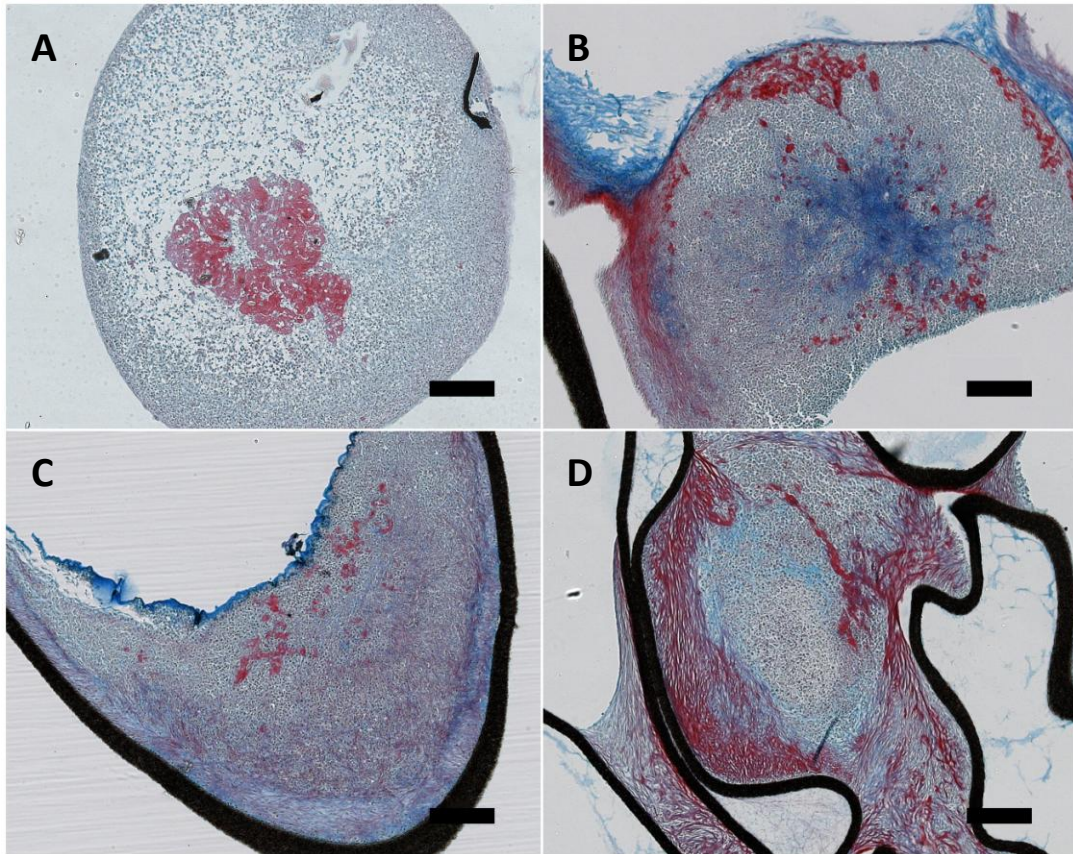
Figure 4.5. Alcian blue and Sirius red staining of fetal cell pellets showing typical expression in pellets at day 1 (A) and pellets at day 21 in organotypic ALI culture under basal (B), osteogenic (C) and chondrogenic (D) conditions. The red collagen stain present at day 1 (A) is Type I collagen carried over from monolayer culture. Scale bars are 200µm.

4.3.3. Histological analysis of 28 day organotypic ALI culture

Fetal cell pellets containing 3×10^5 cells were grown in organotypic ALI culture for up to 28 days under basal, osteogenic (+BMP-2) and chondrogenic conditions. Pellets from later time points (day 14 onwards) were found to express high levels of matrix, resulting in difficulty in extraction of RNA and protein from the samples. Therefore, initial analysis of organotypic ALI culture was predominantly performed by histology. Paraffin wax embedded samples derived from over 6 separate fetal femurs were sectioned and stained for collagen and proteoglycan matrix using Alcian blue/Sirius red histology. At day 1, pellets from all conditions expressed an undifferentiated phenotype, staining equally for proteoglycan and collagen (Figure 4.6). By day 28 of organotypic ALI culture basal-treated pellets expressed the most inconsistent phenotypes between patients but were generally found to express a mixed core of undifferentiated cells, collagen and proteoglycan bordered by aligned collagen, specifically at sites of adhesion (Figure 4.7). Pellet size was found to be crucial to the phenotype of pellets at day 28. Smaller pellets expressed higher levels of collagen both at the borders and within the core of the pellet, whilst larger pellets expressed well characterised cores of proteoglycan with reduced levels of collagen.

The majority of chondrogenic pellets were found to consistently express a core of proteoglycan bordered by large amounts of aligned collagen (Figure 4.8). The levels of collagen expressed by pellets was affected by patient variation and the size of the pellet. In pellets comprising less than 0.8mm in diameter, after 28 days of culture, the phenotype was characterised by a large amount of collagen formation with a small proteoglycan core, with the pellets showing very little growth in size. It was not uncommon for extremely small pellets to express a chiefly collagenous phenotype, with negligible proteoglycan. In contrast, pellets starting at over 0.8mm in diameter expressed a more cartilaginous phenotype at day 28, with a larger proteoglycan core and reduced levels of collagen expression (Figure 4.9).

Osteogenic pellets treated both with and without BMP-2 were found to express a phenotype strongly resembling the phenotype seen in the developing fetal femur (Figures 4.10 and 4.11). Osteogenic pellets expressed a large proteoglycan core containing small amounts of collagen, bordered by aligned collagen at sites of adhesion and at the edges of the pellets. Lacunae formation was also observed within the proteoglycan core, confirming the chondrogenic phenotype. Negligible difference was

seen between pellets of equal size when treated with and without BMP-2. However, it was noted that pellets not treated with BMP-2 showed a reduced rate of growth over 28 days of culture and pellets treated with BMP-2 were, in the majority of samples, found to be larger than those without BMP-2, potentially suggesting a BMP-2 induced increase in proliferation and growth. Due to their reduced size, pellets not treated with BMP-2 were often found to express a higher ratio of collagen than proteoglycan.

Despite all samples being seeded at the same density, it was noted that pellets from different samples demonstrated a variation in pellet size at setup of organotypic ALI culture. No correlation between femur age and propensity for specific pellet size was noted. Therefore, this variation appeared to be due to the inherent differences between patients, rather than an artefact of the stage of development at which cells were harvested. Starting pellet size was found to be crucial to the differentiation and growth of pellets over the 28 days of culture as it was noted that pellets less than 0.8mm in diameter at day 1 typically exhibited minimal growth and differentiation. Smaller pellets were found to be composed of high levels of supportive collagen which inhibited differentiation as the majority of the pellet was committed to maintaining the pellet structure. In contrast, pellets over 0.8mm in diameter at day 1 typically exhibited growth, demonstrated by an increase in pellet diameter, as well as expressing differentiation of the cell pellets.

Specific collagen expression was determined by fluorescent immunostaining for Type I and Type II collagen. At day 1, pellets expressed no new Type I collagen, but maintained small aggregates of Type I collagen recognisable as cross-over from monolayer culture (Figure 4.12 A). Type II collagen expression was variable between samples but was found to be expressed at day 1 throughout the pellet (Figure 4.12 B). At day 28, in samples treated with basal conditions, equal amounts of Type I and Type II collagen were found to be expressed at sites of adhesion and around the pellet edge (Figure 4.12 C,D). Negligible Type I collagen was found within the pellet core, while Type II collagen was expressed in small amounts throughout the pellet. Immunostaining of chondrogenic pellets again demonstrated both Type I and Type II collagen in approximately equal concentrations at sites of cell-confetti adhesion and at the pellet border. The pellet core expressed low levels of Type I collagen and large amounts of

Type II collagen (Figure 4.12 E,F). Sites of cell-air interface were principally composed of aligned Type I and II collagen. In osteogenic pellets (with BMP-2), Type I collagen was found at sites of adhesion and around the pellet boundary (Figure 4.12 G) and Type II collagen was expressed throughout the proteoglycan matrix and at the pellet boundary (Figure 4.12 H).

At day 1, expression of alkaline phosphatase (ALP) and Osteopontin (OPN) was negligible (Figure 4.13 A,B). Both ALP and OPN were expressed at sites of adhesion and at the pellet border in both basal and osteogenic pellet cultures at day 28 (Figure 4.13 C,D,G,H). This expression corresponded with areas of aligned collagen. OPN expression was also present within the pellet core in basal and osteogenic cultures, while ALP was absent. Negligible expression of ALP and OPN were found within chondrogenic pellets (Figure 4.13 E,F).

Immunostaining was also performed to determine the expression of the early chondrogenic marker, SOX9 (Figure 4.14). SOX9 expression was present within fetal cell pellets at day 1 and in all media conditions at day 28, with expression enhanced in osteogenic pellets than in basal and chondrogenic. Staining for the late osteogenic marker Osteocalcin was negligible in all samples.

In summary, effective culture and differentiation required FFDC pellets to have an initial diameter greater than 0.8mm, whereupon treatment with osteogenic media would result in a mimicry of the normal fetal femur development, characterised by a predominantly chondrogenic phenotype bordered by collagen and low levels of early osteogenic differentiation. Treatment of pellets with chondrogenic media failed to induce a true cartilage phenotype, instead resulting in a mixed phenotype of bone and cartilage-like tissue, demonstrated by a core of proteoglycan bordered by high levels of aligned Type I and Type II collagen.
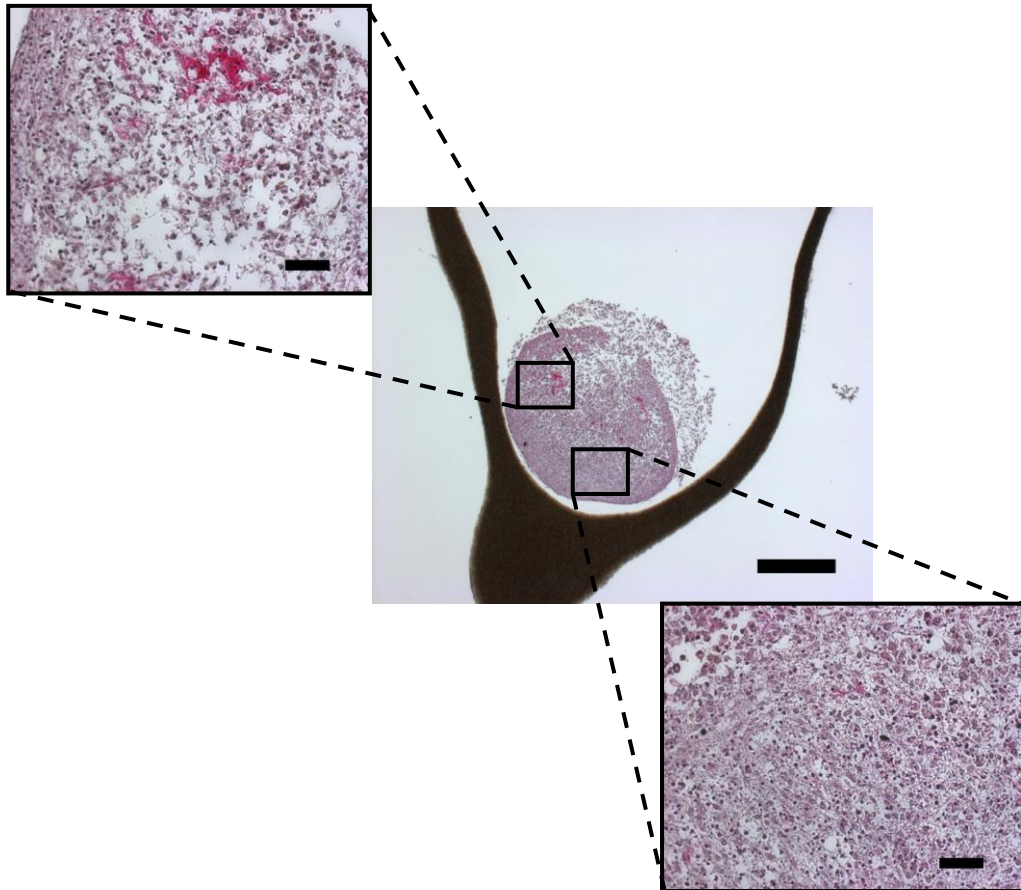
Figure 4.6. Typical example of Alcian blue (proteoglycan) and Sirius red (collagen) staining on sectioned samples from pellets at day 1 in basal culture. All pellets treated with the three media conditions were found to express the similar phenotypes at day 1. Scale bar for centre image: 500µm; for surrounding images: 50µm.
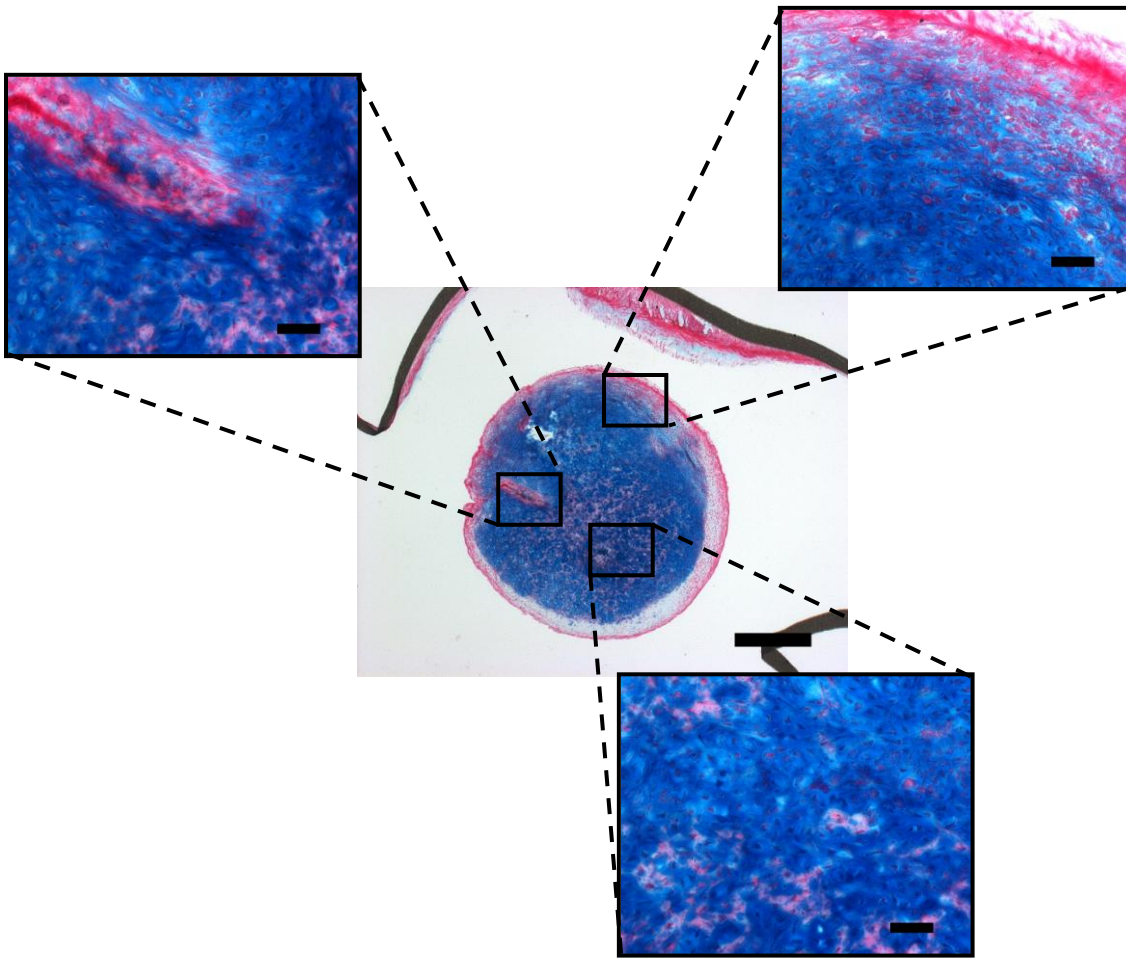
Figure 4.7. Typical example of Alcian blue (proteoglycan) and Sirius red (collagen) staining on sectioned samples from pellets after 28 days in basal conditions. Expanded images demonstrate the location-dependent differentiation of cells, with the pellet core expressing large amounts of proteoglycan and the pellet edge expressing large amounts of aligned collagen. Scale bar for centre image: 500µm; for surrounding images: 50µm.
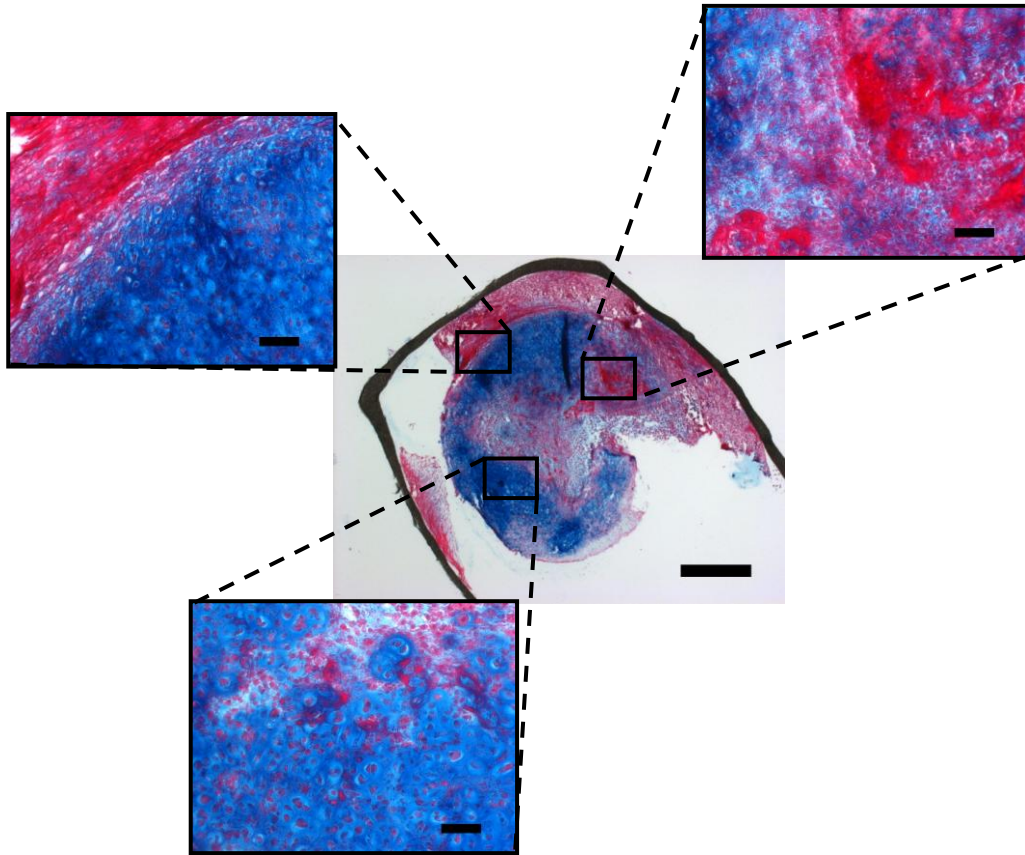
Figure 4.8. Typical example of Alcian blue (proteoglycan) and Sirius red (collagen) staining on sectioned samples from pellets after 28 days in chondrogenic conditions. Expanded images demonstrate the location-dependent differentiation of cells, with the pellet core expressing large amounts of proteoglycan and the pellet edge expressing large amount of aligned collagen. Scale bar for centre image: 500µm; for surrounding images: 50µm.
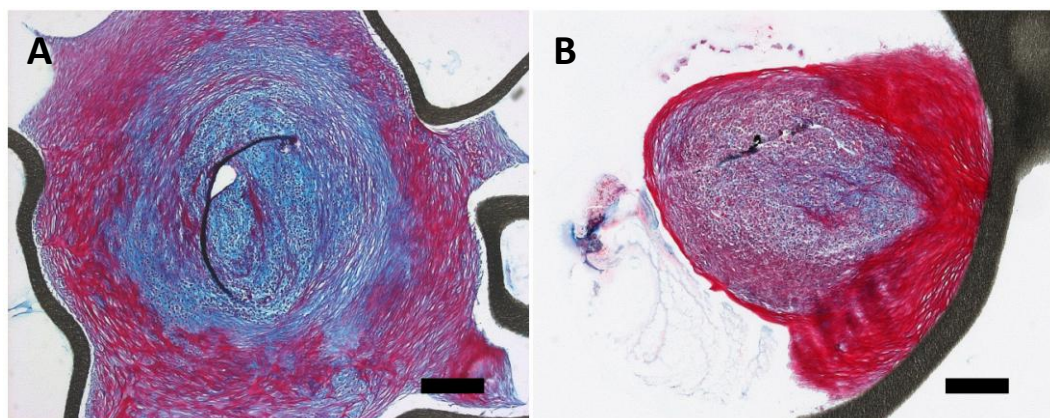
Figure 4.9. Effect of pellet size on fetal femur-derived cell pellets treated for 28 days in chondrogenic media. (A) Pellet greater than 0.8mm at day 1, (B) pellet less than 0.8mm at day 1. Scale bars; 200µm.
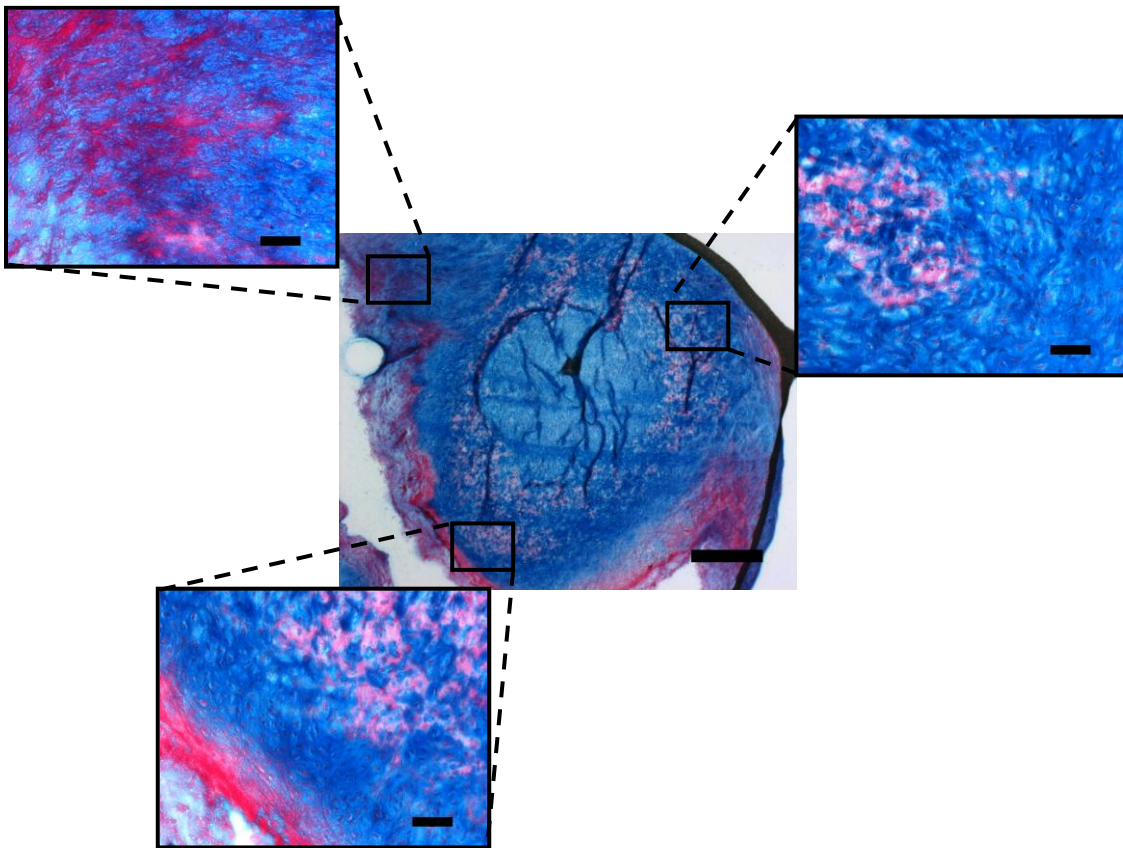
Figure 4.10. Example of Alcian blue (proteoglycan) and Sirius red (collagen) staining on sectioned samples from pellets after 28 days in osteogenic conditions. Expanded images demonstrate the location-dependent differentiation of cells, with the pellet core expressing large amounts of proteoglycan and the pellet edge expressing large amount of aligned collagen. Scale bar for centre image: 500µm; for surrounding images: 50µm.
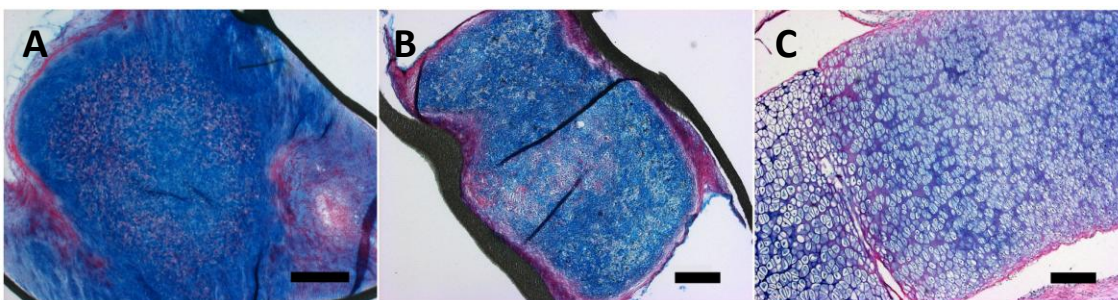
Figure 4.11. Comparison of fetal femur-derived cell pellets treated for 28 days in osteogenic media with BMP-2 (A) and without BMP-2 (B) and a fetal femur control (C). Fetal pellets with and without BMP-2 express similar phenotypes, with those treated with BMP-2 being larger. Fetal pellets treated with osteogenic media express phenotypes strongly resembling that of the developing femur, with a proteoglycan-rich cartilaginous core bordered by collagen. Scale bars; (A) 500µm, (B, C) 200µm.
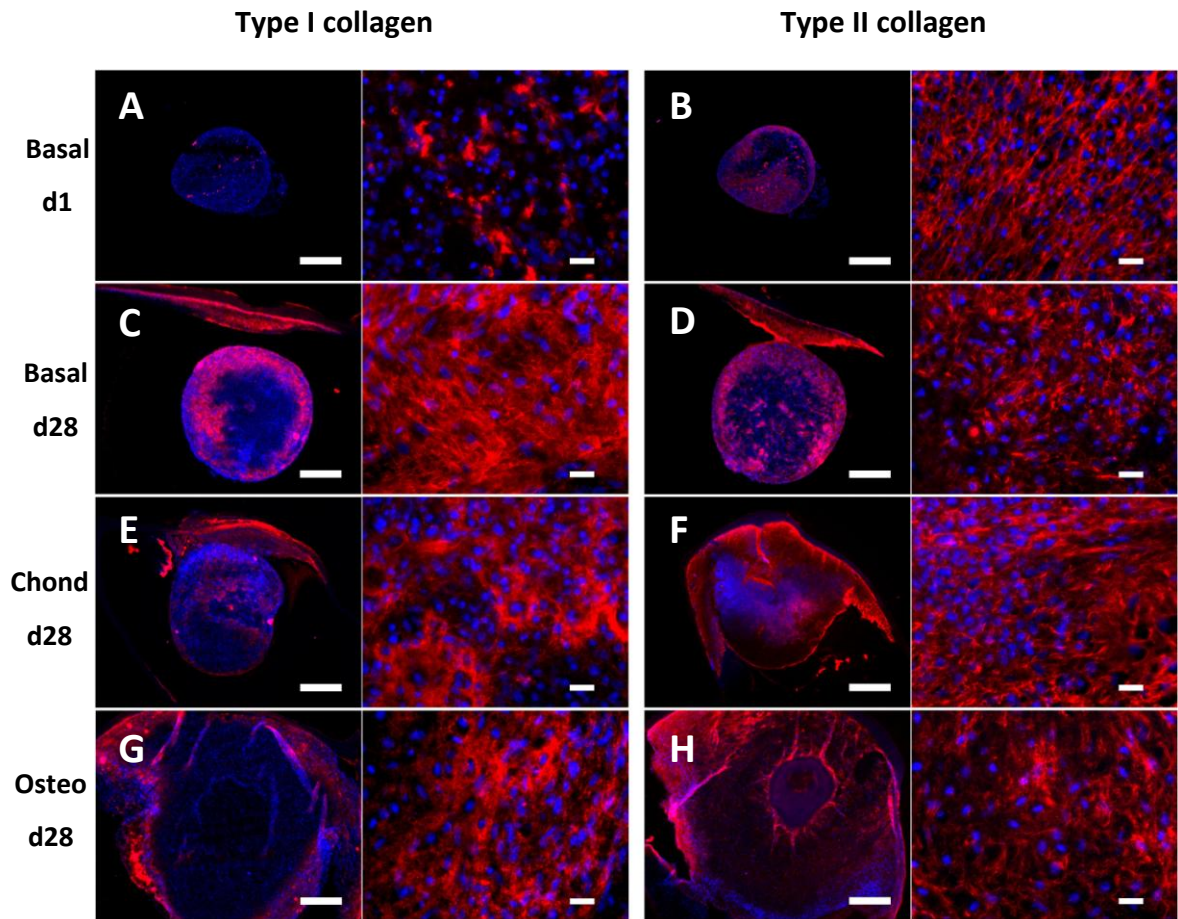
Figure 4.12. Whole pellet and high magnification images of fluorescent immunostaining for Type I and Type II collagen. Bone-specific Type I collagen (red) and cell nuclei (blue) on sectioned samples from pellets at day 1 (A); day 28 basal (C); day 28 chondrogenic (E) and day 28 osteogenic (+BMP-2) (G). Cartilage-specific Type II collagen (red) and cell nuclei (blue) on sectioned samples from pellets at day 1 (B); day 28 basal (D); day 28 chondrogenic (F) and day 28 osteogenic (H). Scale bars: Whole pellet, 500µm; high magnification, 20µm.

Alkaline phosphatase　　　　　**Osteopontin**
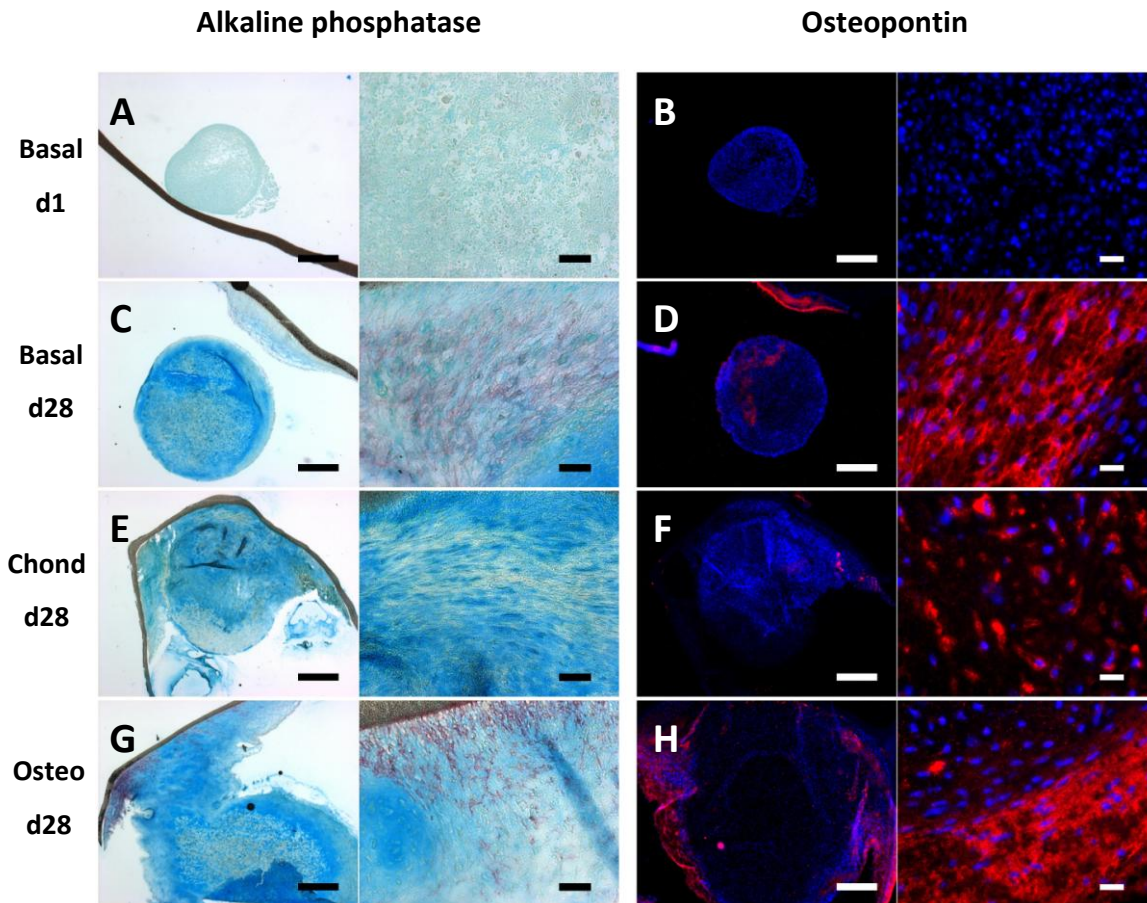
Figure 4.13. Whole pellet and high magnification images of the osteogenic markers alkaline phosphatase and Osteopontin. Alkaline phosphatase staining on sectioned samples from pellets at day 1 (A); day 28 basal (C); day 28 chondrogenic (E) and day 28 osteogenic (+BMP-2) (G). Osteopontin (red) and cell nuclei (blue) staining on sectioned samples from pellets at day 1 (B); day 28 basal (D); day 28 chondrogenic (F) and day 28 osteogenic (H). Colour scale bars: Whole pellet, 500μm; high magnification, 50μm. Fluorescent scale bars: Whole pellet, 500μm; high magnification, 20μm.
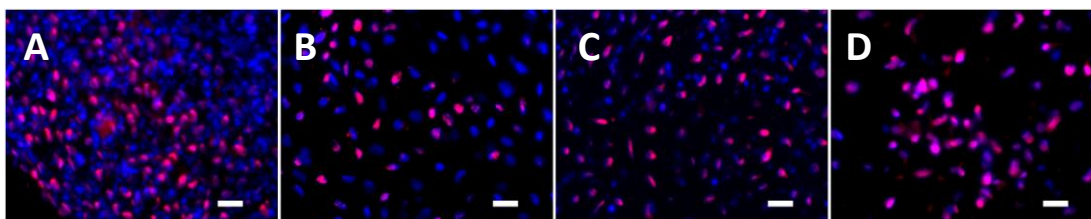
Figure 4.14. SOX9 expression (red) and cell nuclei (blue) in sectioned samples from pellets at day 1 (A); day 28 basal (B); day 28 chondrogenic (C) and day 28 osteogenic (D).

4.3.4. Biochemical analysis of alkaline phosphatase activity

Analysis of the specific alkaline phosphatase activity (Figure 4.15) in samples from 4 separate fetal populations (n=4 pellets/sample, analysis repeated 3 times for each sample) demonstrated the levels of variation between patients. By day 28 of organotypic culture the levels of ALP expression were significantly greater in cultures treated with osteogenic media in all samples. Basal expression of ALP was significantly greater than observed in chondrogenic cultures in 3 of the 4 populations. Chondrogenic cultures were consistently observed to express minimal ALP activity.
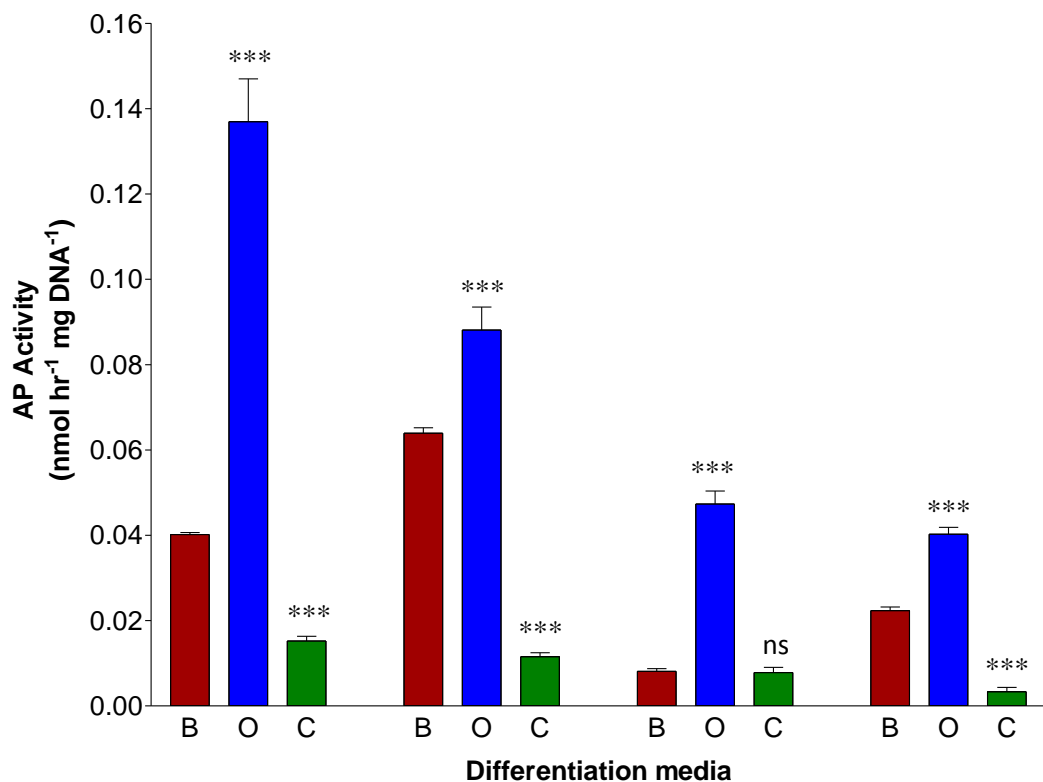
Figure 4.15. Biochemical analysis of specific alkaline phosphatase activity in 4 separate fetal cell populations after 28 day organotypic ALI culture (BMP-2 included in osteogenic conditions). Alkaline phosphatase concentration and total DNA concentration were compared to provide the specific alkaline phosphatase activity, n=4. Key: B, Basal; O, Osteogenic; C, Chondrogenic. Data represents mean ± SD; ns = non-significant, *** = p ≤ 0.001.

4.3.5. Molecular analysis of 28 day organotypic ALI culture

4.3.5.1. SOX9

During development, *SOX9* is expressed in all chondroprogenitors and non-hypertrophic chondrocytes and is a key marker for chondrogenesis. *SOX9* expression was significantly ($p<0.05$ or greater) increased in pellets treated with osteogenic and chondrogenic media over 28 days of culture, while only half of the samples cultured in basal conditions demonstrated a significant increase in *SOX9* expression (Appendix 5). By day 28 of culture, *SOX9* expression was significantly greater ($p<0.01$ or less) in osteogenic conditions than in basal or chondrogenic conditions in all samples (Figure 4.16). Pellets in chondrogenic conditions expressed *SOX9* at levels equal to or greater than basal samples. These results indicate a strong chondrogenic phenotype experienced in pellets treated with osteogenic media. Pellets treated with chondrogenic media also experienced a chondrogenic phenotype, albeit significantly less than pellets in osteogenic media.

4.3.5.2. Type II collagen

Type II collagen is another key marker for chondrogenesis. Synthesised by chondrocytes, Type II collagen is prevalent throughout the extracellular matrix of cartilage tissue. All samples treated with osteogenic media demonstrated very significant increase ($p<0.005$) in Type II collagen expression between day 1 and day 28 of culture. The majority of samples (4 out of 6) treated with basal media exhibited no significant change in expression over 28 days of culture, while treatment with chondrogenic media resulted in half of the samples demonstrating significant increase and the other half demonstrating negligible change in expression (Appendix 5). By day 28, all populations demonstrated a significantly greater ($p<0.001$) expression of Type II collagen in osteogenic samples than the other two conditions, with chondrogenic pellets expressing significantly higher levels ($p<0.001$) than basal pellets in all but one sample (Figure 4.17). This coincides with the histological analysis of Type II collagen, which demonstrates a high level of Type II collagen throughout pellets in osteogenic conditions and enhanced collagen matrix in pellets treated with chondrogenic conditions in comparison to basal cultures.

124

4.3.5.3. RUNX2

RUNX2 is essential for induction of chondrocyte hypertrophy, as well as differentiation of osteoblasts. As such, it plays a key role in the transformation of cartilage to bone via endochondral ossification. Comparison of samples at day 1 and day 28 demonstrated negligible change in *RUNX2* expression in the majority of samples treated with basal media, but demonstrated significant increase of *RUNX2* expression in samples treated with osteogenic and chondrogenic media for 28 days (Appendix 5). By day 28, all but one of the samples analysed demonstrated significantly higher levels of *RUNX2* in chondrogenic pellets than the basal pellets ($p<0.05$ or less), suggesting that this condition resulted in an increase in *RUNX2* expression (Figure 4.18). 4 out of 7 samples showed significant increase in expression between osteogenic and basal conditions ($p< 0.05$ or less). This data suggests that both osteogenic and chondrogenic conditions induce upregulation of *RUNX2* expression. In the majority of samples (4 out of 7), *RUNX2* expression between osteogenic and chondrogenic conditions demonstrated no significant difference, while the remaining samples vary between osteogenic and chondrogenic conditions demonstrating higher expression than the other. Taken as a whole, these results suggest that both osteogenic and chondrogenic media induce *RUNX2* expression at similar levels, indicative of chondrocyte hypertrophy and early osteogenesis.

4.3.5.4. Alkaline phosphatase (ALP)

Alkaline phosphatase is found on the surface of osteoblasts and is thought to play a key role in the calcification of bone. *ALP* is regularly used as a marker for bone formation. Samples treated with basal and osteogenic media demonstrated significant increase in *ALP* expression over 28 days in culture, while only half of the samples treated with chondrogenic media demonstrated significant increase, with the other half demonstrating negligible change (Appendix 5). By day 28, osteogenic conditions demonstrated a significantly larger expression of *ALP* than chondrogenic conditions in all but one population ($p<0.05$ or less, Figure 4.19), corresponding with the histological analysis. Basal conditions expressed a large degree of variation in *ALP* activity, being greater than osteogenic conditions in some populations and less in others. The reason for the diverse differences between basal and osteogenic conditions is unknown, but was likely due to natural variation between populations and not a result of fetal femur

age or other known variables, as cells from femurs of similar ages demonstrated markedly different *ALP* expression. Chondrogenic *ALP* expression was minimal and less than that of basal conditions in all populations.

4.3.5.5. Type I collagen

The osteogenic marker, Type I collagen, comprises approximately 80-90% of all protein in the extracellular matrix of bone. Type I collagen expression was significantly increased in comparison to day 1 expression levels in the majority of samples treated with basal and chondrogenic media for 28 days, while only half of the samples treated with osteogenic media demonstrated significant increase, with the other half demonstrating negligible change (Appendix 5). By day 28 of culture, Type I collagen expression was significantly greater in chondrogenic conditions than in basal conditions in all but one population ($p < 0.05$ or less) and was significantly greater in chondrogenic conditions than in osteogenic conditions in all samples (Figure 4.20). This coincides with histological analysis that demonstrates a large quantity of Type I collagen in chondrogenic pellets in comparison to osteogenic pellets. As observed in the analysis of ALP expression, the pellets from basal conditions exhibit high levels of variation in their relative expression of Type I collagen.

4.3.5.6. Osteocalcin

Osteocalcin is secreted by osteoblasts and is considered a marker for late stages of osteoblast differentiation. Negligible change was observed in Osteocalcin expression when pellets from day 1 and day 28 of culture were compared for samples grown in basal, osteogenic and chondrogenic conditions (Appendix 5). In the majority of populations (4 out of 6), by day 28, no significant difference was observed between Osteocalcin expression in basal, osteogenic and chondrogenic conditions and no obvious trend could be distinguished in Osteocalcin expression (Figure 4.21). In those populations where Osteocalcin expression does show a significant change between conditions, expression of Osteocalcin is lower in osteogenic and chondrogenic conditions than in basal. This data, supported by the lack of positive Osteocalcin staining in pellets, indicates that no late osteogenic activity can be attributed to induction by any of the media conditions.

126

In summary, a high level of variation was observed between different populations in the expression of specific genes in pellets grown in basal conditions, hinting at natural diversity between separate populations. While there is no distinct known reason for the variance observed in basal culture, analysis of the samples used and their results confirmed that this diversity was not due to the age of the fetal femur the cells were isolated from. However, it is hypothesised that the variance is due to natural variation in cell differentiation between separate populations, and variance in starting pellet diameter at day 1. It has already been noted that despite matching seeding densities, different populations of FFDCs will establish different pellet sizes, a factor that is also known to affect differentiation (see Section 4.3.3). Despite the variance observed, organotypic ALI culture of pellets in osteogenic media resulted in a recurring molecular phenotype, defined by an increased expression of *SOX9*, Type II collagen, *RUNX2* and *ALP*, with variable levels of Type I collagen expression. These results are indicative of a strong chondrogenic phenotype beginning to undergo chondrocyte hypertrophy and early bone formation. Pellets cultured in chondrogenic media also demonstrated an increase in *SOX9, RUNX2* and Type II collagen expression, albeit at levels less than samples treated with osteogenic media, suggestive of some chondrogenic activity. Pellets in chondrogenic media expressed significantly higher levels of Type I collagen than any other condition but expressed negligible *ALP*, indicating early osteogenic activity but lack of matrix calcification.
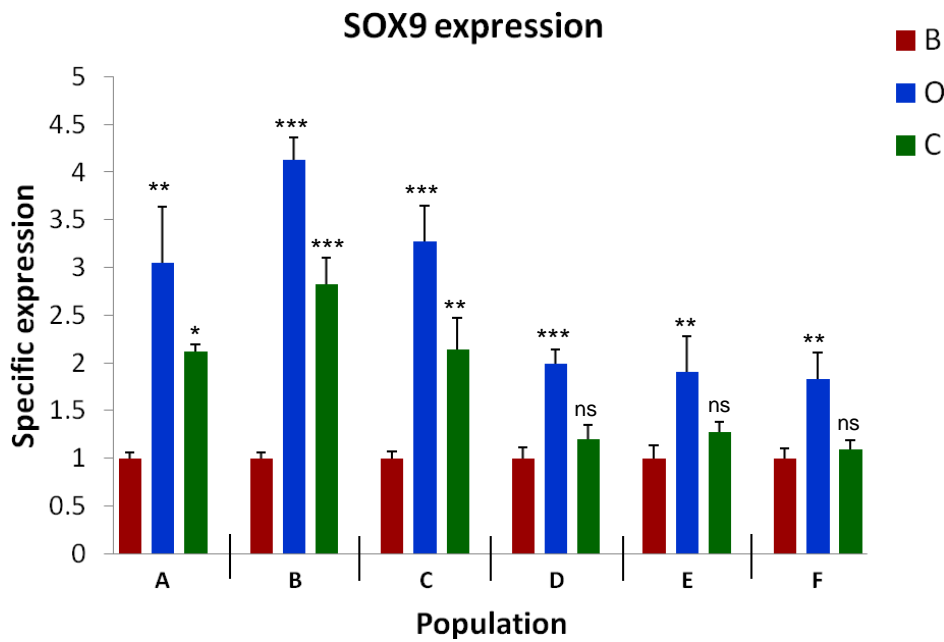
Figure 4.16. Expression of *SOX9* in various fetal cell populations grown in organotypic conditions. Gene expression was compared between basal, osteogenic and chondrogenic treated samples at d28. Key: B, Basal; O, Osteogenic; C, Chondrogenic. Data represents mean ± SD, n=3. Statistical significance of increase/decrease compared to basal conditions shown as: ns = non significant,* = p<0.05, ** = p<0.01, *** = p<0.001.
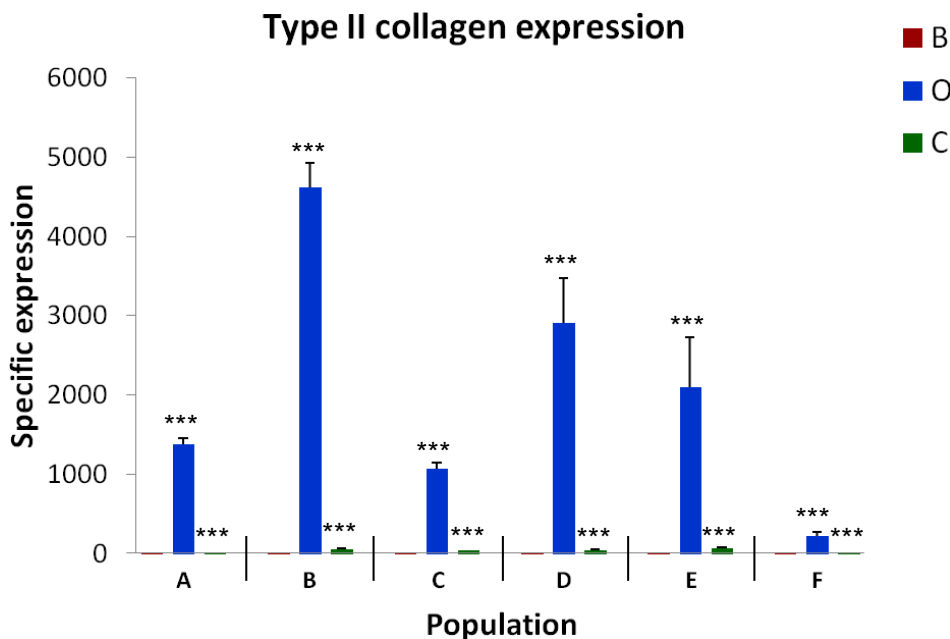
Figure 4.17. Expression of Type II collagen in various fetal cell populations grown in organotypic conditions. Gene expression was compared between basal, osteogenic and chondrogenic treated samples at d28. Key: B, Basal; O, Osteogenic; C, Chondrogenic. Data represents mean ± SD, n=3. Statistical significance of increase/decrease compared to basal conditions shown as: ns = non significant, *** = p<0.001.

128
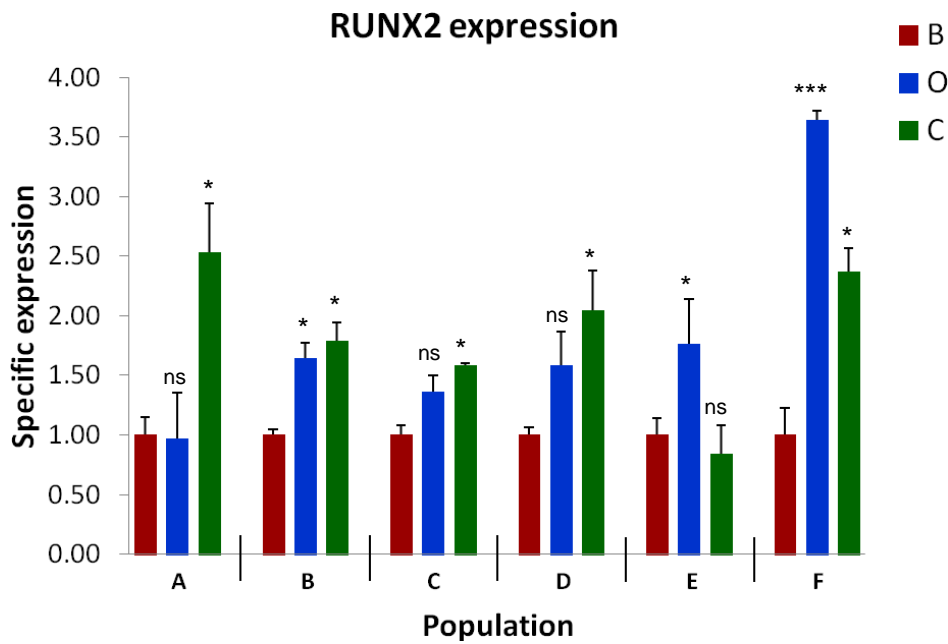
Figure 4.18. Expression of *RUNX2* in various fetal cell populations grown in organotypic conditions. Gene expression was compared between basal, osteogenic and chondrogenic treated samples at d28. Key: B, Basal; O, Osteogenic; C, Chondrogenic. Data represents mean ± SD, n=3. Statistical significance of increase/decrease compared to basal conditions shown as: ns = non significant,* = p<0.05, *** = p<0.001.
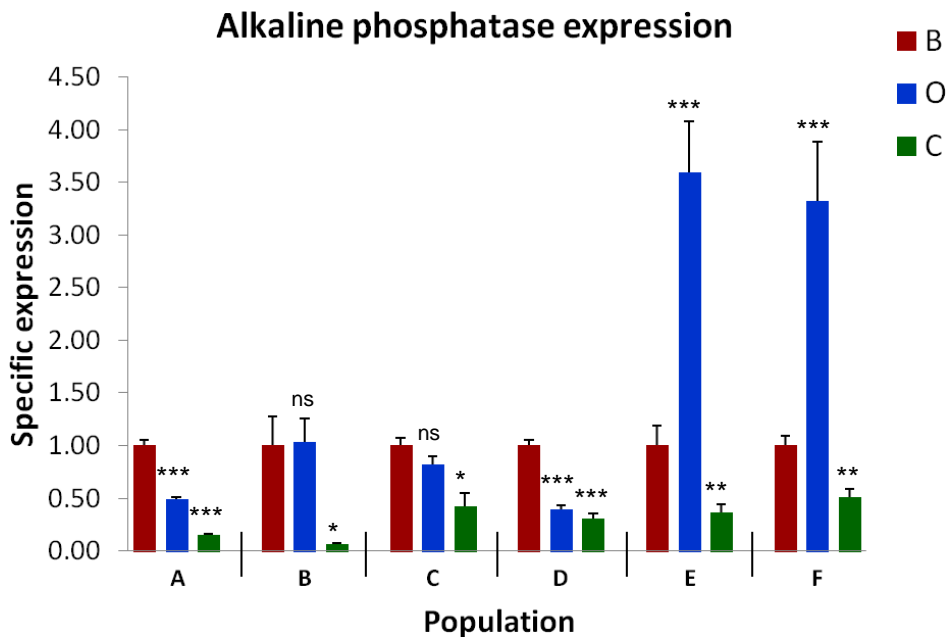
Figure 4.19. Expression of *ALP* in seven different fetal cell populations grown in organotypic conditions. Gene expression was compared between basal, osteogenic and chondrogenic treated samples at d28. Key: B, Basal; O, Osteogenic; C, Chondrogenic. Data represents mean ± SD, n=3. Statistical significance of increase/decrease compared to basal conditions shown as: ns = non significant,* = p<0.05, ** = p<0.01, *** = p<0.001.

129
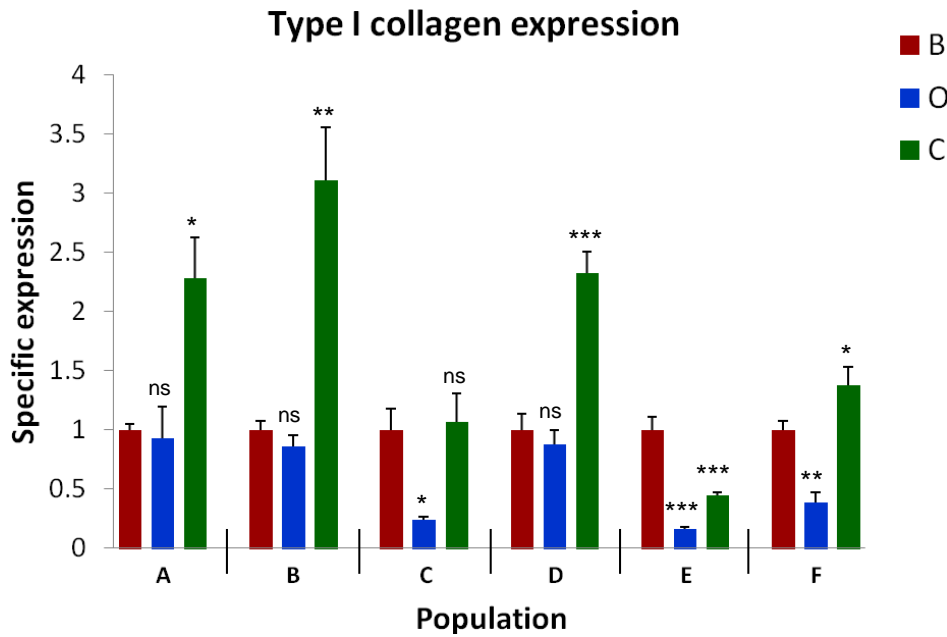
Figure 4.20. Expression of Type I collagen in six different fetal cell populations grown in organotypic conditions. Gene expression was compared between basal, osteogenic and chondrogenic treated samples at d28. Key: B, Basal; O, Osteogenic; C, Chondrogenic. Data represents mean ± SD, n=3. Statistical significance of increase/decrease compared to basal conditions shown as: ns = non significant,* = $p<0.05$, ** = $p<0.01$, *** = $p<0.001$.
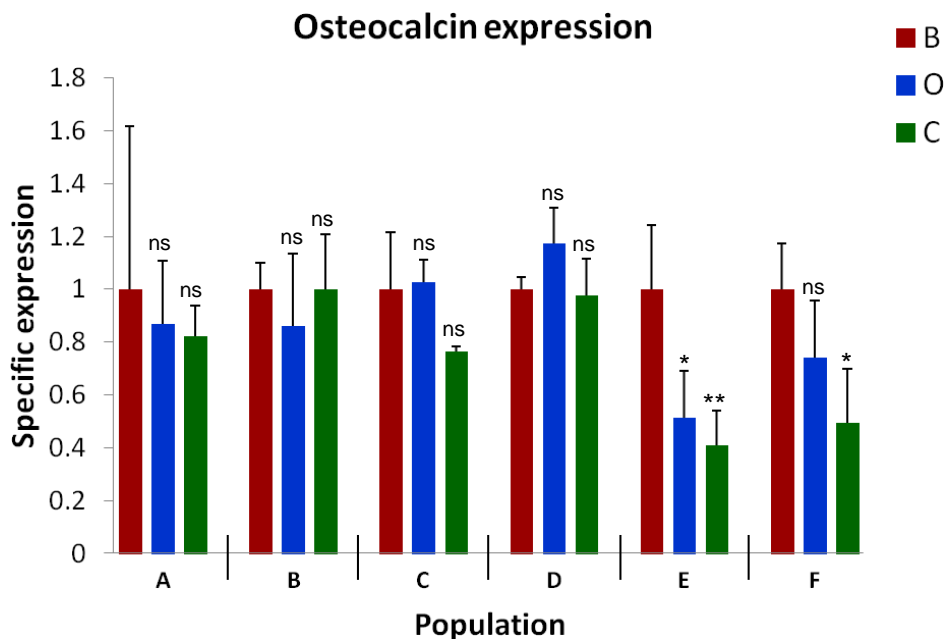
Figure 4.21. Expression of Osteocalcin in various fetal cell populations grown in organotypic conditions. Gene expression was compared between basal, osteogenic and chondrogenic treated samples at d28. Key: B, Basal; O, Osteogenic; C, Chondrogenic. Data represents mean ± SD, n=3. Statistical significance of increase/decrease compared to basal conditions shown as: ns = non significant,* = $p<0.05$, ** = $p<0.01$.

130

4.3.6. Effects of different differentiation-factors on the organotypic model

4.3.6.1. Removal of dexamethasone from differentiation media

Samples from 6 separate populations treated with osteogenic and chondrogenic media without dexamethasone were sectioned and stained for collagen and proteoglycan matrix using Alcian blue/Sirius red histology. At day 1, pellets from all conditions expressed an undifferentiated phenotype Identical to that of samples treated with dexamethasone. By day 28 of organotypic ALI culture, removal of dexamethasone from the chondrogenic media resulted in consistent expression of a chondrogenic phenotype when pellets were greater than 0.8mm in diameter at day 1; characterised by proteoglycan bordered by small amounts of supporting collagen (Figure 4.22). Pellets less than 0.8mm in diameter produced higher levels of supporting collagen similar to those treated with dexamethasone, confirming the role of pellet size on differentiation. Pellets treated with osteogenic media without dexamethasone expressed a phenotype closely matching that of pellets treated with dexamethasone, and therefore similar to the phenotype of the developing femur, but with a reduced size at day 28, resulting in slightly higher levels of collagen expression (Figure 4.23).
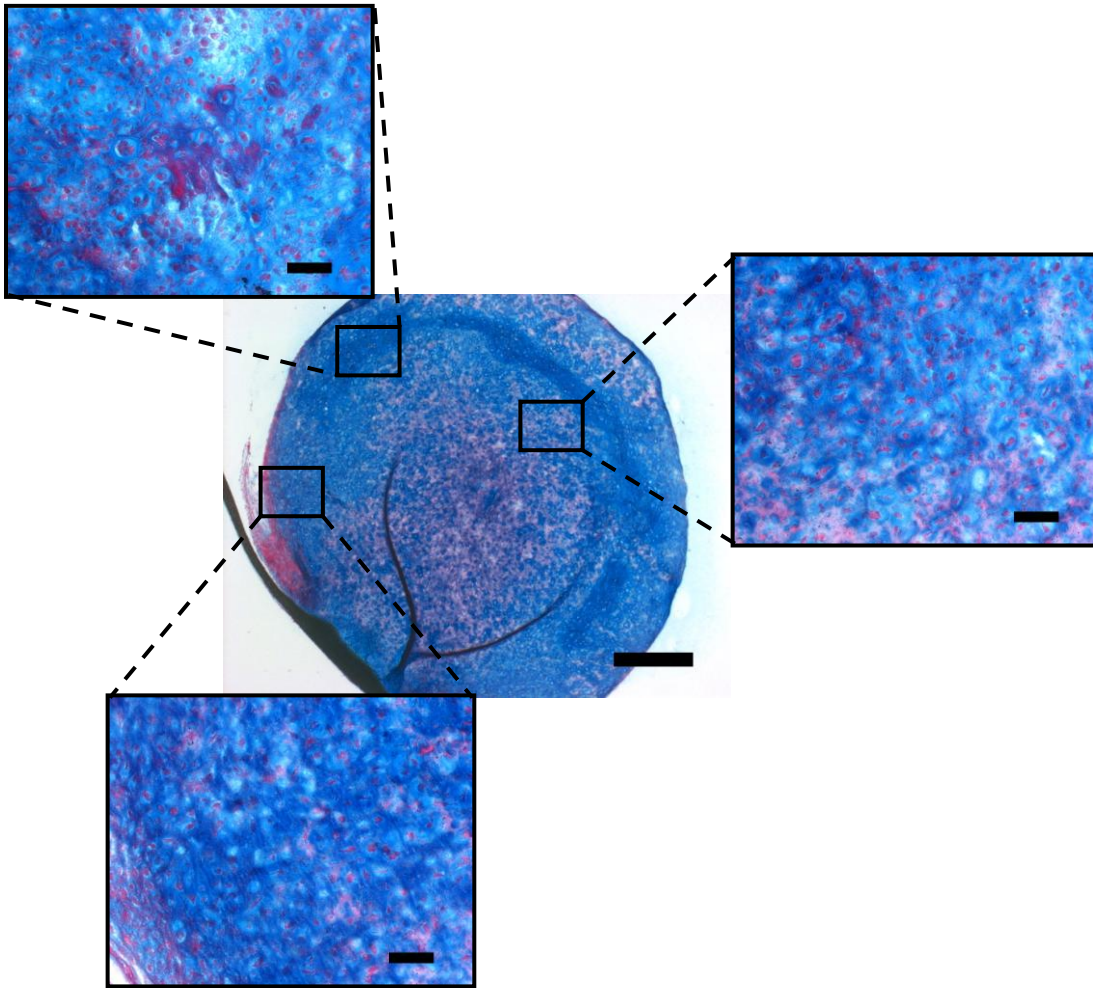
Figure 4.22. Example of Alcian blue (proteoglycan) and Sirius red (collagen) staining on sectioned samples from pellets after 28 days in chondrogenic conditions without dexamethasone (>0.8mm diameter at day 1). Expanded images demonstrate the location-dependent differentiation of cells, with the pellet core expressing large amounts of proteoglycan and the pellet edge expressing minimal aligned collagen. Scale bar for centre image: 500µm; for surrounding images: 50µm.
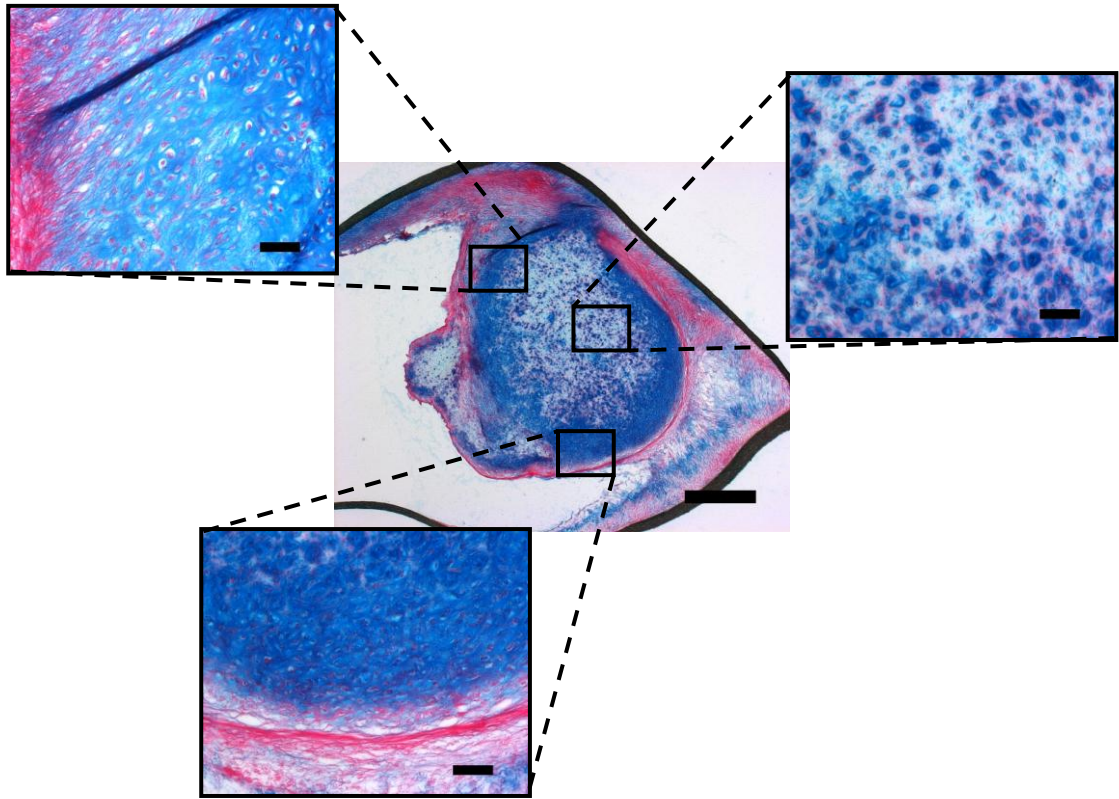
Figure 4.23. Example of Alcian blue (proteoglycan) and Sirius red (collagen) staining on sectioned samples from pellets after 28 days in osteogenic conditions without dexamethasone (>0.8mm diameter at day 1). Expanded images demonstrate the location-dependent differentiation of cells, with the pellet core expressing large amounts of proteoglycan and the pellet edge expressing large amount of aligned collagen Scale bar for centre image: 500µm; for surrounding images: 50µm.

At day 28, samples treated with chondrogenic media without dexamethasone demonstrated minimal Type I collagen, only located at the pellet edge and sites of cell-confetti adhesion (Figure 4.24 A), while Type II collagen was expressed throughout the pellet and in high levels at the pellet border (Figure 4.24 B). Similar to pellets treated with dexamethasone, sites of cell-air interface were composed of aligned Type I and II collagen. Expression of collagen in osteogenic pellets without dexamethasone was comparative to those treated with dexamethasone, with Type I collagen expressed at sites of adhesion and around the pellet boundary (Figure 4.24 C) and Type II collagen expressed throughout the proteoglycan matrix and at the pellet boundary (Figure 4.24 D).

At day 28 without dexamethasone, no expression of ALP was found within chondrogenic pellets (Figure 4.25 A), but was expressed at sites of adhesion and at the pellet border in osteogenic pellet cultures (Figure 4.25 C). This expression corresponded with areas of aligned collagen. Modest OPN expression was present within the pellet core of both chondrogenic and osteogenic cultures, but was found in significant levels in osteogenic pellets at the pellet border and sites of cell-confetti adhesion (Figure 4.25 B,D). SOX9 was present within both osteogenic and chondrogenic fetal cell pellets at day 28 without dexamethasone (Figure 4.26). Expression of SOX9 was stronger in chondrogenic pellets than in those treated with osteogenic media. As with pellets treated with dexamethasone, staining for the late osteogenic marker Osteocalcin was negligible in all samples.

In summary, provided pellets were greater than 0.8mm in diameter at day 1 of culture, removal of dexamethasone resulted in induction of a strong cartilage-like phenotype In samples treated with chondrogenic media, characterised by high levels of proteoglycan, Type II collagen, and SOX9. Minor Type I collagen and negligible ALP expression further indicated a chondrogenic phenotype. Removal of dexamethasone from osteogenic media resulted in minimal difference to previous samples cultured with dexamethasone, characterised by a cartilaginous core, bordered by region undergoing early osteogenesis. A decrease in pellet growth over 28 days and a reduced expression of SOX9 was noted in osteogenic conditions. Both conditions expressed modest expression of OPN, especially at sites of Type I collagen expression such as the pellet border, indicative of low levels of chondrocyte hypertrophy and osteogenesis.
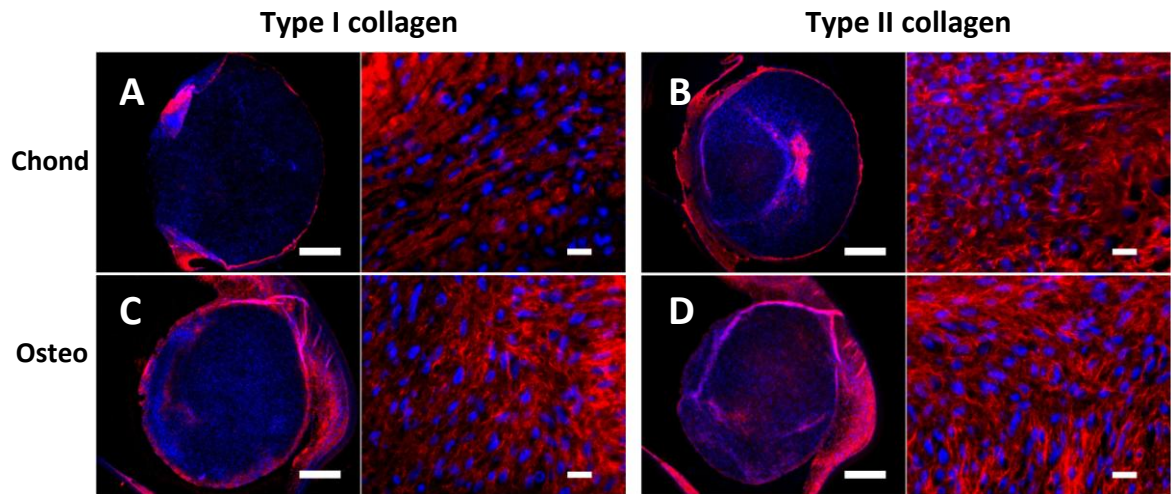
Figure 4.24. Whole pellet and high magnification images of fluorescent immunostaining for Type I and Type II collagen. Bone-specific Type I collagen (red) and cell nuclei (blue) on sectioned samples from pellets at day 28 without dexamethasone. (A) Chondrogenic and (C) osteogenic. Cartilage-specific Type II collagen (red) and cell nuclei (blue) on sectioned samples from pellets at day 28 without dexamethasone. (B) Chondrogenic and (D) osteogenic. Scale bars: Whole pellet, 500µm; high magnification, 20µm.
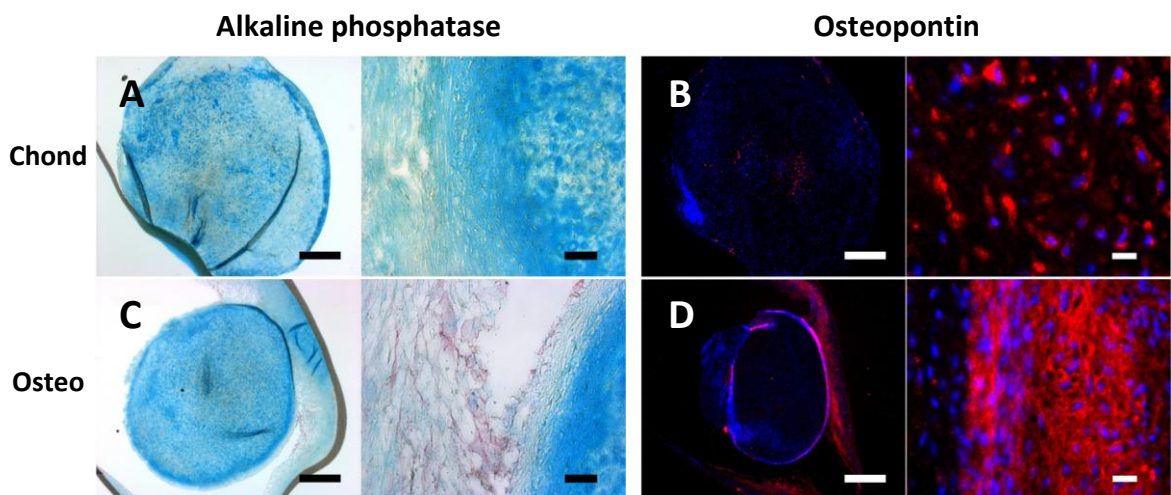
Figure 4.25. Whole pellet and high magnification images of the osteogenic markers alkaline phosphatase and Osteopontin. Alkaline phosphatase staining on sectioned samples from pellets at day 28 without dexamethasone in (A) chondrogenic and (C) osteogenic media. Osteopontin (red) and cell nuclei (blue) staining on sectioned samples from pellets at day 28 without dexamethasone in (B) chondrogenic and (D) osteogenic media. Colour scale bars: Whole pellet, 500µm; high magnification, 50µm. Fluorescent scale bars: Whole pellet, 500µm; high magnification, 20µm.
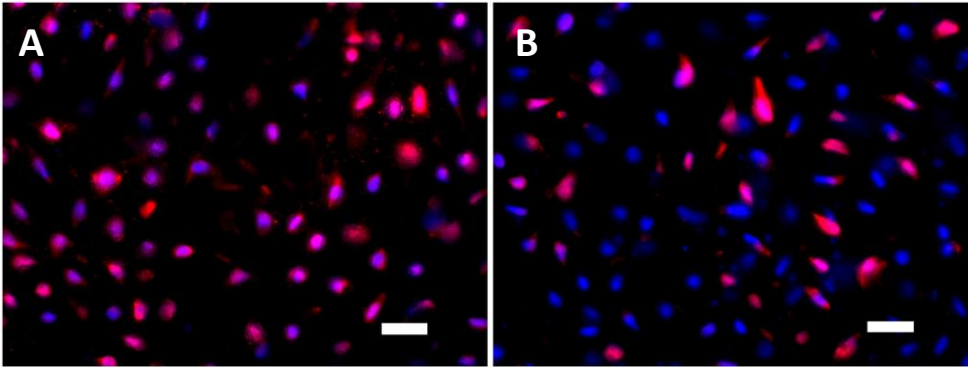
Figure 4.26. SOX9 expression (red) and cell nuclei (blue) in sectioned samples from pellets at day 28 chondrogenic (A) and day 28 osteogenic (B) without dexamethasone. Scale bars: 20μm.

4.3.6.2. Effects of 1,25-dihydroxyvitamin D3 on osteogenic culture

In an attempt to induce a late osteogenic phenotype, vitamin D was added to the osteogenic media and used to culture 3 separate samples for 28 days. Samples were then sectioned and subjected to histological analysis for various osteogenic and chondrogenic markers (Figure 4.27). At day 1, pellets from all conditions expressed an undifferentiated phenotype as seen in all previous experiments. Addition of vitamin D to the osteogenic media resulted in a phenotype expressing a large core of proteoglycan bordered by high levels of both Type I and Type II collagen. Type II collagen was also present within the proteoglycan core, while Type I collagen was absent.

Cultures treated with vitamin D demonstrated expression of ALP greater than in those treated without vitamin D, expressed at sites of adhesion and at the pellet border, especially in areas of aligned collagen. OPN expression was present in significant levels in vitamin D-treated pellets at the pellet border and sites of cell-confetti adhesion but negligible within the pellet core. Minor Osteocalcin staining was observed at the pellet border, located mostly at areas rich in collagen and ALP. Moderate expression of SOX9 was present throughout the pellet at day 28.
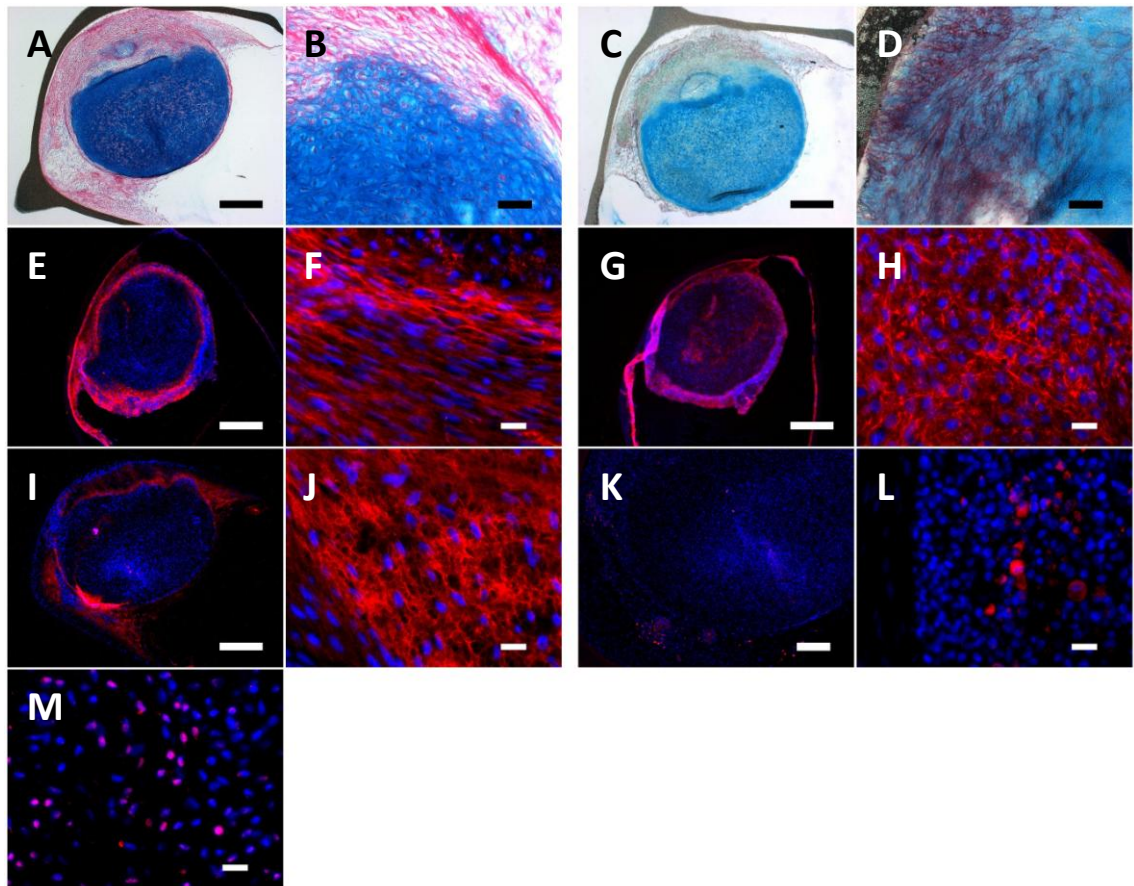
Figure 4.27. Whole pellet and high magnification images demonstrating expression of various osteogenic and chondrogenic markers in vitamin D-treated pellets at day 28. (A, B) Alcian blue (proteoglycan) and Sirius red (collagen) staining; (C, D) alkaline phosphatase staining; (E, F) Type I collagen staining; (G, H) Type II collagen staining; (I, J) Osteopontin staining; (K, L) Osteocalcin staining; and (M) SOX9 staining. Fluorescent images are depicted as the active stain (red) and the nuclear counterstain, DAPI (blue). n=3, colour scale bars: Whole pellet, 500µm; high magnification, 50µm. Fluorescent scale bars: Whole pellet, (E, G, I) 500µm, (K) 200µm; high magnification, 20µm.

4.3.7. Summary of organotypic ALI culture and resulting phenotypes

| Media condition | Expression of specific markers | | | | | | | | | | | Phenotype |
| | Proteoglycan core | Type I Collagen | | Type II Collagen | | ALP | | OPN | | SOX9 | | |
		C	B	C	B	C	B	C	B	C	B	
Basal	++	+	++	++	++	-	+	+	++	+	+	Cartilage/bone
Osteogenic												
+Dex	+++	-	++	+++	+++	-	+	-	++	++	++	Fetal femur-like
-Dex	++	-	++	+++	+++	-	+	-	++	+	+	Cartilage/bone
Vitamin D	++	-	+++	+++	+++	-	++	-	++	+	+	Cartilage/bone
Chondrogenic												
+Dex	++	++	++	+++	+++	-	-	-	-	++	++	Cartilage/bone
-Dex	+++	-	+	++	++	-	-	-	-	+++	++	Cartilage

Table 4.2. Summary of histological analysis of fetal femur cell pellets under different differentiation conditions for 28 days. Specific marker expression at the pellet core (C) and the pellet edge (B) is shown. Data applies only to pellets greater than 0.8mm diameter at day 1. Key: C, core; B, pellet border; ALP, alkaline phosphatase; OPN, Osteopontin; Dex, dexamethasone; +++ = ubiquitous/strong expression, ++ = moderate expression, + = minor expression, - = negligible/no expression.

4.4. Discussion

FFDCs have been shown to possess multipotentcy and are able to undergo differentiation into bone and fat in monolayer culture and chondrogenic differentiation in 3D pellet cultures (Mirmalek-Sani et al. 2006). Furthermore, previous studies have demonstrated the ability of scaffold-based FFDCs to aid in regeneration of bone defects in mice (Kanczler et al. 2009). However, very few studies have investigated the potential of these cells as a model for skeletal tissues. As previously mentioned, use of organotypic ALI culture has been demonstrated as a successful method for mimicking normal tissue growth *ex vivo*. This study has demonstrated the growth and differentiation of fetal femur-derived cell pellets in 3D organotypic ALI culture when treated with basal, osteogenic and chondrogenic media, demonstrating the potential use of organotypic ALI culture in *ex vivo* 3D expansion and in development of a novel model for skeletogenesis.

Fetal femur-derived cell populations were extracted from fetal femurs ranging in age from 7 to 12 weeks post-conception. Cells extracted from distinct patients express different differentiation and growth potential when cultured in pellet form. This inherent variation was evident in pellet growth during culture over 28 days and caused substantial variation in results of different cell populations treated under identical conditions. Due to this, analysis of the effects of basal, osteogenic and chondrogenic media proved problematic, requiring multiple repeats to determine the standard effect of organotypic ALI culture. For pellet culture to be considered for high throughput screening, it would be essential to ensure that all samples, regardless of their sample source, maintain the same level of growth and differentiation. Pre-testing of fetal populations to determine their growth potential would aid in this goal and allow custom seeding densities to be chosen for each sample to ensure production of pellets capable of correct differentiation.

From all conditions tested on pellets in organotypic ALI culture, it was found that two provided potential models for skeletal tissues. Growth of pellets in osteogenic media with dexamethasone was found to mimic the phenotype of the fetal femur (Mackie et al. 2008), suggesting that the addition of osteogenic media stimulated the fetal cell pellet to undergo the development and differentiation observed in fetal femurs, with production

of a cartilage anlage and the commencement of endochondral ossification. The fetal femur-like phenotype was confirmed by the presence of SOX9-expressing, lacunae-based chondrocytes immersed in a proteoglycan and Type II collagen-rich matrix, bordered by an osteogenic bone collar composed of a Type I collagen, Osteopontin and alkaline phosphatase-rich periosteum-like region. This confirmed the ability to establish a potential model for early skeletal development using organotypic pellet culture. The addition of BMP-2 lead to a substantial increase in cell proliferation and proteoglycan matrix deposition, demonstrating a growth-stimulating activity as well as acting as an osteogenic factor.

Previous studies have demonstrated that 3D pellet culture is conducive for chondrogenic differentiation of cartilage-derived cells (Tare et al. 2005) and that organotypic ALI culture can maintain populations of chondrocytes (Bujia et al. 1993). In this study, organotypic ALI culture of FFDC pellets in chondrogenic media without dexamethasone resulted in a strong cartilaginous phenotype (Table 4.2), thus offering a potential model for cartilage development and for use in drug screening. Dexamethasone is considered to be essential for *in vitro* induction of both osteogenic (Yamanouchi et al. 1997) and chondrogenic cell differentiation (Derfoul et al. 2006). However, in contrast to this, only those samples treated with chondrogenic media without dexamethasone resulted in a chondrogenic phenotype, while addition of dexamethasone to chondrogenic organotypic ALI cultures appeared to induce an increase in osteogenic differentiation, evidenced by the increased expression of Type I collagen and RUNX2. This data, in combination with previous studies demonstrating that addition of dexamethasone induces ALP expression in chondrogenic pellet culture (Stewart et al. 2008), suggests that dexamethasone induces osteogenic differentiation in 3D pellet culture. However, removal of dexamethasone from samples cultured in osteogenic media does not prevent osteogenesis but instead results in a reduction in pellet growth, confirming that dexamethasone also plays a role in inducing proliferation during osteogenesis.

While many pellets expressed high levels of Type I collagen, Osteopontin and low levels of alkaline phosphatase, it was found that none of the conditions used were able to produce a mature bone phenotype, with all samples maintaining a core of

140

proteoglycan and very few expressing significant amounts of Osteocalcin or other late bone markers. A study performed by Muraglia et al. (2003) demonstrated that after chondrogenic differentiation of hBMSC pellets to induce cartilaginous tissue, further treatment with osteogenic media resulted in the formation of a bony collar around a cartilage core (Muraglia et al. 2003). This phenotype matches that observed in organotypic ALI culture of FFDC pellets in osteogenic conditions, indicating that the predominantly chondrogenic nature of FFDCs limits the amount of osteogenic differentiation that can occur. Thus, establishment of mature bone using these cells may require a longer culture period or conditions beyond addition of dexamethasone, ascorbate and BMP-2 to induce the formation of bone. However, neither the addition of β-glycerophosphate (work performed by undergraduate medical students, Appendix 6), known to increase matrix calcification (Chang et al. 2000) or 1,25-dihydroxyvitamin D, known to stimulate late osteogenesis (Jorgensen et al. 2004) were able to produce a true bone phenotype, although addition of vitamin D did induce a higher expression of bone-specific markers such as ALP, Type I collagen and OCN. Use of other cell lines such as adult hBMSCs are more likely to offer a strong bone phenotype. Indeed, early tests demonstrated that hBMSC pellets under basal conditions, naturally differentiate towards an osteogenic phenotype (see Appendix 7).

Pellets treated with chondrogenic media regularly produced a phenotype strongly resembling a mix of both bone and cartilage as evidenced by cores of proteoglycan bordered by large quantities of both Type I and Type II collagen. Organotypic ALI culture is carried out at atmospheric oxygen concentrations, in contrast to chondrogenesis *in vivo*, which normally occurs in avascular, hypoxic conditions (Shea & Miller 2005). The high concentration of oxygen may have been responsible for the mixed phenotype produced, as even in cell pellets treated with chondrogenic media, sites of air-pellet interaction were exposed to conditions conducive to osteogenic differentiation. This theory was expounded by the presence of increased levels of Type I collagen and decreased levels of Type II collagen towards sites of air-pellet interaction.

In pellets from all different media conditions, Type I collagen was predominantly found surrounding the pellet at sites of pellet-air interaction, whilst Type II collagen was found at sites of cell-confetti adhesion. This suggests a role for oxygen concentration in the

differentiation of cells in organotypic ALI culture. It was theorised that cells at sites of adhesion and near the liquid-pellet interface were exposed to a lower oxygen concentration in comparison to cells at the pellet-air interface, leading to an enhanced chondrogenic phenotype. Initial results for fetal femur cell pellets cultured in hypoxic (<5% oxygen) organotypic ALI culture were in conflict with this theory, as they exhibited an enhanced osteogenic phenotype in cell pellets grown in all conditions, evidenced by an increase in Type I collagen expression (see Appendix 8). Culture of pellets in hypoxic conditions also led to an increase in cell necrosis, thus further repeats of fetal cell pellets under hypoxic organotypic ALI culture would need to be performed before this phenotype can be confirmed. Another theory for the unusual phenotypes observed in organotypic ALI culture was the serum content of specific media types. Preliminary results concluded that phenotypes expressed by pellets treated were relatively unaffected by serum concentration other than in size. However, it was noted that the addition of serum appeared to initiate a greater osteogenic response in pellets treated with chondrogenic media (see Appendix 9).

In conclusion, this study has demonstrated that organotypic pellet culture of FFDCs presents a potential model for both cartilage and early bone development that mimics *in vivo* conditions. However, the high levels of variation in marker expression observed between different populations of pellets grown in basal conditions highlighted a significant factor in maintaining reproducibility. Patient variation was observed to affect not only the differentiation of cells but also the ability of cells to form adequate 3D structures. Analysis of pellets demonstrated that significant pellet diameter at day 1 (greater than 0.8mm) is crucial for maintaining reproducible results in osteogenic and chondrogenic conditions. To prevent anomalous results, it is essential that the growth potential of each population be determined before organotypic ALI culture to ensure suitable pellet diameter is obtained at day 1. By ensuring adequate pellet size in each population, the organotypic protocol can be used to further analyse the effects of specific growth factors on cartilage and bone differentiation and would enable a better understanding of the processes involved in early skeletogenesis. Future work using these techniques could involve the use of different mesenchymal cell lines such as adult bone marrow cells to establish further models for skeletogenesis.

142

Chapters 3 and 4 have investigated the characteristics of FFDCs and their potential for use in tissue engineering protocols. In these chapters, it was shown that isolated FFDC populations demonstrate heterogeneity and contain multiple subpopulations, a trait common to most primary cell populations. The presence of multiple subpopulations can affect the growth potential and differentiation of a cell population in culture, as well as inhibit efficient characterisation. Thus, the isolation of specific subpopulations of cells for characterisation is a well established goal in stem cell research. While many protocols currently exist for separation of subpopulations, there is a paucity of methods that can offer isolation of 100% pure populations. Chapters 5 and 6 describe the development of novel devices for isolation of specific cell populations according to immunofluorescent marker expression.

CHAPTER 5

DEVELOPMENT OF A DIELECTROPHORETIC DEVICE TO TRAP AND RECOVER CELLS

In collaboration with Dr Rupert Thomas, School of Electronics and Computer Science, University of Southampton

Cell biology by Peter Mitchell
Device preparation by Dr Rupert Thomas
Microfluidic isolation of cells by both parties

5.1. Introduction

It remains a clinical necessity to develop technologies that enable recognition and isolation of specific cell types in order to provide sufficient cell populations for use in tissue regeneration. Isolation of MSCs from bone marrow extracts is simplified by the fact that MSCs/progenitor cells will adhere to tissue culture plastic when cultured while haematopoietic and endothelial cells will not (Oreffo et al. 2005). The standard method used to identify MSCs is the colony forming unit-fibroblastic (CFU-F) assay, which produces fibroblastic, heterogeneous populations (Gronthos et al. 1994). In order to further isolate specific cells, stage-specific markers are required. However, due to the lack of knowledge surrounding the biochemical and phenotypic structure of these cells and the sharing of common features with other cells, both epithelial and endothelial; very few MSC-specific markers have been identified to date and none of these have been accepted as a definitive marker for the MSC phenotype (Baksh et al. 2004). Current markers known to enrich for MSCs include STRO-1, CD44, CD49a, CD63, CD73, CD90, CD105, CD106 and CD166 (Gronthos et al. 1994;Pittenger et al. 1999;Minguell et al. 2001;Stewart et al. 2003;Jones et al. 2006).

Populations of MSCs are often heterogeneous and the presence of sub-populations can seriously affect the overall analysis of the cell population. In order to produce accurate and cell-specific analysis, one approach is to use single-cell analysis. It is estimated that only 1/100,000 nucleated cells derived from bone marrow is a stem cell (Connolly et al. 1989), therefore it is essential that an effective method of isolation is found to isolate stem-like cells. The majority of research into enrichment and isolation of the MSC from bone marrow cells has been carried out by fluorescence activated cell sorting (FACS) (Radbruch 1999) and the similar technique, magnetic activated cell sorting (MACS) (Miltenyi et al. 1990). However, these techniques are time consuming and neither approach provides 100% enrichment for the marker(s) in question. An alternative approach for the selection of specific cell populations is offered through the use of microfluidic techniques for isolation and characterisation of individual cells. Furthermore, microfluidic devices offer new methods for the characterisation of selected cell populations. Microfluidic devices can provide the means to manipulate and trap single cells. Contact-free immobilisation prevents damage to, or interference with the cells that could lead to false data from samples. To date, a variety of non-contact

microfluidic cell isolation techniques exist (Johann 2006), based on optical (Ozkan et al. 2003), acoustic (Kim et al. 2004;Kriel et al. 2006), magnetic (Inglis et al. 2004;Kimura et al. 2005) and dielectrophoretic devices.

Dielectrophoresis (DEP) is the phenomenon whereby polarisable particles exposed to non-uniform electric fields experience a net force directed towards locations with either increasing or decreasing field intensity. If the electric field is uniform, then the attraction between the dipolar charges and the electric field is equal and opposite and there is no net movement of the particle unless it carries its own net charge (Hughes 2002). The strength of the DEP force is dependent on a variety of factors including the particles' dielectric properties, determined by the physical properties of the particle such as the size and shape and the interior structure; the medium; and the frequency of the electric field (Pohl 1978). By varying the frequency of the electric field, it is therefore possible to non-invasively distinguish between different cells and particles. DEP can be classified into two types: positive and negative DEP. Which of these forces a particle experiences is dependent on its permittivity relative to its surrounding medium. When the permittivity of the medium is less than that of the particles' then the net-force causes the particle to move towards the increasing field gradient. This is known as positive DEP (pDEP). However, in negative DEP (nDEP), the permittivity of the medium is greater than the particles, causing the particle to be repelled from areas of high electric energy (Medoro et al. 2007). Negative DEP has many advantages over pDEP, notably the ability to suspend particles above a surface for non-contact isolation of single cells, a property especially important for the study of adherent cells. Technological advancements in the production of electrodes with micro-sized features have led to an increase in the availability of DEP. Different electrode configurations have been designed for DEP, each providing different properties for particle manipulation, for example, the quadrupole electrode uses four electrodes to immobilise and levitate a single particle via negative DEP and offers a method to separate specific cells for characterisation (Voldman et al. 2003) (Figure 1.25). The introduction of octopole electrode designs into DEP (Schnelle et al. 1993) allowed the creation of nDEP cages. In this layout, electrodes are placed on both the top and bottom surfaces of a trap; the fields produced are able isolate a single cell in the middle of a flow channel, allowing single-cell isolation from a flow of cells (Manaresi et al. 2003). More recent techniques

148

have looked at using computer-run recognition programs to selectively trap specific cells such as those expressing certain levels of fluorescence (Thomas et al. 2009).

In essence, microfluidic devices offer two different methods for cell separation; cell sorting and cell trapping. Cell sorting involves active manipulation of cells using an external force within a fluid flow in order to guide cells of interest to specific channels or areas of interest away from unwanted cells (Chen et al. 2008). Cell trapping is used to retain or delay cells in a fluid flow while unwanted cells are removed, thereby separating cells of interest from a population. Cell trapping devices enable a high degree of enrichment as small numbers of cells can be isolated with minimal unwanted cell contamination. Trapping methods also facilitate cell recovery as there is no need to accurately divide the fluid flow as is normally required to recover populations from a cell sorter. Cells separated by trapping can also be retained for on-chip analysis (Johann 2006). The potential use of dielectrophoresis ring electrode traps have been previously demonstrated to immobilise single cells in physiological media (Thomas et al. 2009). Activation of a ring traps draw a cell towards the centre of the ring, suspending it above the substrate. All other cells outside the trap are repelled by the dielectrophoretic field, resulting in each trap only containing a single cell. The aim of this study was to demonstrate the potential use of an array of ring electrodes for the isolation of specific subpopulations from a heterogeneous population of human osteosarcoma cells with 100% purity.

5.2. Methods & Materials

5.2.1. Cell lines

This study utilised MG-63 cells, an osteoblast-like cell line with a fibroblastic morphology, derived from a human osteosarcoma. These cells were purchased from ATCC and were used as an established alternative to primary skeletal cell lines due to their osteogenic characteristics and expression of various osteoblast and skeletal stem cell markers including STRO-1.

5.2.2. Cell labelling

To aid in identification of cells during microfluidic isolation and separation of cell types, Vybrant™ labelling solutions DiD and DiO were used to establish fluorescent cell populations. Dissociated cells were centrifuged, washed with PBS and suspended in a solution of 10µl DiO/DiD stock in 1ml PBS for 7 min at 37°C. After incubation, cells were washed twice with PBS and suspended in flow media (see Section 5.2.4). For ease of recognition, green fluorescent cell lines were used for positive samples (to be trapped) and red fluorescent cells for negative samples. As an alternative to DiO-stained positive populations, established cell lines were transfected with recombinant GFP using the Amaxa Nucleofector® system, a non-viral system that utilises cell-specific buffer solutions and electroporation to transfect cells with foreign DNA. Cell cultures were trypsinised and gently centrifuged for 5 minutes at 90g then resuspended in 100µl of cell-specific nucleofector solution containing appropriate amounts of pmaxGFP plasmid, transferred to a certified Amaxa cuvette and electroporated under an optimised protocol on the Nucleofector® system. Cells were transferred to culture media and seeded onto 6-well plates or T75 culture flasks for recovery. After 24hrs in culture, transfected cells were dissociated and counterstained with DiD for use in cell trapping experiments. Transfection efficiency varied between cell types but on average ranged from 50-60% of the viable population being positive for GFP (Figure 5.1). Cells stained with cell tracker green failed to maintain cell viability after staining and Vybrant CFDA populations were unable to establish viable populations after passage, indicating their lack of suitability as long-term viability markers. Cells stained with Vybrant DiD and DiO stains or transfected with GFP were found to maintain cell viability after staining/transfection and after passage. However, GFP populations exhibited a large degree of variation in the levels of fluorescence exhibited by cells, increased by passage.

150

5.2.3. Microfluidic device

Microfluidic chips were designed by Dr Nicolas Green (Electronics and Computer Science, University of Southampton) using CAD/CAM software and fabricated by Philips Electronics UK Ltd (Guildford). Inlet and outlet ports were drilled in to the chip using electro-chemical spark erosion and anisotropic conductive film bonding was used to connect the electrodes on the chip to an external circuit board through a flexible PCB, to allow connection of the chip to the signal generator via a software-run relay board. Microfluidic trapping of cells via the relay board was performed using an automated MATLAB script that allowed manual or automatic activation and deactivation of individual traps, facilitating selection and trapping of specific cells (see Appendix 10). Live images grabbed from a digital video camera were compared with a stored background image to identify moving objects. The size, colour and intensity of each object was determined, and traps activated as positively-identified cells passed overhead. Video files of cell isolations were also recorded through the MATLAB software for future reference. Microscopic observations were made through a bespoke fluorescent microscope with a uEye 2230c colour CCD camera and a Nikon PlanFluor x4 objective lens. Illumination was provided by a 'white' LED (5500K CCT - Lumiled Luxeon), and red (635nm, 200mW) and blue (473nm, 30mW) lasers (Laserglow) were used for epifluorescence observations with a dual-band polychroic mirror (FITC/CY5 – Chroma, USA) and emission filter (FF01-538/685-25 - Laser 2000, UK). Introduction of flow media and cell solutions was performed using a syringe pump to provide consistent flow of media. Flow rate during trapping was set at 2 μl/min for optimal dielectric manipulation whilst also preventing sedimentation. Recovery of cells was performed at 5 μl/min. Traps were set at electrical excitation of 5 MHz, 10vpp; provided by a function generator. Use of flow valves enabled easy transition between alternating input syringes containing flow media or cell solution and between waste collection and positive cell collection. An overview of the microfluidic setup is shown in Figure 5.2 (additional schematics can be found in Appendix 10).

5.2.3.1. Quantification and prevention of cell adhesion

To determine the extent that cells would adhere to the chip surface without trapping, macro-scale experiments were carried out to test a variety of different coatings. Using a hydrophobic pen, 1.5cm^2 regions were marked on plain glass slides. 200μl solution

containing 1×10^3 cells was dispensed into the marked region and incubated for up to 30 minutes. Slides were then rinsed with running PBS to remove the cell solution and the number of cells adhered were counted in 4 sections of the marked region using microscopy.

5.2.4. Dielectrophoretic trapping

Fluorescently-labelled cell lines (red for negative and green for positive) were mixed at various ratios of red to green (2:1, 4:1, 10:1 etc.) and suspended in DMEM containing 10% Dextran-70 (flow media) to provide neutral buoyancy. Cell solutions were then introduced into a microfluidic chip previously cleaned and sterilised using virkon, ethanol and PBS washes, incubated with 5% BSA in PBS to coat the glass and reduce cell adhesion/sticking, then washed with PBS and flow media. Traps were set at a frequency of 5 MHz and voltage of 10 VPP (volts point-to-point) and the device was cooled to 10 to 12°C to provide optimal conditions. Positive cells could be trapped manually or via the use of computer controlled software. Upon trapping of cells, flow was continued until all remaining non-trapped cells had been collected into the waste tube. Traps were then deactivated and trapped cells washed into a 384-well plate for analysis. After collection of trapped cells, DMEM plus 20% FCS was added to each well to improve cell viability and speed of recovery. The total number of cells collected was counted using phase confocal microscopy, while fluorescent microscopy was used to determine the ratio of positive and negative cells.
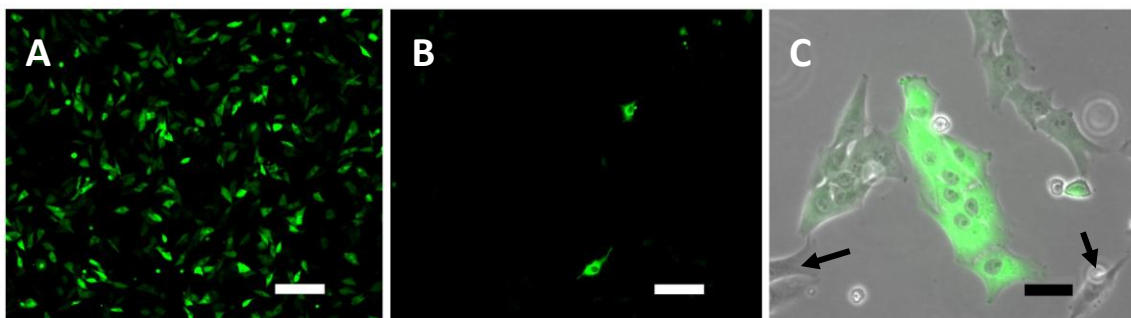
Figure 5.1. Images of GFP+ MG-63 cells 2 days after transfection (A) and 1 week after transfection, after passage (B). Transfection of cells with GFP resulted in varying levels of fluorescence (C) from none (arrowed) to intense fluorescence. Scale bars: (A, B) 100µm, (C) 20µm.
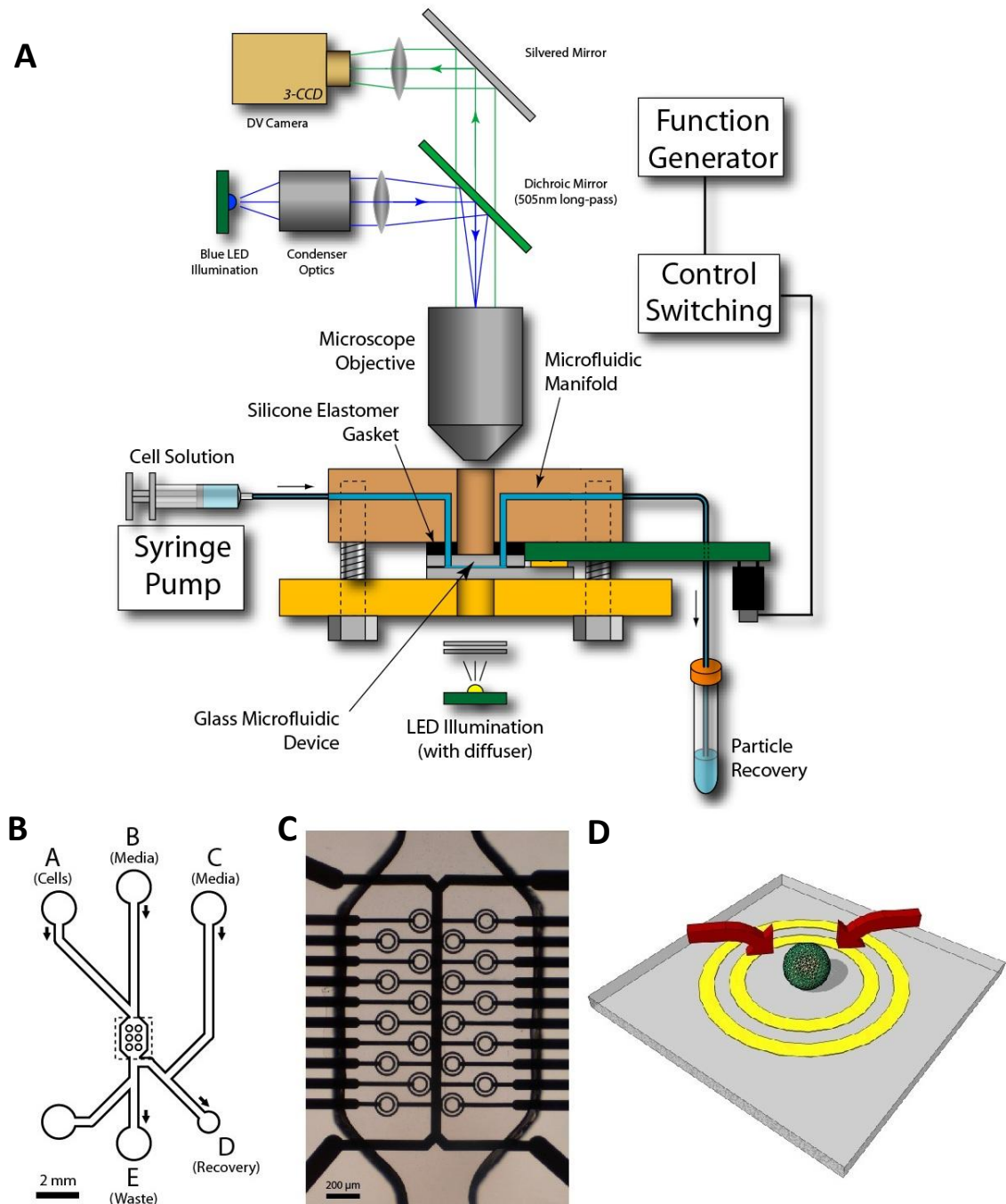
Figure 5.2. (A) Overview of the microfluidic setup (Thomas 2006). (B) Diagram of the microfluidic channel on the device. The channel is 95µm deep, 350µm wide increasing to 950 µm around the ring electrodes. (C) Photograph of the ring electrodes and microfluidic channel in the centre of the device. (D) Concept drawing of a single cell dielectrophoretic trap. The DEP force (arrows) direct the cell down and towards the centre of the ring electrodes. Figure adapted from (Thomas et al. 2010).

5.3. Results

5.3.1. Microfluidic isolation of cells

5.3.1.1. Preliminary experiments

Preliminary tests into the use of microfluidic devices for isolation and retrieval of cells were carried out using three different cell trapping chip designs. Initial tests of novel chip designs were performed by Dr Rupert Thomas using polystyrene fluorescent beads. In all cases, isolation and/or retrieval failed due to inherent problems with the chip design (Table 5.1).

From the preliminary tests, it was discovered that for optimal conditions, chips must be sealed with glass rather than silicone in order to maintain a rigid structure and thus a consistent flow rate throughout the chip (Figure 5.3). Whilst failing to isolate specific cells, the preliminary tests demonstrated the ability of microfluidic devices to trap specific cells.

Test number	Positive	Negative
1	Functional traps, able to isolate fluorescent beads	15µm channel too small for MG-63 cells
2	100µm channel large enough for cells, good consistent flow rate	Manufacture-induced damage, majority of traps non-functional
3	Functional traps, large enough for cells	Use of non-rigid silicone wafer to seal chips caused issues with fluid flow

Table 5.1. Summary of the positive and negative characteristics of the preliminary tests.
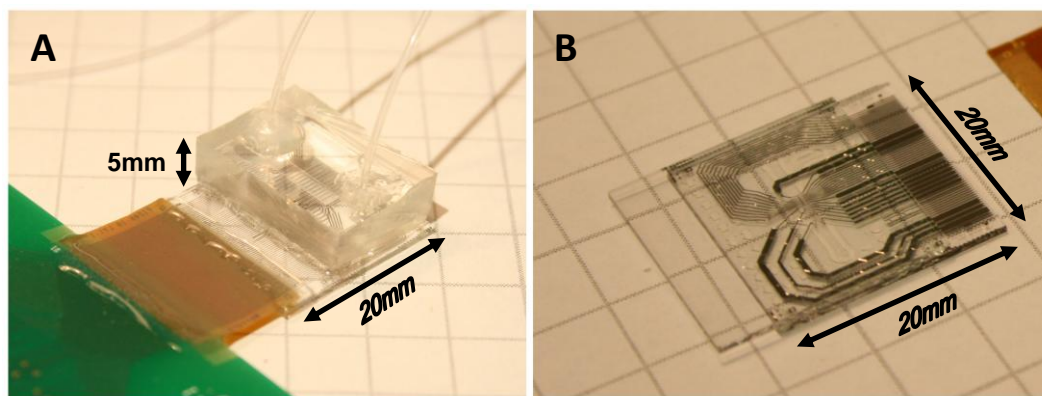
Figure 5.3. Examples of silicone (polydimethylsiloxane) (A) and glass (B) sealed chips.

5.3.2. Isolation and retrieval of Vybrant-stained cells

Red and green fluorescent stained MG-63 cell populations were mixed at a 4:1 ratio of red to green. Cell mixtures were then inserted into the microfluidic device and trapping initiated. From a 4:1 mixture it was possible to identify and trap up to 8 positive green cells. In initial experiments it was found that recovery of pure green populations was prevented by contamination with negative red cells (Table 5.2 runs 1-5). In some cases this contamination came from red cells getting stuck within traps but the majority of contamination came from non-specific adhesion of cells to the chip surface (Figure 5.4). These cells adhered strongly enough to resist normal trapping flow rates but not sufficiently for recovery flow rates, preventing removal of the cells before recovery of the trapped positive cells. On average the purity of green cells was increased from 20% to 50 to 60%. This remained short of the 100% purity desired.

Cooling the device to 10 to 12°C, in addition to use of a 5% BSA anti-adhesion coating (see Section 5.3.2.1) and suspension of cells in DMEM plus 10% Dextran-70 to provide neutral buoyancy, significantly reduced non-specific adhesion, enabling the removal of most, if not all non-trapped cells before recovery (Figure 5.5). This increased the purity of recovered positive cells to a consistent 100% (Table 5.2 runs 6-9). However, a major problem noted with all results was that recovered cells stained with DiD and DiO lacked viability and failed to adhere to tissue culture surfaces after 24 and 72 hours, whilst unsorted control populations maintained viability (Figure 5.6). This suggested that either the dielectrophoretic trapping or the low seeding density after recovery had a negative effect on cell viability.

Run no.	Red stain	Red recovered	Red adhered	Green stain	Green trapped	Green recovered	Green adhered	Green purity
1	DiD	12	0	CTG	8	15	0	55%
2	DiD	6	0	CTG	5	9	0	60%
3	DiD	10	0	CTG	5	11	0	52%
4	DiD	20	1	DiO	6	16	0	44%
5	DiD	1	0	DiO	2	2	0	67%
6	DiD	0	0	DiO	4	4	0	100%
7	DiD	0	0	DiO	5	2	0	100%
8	DiD	0	0	DiO	5	3	0	100%
9	DiD	0	0	DiO	3	3	0	100%

Table 5.2. Summary of chronologically separate recovered stained populations. Runs 1-5 demonstrate early experiments hampered by cell sticking and red cell contamination, while runs 6-9 represent trapping using an optimised protocol. Key: DiD, Vybrant DiD; DiO, Vybrant DiO; CTG, cell tracker green.
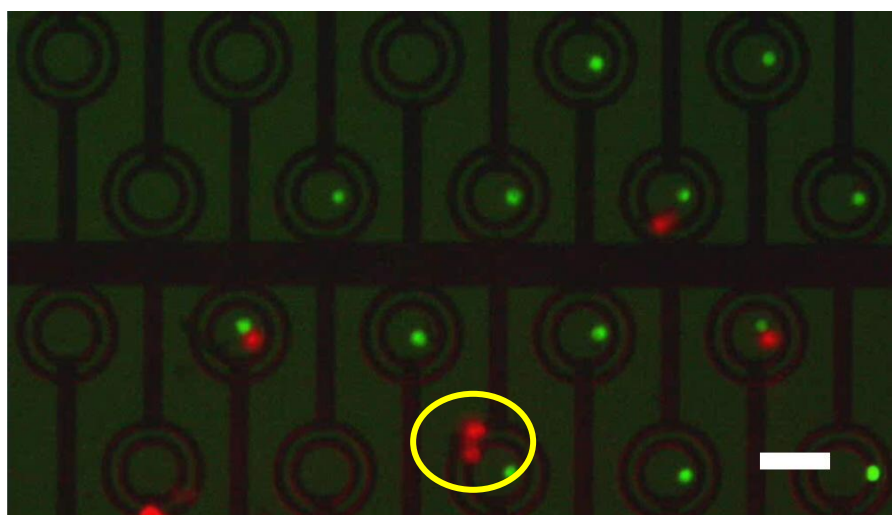
Figure 5.4. Screenshot of trapped MG-63 cells. Examples of adhered cells can be seen circled in yellow. Green cells are stained with Vybrant DiO and act as the cell of interest, while red cells are stained with Vybrant DiD and act as unwanted cells. Scale bar; 100μm.
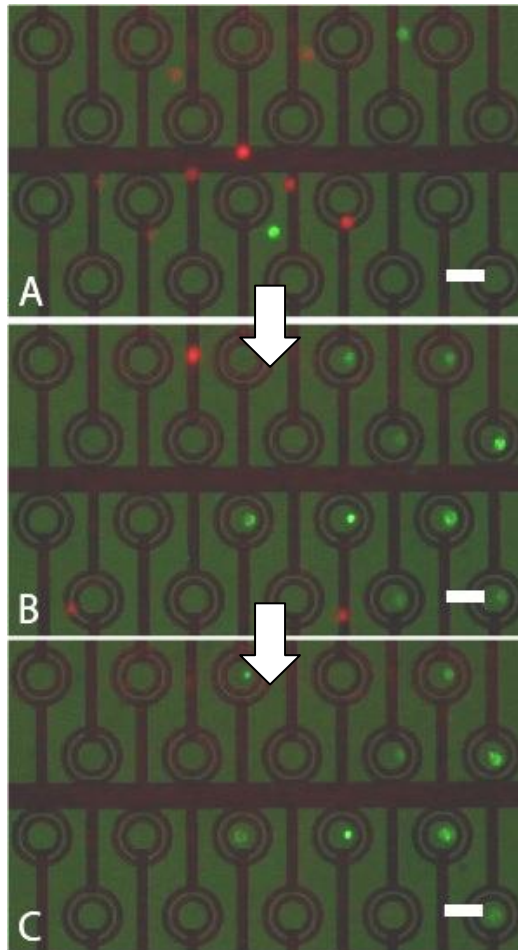
Figure 5.5. Still frames taken from the video at intervals during cell trapping: (A) prior to trapping, (B) after trapping, and (C) after washing. Scale bars; 100µm.
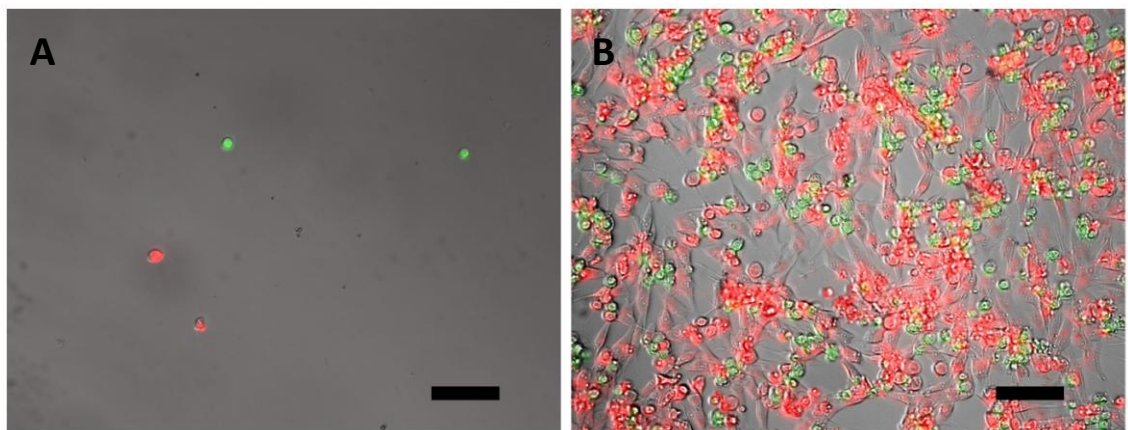
Figure 5.6. Microfluidic isolation of cell tracker green and Vybrant DiD stained cells. An example of an impure batch of recovered cells is shown in (A) and an unsorted control sample of cells is shown in (B). While the control population demonstrates cell adherence, isolated cells fail to readhere to tissue culture plastic. Scale bars: 100µm.

5.3.2.1. Quantification and prevention of cell adhesion

Cells incubated on plain glass slides were found to adhere rapidly, with cells adhering in less than 5 minutes and the majority of cells observed to be adherent after 10 minutes of incubation (Figure 5.7). Therefore the adhesion of cells in all following tests were measured at 5 minutes (Figure 5.8) and 20 minutes (Figure 5.9). Of all coatings tested, 5% BSA, 1% Agarose and 1% Agarose/APES ((3-aminopropyl)triethoxysilane) were deemed the most effective at preventing cell adhesion. In addition to testing coatings for the glass chips, various media additives were tested. These included the addition of various molecular weights of PEG (polyethylene glycol) and trypsin. None of the additives were found to have any substantial effect on cell adhesion to glass slides.

5.3.2.2. Cell viability

Recovered populations of trapped Vybrant DiD/DiO stained cells failed to adhere to tissue culture plastic, prompting an investigation into the effect of the microfluidic device on cell viability. Control samples were established at recovery seeding density (<10 cells per well in a 384 well plate) for each stage of the microfluidic protocol and viewed after 24 and 72 hours. Results showed that after 24 hours, Cells at all stages, (including after being run through the device without trapping), still maintained viability. However, it was noted that cells left in suspension for long periods of time, both at 4°C and 18°C demonstrated severely reduced viability (Figure 5.10). Negligible differences were noted between cell counts at 24 and 72 hours, indicating that no proliferation had occurred despite cell adhesion and viability.
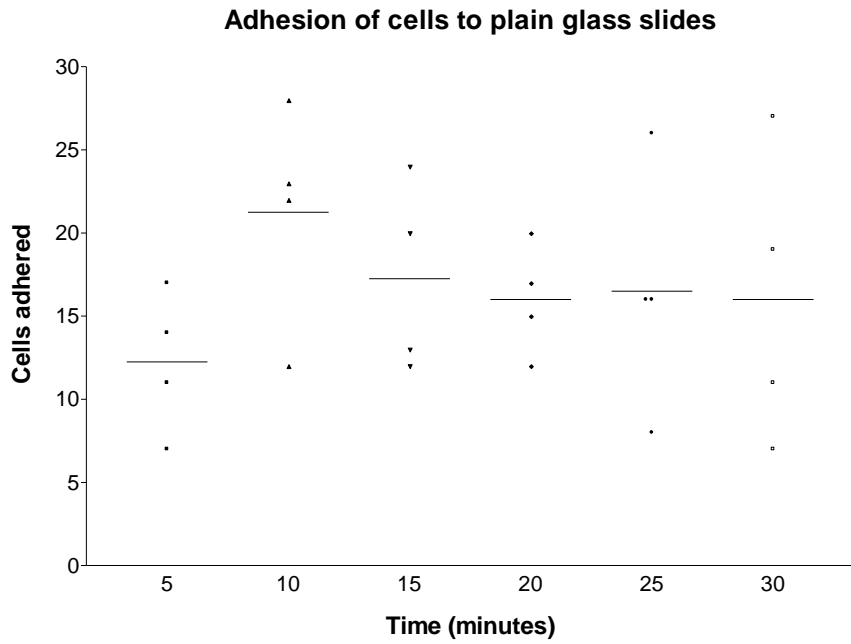
Figure 5.7. Graphic representation of MG-63 cell adhesion on plain glass over 30 minutes. Individual experiments (n=4) are shown by points, with mean demonstrated by a straight line.
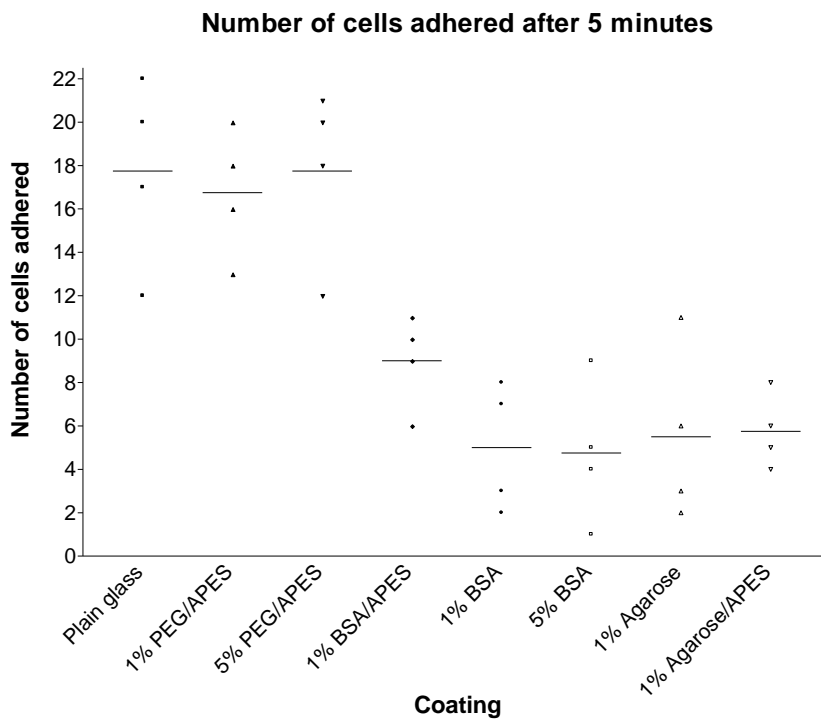
Figure 5.8. Graphic representation of MG-63 cell adhesion on coated slides after 5 minutes. Individual experiments (n=4) are shown by points, with mean demonstrated by a straight line. Key: APES, (3-aminopropyl)triethoxysilane; PEG, poly(ethyleneglycol)diacid 600; BSA, bovine serum albumin.

159
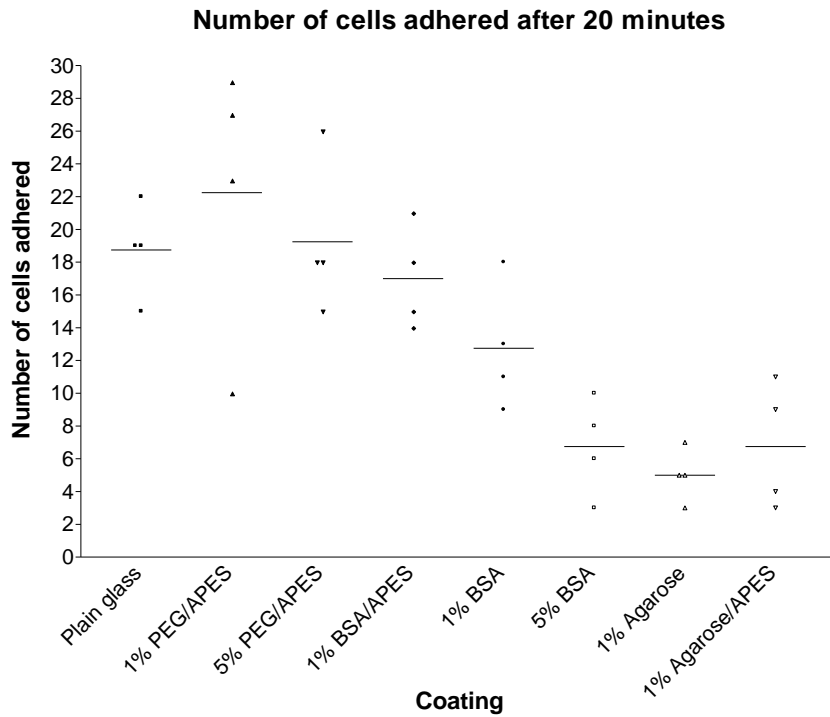
Figure 5.9. Graphic representation of MG-63 cell adhesion on coated slides after 20 minutes. Individual experiments (n=4) are shown by points, with mean demonstrated by a straight line. Key: APES, (3-aminopropyl)triethoxysilane; PEG, poly(ethyleneglycol)diacid 600; BSA, bovine serum albumin.
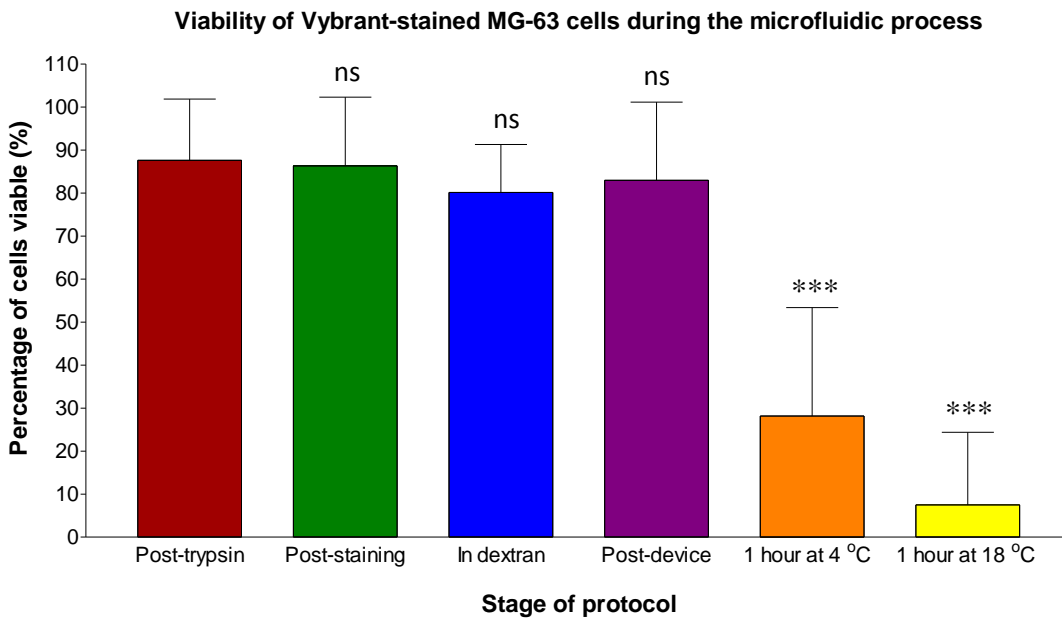
Figure 5.10. Percentage of Vybrant-stained cells viable at each stage of the microfluidic process when seeded at recovery density. Samples were viewed 24 hours after seeding. Data shown as mean $\pm$ SD, n $\geq$ 6. Statistical analysis performed in comparison to post-trypsin control; ns = non-significant, *** = $p < 0.001$.

5.3.3. Microfluidic isolation of GFP⁺ MG-63

MG-63 cell populations transfected with GFP exhibited less uniform expression of fluorescence than stained cells but demonstrated consistent viability throughout testing (Figure 5.11). GFP⁺ cells were mixed with Vybrant DiD stained cells at ratios varying from 2:1 to 4:1 red to green (according to the rough percentage of a transfected population expressing GFP).

Out of a total of 4 runs using GFP transfected cells, it was possible to identify and trap between 2-5 positive cells. All tests recovered 100% purity of GFP⁺ cells. In addition, approximately 53% (range: 33-80%) of recovered cells maintained viability and adhered to tissue culture surfaces within 24 hours (Table 5.3, Figure 5.12). After 72 hours only one of the recovered populations had demonstrated proliferation, while all others failed to proliferate (Figure 5.13). Suggesting that while recovered cells are able to readhere to tissue culture plastic, the stress they are exposed to during trapping severely inhibits normal cell growth.

To test the proliferative ability of GFP transfected cells, control populations were set up at approximately 10 cells per well (384-well plate) and cultured for 12 days to allow ample time for recovery and growth. Proliferation of cells was only observed in wells containing more than 10 cells, while wells containing less than 10 cells were found to lose viability and detach within a few days (Table 5.4, Figure 5.14). This suggested a requirement for a minimum number of cells to be seeded per well to enable cell recovery and growth, offering an explanation as to the poor viability of the small numbers of trapped and recovered cells (<10 cells).
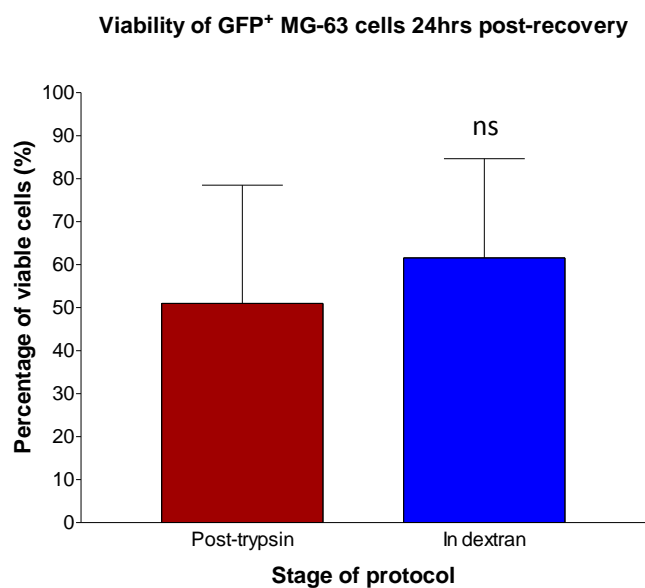
Figure 5.11. Percentage of GFP-transfected cells viable at pre-dielectrophoresis stages of the microfluidic process when seeded at recovery density. Data shown as mean ± SD, $n \geq 6$. Statistical analysis performed in comparison to post-trypsin control; ns = non-significant.

Run no.	Red recovered	Red adhered	Green recovered	Green adhered	Green purity
1	0	0	4	2	100%
2	0	0	5	4	100%
3	0	0	3	1	100%
4	0	0	2	1	100%

Table 5.3. Summary of recovered GFP+ MG-63 populations after 24 hours, n=4.
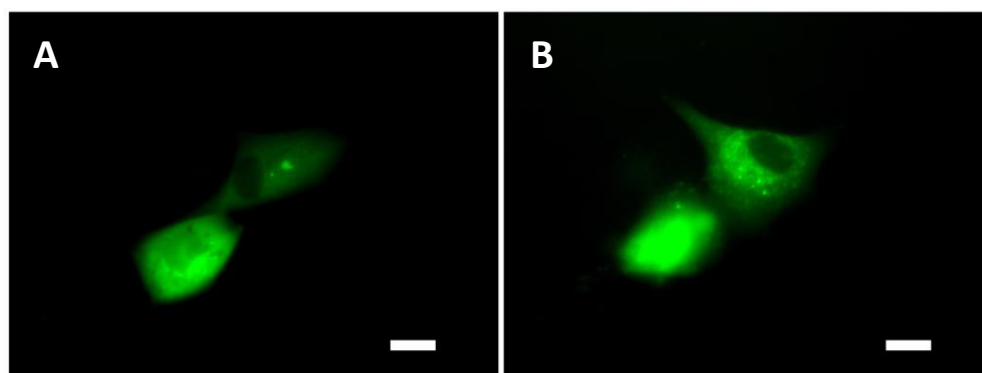
Figure 5.12. Examples of GFP+ MG-63 cell viability 24 (A) and 72 hours (B) after recovery. Scale bars: 20μm.
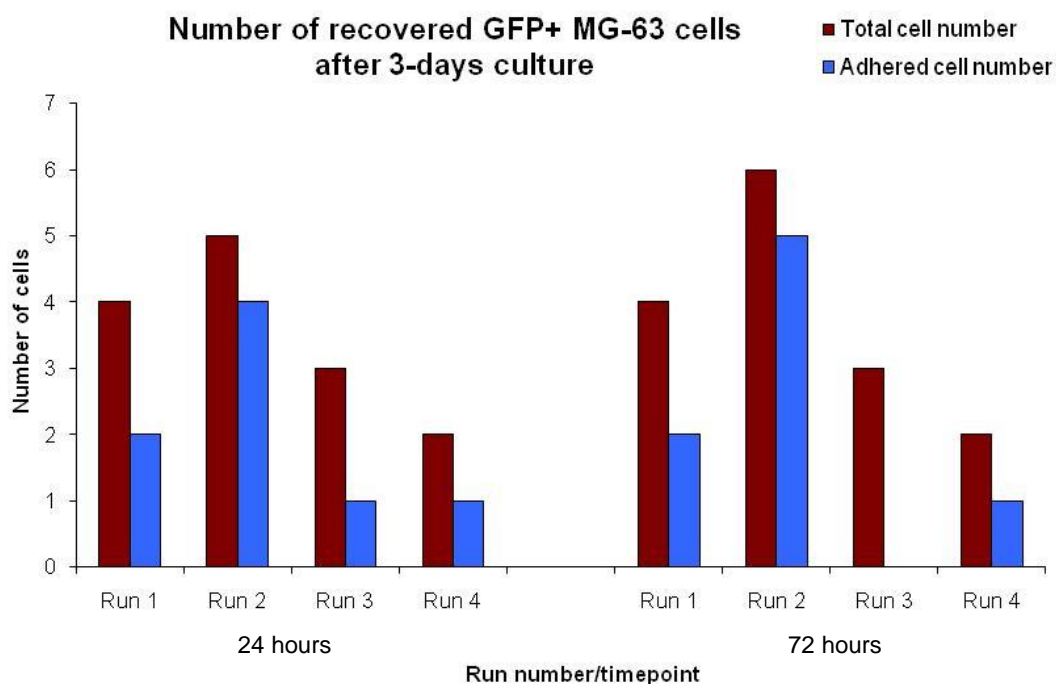
Figure 5.13. Total number of cells vs. viable cells for recovered GFP+ cells at 24 and 72 hours post-recovery (n=2 populations, 2 runs/population).

Sample	Initial adhered cell count	Adhered cell count after 12 days
1	11	0
2	16	>50
3	8	0
4	7	0
5	15	>50
6	11	>20
7	4	3
8	10	0
9	9	0
10	14	>50
11	9	0
12	6	0

Table 5.4. Analysis of cell growth and proliferation in control cultures of MG-63 cells after 12 days culture following seeding at 1 to 20 cells per well.

.
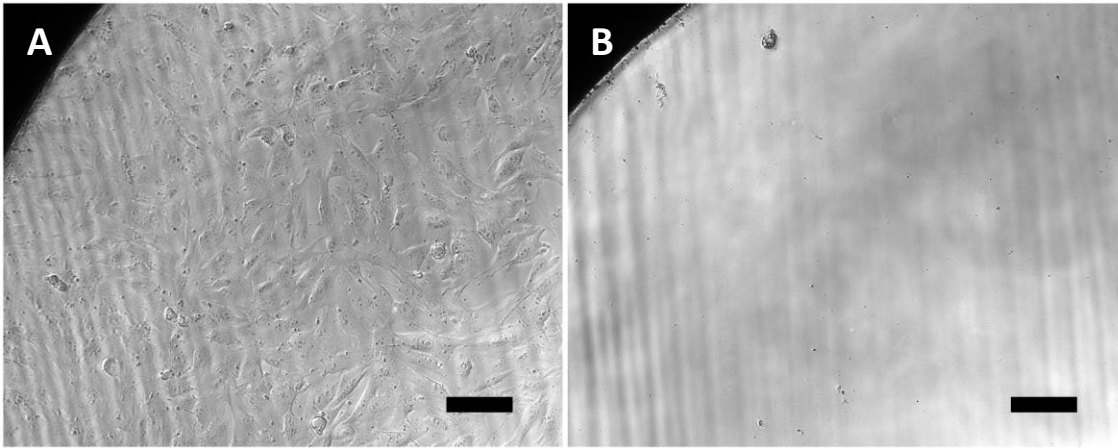
Figure 5.14. Images of MG-63 control populations after 12 days, demonstrating proliferation in wells seeded at more than 10 cells/well (A) and lack of proliferation, resulting in cell death and detachment in wells seeded at less than 10 cells/well (B). Scale bars; 50µm.

5.4. Discussion

Previous studies into characterisation of mesenchymal stem cells have highlighted the need to isolate and purify specific populations of cells for analysis due to the lack of knowledge surrounding the biochemical and phenotypic structure of these cells (Baksh et al. 2004). The majority of current techniques for the isolation and separation of cells from a mixed population have failed to provide pure populations of recovered cells. This study has demonstrated that individual human cells can be isolated and recovered from a heterogeneous population, using nDEP ring traps, to provide an enriched population. Eight separate sorting operations demonstrated recovery of 100% pure populations of specific cells. This shows that despite limitations discussed later in this section, specific individual cells can be selected and manipulated from a heterogeneous population.

The low number of available traps, the linear layout of the traps and the need to compromise between filling all available traps and how long cells were exposed to the sorting process resulted in the output of recovered cells being low in comparison to other existing techniques used for cell enrichment, with the duration of each sorting operation limited by the gradual decrease in cell viability the longer cells spend out of culture. In addition, actuation of flow control valves during washing stages was found to introduce a displacement into the fluid, often with magnitude sufficient to dislodge cells trapped in the ring electrodes. Hence, a small number of trapped cells would be lost during the sorting operation as they would be displaced from traps before recovery. Recovery of cells after trapping typically resulted in a 25% yield of trapped cells, resulting in a further reduction in the number of output cells of interest. However, this could be easily addressed by up-scaling the device to provide a larger number of traps and modifying the layout of the traps to a non-linear pattern so that more cells were likely to be exposed to traps during the sorting process. Alternatively use of a CMOS chip would provide high numbers of traps in any desired layout (Manaresi et al. 2003).

Cells in contact with or moving slowly near to a surface were liable to become attached. These cells could then detach at a later time, particularly at points when the flow rate was increased such as during recovery. This is likely to lead to non-target cells being recovered and contaminating the isolated sample. It was discovered that cells adhered to plain glass within 5 minutes, even when suspended in trypsin, suggesting that adhesion

was due to forces other than cell-produced proteins. To limit cell-surface interactions, the microfluidic channel was designed so that channels to and from the area containing the ring electrodes were narrower, increasing fluid velocity and reducing the likelihood of cell attachment. Additionally, coating the surface of the glass chip with 5% BSA to prevent adhesion, coupled with addition of Dextran-70 to the media to provide a near-neutral buoyancy to prevent cells dragging along the chip surface, substantially reduced cell adherence; even in those trapped and held stationary for up to 20 minutes. The design of the microfluidic channel is crucial if pure populations are to be recovered (Sims & Allbritton 2008). Separate inlets were provided for input of cells and buffer so that non-target cells could be flushed away effectively. Separate outlets were also applied for the recovery of isolated cells and waste. Care was taken to keep the recovery outlet clean and devoid of cells so that non-target cells were not released into the fluid flow during recovery. An additional washing inlet was provided so that media could flow into the device along the recovery outlet, preventing cells entering the recovery outlet until non-target cells had been sufficiently flushed out.

After trapping experiments were performed it was discovered that in all cases, recovered cells stained with Vybrant DiO failed to adhere to tissue culture plastic, whilst most samples transfected with GFP and were able to readhere to tissue culture plastic after trapping and recovery. Trapped GFP+ cells were recovered into a microplate by aliquoting 40µl of the eluent per well. This resulted in cell densities of approximately 1-3 cells per well. Despite the majority of cells adhering to the culture plate, as the numbers of cells recovered to each well failed to reach the numbers required to maintain a healthy population, the cells showed extremely slow recovery rates and negligible levels of proliferation were observed in recovered populations, with almost all trapped cells succumbing to cell death and detaching from the culture surface within a week. From observation of recovered populations and viability controls at all stages of the microfluidic protocol it was proposed that reduction in viability was not caused by any one process, but rather the combined effects of multiple stimuli, including cells becoming stressed by staining (DiO was particularly stressful on cells), held for sustained periods in suspension, being exposed to a dielectric field during trapping and/or an extremely low seeding density during recovery, as interestingly, cells had to be seeded at densities greater than ten cells per well to maintain a stable population and proliferate.

166

The dielectrophoretic traps operate by producing a large gradient in the electric field in the region surrounding the traps, this can alter the electrical potential across the membrane of a cell (Grosse & Schwan 1992). Numerical simulation of the electric field indicates that the traps are unlikely to induce a transmembrane potential within cells immobilised in the traps that exceeds harmful values. However, localised heating of the media will also occur, particularly as the physiological media used is quite conductive (Glasser & Fuhr 1998). Simulations indicate that the substrate temperature inside a trap would not exceed a 12°C rise from the local ambient temperature (Thomas et al. 2009). For example, if the device is cooled to 10°C during trapping, the maximum temperature experienced by cells is approximately 22°C directly above the electrodes (Thomas 2010), demonstrating that it is possible to set the substrate temperature within a range that is unlikely to cause long-term harm to cells when exposed for short periods of time. However, cells in the vicinity of a trap may still experience a thermal gradient that increases cellular stress.

In conclusion, this study demonstrates that isolation and recovery of specific cells is possible using dielectrophoretic ring traps. While this device is capable of isolating and recovering only small numbers of cells, thus hindering reestablishment of stable somatic cell populations, the system offers a route for the isolation and recovery of pure populations of specific cells. Addition of integrated on-chip analytical devices such as those for single-cell mRNA analysis (Ottesen et al. 2006;Marcus et al. 2006) would negate the need for high cell throughput, allowing direct genomic characterisation of small populations of recovered cells. Alternatively, application of more traps coupled with a non-linear arrangement would enable recovery of sufficient cell numbers to allow recovered somatic cell populations to maintain viability and proliferation. The trapping device discussed here also offers potential for isolation and culture of specific cells on-chip as previously described by (Yamaguchi et al. 2009). With the discovery of sufficient surface antigens that enable identification and labelling of stem cells with fluorescent markers, ring trap systems offer a potential for isolation and recovery of stem cells from a heterogeneous population, which typically maintain viability and proliferation even when cultured as single cells. These studies illustrate the potential of such a dielectrophoretic device for cell isolation from heterogeneous populations and the implications therein for cell sorting of somatic populations.

CHAPTER 6

DEVELOPMENT OF A FLUORESCENT-ACTIVATED, DIELECTROPHORETIC MICROFLUIDIC CELL SORTING DEVICE

In collaboration with Dr Rupert Thomas, School of Electronics and Computer Science, University of Southampton

Cell Biology by Peter Mitchell
Device preparation by Dr Rupert Thomas
Microfluidic isolation of cells by both parties

6.1. Introduction

As discussed in Chapter 5, an alternative to trapping devices for cell separation is cell sorting, where an external force is used to manipulate cells of interest within a fluid flow. Separation of cells with distinct characteristics such as difference in size can be performed with greater ease than isolating for less obvious differences such as marker expression. For example, previous studies have isolated nucleated red blood cells with up to 99.99% efficiency based on size and natural magnetism (Huang et al. 2008) or have efficiently separated cells based on distinct dielectrophoretic properties with purity up to 99% (Wang et al. 2005;Gascoyne et al. 2009).

Isolation of similar cells based on marker expression currently requires the use of external identifiers such as stains and antibodies. Currently, the main techniques for marker-based cell sorting consist of fluorescence activated cell sorting (FACS) (Radbruch 1999) and magnetic activated cell sorting (MACS) (Miltenyi et al. 1990). However, these techniques are time consuming and neither approach provides 100% enrichment for the marker(s) in question. The majority of existing microfluidic marker-based sorting devices are simply miniaturised versions of FACS and MACS (Wolff et al. 2003;Adams et al. 2008;Wu et al. 2010) and have yet to provide a consistent method for the recovery of pure cell populations of specific cells, as, to date, recovered populations typically contain small numbers of unwanted cells. For example, a study by Wang and co-workers demonstrated recovery of GFP-labelled HeLa from unstained cells using optical forces to manipulate cells towards collection or waste outputs. This method enabled sorting of more than 10,000 cells but only provided recovery of 82-98% pure GFP-positive populations (Wang et al. 2005).

The isolation of pure populations of specific skeletal cells was previously enabled by use of a novel DEP-based trapping device as discussed in Chapter 5. However, this device was limited in the number of cells that could be retrieved. In addition, recovered cells were unable to establish viable populations. Sorting methods are designed to offer a higher throughput of cells than trapping devices, thus providing a larger number of cells for analysis and/or growth. However, this increased throughput is often hampered by a decrease in purity. The aim of this study set out to utilise DEP technology to create a microfluidic-based cell sorter that would continue to provide 100% purity whilst also

enabling recovery of larger numbers of sorted cells for analysis or establishment of viable cell populations.

6.2. Methods

6.2.1. Cell lines

This study utilised MG-63 cells for initial studies as an established and robust alternative to primary skeletal cell lines due to their expression of the skeletal stem cell marker, STRO-1. Later experiments were performed with primary hBMSC populations (see Section 2.2 for culture protocols).

6.2.2. Microfluidic device

To enable the recovery of an enriched sample from a heterogeneous population a device with two separate outputs, one for the cells of interest (positive fraction) and one for the remainder of the cells (waste), was fabricated by Katie Chamberlain at the Southampton Nanofabrication Centre, University of Southampton. A nDEP-based sorting gate comprising of 3 pairs of electrodes was used to manipulate cells towards the desired output (Figure 6.1). During sorting, the electrodes default setting was to deflect cells towards the waste. When a cell of interest was recognised, the electrodes switched to deflect the cell towards the positive channel, reverting back to the default setting once the cell past the sorting gate. This allowed isolation of cells from the population as a whole. Cell recognition and control of the electrodes was facilitated by automated software written in MATLAB by Dr Rupert Thomas (ECS, University of Southampton). Fluorescence-based optical detection was utilised to allow the software to track cells, with positive cells expressing a fluorescent intensity significantly different to negative cells. The sorting chips were fitted into a holder that enabled connection of the chip to the fluid inputs and outputs. Connective tubing between the chip and sources of media/recovery devices were all fitted with simple on/off valves to enable control of buffer flow during use. Use of valves to isolate specific inputs or outputs helped to ensure that the positive recovery channel was isolated from unwanted cells during cell loading, as well as preventing contamination of sorted populations during recovery (Figure 6.2). During wash cycles, bleach, 70% ethanol, sterile PBS and sterile buffer were fed into the chip through one of the input channels via a syringe pump to prepare the device for use with live cells. A syringe pump was also used to enable recovery of

sorted cells, as the higher throughput of buffer facilitated rapid recovery and removal of any stuck or adhered cells. Control of fluid flow during required finer control than offered by syringe-fed input, therefore sorting was performed using gaseous pressure on fluid input and output tubes using a Fluigent MFCS-4C pressure controller. Use of a Fluigent Flowell allowed individual measurement and fine manipulation of the pressure and thus the flow rate in each channel of the microfluidic chip.

6.2.3. Cell sorting

Initial tests determined that for optimal sorting, the device was run at a flow rate of 40nl/min and a cell density of $3x10^5$/ml. Cell manipulation was carried out at 9vpp, 5Mhz, as this provided a suitable balance between maintaining cell viability and providing a dielectrophoretic field strong enough to manipulate cells (see Section 6.3.4). Automated software written in MATLAB by Dr Rupert Thomas (Electronics and Computer Science, University of Southampton) was designed to recognise and selectively isolate green fluorescent cells (see Appendix 10). The software was limited in that the system required all cells to express some form of fluorescent marker as the software was unable to distinguish unstained cells from the background on the chip. To solve this issue, all cells were labelled with DiD Vybrant (red) to make them visible to the image capture device. Sorting could be performed fully automated, allowing the software to make all decisions on cell separation or via use of a semi-manual approach, where the user observed the automated sorting and manually intervened to remove incorrectly isolated cells by altering the flow of buffer.

For positive cells, either a fraction of the population were further labelled with Vybrant DiO (green, positive control, see Section 5.2.2) or the whole population was immunostained for STRO-1. In Vybrant-stained experiments, cells were mixed at a 4:1 ratio of red to green. MG-63 cells cultured at low density, up to approximately 60% confluence, strongly express STRO-1, thus providing an ideal population of cells for use in development of the device for STRO-1+ cell isolation.

6.2.4. Fluorescent labelling for cell tracking

Populations of hBMSC and MG-63 cells were dissociated from tissue culture plastic using accutase (1X solution, Sigma A6964), suspended in sort buffer (PBS + 1% BSA + 5mM EDTA + 25mM HEPES) and labelled using immunostaining for STRO-1. To

provide fluorescent marking of STRO-1 positive cells, cells were incubated in a 1:1 mix of sort buffer and mouse anti-human STRO-1 primary antibody for 45 minutes, washed and then incubated in sort buffer containing a goat anti-mouse Alexa-fluor 488-conjugated secondary antibody (1:200 dilution). To counterstain all viable cells red and enable observation of all cells within the microfluidic device, the Vybrant cell dye DiD was applied to cells post-immunostaining in a 1:200 dilution in PBS and incubated for 7 minutes at 37°C. Cells were then washed twice and resuspended in neutral buoyancy buffer for use in sorting experiments. The majority of MG-63 cells displayed some STRO-1 expression but only around 10 to 20% strongly expressed STRO-1 and exhibited a ubiquitous green fluorescent stain. As expected from previous STRO-1 isolation research, approximately 10 to 15% of hBMSCs (per population) expressed STRO-1 at detectable levels.

6.2.5. Cell recovery

Recovery methods for initial tests involved collection of positively selected cells to a sterile 2ml vial. Cells were suspended in buoyancy buffer, with addition of media to the recovered cells to reduce the buoyancy of the cell suspension. The vial was then centrifuged and the cells resuspended in fresh culture media plus 20% FCS before being seeded onto a 96-well plate. Later experiments involved recovery of cells directly to a 96-well plate. The majority of sorted cells were observed to be suspended within the first 100 to 200µl of buffer, allowing recovery of the cells to the same well. Media was then added to wells containing recovered cells to reduce buoyancy and the plate centrifuged to allow resuspension of the cells in culture media plus 20% FCS and 1% penicillin/streptomycin.

6.2.6. Genotyping isolated populations

To provide enough RNA for analysis, isolated STRO-1+ cells were seeded onto 96-well tissue culture plates and grown until approximately 100 to 200 cells were available for RNA extraction. Extracted RNA was subjected to two rounds of RNA amplification using the Arcturus RiboAmp HS PLUS kit (Applied Biosystems, KIT0525). Amplification of the RNA provided sufficient quantities for cDNA synthesis using the RT² first strand cDNA kit (SABiosences, C-03) and analysis using the RT² Profiler™ PCR Array (SABiosciences, PAHS-082) for mesenchymal stem cell markers from SABiosciences. Only genes with a Ct less than 25 were considered relevant.
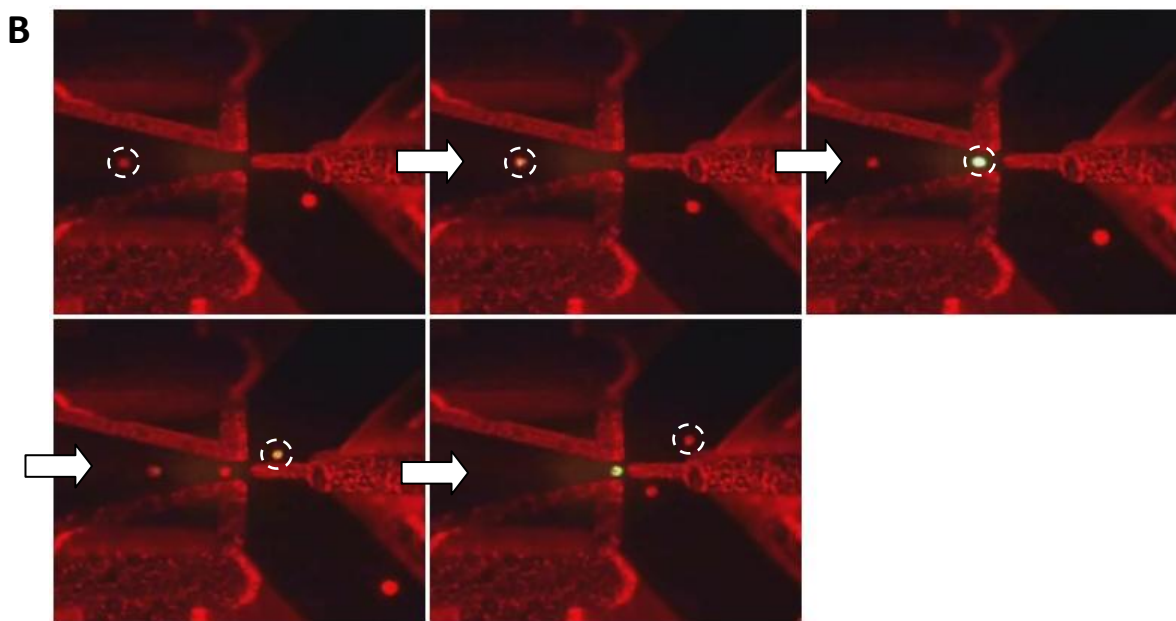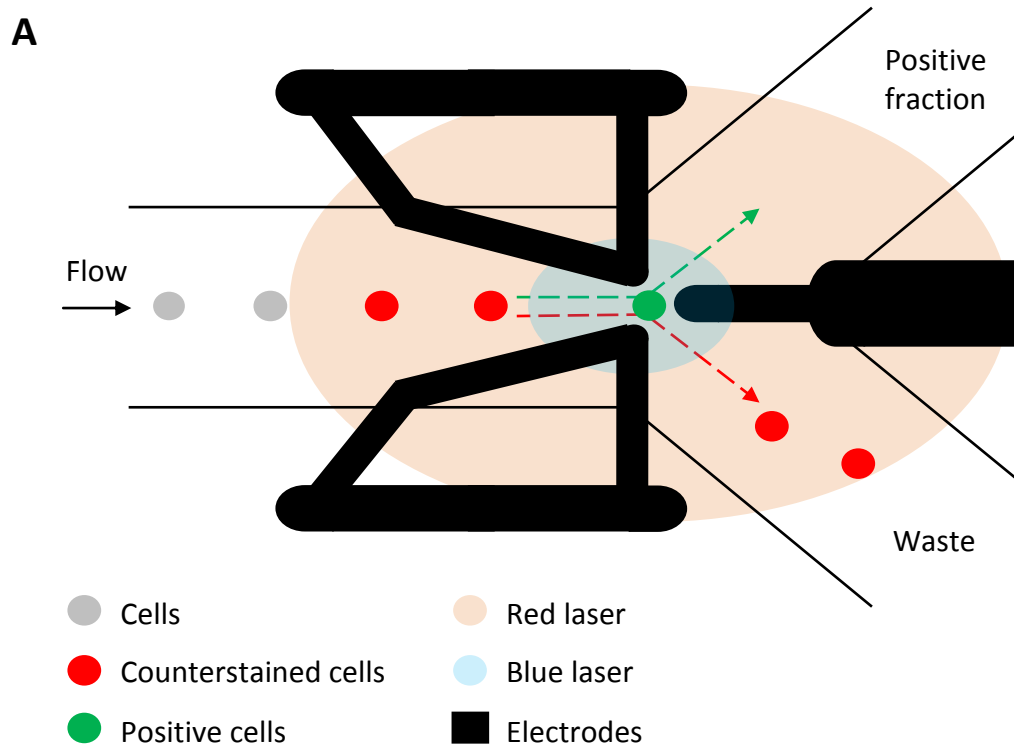
Figure 6.1. A schematic representation of microfluidic based cell sorting (A) and an image of the device positively selecting for a green fluorescent cell (circled) from a heterogeneous population (B).
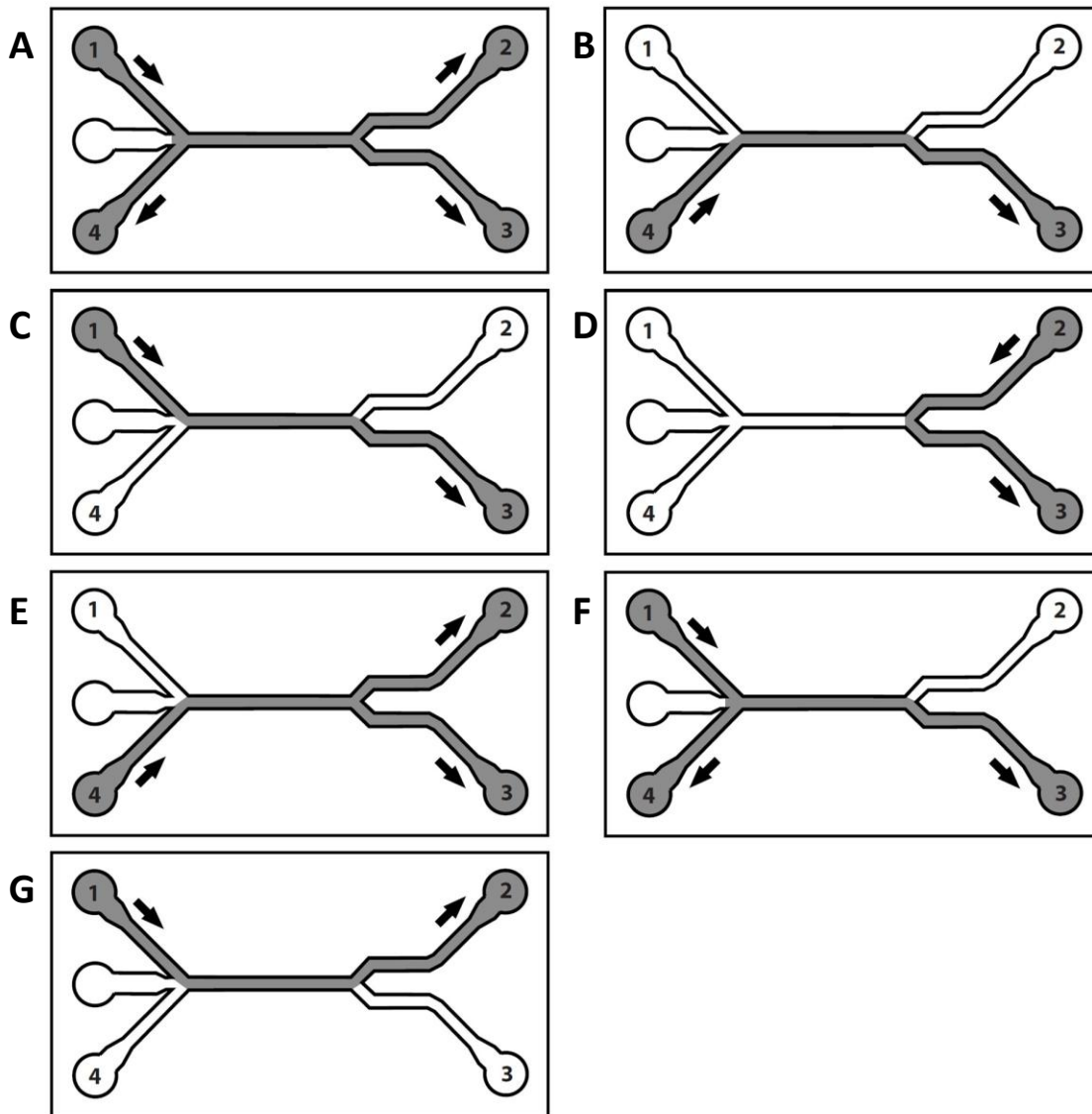
Figure 6.2. Schematic diagram of valve operation during device preparation (A-D), sorting (E) and recovery (F,G) (Figure courtesy of Dr Rupert Thomas, University of Southampton (Thomas 2006)). (A) the syringe pump is used to run sterile sorting buffer through the microfluidic device; (B) cells are introduced into the system; (C) the 'waste' output is flushed clean with buffer; (D) unsorted cells are removed from the 'positive fraction' outlet by flowing buffer back along the channel; (E) cells are sorted between the two outputs; (F) unsorted cells are flushed from the system into the 'waste' output; (G) sorted 'target' cells are flushed from the 'positive fraction' outlet and collected.

6.3. Results

6.3.1. Selection of a suitable cell buffer

Microfluidic sorting is a time-consuming process both in preparation of cells and in running cells through the device. In order to successfully isolate cells from heterogeneous populations, the cells must remain non-adherent and maintain their viability whilst in suspension. Established and primary skeletal cell populations are adherent and become sticky when kept in a single cell suspension for long periods of time. It was therefore essential to ensure that the cells were maintained in a suitable buffer that could maintain a viable single cell suspension for as long as possible.

6.3.1.1. Selection of a buffer to maintain single cell suspension and prevent cell adherence

To test the ability of potential buffers to maintain a single cell suspension, an established cell line (MG-63) and primary cell culture (hBMSCs) were dissociated from tissue culture flasks and resuspended in relevant sort buffer. The suspensions were then observed at room temperature (21°C) or 4°C for up to 4 hours to determine the level of cell adhesion. Cell suspensions were agitated every 30 minutes to maintain the cell suspension.

Sorting of cells in their normal culture medium (DMEM/αMEM) proved beneficial as the buffer was ideal for maintaining cell viability and also facilitated recovery of cells after sorting as cells could be seeded directly from sorting. However, tests using culture medium as a sort buffer demonstrated a high level of cell settling and adherence to container surfaces and other cells, confirming culture media as unsuitable for cell sorting. No significant difference was noted between cells stored at 4°C and those at room temperature.

Based on existing in-house sorting buffer recipes used for maintenance of cells in FACS and MACS, a suitable buffer was designed to replace culture media as the cell buffer during sorting. It was found that PBS (Ca/Mg^{2+} free) plus 1mM EDTA, 25mM HEPES and 1% BSA, maintained a cell suspension for over 4 hours with minimal cell-cell clumping (approximately 13% of the cells were clumped) but high levels of cell-

container adherence. No significant difference was noted between cells stored at 4°C and those at room temperature.

In order to maintain a single cell suspension and prevent settling and adhesion of cells to their container, a high molecular weight sugar, Dextran-70, was added to the sorting buffer. It was calculated that approximately 11% Dextran-70 (w/v) was required to induce neutral buoyancy. It was therefore decided that 10% Dextran-70 would be used to provide a buoyancy level that significantly reduced the settling of cells and limited the level of clumping, whilst not completely preventing cells from settling over time. After 4 hours, both 4°C and room temperature samples demonstrated negligible levels of cell settling and adherence to the container, as well as minimal cell-cell clumping (approx. 8% of cells).

6.3.1.2. Viability of cells in buffer

Viability was assessed using the Guava EasyCyte™ Mini System (Millipore) at various timepoints up to 4 hours under room temperature and at 4°C. Cells suspended for over 4 hours were then seeded onto tissue culture plastic to determine their ability to recover and proliferate.

At room temperature (21°C), both established and primary cells demonstrated some loss of viability when suspended in culture media for 4 hours, although significant (p<0.001) loss was only observed in primary cells. Despite decreased viability, both established and primary cells were able to maintain a healthy population of cells after seeding. In both sort buffer and buoyancy buffer, cells maintained their viability for over 4 hours at room temperature and cells suspended in both buffers demonstrated readherance and cell proliferation (Figure 6.3 A,C; Figure 6.4 A,C,E,G,H,J).

At 4°C, cells from established and primary cultures maintained viability for over 4 hours in all buffers and demonstrated readherance and proliferation of cells (Figure 6.3 B,D; Figure 6.4 B,D,F,H,I,K).

178
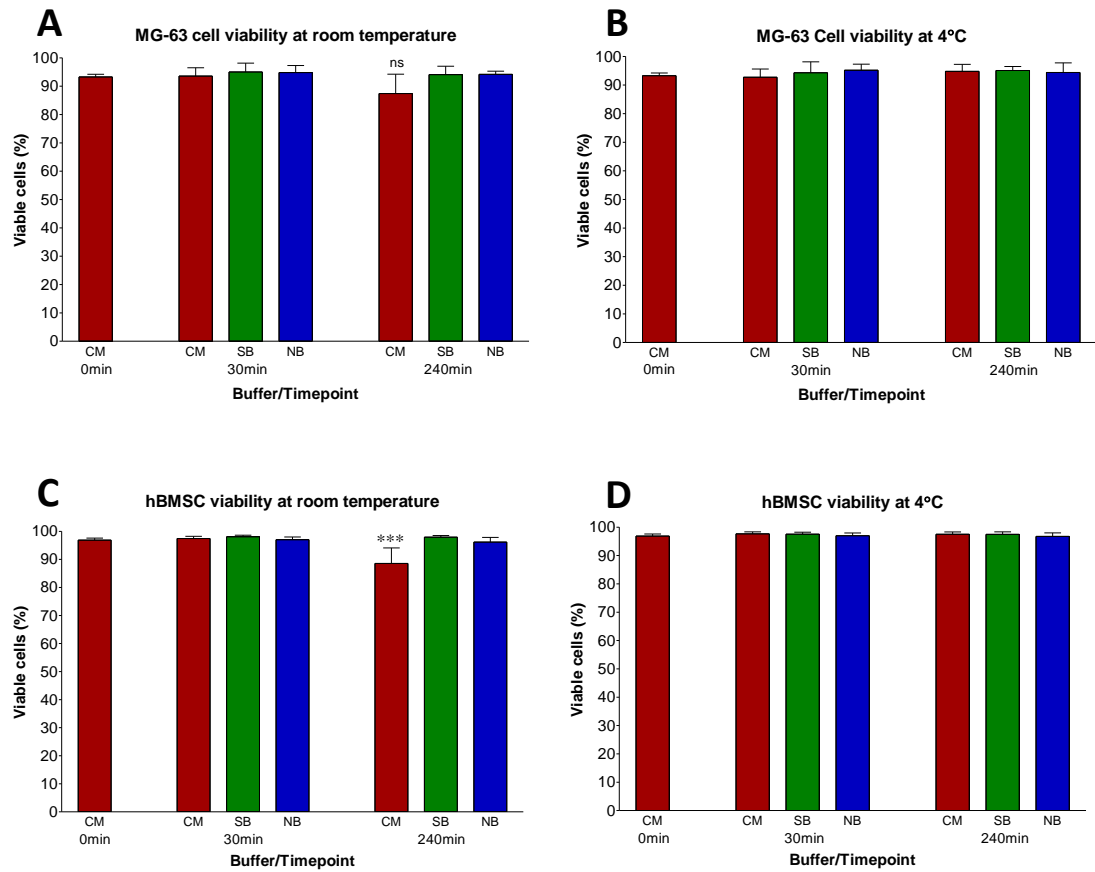
Figure 6.3. Guava-assessed viability of established and primary cell lines suspended in different sorting buffers for up to 4 hours. (A) MG-63 at room temperature (21°C), (B) MG-63 at 4°C, (C) hBMSCs (p0) at room temperature (21°C), (D) hBMSCs at 4°C. Key: CM, culture media (red); SB, sort buffer (green); NB, sort buffer plus 10% Dextran-70 (blue). Results shown as mean ± SD, n ≥ 3, *** = p<0.001, ns = not significant.
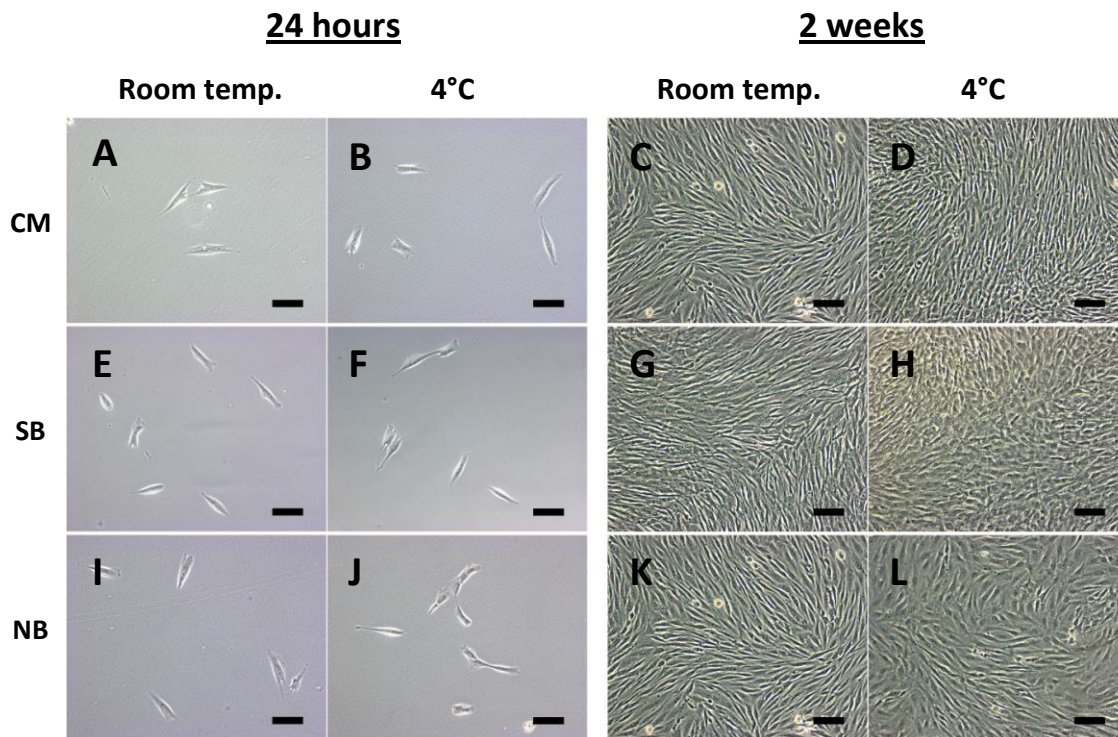
Figure 6.4. Images of MG-63 following 4 hours incubation in sorting buffers at 24 hrs post-seeding (left column) and 2 weeks post-seeding (right column). Cells incubated in DMEM buffer at room temperature (A, C) and at 4°C (B, D). Cells incubated in Sort buffer at room temperature (E, G) and at 4°C (F, H). Cells incubated in buoyancy buffer at room temperature (H, J) and at 4°C (I, K). Key: CM, culture media; SB, sort buffer; NB, sort buffer plus 10% Dextran-70. Scale bars: 100µm.

6.3.2. Cell dissociation tests

6.3.2.1. Dissociation of confluent MG-63 cells:

The method used for cell dissociation plays a key role in preventing cell clumping and in establishing a single cell suspension, critical for effective microfluidic cell sorting. In order to find the best protocol, a variety of different cell dissociation solutions, including trypsin, Accutase (Sigma, A6964), Accumax (Sigma, A7089), trypsin/collagenase and enzyme-free dissociation fluid, were tested on confluent MG-63 cell populations (Figure 6.5). The resulting dissociated cells were re-seeded to determine any effect of the solutions on the viability of the cells (Figure 6.6).

Trypsin dissociation of cells proved extremely effective (5 minutes at 37°C) although significant cell clumping was observed due to the expression of collagen matrix not degraded by the trypsin enzyme (Figure 6.5 A). Trypsin dissociated cells maintained their viability and demonstrated successful readherence to tissue culture plastic (Figures 6.5 B and 6.6).

Accutase is a commercially available dissociation buffer that combines protease and collagenolytic activities, designed to maintain a high level of cell viability. Accutase-induced detachment of confluent cells from tissue culture plastic (15 minutes at 37°C) exhibited a significant increase in single cells in comparison to trypsin-dissociated cell suspensions (Figure 6.5 C) and demonstrated high levels of cell readherence and viability (Figures 6.5 D and 6.6). However, accutase-dissociated cell suspensions still maintained small numbers of collagen-induced cell aggregates that interfered with effective cell sorting.

Accumax maintains the protease and collagenolytic activities of accutase together with the addition of DNase and is designed specifically to dissociate cell clumps into single cell suspensions. Accumax proved effective for cell dissociation (15 minutes at 37°C), resulting in the generation of a single cell suspension with minimal clumping of cells (Figure 6.5 E). Accumax dissociation demonstrated a minor deleterious effect on the viability of the cells, with approximately 5% loss in cell readherence in comparison to accutase. However, the difference in viability between Accumax and other dissociation buffers was statistically insignificant (Figure 6.6). This was corroborated as cells maintained a high level of cell recovery and proliferation (Figure 6.5 F).

It was found that use of a collagenase pre-treatment before use of trypsin dissociation resulted in an effective cell dissociation protocol, with very few cell clumps. However, this technique was deemed no more effective than use of Accumax or Accutase, whilst having the drawback that collagenase treatment required incubations of greater than 30 minutes. Use of enzyme-free dissociation buffer was ineffective at dissociating cells from tissue culture plastic and cells that did detach did so in cell sheets. It was concluded that Accumax would be used for dissociation of cells for use in sorting experiments due to the high viability and negligible cell clumping resulting from its use.
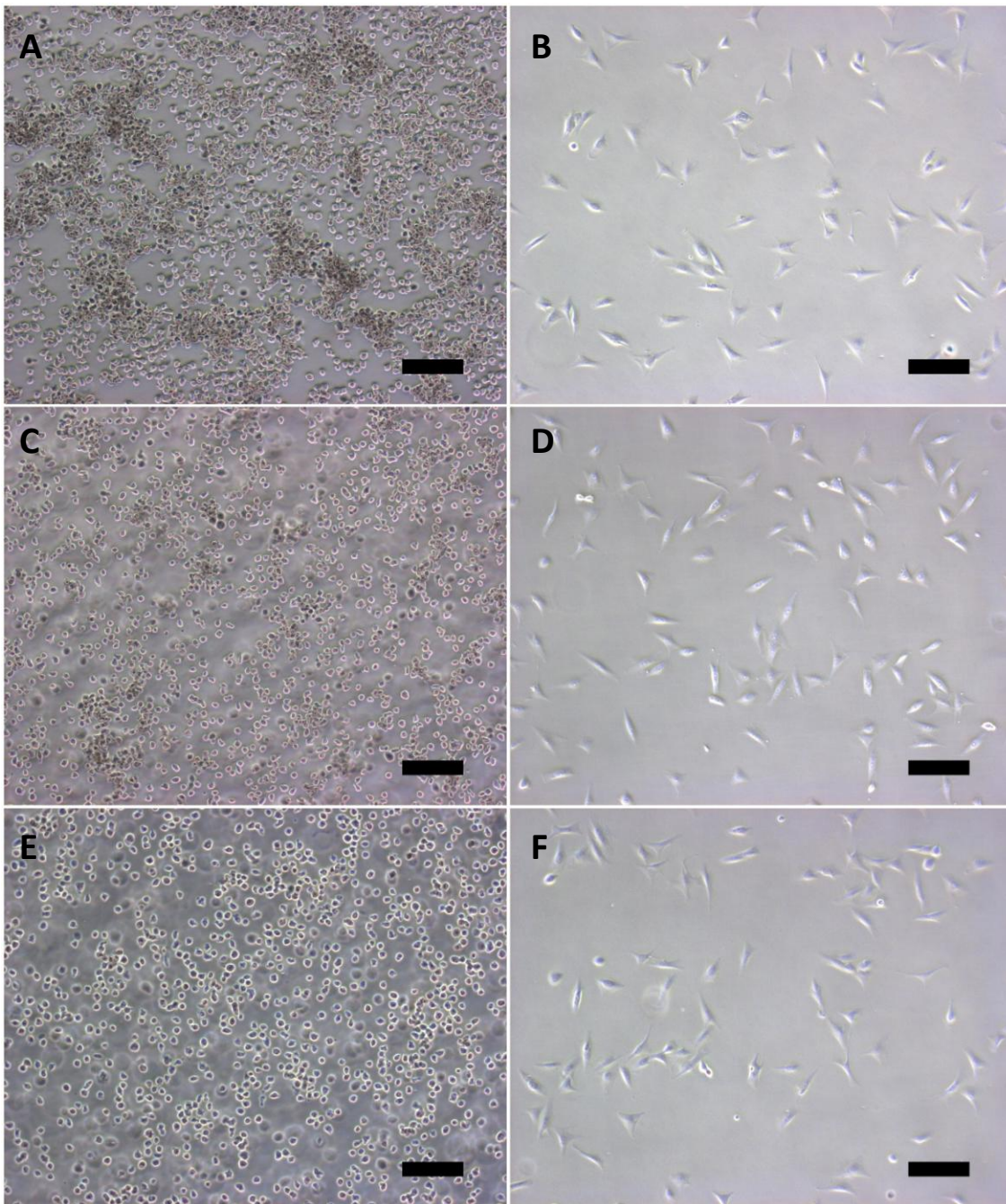
Figure 6.5. Dissociation tests on confluent MG-63 cells. Trypsin dissociation was unable to remove the majority of cell clumps (A) but cells remained viable (B). Accutase dissociation greatly reduced numbers of cell clumps but still maintained a small number of large cell aggregates (C), while cells remained viable (D). Accumax dissociation resulted in a mostly single cell suspension (E) and cell viability demonstrated no significant difference to that seen with other dissociation buffers (F). Scale bars: 200µm.
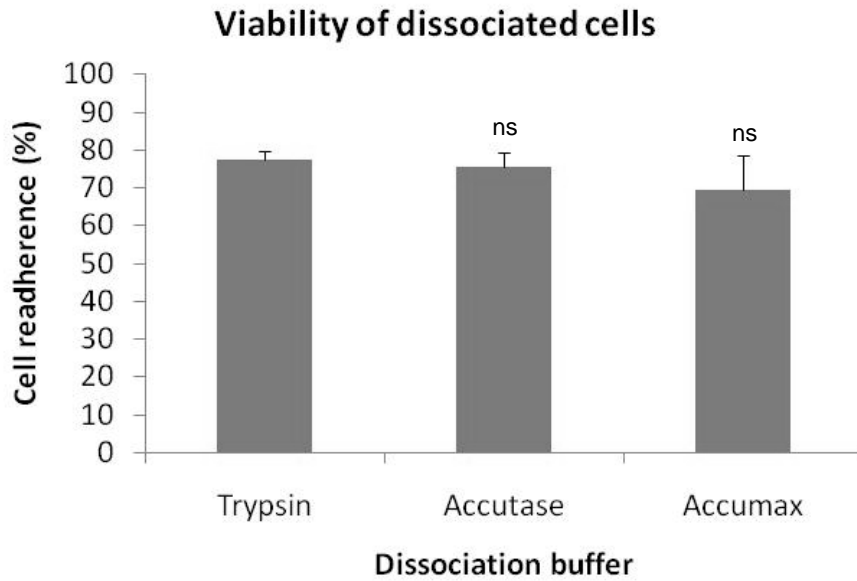
Figure 6.6. Readherence of cells 24hrs post-dissociation. Results are shown as mean ± SD, n = 4, ns = not sigificant.

6.3.2.2. Dissociation of hBMSC cells

When grown in monolayer culture for extended periods of time, hBMSCs are known to produce large amounts of collagenous matrix. The presence of this matrix was extremely detrimental to the establishment of a single cell suspension as large amounts of collagen-adhered cell clumps remained. Use of trypsin-collagenase and buffers with collagenolytic activity (Accutase and Accumax) were found to significantly reduce the level of clumping. However, it was found that collagenase-treated cell suspensions contained large amounts of debris and cells readily coalesced within a short period of time post-dissociation, suggesting a remaining presence of collagen. Modification of the hBMSC growth protocol presented the ideal method of reducing collagen-induced cell aggregates. After isolation from bone marrow, cells were seeded at high density and allowed to adapt to monolayer culture and to establish for 6 days, during which minimal collagen production occurred. After 6 days, at which time cells reached 50% confluence, the flasks were dissociated using accutase. Populations of cells grown and dissociated using this protocol were found to maintain single cell suspensions with minimal clumping for up to 4 hours post staining, facilitating microfluidic isolation of cells.

6.3.3. Effects of staining on cell viability

Staining of cells with fluorescent markers was essential for identification of positive and negative cell fractions. A variety of different cell markers, including cell tracker green, Vybrant CFDA, Vybrant DiD and Vybrant DiO, were tested on multiple populations of MG-63 cells (n>3) to determine the effects of the stains on cells for microfluidic sorting (Figure 6.7). The Vybrant dyes DiD (red) and DiO (green) were chosen as a rapid and uncomplicated method for fluorescent cell staining during development of the sorting protocol and for background staining of all cells. Whilst immunofluorescent staining was used for labelling of specific cell markers such as STRO-1.

Unstained populations of MG-63 cells demonstrated an average of 87% cell readherence for up to 4 hours post-staining when not subjected to the microfluidic process. Cells that were processed through the microfluidic device demonstrated a statistically insignificant drop in readherence to 81% on average. While not statistically significant, this minor loss of readherence indicated that the microfluidic device may have had a small detrimental effect on cell viability.

The ethanol-based DiD stain maintained readherence of unprocessed cells at 86% when kept for up to 4 hours in suspension, confirming the negligible effects of this dye on cell viability. However, DiD-stained cells processed through the microfluidic device induced a significant ($p<0.01$) reduction in cell readherence to a 71% average; a 10% drop in viability in comparison to processed unstained cells. This suggested a synergistic detrimental effect of both the staining and the microfluidic device on cell viability.

Addition of the dimethylformamide based Vybrant stain, DiO, alongside DiD was found to cause notable loss of viability in both microfluidic-processed and -unprocessed populations of MG-63 cells. Viability of DiD/DiO-stained cells was significantly less than that of unstained and DiD-stained cells immediately post-staining ($p<0.001$). Viability continued to drop significantly over 4 hours in suspension ($p<0.001$), with average cell adherence for unprocessed cells dropping from 67% post-staining to 42% after 4 hours in suspension. Processed populations demonstrated severe loss of viability, with an average of 16% readherence of cells.

184

Cells that underwent immunofluorescent staining for STRO-1/DiD demonstrated average cell readherence of 73% immediately post-staining; a significant decrease in comparison to unstained cells (p<0.01), but maintained viability for up to 4 hours in suspension when unprocessed. Thus the long immunostaining protocol and inherent stress from high levels of manipulation resulted in detrimental effects on cell viability. Coupled with exposure to the microfluidic process, cell readherence dropped to an average of 55%, again highlighting the detrimental synergy of staining- and microfluidic-induced stress. While the reduction in viability was not ideal, immunostained cells still maintained a level of readherence considered satisfactory for cell isolation and recovery.
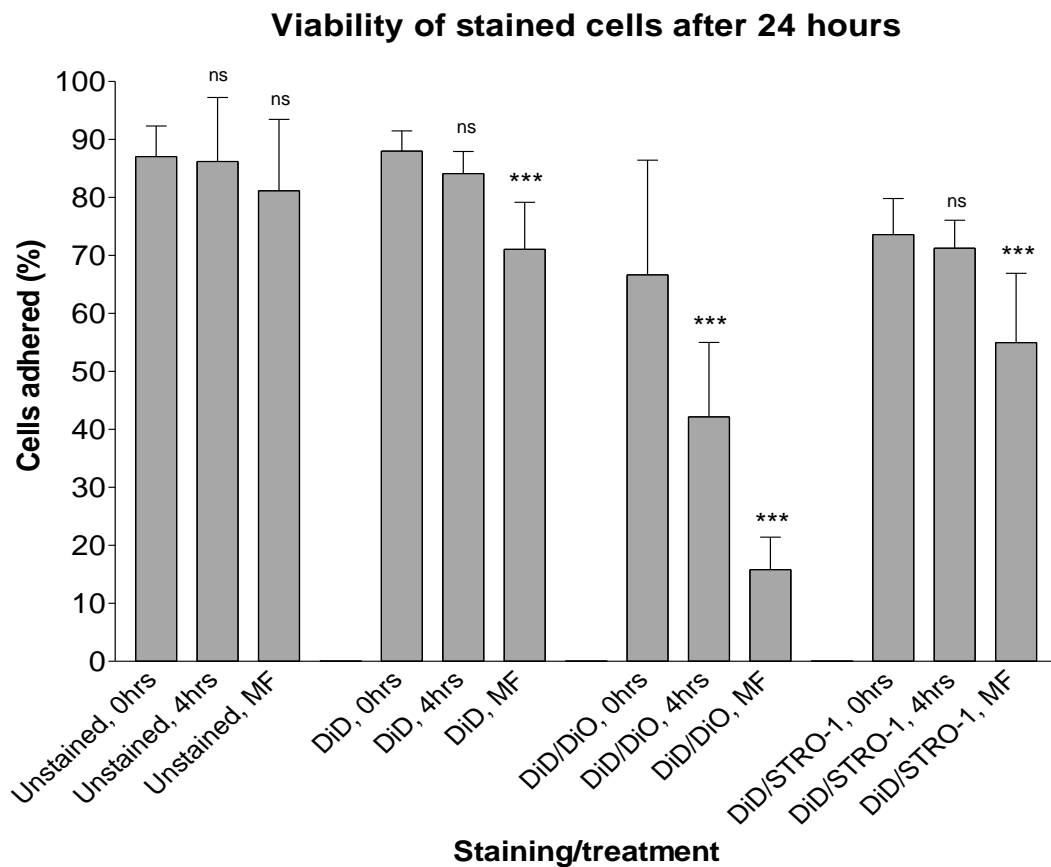
Figure 6.7. Viability of vybrant-stained, unsorted and sorted cells after 24 hours. Readherence of cells 0 hours post-staining (0hrs), 4 hours post-staining (4hrs) and post-microfluidic sorting (MF) was observed for unstained cells, DiD-stained cells, DiD/DiO stained cells and DiD/STRO-1 stained cells. Results are shown as mean ± SD, n ≥ 3. For each staining protocol, comparison to the 0hr control is shown as: ns = not significant, *** = p<0.001.

6.3.4. Selection of the appropriate field strength

Dielectric fields have been known to have detrimental effects on the viability of cells as a consequence of frequency-induced disruption of the cell membrane or voltage-induced heating. Previous work on the trapping device (Chapter 5) had demonstrated the effectiveness of a 5Mhz frequency for maintaining cell viability and a strong manipulative field, as such, this frequency was also used for sorting experiments. A voltage of 9vpp or greater was shown to provide a dielectric field strong enough for cell manipulation. Therefore a voltage dose response was performed to determine the effect of different voltages on cell viability.

MG-63 cells exposed to the dielectric field at both 8vpp and 10vpp demonstrated readherence and proliferation for up to 2 weeks post-exposure, while exposure to 12vpp resulted in complete loss of cell readherence (Figure 6.8). Analysis of cell viability using the Guava EasyCyte™ Mini System demonstrated no significant ($p > 0.05$) loss in cell viability in populations of cells exposed to a field of 10vpp and 5Mhz frequency (Figure 6.9).
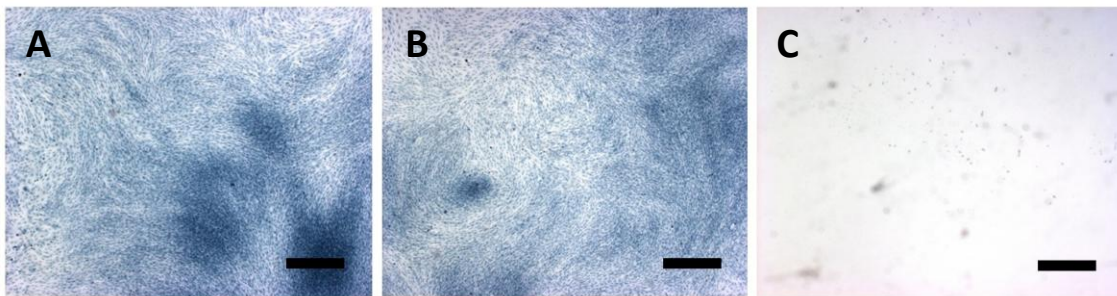
Figure 6.8. Viability and proliferation of MG-63 cells exposed to a dielectric field set at: (A) 8vpp and 5Mhz frequency; (B) 10vpp and 5Mhz frequency; and (C) 12vpp and 5Mhz frequency. Images taken 2 weeks post-exposure and cells were stained for Wigert's haemotoxylin to allow clear observation. Scale bars: 500µm.
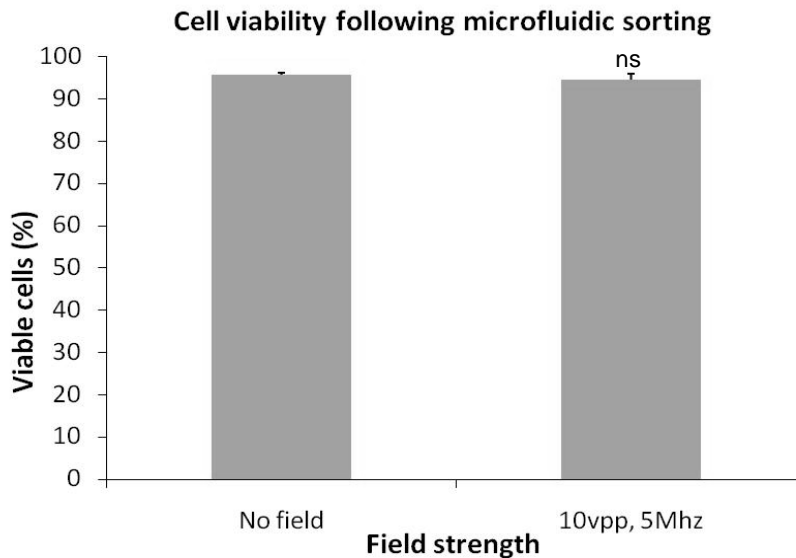
Figure 6.9. Viability of MG-63 cells exposed to 10vpp, 5Mhz electronic field, assessed using the GUAVA Viacount. Populations of unstained (negative) and DiD stained (positive) cells were exposed to the dielectrophoretic field and the viability compared to control populations (unsorted). Results are shown as mean ± SD, n ≥ 3, ns = not significant.

6.3.5. Sorting of fluorescent-stained MG-63 osteoblast populations

Use of the automated software resulted in sorting and recovery of populations with greater than 95% green cells (Table 6.1, Runs 1-4). Red cell contamination of the positive fraction during sorting was caused either by the software being unable to recognise clumps of cells as more than one cell (red cells adhered to green cells were recognised as green), or as a consequence of too many cells being present within the sorting gate at one time, resulting in a loss of field strength and thus reduced ability of the device to prevent cells from entering the positive channel. Reduction of the cell density and improvements to the composition of the suspension of cells (via use of buoyancy buffer) helped to decrease the frequency in errors caused by these issues. Use of a semi-manual approach resulted in consistent sorting of 100% positive (green) populations from heterogeneous cells (Table 6.1, Runs 5-13). Errors in automated cell sorting were found to occur approximately once every 20-30 cells.

Sorting experiments were recorded at 30-45 minutes duration and resulted in an average of 50 positive green cells to be sorted. The output of positive cells was restrained by the slow flow rate required to allow cells to be manipulated correctly and the low numbers of spatially isolated green cells available due to clumping or proximity to negative cells during sorting.

In initial tests where cells were recovered to a sterile 2ml vial before plating, the number of recovered cells was significantly less than that of the cell sorted, with an average loss of around 54% of cells (Table 6.1, Runs 1-6). It was accepted that it was likely a small portion of recovered cells would not be recovered due to settling and adherence to the positive recovery tube during the sort process. However, the loss of such large numbers of cells during recovery was unexpected and considered to be due to cell lysis and loss of cells during centrifugation. It was probable that the stress of centrifugation coupled with the already poor cell viability due to the use of the DiD/DiO dual staining technique and exposure to the dielectrophoretic field resulted in high levels of cell lysis. In later experiments, recovery by direct seeding into 96-well plates exhibited some cell loss, assumed to be due to cell settling in the recovery tube, but demonstrated a marked improvement in recovered cell number in comparison to the centrifugal recovery method, with an average loss of 23% of the cells and some populations only losing 3.5% of the sorted cells during recovery (Table 6.1, Runs 7-13).

Readherence of recovered cells stained with Vybrant DiO was generally poor and only one out of six recovered populations demonstrated proliferation (Table 6.1, Runs 1-6). However, poor recovery was expected as unsorted control populations and previous viability tests demonstrated the detrimental effect of the DiD/DiO dual staining coupled with exposure to the electric field. Early experiments using the DiD/STRO-1 immunostained MG-63 cells also demonstrated poor numbers of readherent cells (~9-20% cell readherence) (Table 6.1, Runs 7-9) due to an unoptimised staining protocol inducing cell stress and loss of viability. Optimisation of the staining protocol in resulted in 54-72% cell readherence in recovered populations (Table 6.1, Runs 10-13), while culture of recovered cells in conditioned media (media previously used to culture cells) aided recovery and establishment of proliferating populations, even in those experiments with low numbers of recovered cells (Table 6.1, Runs 8-13).

Run	Green stain	Sort type	Cells sorted (approx.)	Cells recovered	Cells adhered	Control viability (%)	Sort viability (%)	Green cells	Purity (%)	Proliferated
1	DiO	Automated	50	16	10	71.4	**62.5**	16	**100.0**	No
2	DiO	Automated	80	40	22	62.9	**55.0**	39	**97.5**	Yes
3	DiO	Automated	40	27	7	32.5	**25.9**	27	**100.0**	No
4	DiO	Automated	80	41	11	36.6	**26.8**	39	**95.1**	No
5	DiO	Manual	60	21	4	68.2	**19.0**	21	**100.0**	No
6	DiO	Manual	80	30	11	69.4	**36.7**	30	**100.0**	No
7	STRO-1	Manual	40	34	3	61.5	**8.8**	34	**100.0**	No
8	STRO-1	Manual	70	64	7	51.5	**10.9**	64	**100.0**	Yes
9	STRO-1	Manual	57	55	11	41.4	**20.0**	55	**100.0**	Yes
10	STRO-1	Manual	35	24	13	75.2	**54.2**	24	**100.0**	Yes
11	STRO-1	Manual	25	17	12	71.7	**70.6**	17	**100.0**	Yes
12	STRO-1	Manual	20	12	7	65.5	**58.3**	12	**100.0**	Yes
13	STRO-1	Manual	25	19	12	72.6	**63.2**	19	**100.0**	Yes

Table 6.1. Sorting of fluorescently-stained populations of MG-63 using DiD/DiO or DiD/STRO-1. Cells were recovered to 2ml tubes and centrifuged before resuspension and seeding (runs 1-6) or were recovered directly to 96-well plates in all experiments (runs 7-18). Key: Manual = semi-manual sorting; blue shading = Vybrant stained, automated sorting; red shading = Vybrant stained, semi-manually sorted; green shading = STRO-1 immunostained, semi-manually sorted.

6.3.6. Sorting of fluorescent-stained STRO-1 labelled hBMSC populations

hBMSC populations stained for STRO-1/DiD demonstrated higher levels of clumping than observed in MG-63 cells, resulting in an increase in errors during sorting. The increase in cell aggregates meant fewer spatially isolated green cells were available for positive selection. As a consequence, the numbers of cells that were able to be sorted during the 30-45 minute process was reduced from approximately 50 to 100 cells to an average of 21 cells per run. Use of the semi-manual method for isolation of cells, consistently produced sorted populations with purity of 100% green cells (Table 6.2). Sorted cells were recovered directly to a 96-well plate. Recovery by direct seeding exhibited an average cell loss of 20%, assumed to be due to cell settling in the recovery tube. (Table 6.2).

Immunostained hBMSCs demonstrated poor viability immediately post-staining (Figure 6.10), expressing an average readherence to tissue culture plastic of 47% (range 30-68%), but exhibited no significant decrease in viability when left in suspension for up to 4 hours. Exposure of immunostained hBMSCs to the dielectrophoretic field resulted in significant loss of viability and an average readherence of 20%, demonstrating a similar effect of the microfluidic device/staining protocol to that seen in MG-63 tests.

The poor viability of hBMSCs when exposed to the stresses of staining and subsequent sorting, coupled with the low numbers of cells recovered due to cell clumping, resulted in very few viable cells in recovered STRO-1 positive populations (Table 6.2). It was speculated that this was due to cells not being completely adapted to monolayer tissue culture growth by the time they were harvested for sorting. Despite this, the reduced level of viability was noticeable in cells exposed to the stresses of sorting, with average readherence of 34%, dropping as low as 11% in some samples. Despite the low number of cells, the use of conditioned media, combined with the colony-forming characteristics of STRO-1 positive hBMSCs, enabled establishment of proliferating cells from the small numbers that readhered (Figure 6.11).
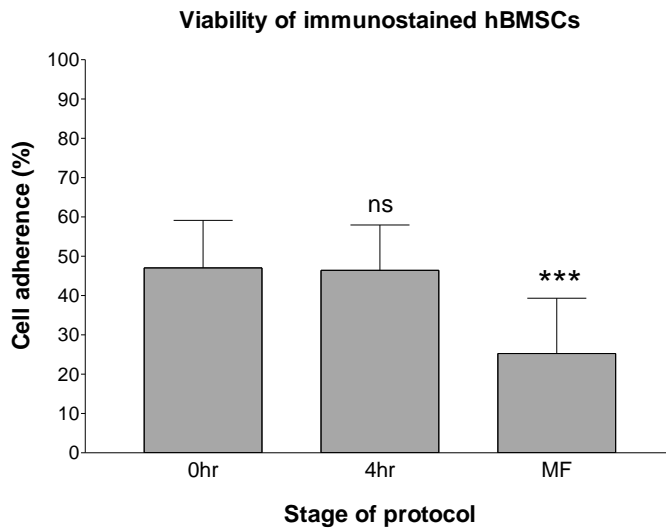
Figure 6.10. hBMSC cell viability after immunofluorescent staining for STRO-1. Readherence of cells was quantified 0 hours post-staining (0hrs), 4 hours post-staining (4hrs) and post-microfluidic sorting (MF). Results are shown as mean ± SD, n ≥ 3, ns = not significant, *** = p<0.001.

Run	Sample	Sort type	Cells sorted (approx.)	Cells recovered	Cells adhered	Control viability (%)	Sort viability (%)	Green cells	Purity (%)	Proliferated
1	F81	Manual	15	9	1	47.9	**11.1**	9	**100.0**	Yes
2	F70	Manual	20	17	7	44.8	**41.1**	17	**100.0**	Yes
3	F70	Manual	20	16	2	44.8	**12.5**	16	**100.0**	Yes
4	F77	Manual	30	20	5	37.9	**25.0**	20	**100.0**	Yes
5	F77	Manual	30	26	5	37.9	**19.2**	26	**100.0**	Yes
6	M79	Manual	10	10	1	30.1	**10.0**	10	**100.0**	Yes

Table 6.2. Sorting of DiD/STRO-1 fluorescently-stained populations of hBMSC. Cells were recovered directly to 96-well plates in all experiments.
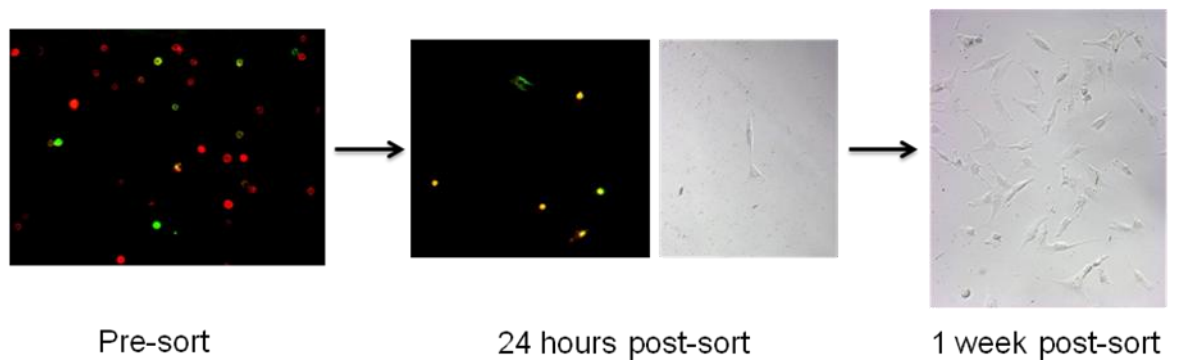
Figure 6.11. Isolation of cells using the microfluidic sorter and subsequent culture.

6.3.7. Provisional genotyping of STRO-1 isolated cells.

Analysis of non-amplified RNA from unsorted populations of hBMSCs demonstrated expression of 43 genes (see Appendix 11), while analysis of amplified RNA from isolated STRO-1 populations demonstrated expression of 27 genes associated with stem cell maintenance and differentiation (Table 6.3). In sorted STRO-1 cells, highest gene expression was demonstrated for *FGF2, ANXA5, RHOA, VIM* and *PIGS*, all of which were present in greater quantities than the housekeeping gene *GAPDH*. All genes highly expressed in sorted populations were also expressed in unsorted cells except for *MITF*, *PPARγ* and *TNF*.

SYMBOL	GENE NAME
ALCAM	activated leukocyte cell adhesion molecule (CD166)
ANPEP	alanyl (membrane) aminopeptidase (CD13)
ANXA5	annexin A5
BDNF	brain-derived neurotrophic factor
CASP3	caspase 3, apoptosis-related cysteine peptidase
COL1A1	collagen, Type I, alpha 1
FGF2	fibroblast growth factor 2
GDF15	growth differentiation factor 15
GTF3A	general transcription factor IIIA
HAT1	histone acetyltransferase 1
HDAC1	histone deacetylase 1
ITGA6	integrin, alpha 6
ITGAV	integrin, alpha V
ITGB1	integrin, beta 1
KITLG	KIT ligand
MITF	microphthalmia-associated transcription factor
NT5E	5'-nucleotidase, ecto
NUDT6	nudix (nucleoside diphosphate linked moiety X)-type motif 6
PIGS	phosphatidylinositol glycan anchor biosynthesis, class S
PPARG	peroxisome proliferator-activated receptor gamma
RHOA	ras homolog gene family, member A
SLC17A5	solute carrier family 17 (anion/sugar transporter), member 5
SMAD4	SMAD family member 4
THY1	Thy-1 cell surface antigen (CD90)
TNF	tumor necrosis factor
VCAM1	vascular cell adhesion molecule 1 (CD106)
VIM	vimentin

Table 6.3. List of genes highly expressed in microarray molecular analysis of isolated STRO-1+ hBMSC populations. Genes with a Ct ≤ 25 are shown. Genes are normalised against *GAPDH*, n=3.

192

6.4. Discussion

Studies using microfluidic trapping have demonstrated high purity but relatively low numbers of recovered cells (Thomas et al. 2010), while previous studies using microfluidic cell sort devices have demonstrated high throughput and enrichment of cells using both magnetic and fluorescent antibodies for specific markers, but have failed in the isolation of 100% pure populations of cells of interest (Kim et al. 2008b). This study has demonstrated that through use of a novel nDEP sorter; small numbers of viable, 100% pure STRO-1+ cell populations can be separated and recovered from heterogeneous populations of MG-63 osteosarcoma cells and hBMSCs.

While the sorting device is effective at isolating specific cells, maintaining cell viability during the sorting process can be difficult. Immunostaining of cells to allow fluorescence-based sorting resulted in significantly decreased viability, most likely due to the stress of repeated manipulation and being kept in suspension for extended periods of time. In addition to the stress of staining, exposure to the microfluidic device was demonstrated to induce a further loss of viability. While neither the staining or device-induced stresses were great enough by themselves, when coupled, the viability of cells was significantly reduced. This data confirmed the trend seen in the microfluidic trapping device (Chapter 5), in that the reduction in viability of sorted cells was a result of the combined effects of multiple stimuli, including cells becoming stressed by staining, being held for sustained periods in suspension and being exposed to a dielectrophoretic field.

The high level of clumping observed during cell sorting is believed to be due to collagen produced by skeletal tissue cells when grown in monolayer culture. Monolayer cultures are known to produce high levels of collagenous matrix when at high levels of confluence (approx. > 70%). Use of collagenase-based dissociation buffers (trypsin/collagenase B or accutase dissociation) resulted in breakdown of the collagen fibres and was effective at releasing single cells into suspension. However, it was noted that collagen debris remained in the cell solution and aided cell clumping during sorting. Therefore it was deemed essential that populations contain as little collagen as possible before dissociation and use in sorting. To enable this, cells grown for use in the microfluidic device were kept at low confluence by seeding at low density. By seeding

at low densities (approx. 5% confluence) and ensuring cells were under 50% confluence before passage or use in the device, it was possible to establish populations of cells with very little collagen deposition, thus reducing the level of clumping. Culture of cells at such low densities was further beneficial as it aided maintenance of STRO-1 expression in cells.

Due to the robustness of the MG-63 cell line, using the optimised protocol it was possible to recover populations of sorted STRO-1+ cells with minimal loss of viability even when using low density cultures (average loss of 10%), enabling establishment of viable, proliferative somatic cell populations. In contrast, hBMSCs demonstrated substantial loss of viability. Normally, hBMSCs are grown for up to 2 weeks after extraction from bone marrow, enabling the cells to adapt to monolayer culture and establish robust, viable populations. However, to ensure a collagen-free population, cells were seeded at low density and only cultured for 6 days before dissociation and use in cell sorting. It is possible that due to this shortened incubation period, the hBMSCs were not fully adapted to *ex vivo* culture and as such, demonstrated decreased robustness, leading to substantial loss of viability when exposed to the stress of staining and sorting. If true, this highlights a trade off between maintaining a robust culture that can maintain viability during the microfluidic protocol and ensuring that populations are not allowed to remain in culture long enough or at confluence levels that stimulate high levels of collagen production.

Recovery of cells after sorting typically resulted in a 68% yield of isolated STRO-1+ cells, highlighting a loss in the number of output cells of interest. The loss observed was believed to be due to settling of cells within the device whilst awaiting recovery, coupled with loss of cells during centrifugation and resuspension in conditioned media post-recovery. With a suitably sized population of sorted cells, this loss of cells is not detrimental to the establishment of a viable population. However, in samples demonstrating high levels of clumping or low numbers of STRO-1+ cells, this loss may lead to issues in establishment of populations or direct analysis of cells. This fault could be addressed by increasing the initial output of sorted cells.

Despite low density culture and use of collagenase-based dissociation, hBMSC populations in suspension demonstrated higher levels of clumping than observed in MG-63 cells, despite use of neutral buoyancy buffer to prevent cell settling, resulting in an increase in errors during sorting and fewer spatially isolated green cells available for positive selection. This, in turn, resulted in sorting and recovery of very few STRO-1+ hBMSC cells. However, due to the colony-forming nature of these cells, it was possible to establish readherence and proliferation of the recovered STRO-1 cells. Ideally, analysis would be performed directly after sorting to ensure that all cells were STRO-1+, as seeding and culture of the cells would increase the risk of re-introducing a heterogeneous population due to differentiation while in culture. Unfortunately, due to the low numbers of cells recovered, it was essential to culture the cells for a minimum of a week before extraction of RNA to ensure cells were viable. In an effort to prevent differentiation of the recovered STRO-1+ populations, sorted cells were only cultured until roughly 50% confluent.

Due to the low numbers of cells, to provide sufficient quantities of RNA to allow analysis, extracted RNA was subjected to two rounds of RNA amplification. Amplification of the unsorted cells was not recommended due to the risk of removing the heterogeneity of the cells by selecting such a small sample of the population. The amplification process is known to cause reduction in RNA sequence length, which can lead to bias towards certain nucleic acid sequences (Croner et al. 2009). Analysis of the housekeeping genes between amplified (sorted cells) and non-amplified (unsorted cells) samples confirmed this bias. All housekeeping genes except for *GAPDH* demonstrated a loss of expression in amplified RNA, confirming amplification-induced bias due to shortening of sequence length. Thus, microarray results for RNA from isolated STRO-1+ populations could not be directly compared to those for unamplified RNA from heterogeneous, non-isolated populations. Ideally, samples of both amplified and unamplified unsorted cells would have been analysed to give a clearer picture of the effects of amplification, however, due to restrictions on funding, this was not possible in this study. Despite the known risk of bias in amplified samples, amplification is a random process, therefore the use of multiple samples to provide $n \geq 3$, can reduce the risk of interpreting false signals. Thus, if a gene demonstrates high expression in all samples, it can be conferred that the gene is present in the cells and that the result is not

a consequence of amplification bias. Due to this, only those genes demonstrating similar results in all separate populations were considered relevant.

Isolated STRO-1 populations were abundant for a number of genes present in stem cell and early progenitor populations, including the stem cell/MSC markers, *FGF2* (maintenance of cell proliferation/renewal (Vallier et al. 2005)), *ALCAM* (MSC marker (Bruder et al. 1998;Arai et al. 2002)), *VCAM1* (MSC marker (Kolf et al. 2007)) and *GTF3A* (MSC-marker (Garrett-Sinha et al. 1996)) and the stem cell differentiation-inducing genes *NUDT6* (Asa et al. 2001)), *BDNF* (Long et al. 2005)) and *HDAC1* (Dovey et al. 2010)). In particular, *FGF2* was extremely abundant, suggesting a highly proliferative phenotype.

As mentioned above, due to the nucleic acid amplification required to analyse RNA from STRO-1+ cells, direct comparison of sorted and unsorted cells was unreliable. However, it was noted that in relation to *GAPDH* expression, the genes for *ANXA5, FGF2, PIGS, RHOA, VIM, GTF3A, HDAC1* and *NT5E* were all found to have substantially greater expression in sorted STRO-1+ cells than in unsorted cells, while *ITGB1* and *COL1A1* were expressed at much lower levels in STRO-1+ than in unsorted cells. If it was assumed that the differences in gene expression were not due to amplification bias, then the fact that sorted cells express greater levels of stem cell markers *FGF2, GTF3A* and *HDAC1* may confirm a less differentiated phenotype for STRO-1+ cells. However, abundance of genes expressed during adipogenesis (*PPARγ*) and skeletogenesis (*COL1A1, GDF15, SMAD4, CASP3, ANXA5* and *MITF*) suggested that the STRO-1+ cells recovered still maintained a level of heterogeneity.

In conclusion, this study illustrates the potential of this dielectrophoretic device for cell isolation from heterogeneous populations. While this device is hampered by issues that limit the number of cells that can be isolated and recovered, such as cell clumping and stress of manipulation, this device is capable of isolating and recovering small cell populations with 100% purity using a dielectrophoretic sorting gate, in contrast to previous sorting devices that have a high throughput but fail to produce pure populations (Kim et al. 2008b). Application of techniques to reduce cell clumping and improve the single cell suspension would enable higher throughput of cells for recovery

196

and analysis, while potentially enabling fully automated sorting whilst maintaining 100% purity. Application of a upgraded automated system, able to recognise and remove errors without the need for manual intervention, would reduce run times and may also enable multiple sorting gates to be run in parallel, further increasing the cell output for analysis. Alternatively, should the number of cells recovered not increase, introduction of a suitable method for direct analysis of small numbers of cells such as the Fluidgm Biomark™ (Narsinh et al. 2011) or integration of on-chip PCR analysis (Ottesen et al. 2006;Marcus et al. 2006) would enable use of the device for analysis of the recovered cells. In addition to single marker selection, use of sequential sorting gates offers potential for the isolation of cells stained for multiple markers during one sorting run.

CHAPTER 7

FINAL DISCUSSION

7.1. Discussion

With the increasing rise in population and life-expectancy, there is an urgent socio-economic and clinical challenge to develop strategies for the repair of cartilage and bone lost as a consequence of trauma, disease or natural degeneration. Stem cell based tissue engineering is viewed as a promising approach for orthopaedic reparative medicine that requires the spatially and temporally coordinated application of a suitable population of cells, a biocompatible extracellular matrix or scaffold and specific tissue-inducing growth factors (Sundelacruz & Kaplan 2009).

The choice of cell line for use in tissue engineering is critical, as the cells must be compatible with current and future scaffolds as well as responsive to tissue induction. Both differentiated and undifferentiated cells can be obtained from many types of tissue with relative ease via techniques such as enzyme degradation of extracellular matrix or mechanical disruption of tissue. One issue found with the use of mature, differentiated cells is the loss of their *in vivo* phenotype when grown in culture *in vitro*, and subsequent difficulty in converting them back to the relevant tissue for use in reparative medicine (Goessler et al. 2005). The majority of research is focused on the identification and isolation of specific populations of stem cells and progenitor cells that offer a wide range of uses and are easily adaptable to tissue engineering. Bone marrow is a good source of both stem cells and skeletal progenitor cells, the most highly sought of which is the mesenchymal stem cell. MSCs are considered an ideal candidate for use in therapeutic medicine as they are multipotent, versatile, easy to grow and can be used for transduction of therapeutic genes into a host. However, to date very little is known about the phenotypic characteristics of these cells as the "true" MSC has yet to be isolated and characterised (Bianco et al. 2001). It is estimated that the frequency of MSCs *in vivo* ranges from 1 in 10,000 to 1 in 2,000,000 human bone marrow mononuclear cells, dependant on the age of the patient (Caplan 2007).

Many macroscale methods currently exist for MSC isolation including density centrifugation (Chang et al. 2009), adherence to tissue culture plastic (Friedenstein et al. 1970;Guo et al. 2006), use of selective culture media such as chemically defined media (Johansson & Wiles 1995) and selection for specific properties such as size (Hung et al. 2002) or expression of cell markers by techniques such as MACS and FACS. Attempts

to isolate pure populations of MSCs by MACS and FACS are limited by the paucity of knowledge regarding specific markers for these cells, therefore 'isolated' populations of MSCs regularly include a variety of cell types ranging from multipotent stem cells to differentiated progenitor cells for specific tissues (see Chapters 5 and 6). The heterogeneity of isolated MSC populations can be observed in cell morphology, proliferation and expression of cellular markers (Sengers et al. 2010). Populations of MSCs have been isolated using a variety of markers found on their surface membrane. Potential markers for MSCs include STRO-1, CD73, CD90, CD105, CD106, CD140b, CD146 and CD271 (Salem & Thiemermann 2010). However, none of these are unique to the MSC preventing use of a singular marker for the isolation of MSCs, indeed, according to the International Society for Cellular Therapy, the expression of CD73, CD90 and CD105 and lack of CD34, CD45, CD11a, CD19 and HLA-DR are considered the minimum criteria for defining MSCs (Dominici et al. 2006). Markers for MSCs are also expressed in variable levels throughout isolated populations, thus selection of a suitable cut-off point for marker expression is essential (Chapters 5 and 6). For example, MSCs isolated by FACS using fluorescent antibodies for STRO-1 and CD271 exhibited diverse levels of fluorescent intensity, ranging from bright to dim, indicating the range of stem cell-like properties within isolated populations, with MSC populations with bright STRO-1 and CD271 expression exhibiting the most stem-like properties (Gronthos et al. 2003;Buhring et al. 2007). Thus, identification and isolation of pure MSCs will likely result from recognition of multiple attributes, rather than an individual marker, as identification of a surface marker unique to the MSC remains elusive.

Miniaturisation of laboratory methods using microfluidic, or lab-on-a-chip (LOAC) technology, has become a major area of research, generating a large variety of techniques for cell isolation. Microfluidic devices offer many advantages over standard laboratory equipment as they are economical, adaptable and use very low volumes of reagents, enabling analysis of rare substances and cell types (Manaresi et al. 2003). Microfluidic cell isolation has been performed using acoustic, optic, magnetic and dielectrophoretic (DEP) manipulation (Johann 2006). The use of DEP-based microfluidic devices has enabled both contact (positive DEP) and non-contact (negative DEP) isolation of cells using both trapping and sorting techniques and offers potential

for characterisation of isolated cells (Taff & Voldman 2005;Thomas et al. 2009). This study has shown that isolation of cells from a heterogeneous population is possible using nDEP trap and sorter devices based on optical selection for fluorescent markers. However, a consistent issue found during isolation of cells using dielectrophoretic devices is the maintenance of cell viability. Use of DEP on cells is known to have a deleterious effect on cell health. Cellular protein and DNA can be damaged by high temperatures induced by high voltage fields, while use of low frequencies can result in damage to the cell membrane (Menachery & Pethig 2005). Prolonged exposure to dielectric fields found in devices that trap and hold cells, run a high risk in loss of cell viability, inhibiting the effectiveness of these devices (as demonstrated in Chapter 5). While the electric field can be adapted to minimise the risk of cell deterioration by using high frequencies and low voltages, use of devices that limit exposure to DEP fields, such as constant flow sorting devices, enable reproducible isolation of viable cells for culture or analysis, as the cells are only exposed to the electrical field within the sorting gate (see Chapter 6). The nDEP sorting device used in these studies enabled isolation of STRO-1+ cells with high efficacy, resulting in viable, isolated populations with 100% purity. These devices offer great potential for isolation of cells for tissue engineering or for characterisation. However, for microfluidic devices to become established as viable alternatives for MSC isolation, it is essential that the methodology is robust and results are reproducible. For a device to meet these criteria, the term 'isolation' must be defined. The majority of cell isolation techniques are focused not on achieving pure samples but on enriching a population of cells. For example, high throughput MACS and FACS (both macro and micro) methods produce large populations sorted for specific markers, but fail to prevent a percentage of unwanted cells being recovered. These populations can therefore be referred to as 'enriched' but not pure. To date, microfluidic devices have demonstrated their ability to produce 'enriched' populations according to differences such as size (Gascoyne et al. 2009), viability (Shafiee et al. 2010), and marker expression (Wu et al. 2010), with reproducible results similar to those observed in macro techniques. Therefore it is logical that future development of devices for cell enrichment should be focused on microfluidic techniques.

Devices focused on cell enrichment such as FACS and MACS deal with large numbers, enabling recovery of thousands or more cells, this allows a certain disregard towards the live/dead ratio of recovered cells as the numbers collected are sufficient to establish healthy culture. The microfluidic devices used in this study are currently designed for the isolation and recovery of small numbers of cells (n<30), therefore the ratio of live/dead cells become much more crucial as the low numbers of cells isolated can inhibit large-scale culture of sorted cells. Optimised protocols for the microfluidic sorter used in these studies resulted in recovery of cells with an average of 62% viability, which due to the low numbers of recovered cells (average of 10 viable cells per run) limited establishment of large-scale cultures. However, this device enables recovery of populations with 100% purity for specific marker expression. While enrichment of cell populations is key for isolating specific cells for tissue engineering, the recovery of 100% pure populations is an exciting prospect, as it would enable isolation of rare cells for analysis and culture without risk of contamination with unwanted cells. The microfluidic devices outlined in this study are more suited for isolation of cells for analysis and characterisation rather than establishment of large-scale culture. However, despite the low cell numbers involved, recovery and culture of single cells with clonogenic potential, such as MSCs, would be possible using these devices.

In addition to cell isolation, microfluidic devices also offer a method for direct cellular characterisation based on the electronic potential of the cells using techniques such as electrochemical impedance spectroscopy (EIS). Integration of devices that enable high-throughput EIS characterisation of cells (Cheung et al. 2005) with cell sorting technology would facilitate label-free sorting of cell lines according to their dielectric properties. Studies have shown that similar cells such as normal and cancerous cells have demonstrated statistically significant differences in their dielectric properties (Ermolina et al. 2001;Egot-Lemaire et al. 2009), but in terms of stem cell recovery, it has yet to be seen whether the dielectric charge of the cells of interest (e.g. STRO-1+ cells) is sufficiently different to the remainder of the population to enable high-throughput isolation.

Cells derived from fetal femurs offer a potential alternative to adult bone marrow-derived cells as a source for skeletal stem cells. Fetal cells offer an improvement over adult-derived cells as they demonstrate increased proliferation, greater plasticity, are ideal targets for gene transfer and have decreased immunogenicity (Lanza et al. 2007). However, issues arise in the ethics of fetal femur use as sample acquisition is linked to the practice of abortion. Multiple studies have demonstrated the multipotency of cells isolated from fetal femurs and FFDCs have been shown to express many of the markers thought to be expressed by adult-derived MSCs, including STRO-1, CD73, CD105, CD44, CD90 and CD106 (Zhang et al. 2009). Populations of FFDCs have also demonstrated various expression of early stem cell markers such as OCT-4, NANOG and SOX2. For example, this study found no expression of the ES cell marker OCT-4 in FFDCs, but did find ubiquitous expression of SOX2, while other studies have demonstrated the presence of both NANOG and OCT-4 in FFDCs (Guillot et al. 2007;Zhang et al. 2009) and others have demonstrated a lack of expression of both NANOG and OCT-4 (Mirmalek-Sani et al. 2006). The majority of previous studies indicate the presence of early stem cell markers and a higher proliferative rate within fetal tissue-derived cells, suggesting that FFDCs maintain ES cell-like characteristics. However, use of FFDCs in tissue engineering is inhibited by the high level of patient variation as observed in organotypic ALI culture of FFDC pellets (Chapter 4). For FFDCs to be considered as a reliable source of cells for use in tissue regeneration, further work is required to determine the presence of all sub-populations within explanted FFDCs as fetal femurs are a heterogeneous mix of chondrocytes, fibroblasts, early osteoblasts, MSCs and other cells.

To remove patient variation and establish a more homogeneous, proliferative population for use in tissue engineering fetal femur cells can be cultured in CDM supplemented with Activin A and FGF2 as demonstrated in this study and in previous work by Mirmalek-Sani et al. (2009). Addition of skeletogenic factors such as BMP-2 and TGF-β to FFDCs in normal culture media results in differentiation of the cells towards bone and cartilage. However, addition of the bone-inducing factor, BMP-2, to FFDCs cultured in CDM failed to initiate osteogenesis, instead resulting in the a heterogeneous population of fibroblastic cells and a novel cobblestone phenotype. This study has demonstrated that the cobblestone cells induced by BMP-2 demonstrate an early

adipogenic phenotype and data suggests an osteogenic phenotype for the fibroblastic cells observed in CDM + BMP-2 cultures, indicating that BMP-2 induces both early osteogenic (fibroblastic) and adipogenic (cobblestone) differentiation (Mikami et al. 2011).

Monolayer culture has played a key role in the investigation of osteogenic and chondrogenic cells. However, although monolayer culture is able to provide large numbers of cells for tissue engineering, it lacks the mechanical and biochemical interactions to closely replicate growth *in vivo* (Abbott 2003). Indeed, the complex interactions between cells and ECM during skeletogenesis is dependent on a 3D environment (Tortelli & Cancedda 2009). One of the most challenging aspects of skeletal tissue engineering remains the development of 3D *in vitro* models that mimic the complex interactions in bone and cartilage. A large number of studies have been performed using various synthetic and natural 3D scaffolds to support osteogenic and chondrogenic differentiation. However, use of 3D scaffolds is beset by a requirements such as biocompatibility, reproducibility and mimicry of in vivo characteristics including tensile strength, elasticity and degradation rate. Alternative, less complex methods for 3D culture are high-density systems such as micromass or pellet culture, where cells growth and differentiation are supported by ECM produced within an aggregate of cells.

The use of high-density 3D culture methods have been established as suitable for osteogenic and chondrogenic cell differentiation in several studies. For example, human osteoblasts grown in 3D micromass cultures have demonstrated expression of osteogenic markers including Type I collagen, ALP, osteonectin and Osteopontin, as well as demonstrating calcification and Osteocalcin expression at later timepoints (Ferrera et al. 2002), while pellet and micromass cultures are widely used for studying chondrogenesis of MSCs (Scharstuhl et al. 2007;Reger et al. 2008). Standard pellet culture methods have demonstrated limitations in production of tissues such as cartilage, including: necrosis of cells or failure to differentiate in the centre of pellets and induction of fibrocartilage-like features such as Type I collagen expression and chondrocyte hypertrophy (Tare et al. 2005;Pelttari et al. 2008;Mueller & Tuan 2008). Furthermore, high-throughput experiments often require the use of large numbers of

206

polypropylene conical tubes, used to establish and culture the pellets, making the technique time-consuming and inconvenient for long-term culture (Penick et al. 2005). Culture of cells at air-liquid interfaces, provides ready access to medium and gas exchange, enabling viable cell culture at tissue-like densities. The organotypic system used in this study enabled production of two relevant skeletogenic models; one for early bone formation (osteogenic media) and one for cartilaginous tissues. Cells cultured in chondrogenic media without dexamethasone produced predominantly homogeneous chondrogenic tissues with minimal expression of fibrocartilage or bone markers. Organotypic ALI culture also allowed high-throughput, multi-replicate culture of cell pellets, offering an improvement over standard pellet culture. A study by Zhang et al. (2010) demonstrated that micromass culture (where cells are seeded at high density in a small volume) was found to induce larger and more homogenous cartilage tissues, rich with Type II collagen and aggrecan, with reduced Type I collagen expression and chondrocyte hypertrophy in comparison to standard pellet culture (Zhang et al. 2010). However, micromass and pellet culture regularly involve complete suspension of the cell aggregates in medium for the duration of culture, limiting gas exchange. Combining the use of air-liquid interfaces with micromass culture may therefore offer an improved chondrogenic model. While organotypic pellet culture of FFDCs did not facilitate mature osteogenic differentiation, pellet culture has been shown to facilitate rapid maturation of osteoblasts (Jahn et al. 2010), suggesting that use of a cell line that does not favour chondrogenesis, such as adult MSCs or primary osteoblasts would result in the formation of mature bone.

Recent studies have demonstrated the potential of microfluidics for establishing effective 3D *in vitro* tissue culture models. Monolayer-based microfluidic culture platforms have been previously described (Chung et al. 2005;Hung et al. 2005) and microfluidic technology offers many techniques for cell isolation and analysis. A variety of different techniques have been utilised to facilitate microfluidic 3D cell culture, including integration of 3D microstructure scaffolds into the microfluidic channel (Leclerc et al. 2006), suspension of cells in hydrogels (Ling et al. 2007;Kim et al. 2008a) and induction of natural cell aggregation. For example, by chemically modifying cells to express a transient inter-cellular linker, one study was able to establish scaffold-free 3D aggregates of MSCs within a microfluidic device. Addition of

osteogenic media to these MSC aggregates resulted in the production of mineralised matrix, while use of the cellular linker instead of a scaffold facilitated development of a more natural 3D environment (Ong et al. 2008). The integration of 3D on-chip cell culture into microscale cell isolation devices would offer a high degree of control over the culture environment and facilitate development of high-throughput *in vitro* models.

As observed in chapters 3 and 6, obtaining purified mRNA from low numbers of cells, followed by synthesis of cDNA is a laborious and difficult procedure, as the large number of steps required can result in loss of material through factors such as mRNA degradation or incomplete reverse transcription (Marcus et al. 2006). Due to the low numbers of cells isolated from both the laser dissection (cobblestone cell) and microfluidic sorting, it is essential that an adequate method for molecular analysis of low yields of RNA is available. The most common method for such analysis involves amplification of the total RNA (Wang et al. 2000). However, the amplification process is known to cause reduction in RNA sequence length, which can lead to bias towards certain nucleic acid sequences (Croner et al. 2009). Microfluidic technology offers an ideal method for performing high-throughput analysis of small-size cell samples due to the small volume of reagents needed and the potential for automation. Marcus et al. (2006) demonstrated integration of on-chip devices for cell capture, lysis, mRNA purification, cDNA synthesis and purification, with the ability to process up to 100 cells per reaction without the need for amplification of the sample, while another study presented microelectronic chip arrays for both cell separation and gene expression profiling, offering great potential for direct and accurate molecular analysis of specific cell subpopulations isolated from heterogeneous samples (Huang et al. 2002).

In summary, current studies have indicated that microfluidic technology offers an exciting approach for cell isolation from heterogeneous populations, while also displaying potential for on-chip analysis and culture due to the ability to precisely control the device's microenvironment. The ability to isolate pure populations of cells presents a significant breakthrough for skeletal tissue engineering and regenerative medicine, facilitating further examination of the characteristics of skeletal stem cells. Development of strategies to increase the throughput of cells whilst maintaining the high purity of isolated populations would enable future methods for cell isolation to

208

focus on microfluidics. These studies have also shown that organotypic ALI culture of 3D fetal femur-derived cell pellets offers an *in vitro* model for skeletal tissue development with strong potential for analysing the effects of specific drugs and growth factors on the differentiation of cells and that addition of BMP-2 to cells treated with chemically defined media induces an adipogenic phenotype with a novel cobblestone morphology.

7.2. Future directions

- Further examine the use of cells treated with CDM + Activin A/FGF2 in tissue engineering protocols such as organotypic ALI culture.

- Culture CDM + BMP-2-derived cobblestone cells in adipogenic factors to confirm their adipogenic phenotype (by and stain for more markers)

- Determine why addition of BMP-2 induces cells with an adipogenic phenotype In FFDCs treated with CDM + Activin A/FGF2.

- Further examine the phenotype of the fibroblastic cells in cultures treated with CDM + BMP-2.

- Improve the quantity of cells that microfluidic technology can manipulate by developing scale-up protocols such as multiple parallel devices or improving the sorting efficiency.

- Improve the recovery rate of cells from microfluidic devices from an average of 72% to 100%.

- Use the microfluidic device as an alternative to Laser dissection microscopy to isolate and further characterise the cobblestone phenotype observed in FFDCs based on expression of markers such as PPARγ and lipid (via use of the fluorescent lipid stain AdipoRed™).

- Further examine the effects of oxygen concentration and serum content on organotypic pellet culture.

- Further examine the potential of organotypic pellet culture as a model for osteogenesis and chondrogenesis using adult human bone marrow cells and other cell lines.

APPENDICES

Appendix 1. Sample data

List of adult bone marrow samples utilised

Age:	57	67	68	70	70	71	75	77	79	81	88	88	92	101
Sex:	M	M	M	F	M	F	M	F	M	F	F	F	M	M

List of fetal femur samples utilised

Code	Length (mm)	Age (WPC)	Sex	Code	Length (mm)	Age (WPC)	Sex
H1126	6.5	8.7	m	H1259	4.5	7.7	
H1129	7	9.0	m	H1260	5.5	8.0	
H1131	5	7.9	m	H1267	6	8.4	
H1132	5.5	8.0	f	H1269	4.5	7.7	
H1134	3.5	7.3		H1282	4.5	7.7	
H1162	4	7.6	m	H1286	6.5	8.7	
H1168	5	7.9	f	H1288	6	8.4	
H1170	5.5	8.0	f	H1295	5	7.9	
H1172	4.5	7.7		H1296	10	11.0	
H1176	7	9.0		H1301	5	7.9	
H1179	5.5	8.0		H1305	4	7.6	
H1197	unknown	unknown	m	H1328		8.4	
H1199	5.5	8.0	f	H1337	4	7.6	
H1203	4	7.6	m	H1338	7	9.0	
H1206	5	7.9	f	H1339	6	8.4	
H1208	7	9.0	m	H1340	6.5	8.7	
H1213	5	7.9		H1341	6	8.4	
H1214	7	9.0		H1345	5.5	8.0	
H1217	8	9.7	f	H1351	8	9.7	
H1226	8.5	10.0	m	H1352	5.5	8.0	
H1235	4.5	7.7		H1353	4.5	7.7	
H1236	5.5	8.0		H1355	5	7.9	
H1237	7.5	9.3		H1357	5	7.9	
H1244	7.5	9.3	f	H1362	3.5	7.3	
H1246	5	7.9	m	H1363	5	7.9	
H1247	3	7.0	m	H1364	CS19	6.9	
H1248	9	10.3					

Appendix 2. Controls for immunostaining

Positive controls for Type I collagen, Type II collagen, Alkaline phosphatase, Osteocalcin and Osteopontin were performed on sections of fetal femur, examples of which are demonstrated in chapter 3, Figure 3.3. For the following figures, red fluorescent staining represents the expression of the specific marker, while blue staining represents cell nuclei. Scale bars: 20μm.

Negative (A) and positive controls using embryonic stem cell cultures for stem cell markers SOX2 (B) and OCT4 (C).
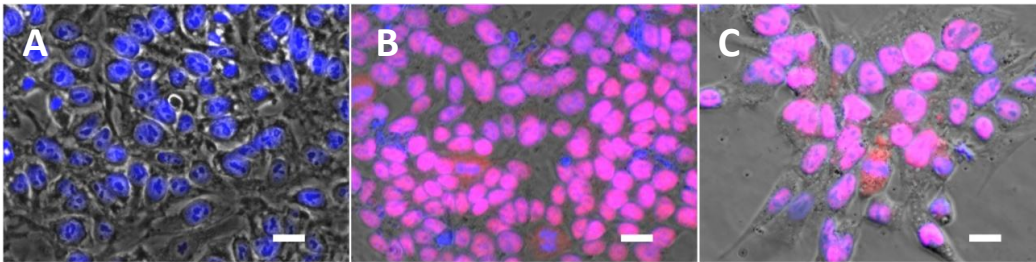
Negative (A) and positive controls using cultured marrow fat layer for adipogenic cell markers PPARγ (B) and FABP4 (C).
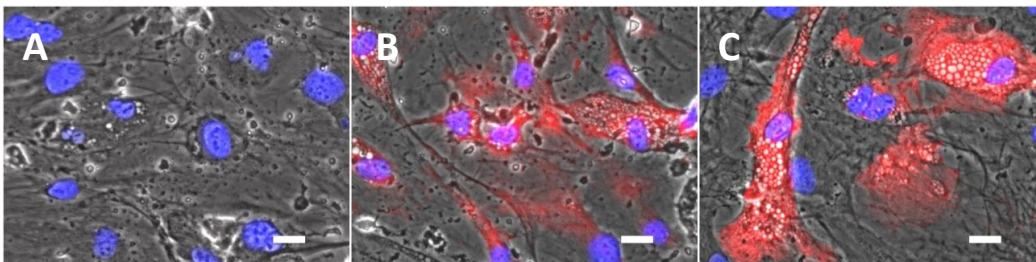
Negative (A) and positive controls using HUVEC cultures for endothelial and haematopoietic cell markers CD105 (B), CD34 (C), CD146 (D), TIE2 (E) and VWF (F).
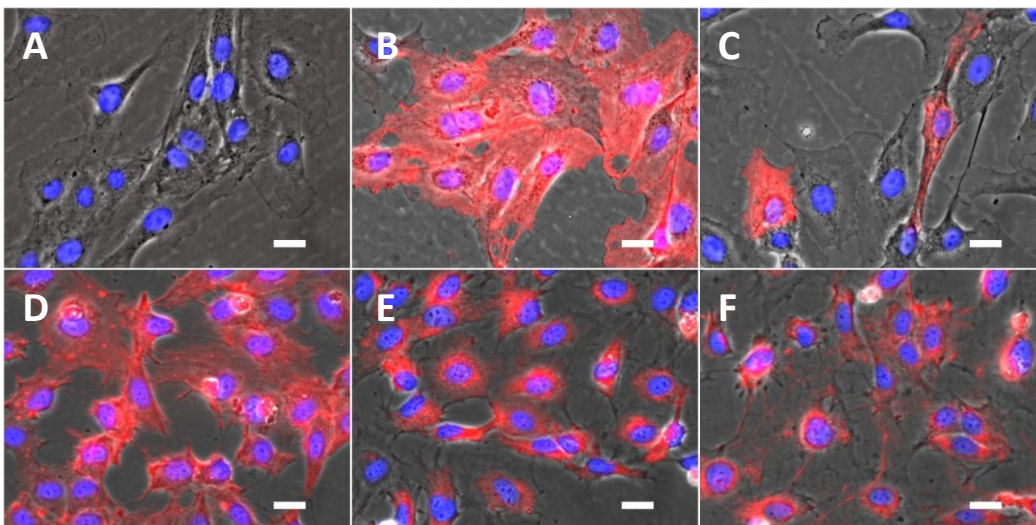
Appendix 3. Additional data for cobblestone cell analysis

Graph demonstrating the amplification plots for the housekeeping gene, GAPDH of 3 separate isolated cobblestone populations. The expected value for GAPDH expression to cross the threshold (red line) is approximately 15 to 16 cycles. RT-PCR of isolated cobblestone samples required 24 cycles or greater to reach the threshold, confirming the inadequate levels of cDNA available.
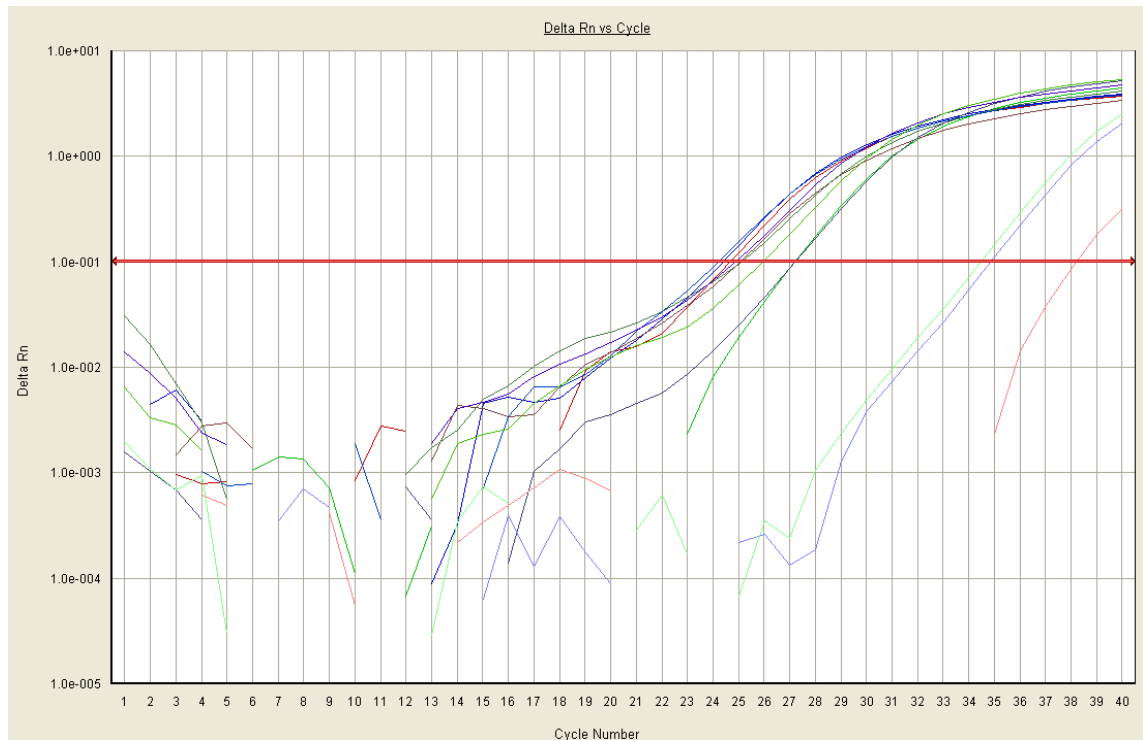
List of genes highly expressed in heterogeneous CDM + BMP-2-treated populations of FFDCs. Only genes that have a Ct less than 25 are shown. n=4 populations.

HETEROGENEOUS POPULATION	
SYMBOL	**GENE NAME**
ALCAM	activated leukocyte cell adhesion molecule
ANPEP	alanyl (membrane) aminopeptidase
ANXA5	annexin A5
CASP3	caspase 3, apoptosis-related cysteine peptidase
CD44	CD44 molecule (Indian blood group)
COL1A1	collagen, Type I, alpha 1
CTNNB1	catenin (cadherin-associated protein), beta 1
ENG	endoglin
FGF2	fibroblast growth factor 2
GDF15	growth differentiation factor 15
GDF5	growth differentiation factor 5
GTF3A	general transcription factor IIIA
HAT1	histone acetyltransferase 1
HDAC1	histone deacetylase 1
ITGA6	integrin, alpha 6
ITGAV	integrin, alpha V
ITGB1	integrin, beta 1
KILTG	KIT ligand
MCAM	melanoma cell adhesion molecule
MMP2	matrix metallopeptidase 2
NES	nestin
NGFR	nerve growth factor receptor
NOTCH1	Notch homolog 1, translocation-associated (Drosophila)
NT5E	5'-nucleotidase, ecto
NUDT6	nudix (nucleoside diphosphate linked moiety X)-type motif 6
PDGFRB	platelet-derived growth factor receptor, beta polypeptide
PIGS	phosphatidylinositol glycan anchor biosynthesis, class S
PTK2	protein tyrosine kinase 2
RHOA	ras homolog gene family, member A
SLC17A5	solute carrier family 17 (anion/sugar transporter), member 5
SMAD4	SMAD family member 4
SMURF1	SMAD specific E3 ubiquitin protein ligase 1
SMURF2	SMAD specific E3 ubiquitin protein ligase 2
SOX9	SRY (sex determining region Y)-box 9
TGFB1	transforming growth factor, beta 1
TGFB3	transforming growth factor, beta 3
THY1	**Thy**-1 cell surface antigen (CD90)
VCAM1	vascular cell adhesion molecule 1
VEGFA	vascular endothelial growth factor A
VIM	vimentin

Appendix 4. Protocol for preparation of alginate/polysaccharide capsules (courtesy of Dr Jodie Babister, University of Southampton)

Preparation of alginate solution

Ultra pure alginate (NovaMatrix, Drammen, Norway) (0.2g) was added to 0.09g sodium chloride and 0.3g d-sodium hydrogen orthophosphate (210mM) and dissolved in 10ml distilled water. The solution was mixed thoroughly for approximately 1 hour and filter sterilized prior to cell encapsulation. Alginate solutions were stored at 4oC for no longer than 1 month.

Preparation of chitosan solution

Chitosan (3g) was added to 1g calcium chloride (50mM), 3ml acetic acid and 200ml distilled water. The solution was thoroughly mixed for 1 hour and autoclaved before use. Chitosan solutions were stored at 4oC prior to use.

Cell encapsulation

After trypsinisation and centrifugation of cells the sodium alginate solution was added to the cell pellet and vortexed to ensure thorough mixing and even distribution of cells throughout the alginate. For capsules treated with transforming growth factor-β3, 10ng/ml (5μl/ml) was added to the alginate solution immediately before the addition of cells. Droplets of alginate (100μl containing approximately 4 x 105 cells) were dispensed onto the surface of the chitosan solution in a petri dish. Capsules, approximately 5mm in diameter, were left in the chitosan in a covered petri dish for 1 hour, following self-assembly, for the attachment of the chitosan shell to occur (Leveque et al., 2002), and were subsequently washed 3 times in α-MEM media. Capsules were held in media supplemented with 10nM dexamethasone, 100μM ascorbate-2-phosphate and 1X ITS premix (insulin – 10μg/ml, transferrin – 5.5μg/ml, selenium – 5ng/ml) for 24 hours and subsequently placed either in 6-well plates, in rotating-bioreactor vessels or into the flow chambers of the perfused bioreactor. To ensure appropriate quantities of cells were obtained, in some experiments isolated cells were pooled prior to encapsulation. Capsules were encapsulated with a variety of cell types including human bone marrow cells, human articular chondrocytes or a mixture of the two cell types.

Appendix 5. Additional data for molecular analysis of organotypic ALI culture

For the following figures: Key: B, Basal; O, Osteogenic; C, Chondrogenic. Data represents mean ± SD, n=3 per population. Statistical significance of increase/decrease compared to day 1 samples shown as: ns = non-significant; * = p<0.05; ** = p<0.01, *** = p<0.005.

Comparison of gene expression at day 1 and at day 28 in organotypic ALI culture of various fetal cell populations. Expression of SOX9 (A), RUNX2 (B), ALP (C), Type I collagen (D) and OCN (E) are shown.
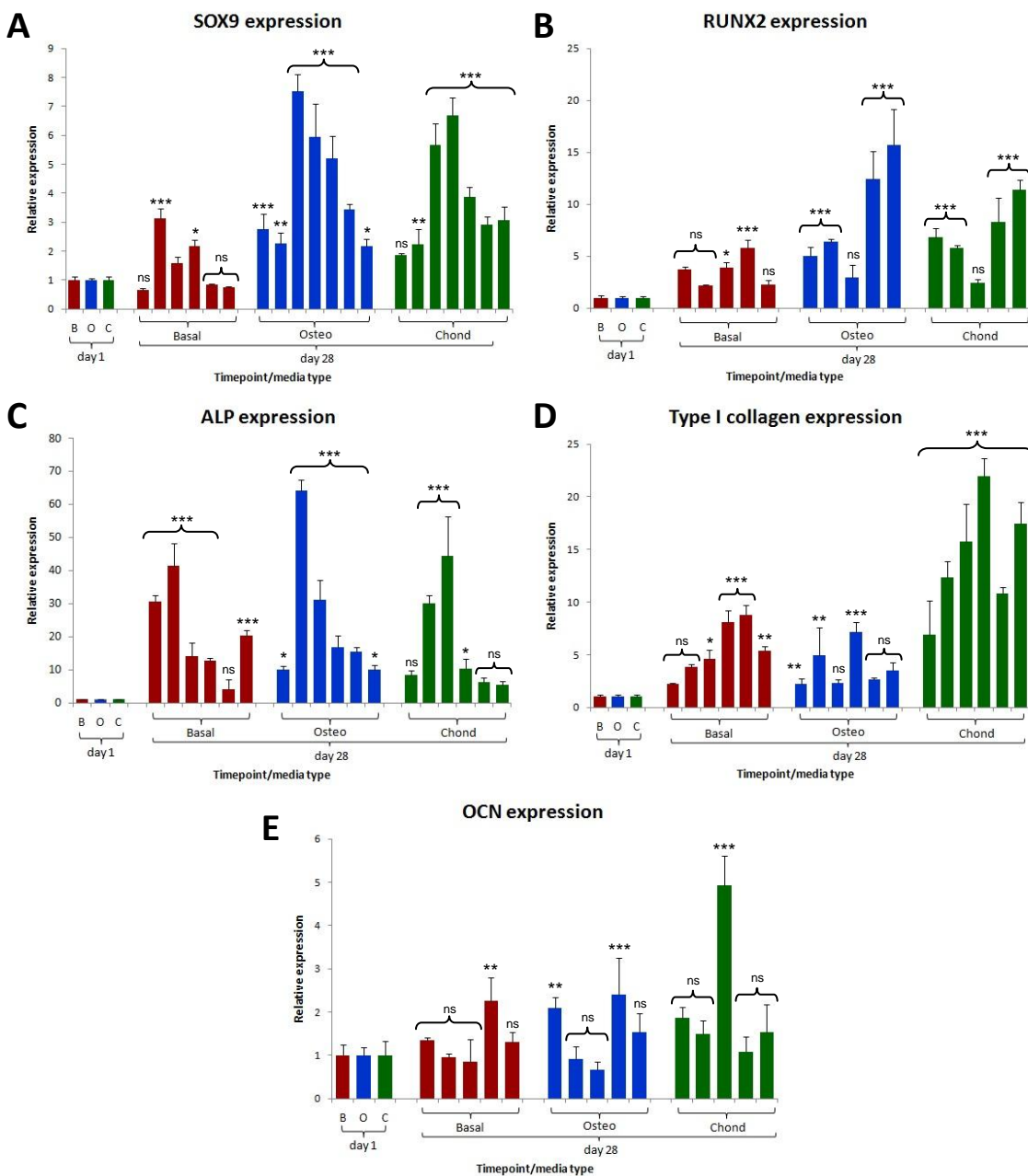
Comparison of Type II collagen gene expression at day 1 and at day 28 in organotypic ALI culture of various fetal cell populations. Separation of basal/chondrogenic results (A) from osteogenic results (B) was required due to significant increase in expression.
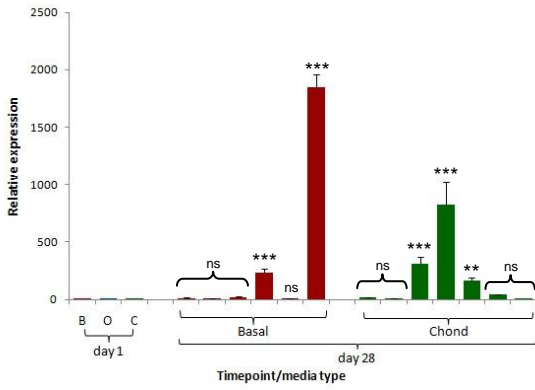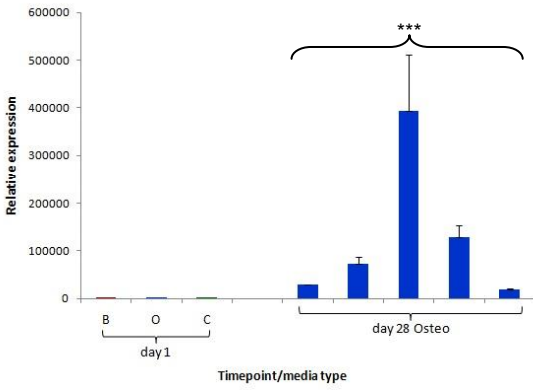
Appendix 6. Effects of β-Glycerol Phosphate on cell pellet differentiation in organotypic ALI culture

Inclusion of Beta-Glycerol Phosphate (β-GP) together with BMP-2 in the standard osteogenic culturing conditions displayed uniform expression of both proteoglycan and collagen throughout the pellet, while immunohistochemistry revealed that culture of pellets with β-GP resulted in a decrease in the overall expression of Type I and II collagen when compared to cell pellet cultures where β-GP was omitted.

Images of histological sections of pellets expanded for 28 days in organotypic ALI culture under standard osteogenic conditions (containing dexamethasone and ascorbate) in the presence of 150ng/ml BMP-2 and Beta Glycerol Phosphate (βGP). Staining is shown for (A) Alcian Blue (proteoglycan) and Sirius Red (collagen matrix) stain, (B) Type 1 Collagen (red) and (C) Type 2 Collagen (red). Blue fluorescence in (B) and (C) is the nuclear counterstain, DAPI. (Figure adapted with permission from undergraduate research student, Charlie Loveday-Jefferson).
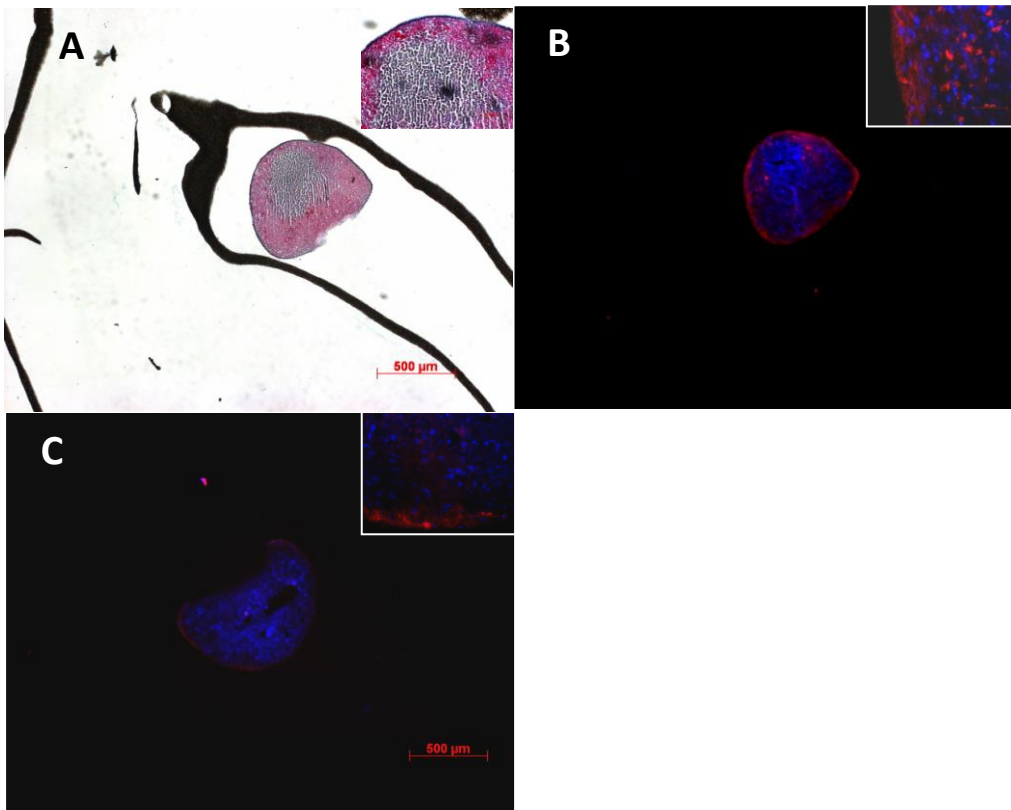
Appendix 7. Preliminary culture of hBMSC pellets in organotypic ALI culture

Preliminary experiments into the culture of hBMSC pellets in organotypic ALI culture were performed under basal conditions. At 21 days of culture, large amounts of aligned collagen and osteoid, coupled with low levels of proteoglycan were found in adult hBMSC pellets, suggesting a strong bone-like phenotype.

Alcian blue (proteoglycan) and Sirius red (collagen) staining on sectioned samples from hBMSC pellets at day 21 under basal conditions (n=2). Scale bar is 500μm.
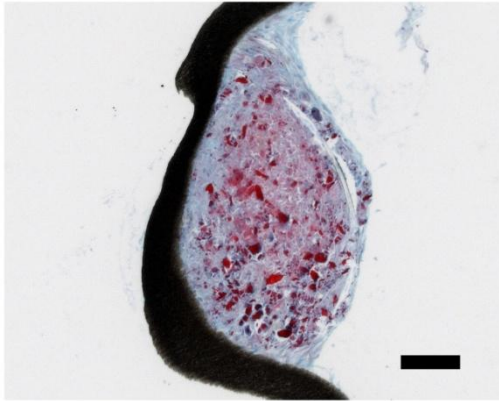
Appendix 8. Effects of hypoxia on differentiation in organotypic ALI culture

To test the effects of oxygen availability on pellets grown at an air-liquid interface, samples were cultured in normal organotypic ALI culture in a hypoxic (~5% oxygen) atmosphere. Pellets grown in all three differentiation medias in hypoxic conditions were found to express growth and differentiation similar to that of normal organotypic ALI culture, including a strong effect of pellet size on the differentiation of the pellets. As with normal organotypic ALI culture, pellets starting approximately less than 0.8mm in diameter produced phenotypes expressing large amounts of collagen and minimal growth, while those over 0.8mm in diameter at day 1 produced a defined proteoglycan pellet core with reduced collagen expression after 28 days of culture. The most distinct difference between hypoxic and normal organotypic ALI culture was the amplified amount of cell death that occurred in osteogenic and chondrogenic cultures, illustrated by the patches void of cells in the pellet cores.

At day 28, samples treated with basal media demonstrated expression of both Type I and Type II collagen, located at the pellet edge but not the pellet core. Pellets treated with chondrogenic media expressed large amounts of Type I collagen throughout the pellet, while Type II collagen was expressed in high levels at the pellet border, with minimal expression in the pellet core. Expression of Type I collagen in osteogenic pellets was situated throughout pellet, with stronger expression at the pellet edge and Type II collagen was expressed throughout the proteoglycan matrix and at the pellet boundary. In all three conditions, sites of cell-air interface were composed of aligned Type I and II collagen, while pellet cores expressed minimal alignment. Alkaline phosphatase expression was only observed in pellets treated with basal media in hypoxic conditions. Osteopontin was expressed at the pellet borders of pellets grown in all conditions.

Alcian blue (proteoglycan) and Sirius red (collagen) staining on sectioned samples from hypoxic pellets at day 28 under basal conditions (pellets greater than 0.8mm at day 1). Scale bar for centre image: 200µm; for surrounding images: 50µm.

Alcian blue (proteoglycan) and Sirius red (collagen) staining on sectioned samples from hypoxic pellets at day 28 under chondrogenic conditions (pellets greater than 0.8mm at day 1). Areas void of cells are recognised by their lack of staining. Scale bar for centre image: 200μm; for surrounding images: 50μm.

Alcian blue (proteoglycan) and Sirius red (collagen) staining on sectioned samples from hypoxic pellets at day 28 under osteogenic conditions (pellets greater than 0.8mm at day 1). Areas void of cells are recognised by their lack of staining. Scale bar for centre image: 200μm; for surrounding images: 50μm.

Fluorescent immunostaining for Type I and Type II collagen (red) on sectioned samples from hypoxic pellets at day 28 of culture in basal media (A, B), osteogenic media (C, D) and chondrogenic media (E, F). Blue fluorescence is the nuclear counterstain, DAPI. Scale bars: Whole pellet, 200μm; high magnification, 20μm
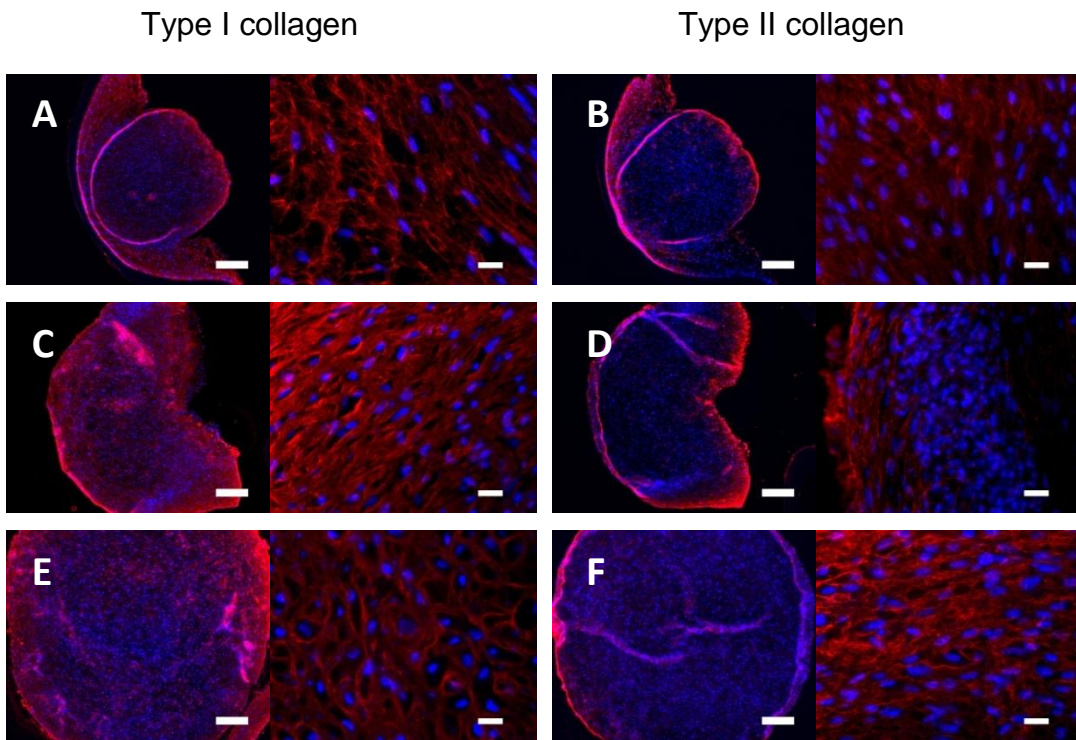
Alkaline phosphatase and Osteopontin staining (red) on sectioned samples from hypoxic pellets at day 28 of culture in basal media (A, B), osteogenic media (C, D) and chondrogenic media (E, F). (A, C and E) counterstained with Alcian blue (proteoglycan) and light green (all tissue), blue fluorescence in (B, D and F) is the nuclear counterstain, DAPI. Colour scale bars: Whole pellet, 500μm; high magnification, 50μm. Fluorescent scale bars: Whole pellet, 200μm; high magnification, 20μm.

Alkaline Phosphatase   Osteopontin
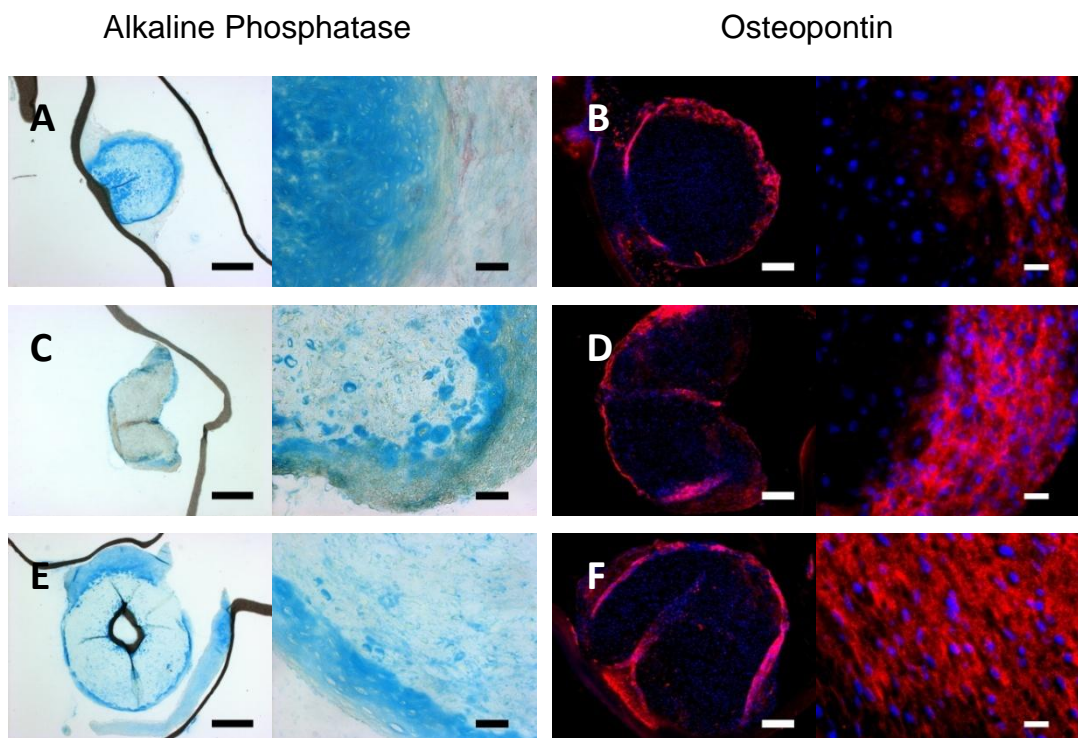
Appendix 9. Effects of serum on cell pellet differentiation in organotypic ALI culture

Chondrogenic media normally contains no serum, whilst osteogenic media contains 10% serum. Thus to test the effects of serum, chondrogenic media was added with 10% serum, whilst osteogenic media was added with no serum content. Results observed during 28 days culture and histological analysis demonstrated that pellets grown in osteogenic conditions without FCS were smaller than those in normal osteogenic conditions but maintained a proteoglycan-rich phenotype bordered by collagen. Due to their smaller size in comparison to normal osteogenic pellet culture, an increase in collagen formation was noted in pellets at day 28 of osteogenic culture without FCS. Type I collagen was present in large amounts at the cell border and at sites of adhesion but not in the pellet core, while Type II collagen was found strongly expressed throughout pellets treated with osteogenic media without FCS. ALP staining was present in basal but only in negligible quantities in osteogenic conditions at sites of pellet-confetti adhesion. Osteopontin was present throughout the pellets treated without FCS. Pellets treated with chondrogenic media with FCS were found to maintain a similar mixed phenotype as observed in normal organotypic ALI culture, but expressed much higher levels of collagen and minimal proteoglycan. Addition of FCS to chondrogenic media did not appear to increase growth of pellets over 28 days. Both Type I and Type II collagen were highly expressed throughout pellets cultured in chondrogenic media with FCS, revealing a mixed phenotype. ALP expression was minimal, while Osteopontin was expressed at the pellet border and a low levels throughout pellets treated with chondrogenic media with FCS.

Alcian blue (proteoglycan) and Sirius red (collagen) staining on sectioned samples from pellets at day 28 under osteogenic conditions without FCS. Scale bar for centre image: 200µm; for surrounding images: 50µm.
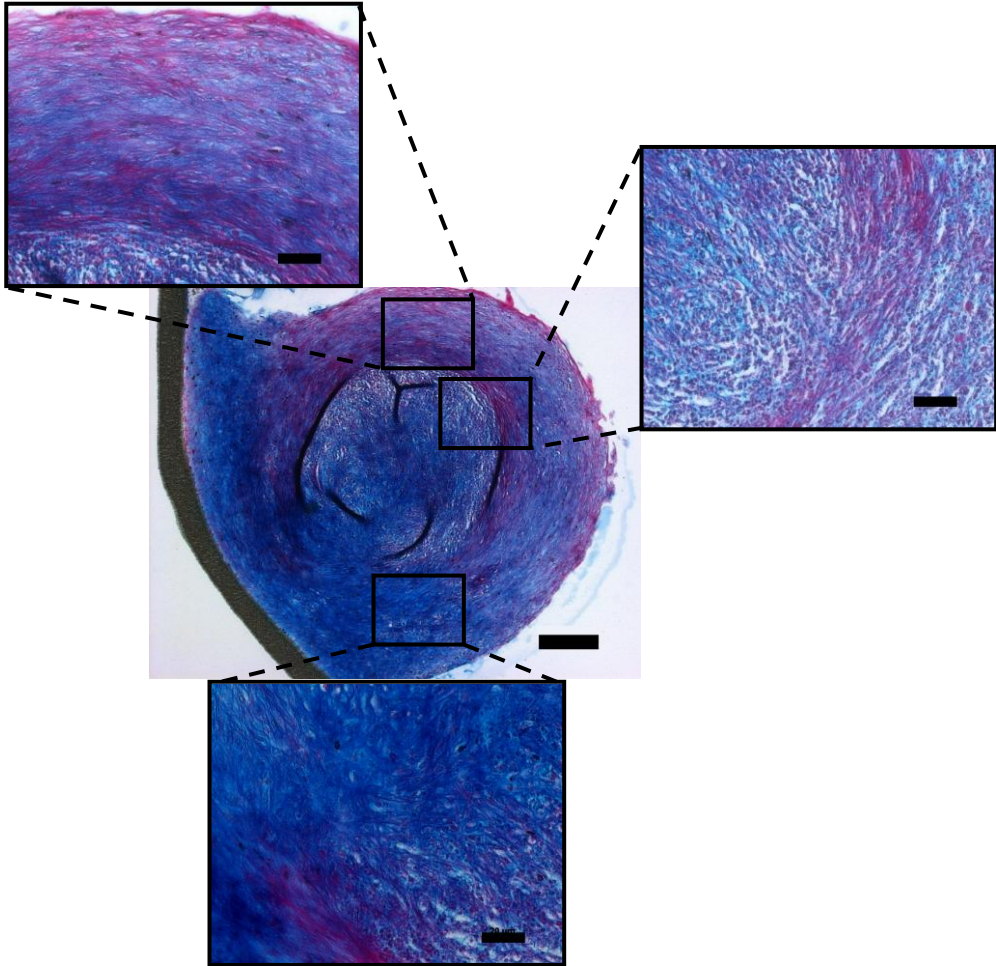
Alcian blue (proteoglycan) and Sirius red (collagen) staining on sectioned samples from pellets at day 28 under chondrogenic conditions with FCS. Scale bar for centre image: 200μm; for surrounding images: 50μm.
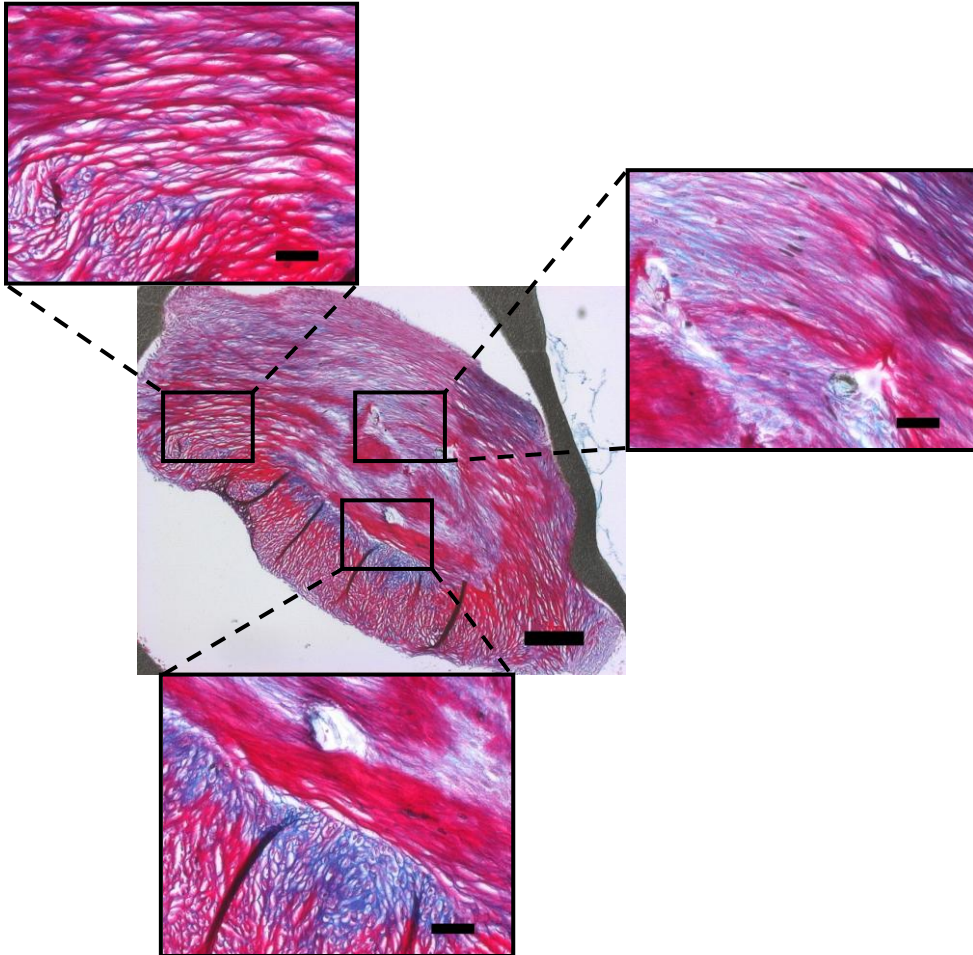
Fluorescent immunostaining for Type I and Type II collagen (red) on sectioned samples from pellets at day 28 of culture in osteogenic media without FCS (A, B) and chondrogenic media with FCS (C, D). Blue fluorescence is the nuclear counterstain, DAPI. Scale bars: Whole pellet, 200μm; high magnification, 20μm

Type I collagen   Type II collagen
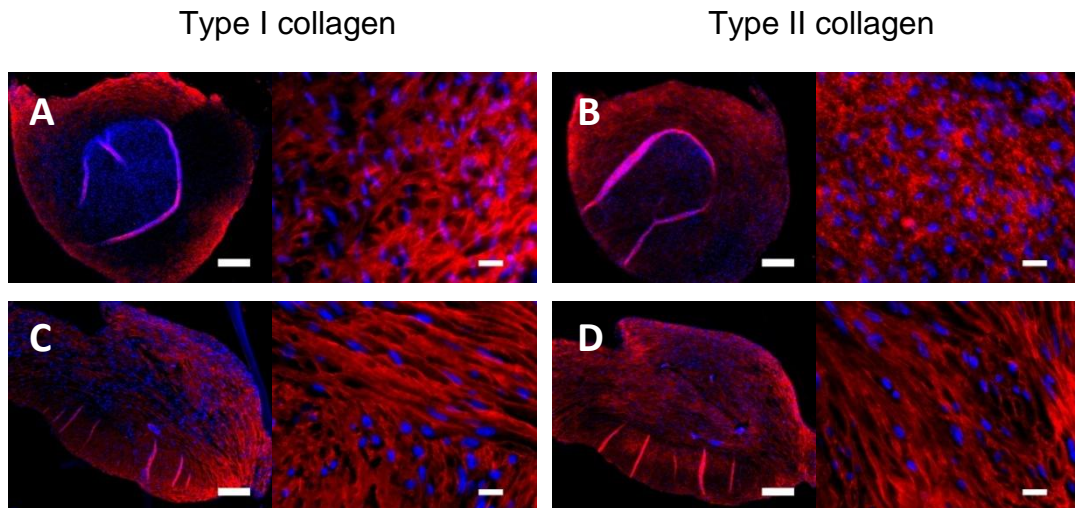
Alkaline phosphatase and Osteopontin staining (red) on sectioned samples from pellets at day 28 of culture in osteogenic media without FCS (A, B) and chondrogenic media with FCS (C, D). (A) and (C) counterstained with Alcian blue (proteoglycan) and light green (all tissue), blue fluorescence in (B) and (D) is the nuclear counterstain, DAPI. Colour scale bars: Whole pellet, 500μm; high magnification, 50μm. Fluorescent scale bars: Whole pellet, 200μm; high magnification, 20μm.

Alkaline phosphatase   Osteopontin
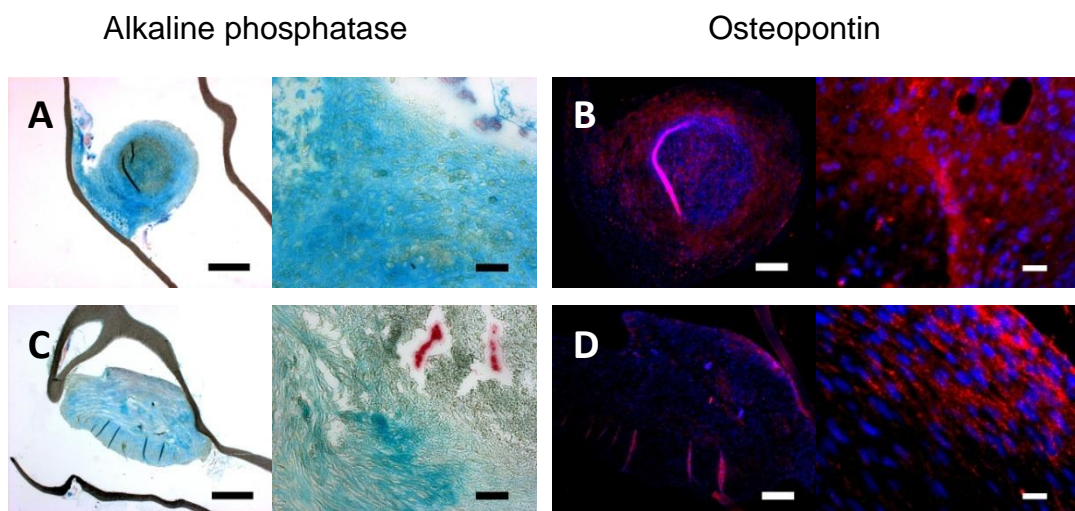
Appendix 10. Additional diagrams and MATLAB scripts for the microfluidic devices (courtesy of Dr Rupert Thomas, Electronics and Computer Science, University of Southampton). Further information regarding chip design and manufacture can be found in Thomas (2010).

Schematic diagram of the fabrication mask for the ring trap multi-layer electrodes (A, B) and a diagram of a completed ring trap device, including the glass electrodes, flexible connector and PCB daughterboard (C).
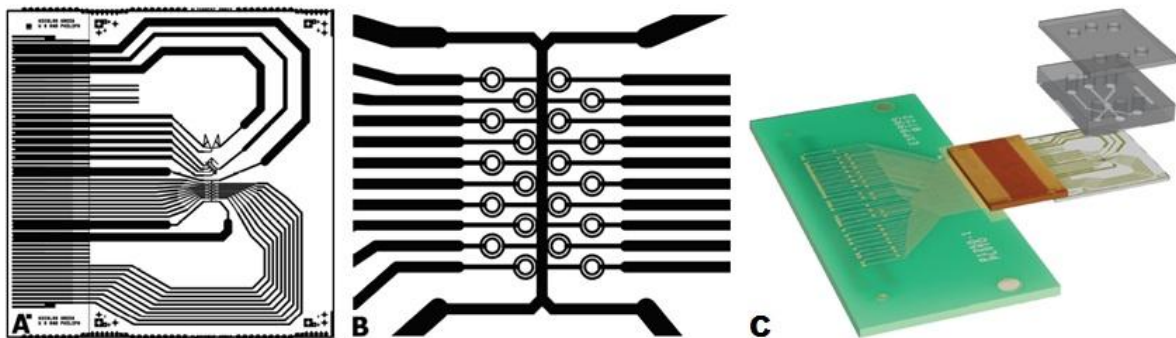
Schematic diagram of valve operation in ring trap devices during trapping (i-ii), washing (iii-iv) and recovery (v-vi)
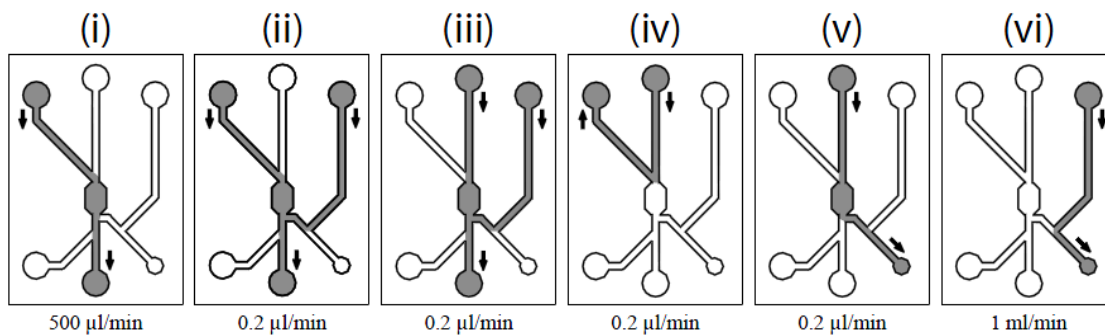
Schematic diagram showing the macrofluidic connections of the trapping device
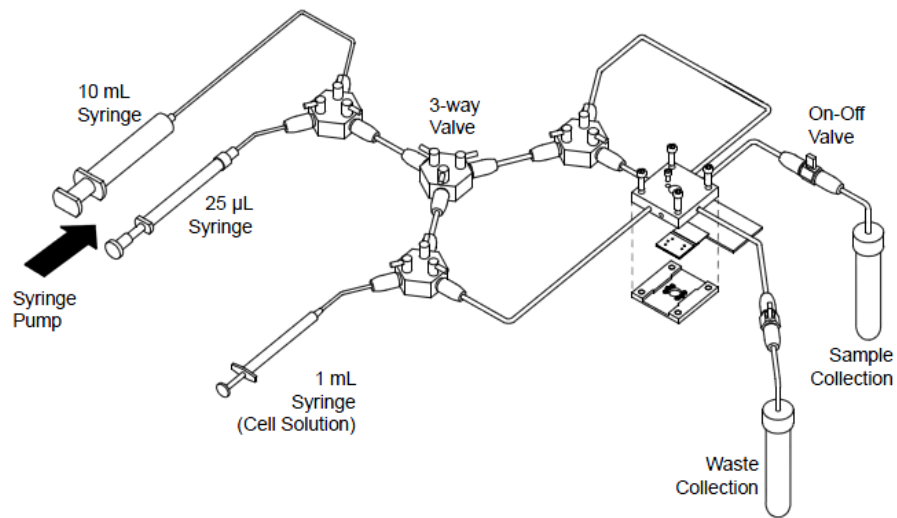
Image of the microfluidic channel (grey) and electrodes (black) of the sorter device
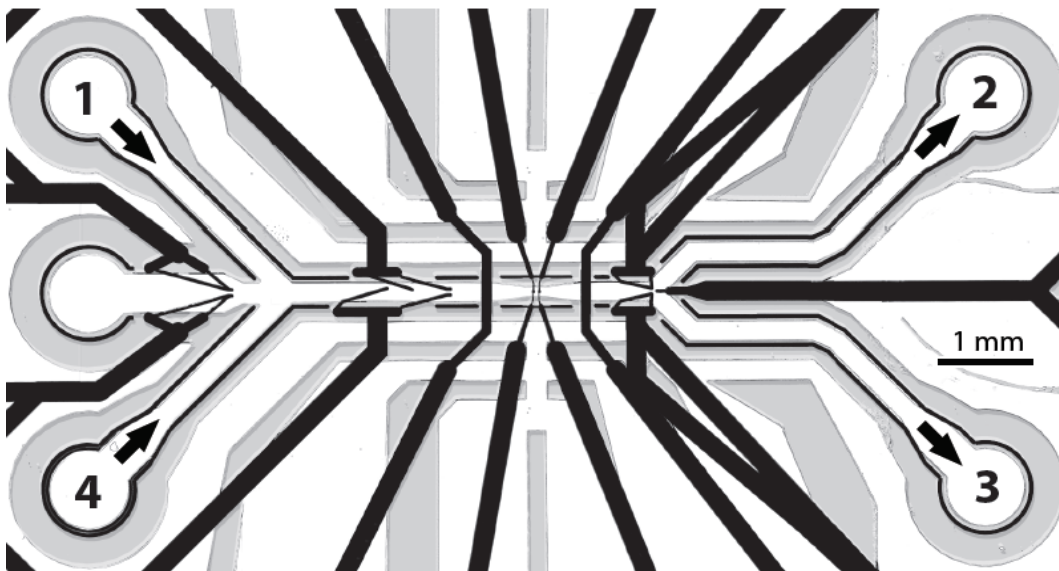
MATLAB script "labelRegions"that enables setup of cell recognition parameters for both trapping and sorting devices

```matlab
function varargout = labelRegions(varargin)
% LABELREGIONS M-file for labelRegions.fig
%      LABELREGIONS, by itself, creates a new LABELREGIONS or raises the existing
%      singleton*.
%
%      H = LABELREGIONS returns the handle to a new LABELREGIONS or the handle to
%      the existing singleton*.
%
%      LABELREGIONS('CALLBACK',hObject,eventData,handles,...) calls the local
%      function named CALLBACK in LABELREGIONS.M with the given input arguments.
%
%      LABELREGIONS('Property','Value',...) creates a new LABELREGIONS or raises the
%      existing singleton*.  Starting from the left, property value pairs are
%      applied to the GUI before labelRegions_OpeningFunction gets called.  An
%      unrecognized property name or invalid value makes property application
%      stop.  All inputs are passed to labelRegions_OpeningFcn via varargin.
%
%      *See GUI Options on GUIDE's Tools menu.  Choose "GUI allows only one
%      instance to run (singleton)".
%
% See also: GUIDE, GUIDATA, GUIHANDLES

% Edit the above text to modify the response to help labelRegions

% Last Modified by GUIDE v2.5 24-Feb-2010 13:20:35

% Begin initialization code - DO NOT EDIT
gui_Singleton = 1;
gui_State = struct('gui_Name',       mfilename, ...
                   'gui_Singleton',  gui_Singleton, ...
                   'gui_OpeningFcn', @labelRegions_OpeningFcn, ...
                   'gui_OutputFcn',  @labelRegions_OutputFcn, ...
                   'gui_LayoutFcn',  [] , ...
                   'gui_Callback',   []);
if nargin && ischar(varargin{1})
    gui_State.gui_Callback = str2func(varargin{1});
end

if nargout
    [varargout{1:nargout}] = gui_mainfcn(gui_State, varargin{:});
else
    gui_mainfcn(gui_State, varargin{:});
end
% End initialization code - DO NOT EDIT

 % --- Executes just before labelRegions is made visible.
function labelRegions_OpeningFcn(hObject, eventdata, handles, varargin)
% This function has no output args, see OutputFcn.
% hObject    handle to figure
% eventdata  reserved - to be defined in a future version of MATLAB
% handles    structure with handles and user data (see GUIDATA)
% varargin   command line arguments to labelRegions (see VARARGIN)

% Choose default command line output for labelRegions
handles.output = hObject;

% Update handles structure
guidata(hObject, handles);

% UIWAIT makes labelRegions wait for user response (see UIRESUME)
% uiwait(handles.figure1);

%load some general variables
config

%initialise counter for regions
tracking.regionCounter = 0;
```

234

```
 %% Video setup
try
    % Create video input object.
    obj = videoinput('winvideo');
    video=obj;

    % Make sure we've stopped so we can set up the acquisition.
    stop(obj);

    % Set video input object properties for this application.
    % Note that example uses both SET method and dot notation method.

    appTitle = 'Video developer';

            %from imaqmotion: set to continously aquire data
    %triggerconfig(obj, 'manual');
    %set(obj, 'Tag', appTitle, 'FramesAcquiredFcnCount', 1, ...
    %    'TimerFcn', @localFrameCallback, 'TimerPeriod', tracking.frame_period);

    %reduce size of video resolution
    res=get(obj,'VideoResolution');
    if res>tracking.target_resolution %if resolution exceeds this value, reduce it
        set(obj,'ROIPosition', [floor((res(1)-tracking.target_resolution(1))/2)
floor((res(2)-tracking.target_resolution(2))/2) tracking.target_resolution(1)
tracking.target_resolution(2)]);
    end

    % Create a spot for the image object display.
    nbands = get(obj, 'NumberOfBands');
    res = get(obj, 'ROIPosition');
    %himage = imagesc(rand(res(4), res(3), nbands));
    himage = image(zeros(res(4), res(3)));

    preview(obj,himage)

    % Clean up the axes.
    ax = get(himage, 'Parent');
    set(ax, 'XTick', [], 'XTickLabel', [], 'YTick', [], 'YTickLabel', []);

    appdata.figureHandles.hFigure = hObject;
    appdata.figureHandles.hImage = himage;
    appdata.figureHandles.hPatch = [];

    tracking.himage = himage;

    %start the video object
    %start(obj);
    %warning off imaq:peekdata:tooManyFramesRequested

    %tracking.background = getsnapshot(obj);

    % Store the application data the video input object needs.
%    appdata.background = [];
%    obj.UserData = appdata;
    %setappdata(0, 'tracking_data_structure', tracking);

catch
%    writeLog('Cannot initialise video hardware.', handles);
    errordlg('Cannot initialise video hardware.','Video Interface','modal');
end

setappdata(0,'tracking_data_structure',tracking);
setappdata(0,'video',video);
set_gui_values(handles);

% --- Outputs from this function are returned to the command line.
function varargout = labelRegions_OutputFcn(hObject, eventdata, handles)
% varargout  cell array for returning output args (see VARARGOUT);
% hObject    handle to figure
% eventdata  reserved - to be defined in a future version of MATLAB
% handles    structure with handles and user data (see GUIDATA)
```

```matlab
% Get default command line output from handles structure
varargout{1} = handles.output;

%% Add region button
% --- Executes on button press in addRegion.
function addRegion_Callback(hObject, eventdata, handles)
% hObject    handle to addRegion (see GCBO)
% eventdata  reserved - to be defined in a future version of MATLAB
% handles    structure with handles and user data (see GUIDATA)

%retrieve tracking data
tracking = getappdata(0, 'tracking_data_structure');

%increment regionCounter
tracking.regionCounter = tracking.regionCounter + 1;

%create trap pre-requisite structure
answer = inputdlg('Enter trap pre-requisite:','Add region',1,{'0'});
tracking.prerequisites(tracking.regionCounter)=str2double(answer);

hbox = imrect(handles.axes1, tracking.tracking_area_position);

%set callback to update register if box is moved
%only changes to most recently added box will be considered!
api = iptgetapi(hbox);
api.addNewPositionCallback(@update_tracking_area_position);

%record current position of region, in case region is never moved
tracking.labelledRegions(tracking.regionCounter,:) = ...
round(tracking.tracking_area_position);

tracking.hbox = hbox;

%set trap quantity value
tracking.nof_regions = tracking.regionCounter;

%store appdata
setappdata(0, 'tracking_data_structure', tracking);

%%% if user changs position of the tracking area, update memory
function update_tracking_area_position(position)
tracking = getappdata(0, 'tracking_data_structure');
%position
tracking.labelledRegions(tracking.regionCounter,:) = round(position);
setappdata(0, 'tracking_data_structure', tracking);

%% Save

% --- Executes on button press in saveDatafile.
function saveDatafile_Callback(hObject, eventdata, handles)
% hObject    handle to saveDatafile (see GCBO)
% eventdata  reserved - to be defined in a future version of MATLAB
% handles    structure with handles and user data (see GUIDATA)

set_button_Callback(hObject, eventdata, handles)

tracking = getappdata(0, 'tracking_data_structure');

if isfield(tracking, 'expsummary')
    if isfield(tracking.expsummary, 'datestamp')
    datex=tracking.expsummary.datestamp;
    else
    datex=datestr(now, 30);
    end
    else
    datex=datestr(now, 30);
end

logfilename=['settings' datex];
dirpath='';
savefilepath=[dirpath logfilename];
```

236

```matlab
save (savefilepath, 'tracking')

function threshold_gain_box_Callback(hObject, eventdata, handles)
% hObject    handle to threshold_gain_box (see GCBO)
% eventdata  reserved - to be defined in a future version of MATLAB
% handles    structure with handles and user data (see GUIDATA)

% Hints: get(hObject,'String') returns contents of threshold_gain_box as text
%        str2double(get(hObject,'String')) returns contents of threshold_gain_box as a
double

% --- Executes during object creation, after setting all properties.
function threshold_gain_box_CreateFcn(hObject, eventdata, handles)
% hObject    handle to threshold_gain_box (see GCBO)
% eventdata  reserved - to be defined in a future version of MATLAB
% handles    empty - handles not created until after all CreateFcns called

% Hint: edit controls usually have a white background on Windows.
%       See ISPC and COMPUTER.
if ispc && isequal(get(hObject,'BackgroundColor'),
get(0,'defaultUicontrolBackgroundColor'))
    set(hObject,'BackgroundColor','white');
end

function r_box_Callback(hObject, eventdata, handles)
% hObject    handle to r_box (see GCBO)
% eventdata  reserved - to be defined in a future version of MATLAB
% handles    structure with handles and user data (see GUIDATA)

% Hints: get(hObject,'String') returns contents of r_box as text
%        str2double(get(hObject,'String')) returns contents of r_box as a double

% --- Executes during object creation, after setting all properties.
function r_box_CreateFcn(hObject, eventdata, handles)
% hObject    handle to r_box (see GCBO)
% eventdata  reserved - to be defined in a future version of MATLAB
% handles    empty - handles not created until after all CreateFcns called

% Hint: edit controls usually have a white background on Windows.
%       See ISPC and COMPUTER.
if ispc && isequal(get(hObject,'BackgroundColor'),
get(0,'defaultUicontrolBackgroundColor'))
    set(hObject,'BackgroundColor','white');
end

function g_box_Callback(hObject, eventdata, handles)
% hObject    handle to g_box (see GCBO)
% eventdata  reserved - to be defined in a future version of MATLAB
% handles    structure with handles and user data (see GUIDATA)

% Hints: get(hObject,'String') returns contents of g_box as text
%        str2double(get(hObject,'String')) returns contents of g_box as a double

% --- Executes during object creation, after setting all properties.
function g_box_CreateFcn(hObject, eventdata, handles)
% hObject    handle to g_box (see GCBO)
% eventdata  reserved - to be defined in a future version of MATLAB
% handles    empty - handles not created until after all CreateFcns called

% Hint: edit controls usually have a white background on Windows.
%       See ISPC and COMPUTER.
if ispc && isequal(get(hObject,'BackgroundColor'),
get(0,'defaultUicontrolBackgroundColor'))
    set(hObject,'BackgroundColor','white');
end

function b_box_Callback(hObject, eventdata, handles)
% hObject    handle to b_box (see GCBO)
% eventdata  reserved - to be defined in a future version of MATLAB
% handles    structure with handles and user data (see GUIDATA)

% Hints: get(hObject,'String') returns contents of b_box as text
```

```matlab
%        str2double(get(hObject,'String')) returns contents of b_box as a double

% --- Executes during object creation, after setting all properties.
function b_box_CreateFcn(hObject, eventdata, handles)
% hObject    handle to b_box (see GCBO)
% eventdata  reserved - to be defined in a future version of MATLAB
% handles    empty - handles not created until after all CreateFcns called

% Hint: edit controls usually have a white background on Windows.
%       See ISPC and COMPUTER.
if ispc && isequal(get(hObject,'BackgroundColor'),
get(0,'defaultUicontrolBackgroundColor'))
    set(hObject,'BackgroundColor','white');
end

%% Set Button
% --- Executes on button press in set_button.
function set_button_Callback(hObject, eventdata, handles)
% hObject    handle to set_button (see GCBO)
% eventdata  reserved - to be defined in a future version of MATLAB
% handles    structure with handles and user data (see GUIDATA)

tracking=getappdata(0, 'tracking_data_structure');

tracking.threshold_gain=str2double(get(handles.threshold_gain_box,'String'));
tracking.threshold_size=str2double(get(handles.threshold_size_box,'String'));
tracking.target_rgb=[str2double(get(handles.r_box,'String'))
str2double(get(handles.g_box,'String')) str2double(get(handles.b_box,'String'))];
tracking.positive_min_size=str2double(get(handles.positive_min_size_box,'String'));
tracking.positive_max_size=str2double(get(handles.positive_max_size_box,'String'));
tracking.negative_min_size=str2double(get(handles.negative_min_size_box,'String'));
tracking.negative_max_size=str2double(get(handles.negative_max_size_box,'String'));

tracking.expsummary.cell1=get(handles.cell1_box,'String');
tracking.expsummary.cell2=get(handles.cell2_box,'String');
tracking.expsummary.ratio=get(handles.ratio_box,'String');
tracking.expsummary.media=get(handles.media_box,'String');
tracking.expsummary.voltage=str2double(get(handles.voltage_box,'String'));
tracking.expsummary.freq=str2double(get(handles.freq_box,'String'));
tracking.expsummary.datestamp=get(handles.datestamp_box,'String');
tracking.expsummary.details=get(handles.details_box,'String');

setappdata(0, 'tracking_data_structure', tracking);

%% Test Snapshot
% --- Executes on button press in test_snapshotbutton.
function test_snapshotbutton_Callback(hObject, eventdata, handles)
% hObject    handle to test_snapshotbutton (see GCBO)
% eventdata  reserved - to be defined in a future version of MATLAB
% handles    structure with handles and user data (see GUIDATA)

tracking=getappdata(0, 'tracking_data_structure');
video=getappdata(0, 'video');
tracking.testframe = getsnapshot(video);
stoppreview(video);

%development testing:
%tracking.testframe = imread('1bead.bmp');
%tracking.background = imread('0bead.bmp');

setappdata(0,'tracking_data_structure',tracking);

output = detect_particles(tracking.testframe,tracking.background,
tracking.threshold_gain, tracking.threshold_size);
imshow(output.bw_I);
[nof,dummy]=size(output.measured_RGB);
match_counter=0;
match_ids=[];
no_match_counter=0;
no_match_ids=[];
for counter=1:nof
```

238

```matlab
    if compare_colours(output.measured_RGB(counter,:), tracking.target_rgb,
tracking.haze_factor, tracking.hue_factor, tracking.stability_factor)
            impoint(gca, output.centroids(counter, 1), output.centroids(counter, 2));
            match_counter=match_counter+1;
            match_ids=[match_ids; counter];
    else
            no_match_counter=no_match_counter+1;
            no_match_ids=[no_match_ids; counter];
    end
end

text_to_output=[num2str(nof) ' objects detected, with ' num2str(match_counter) '
colour/area match(es)'];
writeLog(text_to_output, handles);
for counter2=1:match_counter
    writeLog(['[' num2str(output.measured_RGB(match_ids(counter2),:)) ']  Area: '
num2str(output.area(match_ids(counter2),:))], handles);
end

text_to_output=[num2str(no_match_counter) ' objects detected above size threshold with
colour mis-matches:'];
writeLog(text_to_output, handles);
for counter2=1:no_match_counter
    writeLog(['[' num2str(output.measured_RGB(no_match_ids(counter2),:)) ']  Area: '
num2str(output.area(no_match_ids(counter2),:))], handles);
end

% --- Executes on button press in test_run_button.
function test_run_button_Callback(hObject, eventdata, handles)
% hObject    handle to test_run_button (see GCBO)
% eventdata  reserved - to be defined in a future version of MATLAB
% handles    structure with handles and user data (see GUIDATA)

%image_bank is a collection of frames with particles in for analysis
%image_bank2 is the processed frames in black and white
tracking=getappdata(0, 'tracking_data_structure');
video=getappdata(0, 'video');
tracking.testframe = getsnapshot(video);
test_run_data=[];

counter=1;
temporary_background=tracking.background((tracking.labelledRegions(counter,2):(tracking.
labelledRegions(counter,2)+tracking.labelledRegions(counter,4))),(tracking.labelledRegio
ns(counter,1):(tracking.labelledRegions(counter,1)+tracking.labelledRegions(counter,3)))
,:);
image_bank=uint8(zeros(tracking.labelledRegions(4)+1,tracking.labelledRegions(3)+1,3,50)
);
image_bank2=logical(ones(tracking.labelledRegions(4)+1,tracking.labelledRegions(3)+1,50)
);
frames_with_particles_in_counter=1;

bar = waitbar(0,'Waiting to identify particles...');
target_particle_total=50;

while(frames_with_particles_in_counter<target_particle_total+1)
    testframe = getsnapshot(video);

temporary_frame=testframe((tracking.labelledRegions(counter,2):(tracking.labelledRegions
(counter,2)+tracking.labelledRegions(counter,4))),(tracking.labelledRegions(counter,1):(
tracking.labelledRegions(counter,1)+tracking.labelledRegions(counter,3))),:); %isolate
region
    output = detect_particles(temporary_frame, temporary_background,
tracking.threshold_gain, tracking.threshold_size);
    if output.result
        pause(0.25);
        testframe = getsnapshot(video);

temporary_frame=testframe((tracking.labelledRegions(counter,2):(tracking.labelledRegions
(counter,2)+tracking.labelledRegions(counter,4))),(tracking.labelledRegions(counter,1):(
tracking.labelledRegions(counter,1)+tracking.labelledRegions(counter,3))),:); %isolate
region
        output = detect_particles(temporary_frame, temporary_background,
tracking.threshold_gain, tracking.threshold_size);
            if output.result
```

```matlab
                image_bank(:,:,:,frames_with_particles_in_counter)=temporary_frame;
                image_bank2(:,:,frames_with_particles_in_counter)=output.bw_I;
                test_run_data=[test_run_data;[output.measured_RGB output.area]]
                frames_with_particles_in_counter=frames_with_particles_in_counter+1;
                waitbar(frames_with_particles_in_counter/target_particle_total,bar);
                pause(0.5);
            end
        end
end

close(bar);

setup_data.image_bank=image_bank;
setup_data.image_bank2=image_bank2;
setup_data.test_run_data=test_run_data

setappdata(0,'setup_data',setup_data);
setappdata(0,'tracking_data_structure',tracking);

colourspace_setup_plots()

%% Video Preview
% --- Executes on button press in video_preview_button.
function video_preview_button_Callback(hObject, eventdata, handles)
% hObject    handle to video_preview_button (see GCBO)
% eventdata  reserved - to be defined in a future version of MATLAB
% handles    structure with handles and user data (see GUIDATA)

    tracking=getappdata(0, 'tracking_data_structure');
    video=getappdata(0, 'video');
    res = get(video, 'ROIPosition');
    himage = image(zeros(res(4), res(3)));
    preview(video,himage)
    redraw_regions(handles);

%% Set Background
% --- Executes on button press in set_background.
function set_background_Callback(hObject, eventdata, handles)
% hObject    handle to set_background (see GCBO)
% eventdata  reserved - to be defined in a future version of MATLAB
% handles    structure with handles and user data (see GUIDATA)

    tracking=getappdata(0, 'tracking_data_structure');
    video=getappdata(0, 'video');
    tracking.background = getsnapshot(video);
    setappdata(0, 'tracking_data_structure', tracking);

    writeLog(['Background image set'], handles);

% --- Executes on button press in reanalyse_button.
function reanalyse_button_Callback(hObject, eventdata, handles)
% hObject    handle to reanalyse_button (see GCBO)
% eventdata  reserved - to be defined in a future version of MATLAB
% handles    structure with handles and user data (see GUIDATA)

    tracking=getappdata(0, 'tracking_data_structure');
    process_frame(tracking.testframe,tracking.background)

%% Load
% --- Executes on button press in load_datafile_button.
function load_datafile_button_Callback(hObject, eventdata, handles)
% hObject    handle to load_datafile_button (see GCBO)
% eventdata  reserved - to be defined in a future version of MATLAB
% handles    structure with handles and user data (see GUIDATA)

    %errordlg('Do not move the regions - not supported in this version!.','Region
Setup','modal');
    clear tracking;
    if isappdata(0, 'tracking_data_structure');
        rmappdata(0, 'tracking_data_structure');
    end
    uiload;
```

240

```matlab
        setappdata(0, 'tracking_data_structure', tracking);

        newdatestamp(handles);

        set_gui_values(handles);
        if isfield(tracking, 'labelledRegions')
            redraw_regions(handles);
        end

function newdatestamp(handles)

        tracking=getappdata(0, 'tracking_data_structure');

        tracking.expsummary.datestamp=datestr(now, 30);
        writeLog(['New datestamp set ' tracking.expsummary.datestamp], handles);

        setappdata(0, 'tracking_data_structure', tracking);

%% Redraw gui objects
function redraw_regions(handles)
        tracking=getappdata(0, 'tracking_data_structure');
        [nof,dummy]=size(tracking.labelledRegions);

        for counter=1:nof
            hbox = imrect(handles.axes1, tracking.labelledRegions(counter,:));
        end

%% Write GUI Values
function set_gui_values(handles)
        tracking=getappdata(0, 'tracking_data_structure');
        set(handles.threshold_gain_box,'String',tracking.threshold_gain);
        set(handles.threshold_size_box,'String',tracking.threshold_size);
        set(handles.r_box,'String',mat2str(tracking.target_rgb(1)));
        set(handles.g_box,'String',mat2str(tracking.target_rgb(2)));
        set(handles.b_box,'String',mat2str(tracking.target_rgb(3)));

        if isfield(tracking, 'positive_min_size')
            set(handles.positive_min_size_box,'String',mat2str(tracking.positive_min_size));
            set(handles.positive_max_size_box,'String',mat2str(tracking.positive_max_size));
            set(handles.negative_min_size_box,'String',mat2str(tracking.negative_min_size));
            set(handles.negative_max_size_box,'String',mat2str(tracking.negative_max_size));
        end

        if isfield(tracking, 'expsummary')
            if isfield(tracking.expsummary, 'datestamp')
                set(handles.datestamp_box,'String',tracking.expsummary.datestamp);
            end

            if isfield(tracking.expsummary, 'details')
                set(handles.details_box,'String',tracking.expsummary.details);
            end

            if isfield(tracking.expsummary, 'cell1')

            set(handles.cell1_box,'String',tracking.expsummary.cell1);
            set(handles.cell2_box,'String',tracking.expsummary.cell2);
            set(handles.ratio_box,'String',tracking.expsummary.ratio);
            set(handles.media_box,'String',tracking.expsummary.media);
            set(handles.voltage_box,'String',tracking.expsummary.voltage);
            set(handles.freq_box,'String',tracking.expsummary.freq);

            end
        end

function log_box_Callback(hObject, eventdata, handles)
% hObject    handle to log_box (see GCBO)
% eventdata  reserved - to be defined in a future version of MATLAB
% handles    structure with handles and user data (see GUIDATA)

% Hints: get(hObject,'String') returns contents of log_box as text
```

```matlab
%        str2double(get(hObject,'String')) returns contents of log_box as a double


% --- Executes during object creation, after setting all properties.
function log_box_CreateFcn(hObject, eventdata, handles)
% hObject    handle to log_box (see GCBO)
% eventdata  reserved - to be defined in a future version of MATLAB
% handles    empty - handles not created until after all CreateFcns called


% Hint: edit controls usually have a white background on Windows.
%        See ISPC and COMPUTER.
if ispc && isequal(get(hObject,'BackgroundColor'),
get(0,'defaultUicontrolBackgroundColor'))
    set(hObject,'BackgroundColor','white');
end


function writeLog(text_to_output, handles)
    current_log_text=get(handles.log_box,'String');
    %output=char(current_log_text,text_to_output,' ');
    output=[current_log_text; text_to_output];
    set(handles.log_box,'String',output);


function threshold_size_box_Callback(hObject, eventdata, handles)
% hObject    handle to threshold_size_box (see GCBO)
% eventdata  reserved - to be defined in a future version of MATLAB
% handles    structure with handles and user data (see GUIDATA)


% Hints: get(hObject,'String') returns contents of threshold_size_box as text
%        str2double(get(hObject,'String')) returns contents of threshold_size_box as a
double


% --- Executes during object creation, after setting all properties.
function threshold_size_box_CreateFcn(hObject, eventdata, handles)
% hObject    handle to threshold_size_box (see GCBO)
% eventdata  reserved - to be defined in a future version of MATLAB
% handles    empty - handles not created until after all CreateFcns called


% Hint: edit controls usually have a white background on Windows.
%        See ISPC and COMPUTER.
if ispc && isequal(get(hObject,'BackgroundColor'),
get(0,'defaultUicontrolBackgroundColor'))
    set(hObject,'BackgroundColor','white');
end


function cell1_box_Callback(hObject, eventdata, handles)
% hObject    handle to cell1_box (see GCBO)
% eventdata  reserved - to be defined in a future version of MATLAB
% handles    structure with handles and user data (see GUIDATA)


% Hints: get(hObject,'String') returns contents of cell1_box as text
%        str2double(get(hObject,'String')) returns contents of cell1_box as a double


% --- Executes during object creation, after setting all properties.
function cell1_box_CreateFcn(hObject, eventdata, handles)
% hObject    handle to cell1_box (see GCBO)
% eventdata  reserved - to be defined in a future version of MATLAB
% handles    empty - handles not created until after all CreateFcns called


% Hint: edit controls usually have a white background on Windows.
%        See ISPC and COMPUTER.
if ispc && isequal(get(hObject,'BackgroundColor'),
get(0,'defaultUicontrolBackgroundColor'))
    set(hObject,'BackgroundColor','white');
end


function cell2_box_Callback(hObject, eventdata, handles)
% hObject    handle to cell2_box (see GCBO)
% eventdata  reserved - to be defined in a future version of MATLAB
% handles    structure with handles and user data (see GUIDATA)


% Hints: get(hObject,'String') returns contents of cell2_box as text
%        str2double(get(hObject,'String')) returns contents of cell2_box as a double
```

242

```matlab
% --- Executes during object creation, after setting all properties.
function cell2_box_CreateFcn(hObject, eventdata, handles)
% hObject    handle to cell2_box (see GCBO)
% eventdata  reserved - to be defined in a future version of MATLAB
% handles    empty - handles not created until after all CreateFcns called


% Hint: edit controls usually have a white background on Windows.
%       See ISPC and COMPUTER.
if ispc && isequal(get(hObject,'BackgroundColor'),
get(0,'defaultUicontrolBackgroundColor'))
    set(hObject,'BackgroundColor','white');
end


function media_box_Callback(hObject, eventdata, handles)
% hObject    handle to media_box (see GCBO)
% eventdata  reserved - to be defined in a future version of MATLAB
% handles    structure with handles and user data (see GUIDATA)


% Hints: get(hObject,'String') returns contents of media_box as text
%        str2double(get(hObject,'String')) returns contents of media_box as a double


% --- Executes during object creation, after setting all properties.
function media_box_CreateFcn(hObject, eventdata, handles)
% hObject    handle to media_box (see GCBO)
% eventdata  reserved - to be defined in a future version of MATLAB
% handles    empty - handles not created until after all CreateFcns called


% Hint: edit controls usually have a white background on Windows.
%       See ISPC and COMPUTER.
if ispc && isequal(get(hObject,'BackgroundColor'),
get(0,'defaultUicontrolBackgroundColor'))
    set(hObject,'BackgroundColor','white');
end


function voltage_box_Callback(hObject, eventdata, handles)
% hObject    handle to voltage_box (see GCBO)
% eventdata  reserved - to be defined in a future version of MATLAB
% handles    structure with handles and user data (see GUIDATA)


% Hints: get(hObject,'String') returns contents of voltage_box as text
%        str2double(get(hObject,'String')) returns contents of voltage_box as a double


% --- Executes during object creation, after setting all properties.
function voltage_box_CreateFcn(hObject, eventdata, handles)
% hObject    handle to voltage_box (see GCBO)
% eventdata  reserved - to be defined in a future version of MATLAB
% handles    empty - handles not created until after all CreateFcns called


% Hint: edit controls usually have a white background on Windows.
%       See ISPC and COMPUTER.
if ispc && isequal(get(hObject,'BackgroundColor'),
get(0,'defaultUicontrolBackgroundColor'))
    set(hObject,'BackgroundColor','white');
end


function freq_box_Callback(hObject, eventdata, handles)
% hObject    handle to freq_box (see GCBO)
% eventdata  reserved - to be defined in a future version of MATLAB
% handles    structure with handles and user data (see GUIDATA)


% Hints: get(hObject,'String') returns contents of freq_box as text
%        str2double(get(hObject,'String')) returns contents of freq_box as a double


% --- Executes during object creation, after setting all properties.
function freq_box_CreateFcn(hObject, eventdata, handles)
% hObject    handle to freq_box (see GCBO)
% eventdata  reserved - to be defined in a future version of MATLAB
% handles    empty - handles not created until after all CreateFcns called


% Hint: edit controls usually have a white background on Windows.
%       See ISPC and COMPUTER.
if ispc && isequal(get(hObject,'BackgroundColor'),
get(0,'defaultUicontrolBackgroundColor'))
```

```matlab
    set(hObject,'BackgroundColor','white');
end


function ratio_box_Callback(hObject, eventdata, handles)
% hObject    handle to ratio_box (see GCBO)
% eventdata  reserved - to be defined in a future version of MATLAB
% handles    structure with handles and user data (see GUIDATA)


% Hints: get(hObject,'String') returns contents of ratio_box as text
%        str2double(get(hObject,'String')) returns contents of ratio_box as a double


% --- Executes during object creation, after setting all properties.
function ratio_box_CreateFcn(hObject, eventdata, handles)
% hObject    handle to ratio_box (see GCBO)
% eventdata  reserved - to be defined in a future version of MATLAB
% handles    empty - handles not created until after all CreateFcns called


% Hint: edit controls usually have a white background on Windows.
%       See ISPC and COMPUTER.
if ispc && isequal(get(hObject,'BackgroundColor'),
get(0,'defaultUicontrolBackgroundColor'))
    set(hObject,'BackgroundColor','white');
end


function datestamp_box_Callback(hObject, eventdata, handles)
% hObject    handle to datestamp_box (see GCBO)
% eventdata  reserved - to be defined in a future version of MATLAB
% handles    structure with handles and user data (see GUIDATA)


% Hints: get(hObject,'String') returns contents of datestamp_box as text
%        str2double(get(hObject,'String')) returns contents of datestamp_box as a double


% --- Executes during object creation, after setting all properties.
function datestamp_box_CreateFcn(hObject, eventdata, handles)
% hObject    handle to datestamp_box (see GCBO)
% eventdata  reserved - to be defined in a future version of MATLAB
% handles    empty - handles not created until after all CreateFcns called


% Hint: edit controls usually have a white background on Windows.
%       See ISPC and COMPUTER.
if ispc && isequal(get(hObject,'BackgroundColor'),
get(0,'defaultUicontrolBackgroundColor'))
    set(hObject,'BackgroundColor','white');
end


% --- Executes on button press in new_button.
function new_button_Callback(hObject, eventdata, handles)
% hObject    handle to new_button (see GCBO)
% eventdata  reserved - to be defined in a future version of MATLAB
% handles    structure with handles and user data (see GUIDATA)


newdatestamp(handles)


set_gui_values(handles);


function details_box_Callback(hObject, eventdata, handles)
% hObject    handle to details_box (see GCBO)
% eventdata  reserved - to be defined in a future version of MATLAB
% handles    structure with handles and user data (see GUIDATA)


% Hints: get(hObject,'String') returns contents of details_box as text
%        str2double(get(hObject,'String')) returns contents of details_box as a double


% --- Executes during object creation, after setting all properties.
function details_box_CreateFcn(hObject, eventdata, handles)
% hObject    handle to details_box (see GCBO)
% eventdata  reserved - to be defined in a future version of MATLAB
% handles    empty - handles not created until after all CreateFcns called


% Hint: edit controls usually have a white background on Windows.
%       See ISPC and COMPUTER.
```

244

```matlab
if ispc && isequal(get(hObject,'BackgroundColor'),
get(0,'defaultUicontrolBackgroundColor'))
    set(hObject,'BackgroundColor','white');
end


function positive_min_size_box_Callback(hObject, eventdata, handles)
% hObject    handle to positive_min_size_box (see GCBO)
% eventdata  reserved - to be defined in a future version of MATLAB
% handles    structure with handles and user data (see GUIDATA)

% Hints: get(hObject,'String') returns contents of positive_min_size_box as text
%        str2double(get(hObject,'String')) returns contents of positive_min_size_box as
a double


% --- Executes during object creation, after setting all properties.
function positive_min_size_box_CreateFcn(hObject, eventdata, handles)
% hObject    handle to positive_min_size_box (see GCBO)
% eventdata  reserved - to be defined in a future version of MATLAB
% handles    empty - handles not created until after all CreateFcns called

% Hint: edit controls usually have a white background on Windows.
%       See ISPC and COMPUTER.
if ispc && isequal(get(hObject,'BackgroundColor'),
get(0,'defaultUicontrolBackgroundColor'))
    set(hObject,'BackgroundColor','white');
end


function positive_max_size_box_Callback(hObject, eventdata, handles)
% hObject    handle to positive_max_size_box (see GCBO)
% eventdata  reserved - to be defined in a future version of MATLAB
% handles    structure with handles and user data (see GUIDATA)

% Hints: get(hObject,'String') returns contents of positive_max_size_box as text
%        str2double(get(hObject,'String')) returns contents of positive_max_size_box as
a double


% --- Executes during object creation, after setting all properties.
function positive_max_size_box_CreateFcn(hObject, eventdata, handles)
% hObject    handle to positive_max_size_box (see GCBO)
% eventdata  reserved - to be defined in a future version of MATLAB
% handles    empty - handles not created until after all CreateFcns called

% Hint: edit controls usually have a white background on Windows.
%       See ISPC and COMPUTER.
if ispc && isequal(get(hObject,'BackgroundColor'),
get(0,'defaultUicontrolBackgroundColor'))
    set(hObject,'BackgroundColor','white');
end


function negative_min_size_box_Callback(hObject, eventdata, handles)
% hObject    handle to negative_min_size_box (see GCBO)
% eventdata  reserved - to be defined in a future version of MATLAB
% handles    structure with handles and user data (see GUIDATA)

% Hints: get(hObject,'String') returns contents of negative_min_size_box as text
%        str2double(get(hObject,'String')) returns contents of negative_min_size_box as
a double


% --- Executes during object creation, after setting all properties.
function negative_min_size_box_CreateFcn(hObject, eventdata, handles)
% hObject    handle to negative_min_size_box (see GCBO)
% eventdata  reserved - to be defined in a future version of MATLAB
% handles    empty - handles not created until after all CreateFcns called

% Hint: edit controls usually have a white background on Windows.
%       See ISPC and COMPUTER.
if ispc && isequal(get(hObject,'BackgroundColor'),
get(0,'defaultUicontrolBackgroundColor'))
    set(hObject,'BackgroundColor','white');
end


function negative_max_size_box_Callback(hObject, eventdata, handles)
% hObject    handle to negative_max_size_box (see GCBO)
```

245

```matlab
% eventdata  reserved - to be defined in a future version of MATLAB
% handles    structure with handles and user data (see GUIDATA)

% Hints: get(hObject,'String') returns contents of negative_max_size_box as text
%        str2double(get(hObject,'String')) returns contents of negative_max_size_box as
a double

% --- Executes during object creation, after setting all properties.
function negative_max_size_box_CreateFcn(hObject, eventdata, handles)
% hObject    handle to negative_max_size_box (see GCBO)
% eventdata  reserved - to be defined in a future version of MATLAB
% handles    empty - handles not created until after all CreateFcns called

% Hint: edit controls usually have a white background on Windows.
%       See ISPC and COMPUTER.
if ispc && isequal(get(hObject,'BackgroundColor'),
get(0,'defaultUicontrolBackgroundColor'))
    set(hObject,'BackgroundColor','white');
end

% --- Executes on button press in pushbutton11.
function pushbutton11_Callback(hObject, eventdata, handles)
% hObject    handle to pushbutton11 (see GCBO)
% eventdata  reserved - to be defined in a future version of MATLAB
% handles    structure with handles and user data (see GUIDATA)
```

```matlab
function trapper()
% Adapted from imaqmotion - simple motion detector from Mathworks

%load datafile
    uiload;


appTitle = 'Trapper';


%% DAQ setup
%%% Initialise Box, set Timers, Start, and store handle
%use custom initialise function to open the output and name 2 of the lines
%box is initialised with all outputs *on*

% For NI USB-6009 Box:
% P0.0: Focusing
% P0.1: Gate1
% P0.2: Gate2
% P0.3: Gate3
% P0.4: Gate4
% P0.5: Gate5

try
    [DIOhandle,hwlines] = initialiseInterface()
    %set(DIOhandle,'TimerFcn',@daqcallback);
    %set(DIOhandle,'TimerPeriod',1);
    %start(DIOhandle);
    setappdata(0,'DIOhandle',DIOhandle);
    tracking.currentState=logical([0 0 0 0 0 0 0 0 0 0 0 0 0 0 0 0 0 0 0 0 0 0 0 0 0 0 0 0 0]);
    putvalue(DIOhandle, tracking.currentState);
catch
    'Cannot initialise DAQ hardware interface.'
%    writeLog('Cannot initialise DAQ hardware interface.', handles);
%    errordlg('Cannot initialise DAQ hardware interface.','DAQ Interface','modal');
end


%% Environment setup
%clear region buffer, enable base level pre-requisites
tracking.regions_filled = 0;
tracking.regions_locked_down=[];
tracking.regions_filled_timestamp = clock;
%set first time flag so that video stabilises before acquisition starts
tracking.firsttime=1;


%% Video setup
obj = videoinput('winvideo');

%try
    % Make sure we've stopped so we can set up the acquisition.
    stop(obj);

    % Configure the video input object to continuously acquire data.
%    triggerconfig(obj, 'manual');
%    set(obj, 'Tag', appTitle, 'FramesAcquiredFcnCount', 1, ...
%        'TimerFcn', @localFrameCallback, 'TimerPeriod', tracking.frame_period);

        %reduce size of video resolution
    res=get(obj,'VideoResolution');
    if res>tracking.target_resolution %if resolution exceeds this value, reduce it
        set(obj,'ROIPosition', [floor((res(1)-tracking.target_resolution(1))/2)
floor((res(2)-tracking.target_resolution(2))/2) tracking.target_resolution(1)
tracking.target_resolution(2)]);
    end

    % Check to see if this object already has an associated figure.
    % Otherwise create a new one.
    ud = get(obj, 'UserData');
    if ~isempty(ud) && isstruct(ud) && isfield(ud, 'figureHandles') ...
            && ishandle(ud.figureHandles.hFigure)
        appdata.figureHandles = ud.figureHandles;
```

```
            figure(appdata.figureHandles.hFigure)
        else
            appdata.figureHandles = localCreateFigure(obj, appTitle);
        end

        % Store the application data the video input object needs.
        appdata.background = [];
        obj.UserData = appdata;

        %pre-calculate background sub-images to regions of interest
        [nof,dummy]=size(tracking.labelledRegions);

        for counter=1:nof

tracking.sub_background(:,:,:,counter)=tracking.background((tracking.labelledRegions(cou
nter,2):(tracking.labelledRegions(counter,2)+tracking.labelledRegions(counter,4))),(trac
king.labelledRegions(counter,1):(tracking.labelledRegions(counter,1)+tracking.labelledRe
gions(counter,3))),:);
        end

        %setup video datalogging
        if (tracking.video_logging==1)
            set(obj, 'LoggingMode', 'disk')
            logfilename=['c:\traplogvideos\trapping' datestr(now, 30) '.avi'];
            logfile = avifile(logfilename);
            logfile.Compression = 'wmv3';
            obj.DiskLogger = logfile;
            imaqmem(2e9);
        end

        %leave trigger repeat at inf even if not logging so vidobj keeps
        %running
        set(obj, 'TriggerRepeat', inf);

        % Start the acquisition.
        start(obj);

        t = timer('TimerFcn',{@localFrameCallback, obj}, 'Period', tracking.frame_period,
...
            'StartDelay', 4, 'ExecutionMode', 'fixedRate', 'TasksToExecute', inf);

        start(t);

        % Avoid peekdata warnings in case it takes too long to return a frame.
        warning off imaq:peekdata:tooManyFramesRequested
% catch
%     % Error gracefully.
%     error('MATLAB:imaqmotion:error', ...
%         sprintf('IMAQMOTION is unable to run properly.\n%s', lasterr))
% end

        setappdata(0,'tracking_data_structure',tracking);
        setappdata(0,'vidObj',obj);

%%%%%%%%%%%%%%%%%%%%%%%%%%%%%%%%%%%%%%%%%%%%%%%%%%
function localFrameCallback(obj, event, vid)
% Executed by the videoinput object callback
% to update the image display.

%If the object has been deleted on us,
%or we're no longer running, do nothing.
if ~isvalid(vid) || ~isrunning(vid)
    return;
end

% Access our application data.
tracking = getappdata(0, 'tracking_data_structure');

%setappdata(0,'tracking_data_structure',tracking);

appdata = get(vid, 'UserData');
%background = appdata.background;
```
248

```
% Peek into the video stream. Since we are only interested
% in processing the current frame, not every single image
% frame provided by the device, we can flush any frames in
% the buffer.
%frame = peekdata(vid, 1);
frame = getsnapshot(vid);
if isempty(frame),
    return;
end


flushdata(vid);

%Decide which traps to scan
%Correlate list of filled traps with list of trap hierachy - some traps
%must be filled before others, traps with pre-requisite of zero are filled
%first

%Remove from list traps that have met the pre-requisites but are already
%full

% Separate active regions
%send batch of frames and backgrounds to be chekced

% **TESTing only!!
%frame=imread('testframe.bmp');
%frame=tracking.background;

for counter=1:tracking.nof_regions; %count through each region
    tracking = getappdata(0, 'tracking_data_structure');
    if find(tracking.regions_filled==tracking.prerequisites(counter)) %is pre-requisite
trap filled?
        if isempty(find(tracking.regions_filled==counter, 1)) %is this trap not filled?

sub_frame=frame((tracking.labelledRegions(counter,2):(tracking.labelledRegions(counter,2
)+tracking.labelledRegions(counter,4))),(tracking.labelledRegions(counter,1):(tracking.l
abelledRegions(counter,1)+tracking.labelledRegions(counter,3))),:); %isolate region
            localUpdateFig(sub_frame, tracking.sub_background(:,:,:,counter),counter);
        end
    end
end

% Verify that traps that should be filled really are filled
% Randomly choose one of the traps and verify

verify_region_index=round((rand*length(tracking.regions_filled)+0.5));    %+0.5 to
ensure that region_ID 0 can't be selected
verify_ID=tracking.regions_filled(verify_region_index);
%if verify id is not locked down, verify that the particle is correctly
%trapped
if find(tracking.regions_locked_down==verify_ID)
else
    if verify_ID~=0

sub_frame=frame((tracking.labelledRegions(verify_ID,2):(tracking.labelledRegions(verify_
ID,2)+tracking.labelledRegions(verify_ID,4))),(tracking.labelledRegions(verify_ID,1):(tr
acking.labelledRegions(verify_ID,1)+tracking.labelledRegions(verify_ID,3))),:); %isolate
region
        %tracking.threshold_gain*0.75 is to provide a lower switch off
        %threshold
        output = detect_particles(sub_frame, tracking.sub_background(:,:,:,verify_ID),
tracking.threshold_gain*0.5, tracking.threshold_size);

        if ~isempty(output.area)

            result = compare_colours(output.measured_RGB(1,:), tracking.target_rgb,
tracking.haze_factor*.75, tracking.hue_factor*.75, tracking.stability_factor*.75);

        end
        %   if length(output.area)~=1       %if number of particles is greater or less
than 1

        %if isempty(output.area)       %if no particles are trapped
```

249

```matlab
        %new, stricter verify conditions checks colour as well
        if isempty(output.area)
        %if or(isempty(output.area),~result)
            binID=dec2binvec(2^(verify_ID-1),24);      %generate binary trap reference
            try
                %deactivate trap through DIO
                tracking.currentState = switchOutput(binID,tracking.currentState);

                % Remove trap from filled regions list
                tracking.regions_filled(verify_region_index) = [];
                tracking.regions_filled_timestamp(verify_region_index,:) = [];
                ['Particle not trapped, database corrected.']
                verify_ID
                setappdata(0,'tracking_data_structure',tracking);
            catch
                'Particle not trapped, but could not switch DAQ interface'
            end
        else

            %if particle has been trapped longer than threshold time, lock down
            %the trap
            t1=tracking.regions_filled_timestamp(verify_region_index,:);
            if ((~isempty(t1))&& (etime(clock,t1)>tracking.lockdown_period) && result)
                tracking.regions_locked_down = [tracking.regions_locked_down; verify_ID]
                setappdata(0,'tracking_data_structure',tracking);
            end
        end
    end
end

%check currentState is correct
tracking.currentState = [0 0 0 0 0 0 0 0 0 0 0 0 0 0 0 0 0 0 0 0 0 0 0 0];
for counter=1:length(tracking.regions_filled)
    binID=dec2binvec(2^(tracking.regions_filled(counter)-1),24);
    tracking.currentState = xor(tracking.currentState,binID);
end

%confirm outputs are correctly set
setOutput(tracking.currentState);

%moved out of localUpdateFig - RT 090908
% If the figure has been destroyed on us, stop the acquisition.
if ~ishandle(appdata.figureHandles.hFigure),
    stop(vid);
    %stop(timerfindall);
    return;
end

%%%%%%%%%%%%%%%%%%%%%%%%%%%%%%%%%%%%%%%%%%%%%%%%
function localUpdateFig(frame, background, region_ID)
    % Detect particles in supplied region, and switch DIO accordingly

    tracking = getappdata(0, 'tracking_data_structure');

    %look for particles, and switch on relevant trap
    % currently switches on if any particles in the region match the target
    % RGB
    output = detect_particles(frame, background, tracking.threshold_gain,
tracking.threshold_size);

    if output.result                                %if something has been found
        [nof,dummy]=size(output.measured_RGB);
        for counter=1:nof                           %cycle through all found particles
            output.measured_RGB
            if compare_colours(output.measured_RGB(counter,:), tracking.target_rgb,
tracking.haze_factor, tracking.hue_factor, tracking.stability_factor)
            %if compare_colours(output.measured_RGB(counter,:), tracking.target_rgb,
1,1, 1)
                % Activate trap, if DIO is working generate binary trap reference
                binID=dec2binvec(2^(region_ID-1),24);
                try
                    %activate trap through DIO
                    tracking.currentState = switchOutput(binID,tracking.currentState);
```

250

```matlab
                    % Log trap as filled
                    tracking.regions_filled = [tracking.regions_filled; region_ID];
                    tracking.regions_filled_timestamp  =
[tracking.regions_filled_timestamp; clock];
                    'Trap filled'
                    region_ID

                    setappdata(0,'tracking_data_structure',tracking);
                    return
                catch
                    'Could not switch DAQ interface'
                end
            end
        end
    end


%%%%%%%%%%%%%%%%%%%%%%%%%%%%%%%%%%%%%%%%%%%%

function newState = switchOutput(binID,currentState)
    %tracking = getappdata(0, 'tracking_data_structure');
    DIOhandle = getappdata(0,'DIOhandle');
    newState = xor(currentState,binID);
    try
        putvalue(DIOhandle, newState);
    catch
        'DIO error'
    end
    %tracking.currentState = newState;
    %setappdata(0,'tracking_data_structure',tracking);

function setOutput(newState)
    %tracking = getappdata(0, 'tracking_data_structure');
    DIOhandle = getappdata(0,'DIOhandle');
    %newState = xor(tracking.currentState,binID);
    try
        putvalue(DIOhandle, newState);
    catch
        'DIO error'
    end
    %tracking.currentState = newState
    %setappdata(0,'tracking_data_structure',tracking);

%%%%%%%%%%%%%%%%%%%%%%%%%%%%%%%%%%%%%%%%%%%%%%%
function localDeleteFig(fig, event)

% Reset peekdata warnings.
warning on imaq:peekdata:tooManyFramesRequested

obj = getappdata(0,'vidObj');
tracking=getappdata(0,'tracking_data_structure');

%closepreview;

active_timers=timerfindall;
stop(active_timers);
delete(active_timers);

stop(obj);

if (tracking.video_logging==1)
    aviobj = obj.Disklogger;
    file = close(aviobj)
end

delete(obj)
clear obj


%%%%%%%%%%%%%%%%%%%%%%%%%%%%%%%%%%%%%%%%%%%%%%%
function figData = localCreateFigure(vid, figTitle)
% Creates and initializes the figure.
% % Create a spot for the image object display.
```

```matlab
% nbands = get(vid, 'NumberOfBands');
res = get(vid, 'ROIPosition');
% himage = imagesc(rand(res(4), res(3), nbands));

% Create the image object in which you want to
% display the video preview data.
%vidRes = get(vid, 'VideoResolution');
% imWidth = vidRes(1);
imWidth = res(3);
% imHeight = vidRes(2);
imHeight = res(4);
nBands = get(vid, 'NumberOfBands');

% Create the figure and axes to plot into - off screen
fig = figure('NumberTitle', 'off', 'MenuBar', 'none', ...
    'Name', figTitle, 'unit', 'pixels', 'position', [ 10000 10000 imWidth imHeight ],
'DeleteFcn', @localDeleteFig);

himage = image( zeros(imHeight, imWidth, nBands) );

% Specify the size of the axes that contains the image object
% so that it displays the image at the right resolution and
% centers it in the figure window.
set(gca,'unit','pixels',...
        'position',[ 0 0 imWidth imHeight ]);

preview(vid,himage);
% preview(vid);

%show window, in centre of screen
movegui(fig,'center');

% Clean up the axes.
ax = get(himage, 'Parent');
set(ax, 'XTick', [], 'XTickLabel', [], 'YTick', [], 'YTickLabel', []);

% Create the motion detection bar before hiding the figure.
%[hPatch, hLine] = localCreateBar(ax);
set(fig, 'HandleVisibility', 'off');

% Store the figure data.
figData.hFigure = fig;
figData.hImage = himage;
% figData.hPatch = hPatch;
% figData.hLine = hLine;
```

```matlab
function sorter()
% Adapted from imaqmotion - simple motion detector from Mathworks

%load datafile
    uiload;

appTitle = 'Sorter';

%% DAQ setup
%%% Initialise Box, set Timers, Start, and store handle
%use custom initialise function to open the output and name 2 of the lines
%box is initialised with all outputs *on*

% For NI USB-6009 Box:
% P0.0: Focusing
% P0.1: Gate1
% P0.2: Gate2
% P0.3: Gate3
% P0.4: Gate4
% P0.5: Gate5

try
    [DIOhandle,hwlines] = initialiseInterface()
    %set(DIOhandle,'TimerFcn',@daqcallback);
    %set(DIOhandle,'TimerPeriod',1);
    %start(DIOhandle);
    setappdata(0,'DIOhandle',DIOhandle);
    tracking.currentState=logical([0 0 0 0 0 0 0 0 0 0 0 0 0 0 0 0 0 0 0 0 0 0 0 0 0 0 0 0 0 0]);
    putvalue(DIOhandle, tracking.currentState);
catch
    'Cannot initialise DAQ hardware interface.'
%    writeLog('Cannot initialise DAQ hardware interface.', handles);
%    errordlg('Cannot initialise DAQ hardware interface.','DAQ Interface','modal');
end

%% Environment setup
%clear region buffer, enable base level pre-requisites
tracking.regions_filled = 0;
tracking.regions_locked_down=[];
tracking.regions_filled_timestamp = clock;
%set first time flag so that video stabilises before acquisition starts
tracking.firsttime=1;
tracking.frame_log=[];

vector=linspace(1,1800,200);
tracking.high_sound=0.2*sin(vector);
vector2=linspace(1,2000,200);
tracking.low_sound=0.2*sin(vector2);

    setappdata(0,'tracking_data_structure',tracking);

 tracking.currentState = tracking.gate_closed_condition;
close_gate(1);

%% Video setup
obj = videoinput('winvideo');

%try
    % Make sure we've stopped so we can set up the acquisition.
    stop(obj);

    % Configure the video input object to continuously acquire data.
%    triggerconfig(obj, 'manual');
%    set(obj, 'Tag', appTitle, 'FramesAcquiredFcnCount', 1, ...
%        'TimerFcn', @localFrameCallback, 'TimerPeriod', tracking.frame_period);

        %reduce size of video resolution
    res=get(obj,'VideoResolution');
    if res>tracking.target_resolution %if resolution exceeds this value, reduce it
```

253

```matlab
        set(obj,'ROIPosition', [floor((res(1)-tracking.target_resolution(1))/2)
floor((res(2)-tracking.target_resolution(2))/2) tracking.target_resolution(1)
tracking.target_resolution(2)]);
    end

    % Check to see if this object already has an associated figure.
    % Otherwise create a new one.
    ud = get(obj, 'UserData');
    if ~isempty(ud) && isstruct(ud) && isfield(ud, 'figureHandles') ...
            && ishandle(ud.figureHandles.hFigure)
        appdata.figureHandles = ud.figureHandles;
        figure(appdata.figureHandles.hFigure)
    else
        appdata.figureHandles = localCreateFigure(obj, appTitle);
    end

    % Store the application data the video input object needs.
    appdata.background = [];
    obj.UserData = appdata;

    %pre-calculate background sub-images to regions of interest
    [nof,dummy]=size(tracking.labelledRegions);

    for counter=1:nof

tracking.sub_background(:,:,:,counter)=tracking.background((tracking.labelledRegions(cou
nter,2):(tracking.labelledRegions(counter,2)+tracking.labelledRegions(counter,4))),(trac
king.labelledRegions(counter,1):(tracking.labelledRegions(counter,1)+tracking.labelledRe
gions(counter,3))),:);
    end

        if isfield(tracking.expsummary, 'datestamp')
        datex=tracking.expsummary.datestamp;
    else
        datex=datestr(now, 30);
    end

    repetition_id=1;

    dirlisting=dir('C:\traplogvideos\');
    logfilename=['trapping' datex '_' num2str(repetition_id) '.avi'];
    clear_flag=0;
    clash=0;

    while clear_flag==0
        for counter=1:length(dirlisting)
            if strcmp(dirlisting(counter).name,logfilename)
                clash=1;
            end
        end

        if clash==1
            repetition_id=repetition_id+1;
            logfilename=['trapping' datex '_' num2str(repetition_id) '.avi'];
            clash=0;
        else
            clear_flag=1;
        end
     end

    logfilepath=['c:\traplogvideos\' logfilename];

    %setup video datalogging
    if (tracking.video_logging==1)
        set(obj, 'LoggingMode', 'disk')
        logfile = avifile(logfilepath);
        logfile.Compression = 'wmv3';
        obj.DiskLogger = logfile;
        imaqmem(2e9);
    end

    %leave trigger repeat at inf even if not logging so vidobj keeps
```

254

```matlab
    %running
    set(obj, 'TriggerRepeat', inf);

    % Start the acquisition.
    start(obj);

    t = timer('TimerFcn',{@localFrameCallback, obj}, 'Period', tracking.frame_period,
...
        'StartDelay', 4, 'ExecutionMode', 'fixedRate', 'TasksToExecute', inf);

    start(t);

    % Avoid peekdata warnings in case it takes too long to return a frame.
    warning off imaq:peekdata:tooManyFramesRequested
% catch
%     % Error gracefully.
%     error('MATLAB:imaqmotion:error', ...
%         sprintf('IMAQMOTION is unable to run properly.\n%s', lasterr))
% end

% tracking.clock=[];

    setappdata(0,'tracking_data_structure',tracking);
    setappdata(0,'vidObj',obj);
    close_gate(0);

    %generate text log file
    sort_type='Y-junction';
    handle_text_log;

%%%%%%%%%%%%%%%%%%%%%%%%%%%%%%%%%%%%%%%%%%%%%%%
function localFrameCallback(obj, event, vid)
% Executed by the videoinput object callback
% to update the image display.

%If the object has been deleted on us,
%or we're no longer running, do nothing.
if ~isvalid(vid) || ~isrunning(vid)
    return;
end

% Access our application data.
tracking = getappdata(0, 'tracking_data_structure');

% tracking.clock=[tracking.clock;clock];
% length(tracking.clock)
% clock
%         setappdata(0,'tracking_data_structure',tracking);

tracking.frame_log=[tracking.frame_log; clock];

%setappdata(0,'tracking_data_structure',tracking);

appdata = get(vid, 'UserData');
%background = appdata.background;

frame = getsnapshot(vid);
if isempty(frame),
    return;
end

flushdata(vid);

%if gate is open, check time since gate opened and close if necessary
%else scan for particles

if (tracking.currentState==tracking.gate_open_condition)
    gate_ID=1;
    t1=tracking.gate_open_time;
    if ((~isempty(t1))&& (etime(clock,t1)>tracking.gate_open_period))
        close_gate(gate_ID);
```

```matlab
        end
end


if (tracking.gate_locked_shut==1)
    t1=tracking.gate_lock_time;
    if ((~isempty(t1)) && (etime(clock,t1)>tracking.gate_lock_period))
        tracking.gate_locked_shut=0;
        setappdata(0,'tracking_data_structure',tracking);
    end
else
    counter=1;

sub_frame=frame((tracking.labelledRegions(counter,2):(tracking.labelledRegions(counter,2
)+tracking.labelledRegions(counter,4))),(tracking.labelledRegions(counter,1):(tracking.l
abelledRegions(counter,1)+tracking.labelledRegions(counter,3))),:); %isolate region
    localUpdateFig(sub_frame, tracking.sub_background(:,:,:,counter),counter);
end

%moved out of localUpdateFig - RT 090908
% If the figure has been destroyed on us, stop the acquisition.
if ~ishandle(appdata.figureHandles.hFigure),
    stop(vid);
    %stop(timerfindall);
    return;
end

%%%%%%%%%%%%%%%%%%%%%%%%%%%%%%%%%%%%%%%%%%%%%%%
function localUpdateFig(frame, background, region_ID)
    % Detect particles in supplied region, and switch DIO accordingly

    tracking = getappdata(0, 'tracking_data_structure');

    %look for particles, and switch on relevant trap
    %Counts through detected particles, opens gate if a particle matches
    %target.
    %If any particle is detected that is non-target, gate is immediately
    %closed and locked shut for the lock down period.
    %Gate is automatically closed once target particle leaves tracking
    %area, of after the trap_open_period
    region_ID=1;
    if tracking.gate_locked_shut==0

        output = detect_particles(frame, background, tracking.threshold_gain,
tracking.threshold_size);

        if output.result                              %if something has been found
            response=gate_decision(output);

            switch response
                case 1
                    open_gate(region_ID);
                case 2
                    close_gate(region_ID);
                case 3
                    %active close gate
                    close_gate(region_ID);

                    %lock gate shut for specified period
                     tracking.gate_locked_shut=1;
                     tracking.gate_lock_time=clock;
                     setappdata(0,'tracking_data_structure',tracking);
            end

        else                              %nothing found
            %implement active closing of gate if no particles found
            %*** tracking area must be large enough to track particles
            %until clear of gate!***

            %active close gate
            close_gate(region_ID);
        end
    else
    end
256
```

```matlab
%%%%%%%%%%%%%%%%%%%%%%%%%%%%%%%%%%%%%%%%%%%%%%%
%Gate control functions using DIO

% function open_gate(region_ID)
% tracking = getappdata(0, 'tracking_data_structure');
% DIOhandle = getappdata(0,'DIOhandle');
% tracking.currentState=tracking.gate_open_condition;
% try
%     putvalue(DIOhandle, tracking.currentState);
%     tracking.gate_open_time=clock;
%     setappdata(0,'tracking_data_structure',tracking);
% catch
%   'DIO error'
% end
%
% function close_gate(region_ID)
% tracking = getappdata(0, 'tracking_data_structure');
% DIOhandle = getappdata(0,'DIOhandle');
% tracking.currentState=tracking.gate_closed_condition;
% try
%     putvalue(DIOhandle, tracking.currentState);
%     setappdata(0,'tracking_data_structure',tracking);
% catch
%   'DIO error'
% end


%Gate control functions using GPIB and TTI TGA12104

function open_gate(region_ID)
tracking = getappdata(0, 'tracking_data_structure');
DIOhandle = getappdata(0,'DIOhandle');
%if tracking.currentState ~= tracking.gate_open_condition
    sound(tracking.high_sound,4000)
    tracking.currentState=tracking.gate_open_condition;
%end

try
    putvalue(DIOhandle, tracking.currentState);

%     fprintf(g,'SETUPCH 4');
%     fprintf(g,'PHASE 180');
%
%     fprintf(g,'SETUPCH 3');
%     fprintf(g,'PHASE 0');

    tracking.gate_open_time=clock;
    setappdata(0,'tracking_data_structure',tracking);
catch
    'DIO error'
end
%end


function close_gate(region_ID)
tracking = getappdata(0, 'tracking_data_structure');
DIOhandle = getappdata(0,'DIOhandle');
%if tracking.currentState ~= tracking.gate_closed_condition
 %   sound(tracking.low_sound,4000)
    tracking.currentState=tracking.gate_closed_condition;
%end
%g=getappdata(0,'gpib');
try
    putvalue(DIOhandle, tracking.currentState);
% fprintf(g,'SETUPCH 3');
% fprintf(g,'PHASE 180');
%
% fprintf(g,'SETUPCH 4');
% fprintf(g,'PHASE 0');

    setappdata(0,'tracking_data_structure',tracking);
catch
    'DIO error'
end
%end
%%%%%%%%%%%%%%%%%%%%%%%%%%%%%%%%%%%%%%%%%%%%%%%
```

257

```matlab
function localDeleteFig(fig, event)

% Reset peekdata warnings.
warning on imaq:peekdata:tooManyFramesRequested

obj = getappdata(0,'vidObj');
tracking=getappdata(0,'tracking_data_structure');

active_timers=timerfindall;
stop(active_timers);
delete(active_timers);

closepreview;
stop(obj);

if (tracking.video_logging==1)
    aviobj = obj.Disklogger;
    file = close(aviobj)
end

delete(obj)
clear obj
%%%%%%%%%%%%%%%%%%%%%%%%%%%%%%%%%%%%%%%%%%%%%%%%%%%
function figData = localCreateFigure(vid, figTitle)
% Creates and initializes the figure.
% % Create a spot for the image object display.
% nbands = get(vid, 'NumberOfBands');
res = get(vid, 'ROIPosition');
% himage = imagesc(rand(res(4), res(3), nbands));

% Create the image object in which you want to
% display the video preview data.
%vidRes = get(vid, 'VideoResolution');
% imWidth = vidRes(1);
imWidth = res(3);
% imHeight = vidRes(2);
imHeight = res(4);
nBands = get(vid, 'NumberOfBands');

% Create the figure and axes to plot into - off screen
fig = figure('NumberTitle', 'off', 'MenuBar', 'none', ...
    'Name', figTitle, 'unit', 'pixels', 'position', [ 10000 10000 imWidth imHeight ],
'DeleteFcn', @localDeleteFig);

himage = image( zeros(imHeight, imWidth, nBands) );

% Specify the size of the axes that contains the image object
% so that it displays the image at the right resolution and
% centers it in the figure window.
set(gca,'unit','pixels',...
        'position',[ 0 0 imWidth imHeight ]);

preview(vid,himage);
% preview(vid);

%show window, in centre of screen
movegui(fig,'center');

% Clean up the axes.
ax = get(himage, 'Parent');
set(ax, 'XTick', [], 'XTickLabel', [], 'YTick', [], 'YTickLabel', []);

% Create the motion detection bar before hiding the figure.
%[hPatch, hLine] = localCreateBar(ax);
set(fig, 'HandleVisibility', 'off');

% Store the figure data.
figData.hFigure = fig;
figData.hImage = himage;
% figData.hPatch = hPatch;
% figData.hLine = hLine;
```

258

Appendix 11. Additional data for molecular analysis of sorted STRO-1+ cells

List of genes highly expressed in microarray molecular analysis of unsorted hBMSC populations. Genes are normalised against GAPDH, n=3.

SYMBOL	GENE NAME
ALCAM	activated leukocyte cell adhesion molecule (CD166)
ANPEP	alanyl (membrane) aminopeptidase (CD13)
ANXA5	annexin A5
BDNF	brain-derived neurotrophic factor
BGLAP	bone gamma-carboxyglutamate (gla) protein (Osteocalcin)
CASP3	caspase 3, apoptosis-related cysteine peptidase
CD44	CD44 molecule (Indian blood group)
COL1A1	collagen, Type I, alpha 1
CTNNB1	catenin (cadherin-associated protein), beta 1
ENG	Endoglin (CD105)
FGF2	fibroblast growth factor 2
GDF15	growth differentiation factor 15
GDF5	growth differentiation factor 5 (BMP-14)
GTF3A	general transcription factor IIIA
HAT1	histone acetyltransferase 1
HDAC1	histone deacetylase 1
HGF	hepatocyte growth factor
IL6	interleukin 6
ITGA6	integrin, alpha 6
ITGAV	integrin, alpha V
ITGB1	integrin, beta 1
JAG1	jagged 1 (CD339)
KITLG	KIT ligand
MCAM	melanoma cell adhesion molecule (CD146)
MMP2	matrix metallopeptidase 2 (gelatinase A, Type IV collagenase)
NES	nestin
NT5E	5'-nucleotidase, ecto
NUDT6	nudix (nucleoside diphosphate linked moiety X)-type motif 6
PDGFRB	platelet-derived growth factor receptor, beta (CD140b)
PIGS	phosphatidylinositol glycan anchor biosynthesis, class S
PTK2	protein tyrosine kinase 2
RHOA	ras homolog gene family, member A
RUNX2	runt-related transcription factor 2 (CBFA1)
SLC17A5	solute carrier family 17 (anion/sugar transporter), member 5
SMAD4	SMAD family member 4
SMURF1	SMAD specific E3 ubiquitin protein ligase 1
SMURF2	SMAD specific E3 ubiquitin protein ligase 2
TGFB1	transforming growth factor, beta 1
TGFB3	transforming growth factor, beta 3
THY1	Thy-1 cell surface antigen (CD90)
VCAM1	vascular cell adhesion molecule 1 (CD106)
VEGFA	vascular endothelial growth factor A
VIM	vimentin

Appendix 12. Publications and presentations

Publications:

1. Thomas, R.S.W.*, **Mitchell, P.D**.*, Oreffo, R.O.C., & Morgan, H. 2010. "Trapping single human osteoblast-like cells from a heterogeneous population using a dielectrophoretic microfluidic device." *Biomicrofluidics*, 4, (2) (*Joint first author).

2. Gothard, D., Tare, R.S., **Mitchell, P.D**., Dawson, J.I., & Oreffo, R.O.C. 2011. "In search of the skeletal stem cell: isolation and separation strategies at the macro/micro scale for skeletal regeneration." *Lab on a Chip*, 11, 1206-1220.

Presentations:

1. **Mitchell, P.D**., Oreffo, R.O.C. Human skeletal stem cell enrichment using microfluidic and lab-on-a-chip strategies (2010) (Oral presentation, University of Southampton School Of Medicine Postgraduate Conference, awarded commendation for outstanding talk)

2. **Mitchell, P.D**., Wilson, D.I., Oreffo, R.O.C. Development of a 3D model for skeletogenesis using fetal femur-derived cell populations (2009) (Poster Presentation, University of Southampton School Of Medicine Postgraduate Conference)

3. **Mitchell, P.D**., Wilson, D.I., Oreffo, R.O.C. Development of a 3D model for skeletogenesis using fetal femur-derived cell populations (2009) (Poster Presentation, UKNSCN Annual Scientific Conference, University of Oxford)

Pending publications:

1. **Mitchell, P.D.** & Oreffo, R.O.C. "Development of a novel 3D organotypic model for skeletogenesis using fetal femur-derived cell populations."

2. **Mitchell, P.D**., Thomas, R.S.W., Oreffo, R.O.C. & Morgan, H. " A novel dielectrophoretic sorting device for cell isolation from heterogeneous populations."

GLOSSARY

Adipocyte	Fat cell
Adipo-	Fat
Adipogenesis	Formation of fat cells
Allogeneic	From a non-host (donor) source
Allograft	Tissue from another patient/donor
Autograft	Tissue from the same patient/donor
Autologous	From the host source
Centrifugation	Spinning of cells to produce a pellet
Chondro-	Cartilage
Chondrocyte	Cartilage cell
Chondrogenesis	Formation of cartilage cells
Ex vivo	Outside of body
Genotype	Genetic arrangement
In situ	Within its place
In vitro	Within the laboratory
In vivo	In patient/animal
Lacunae	Cell pits
Organotypic	Organ-like culture
Osteo-	Bone
Osteoblast	Developing bone cell
Osteoclast	Bone remodelling cell
Osteocyte	Mature bone cell
Osteogenesis	Formation of bone cells
Passage	Splitting of cell populations
Phenotype	Physical appearance/expression of distinct markers
Plasticity	Differentiation from one cell type to another
Transfection	Insertion into cell of new genetic information

REFERENCES

Abbott, A. 2003. Cell culture: Biology's new dimension. *Nature*, 424, (6951) 870-872

Abdulrazzak, H., Moschidou, D., Jones, G., & Guillot, P.V. 2010. Biological characteristics of stem cells from foetal, cord blood and extraembryonic tissues. *Journal of the Royal Society Interface*, 7, S689-S706

Adams, J.D., Kim, U., & Soh, H.T. 2008. Multitarget magnetic activated cell sorter. *Proceedings of the National Academy of Sciences of the United States of America*, 105, (47) 18165-18170

Aigner, T. & Stove, J. 2003. Collagens - major component of the physiological cartilage matrix, major target of cartilage degeneration, major tool in cartilage repair. *Advanced Drug Delivery Reviews*, 55, (12) 1569-1593

Akino, K., Mineta, T., Fukui, M., Fujii, T., & Akita, S. 2003. Bone morphogenetic protein-2 regulates proliferation of human mesenchymal stem cells. *Wound Repair and Regeneration*, 11, (5) 354-360

Alison, M. & Sarraf, C. 1998. Hepatic stem cells. *Journal of Hepatology*, 29, (4) 676-682

Arai, F., Ohneda, O., Miyamoto, T., Zhang, X.Q., & Suda, T. 2002. Mesenchymal stem cells in perichondrium express activated leukocyte cell adhesion molecule and participate in bone marrow formation. *Journal of Experimental Medicine*, 195, (12) 1549-1563

Archer, S., Li, T.T., Evans, A.T., Britland, S.T., & Morgan, H. 1999. Cell reactions to dielectrophoretic manipulation. *Biochemical and Biophysical Research Communications*, 257, (3) 687-698

Arnold, W.M. & Zimmermann, U. 1982. Rotation of An Isolated Cell in A Rotating Electric-Field. *Naturwissenschaften*, 69, (6) 297-298

Arnold, W.M. & Zimmermann, U. 1988. Electro-Rotation - Development of A Technique for Dielectric Measurements on Individual Cells and Particles. *Journal of Electrostatics*, 21, (2-3) 151-191

Arora, A., Simone, G., Salieb-Beugelaar, G.B., Kim, J.T., & Manz, A. 2010. Latest Developments in Micro Total Analysis Systems. *Analytical Chemistry*, 82, (12) 4830-4847

Asa, S.L., Ramyar, L., Murphy, P.R., Li, A.W., & Ezzat, S. 2001. The endogenous fibroblast growth factor-2 antisense gene product regulates pituitary cell growth and hormone production. *Molecular Endocrinology*, 15, (4) 589-599

Baksh, D., Song, L., & Tuan, R.S. 2004. Adult mesenchymal stem cells: characterization, differentiation, and application in cell and gene therapy. *Journal of Cellular and Molecular Medicine*, 8, (3) 301-316

Barlow, S., Brooke, G., Chatterjee, K., Price, G., Pelekanos, R., Rossetti, T., Doody, M., Venter, D., Pain, S., Gilshenan, K., & Atkinson, K. 2008. Comparison of Human Placenta- and Bone Marrow-Derived Multipotent Mesenchymal Stem Cells. *Stem Cells and Development*, 17, (6) 1095-1107

Barry, F., Boynton, R.E., Liu, B.S., & Murphy, J.M. 2001. Chondrogenic differentiation of mesenchymal stem cells from bone marrow: Differentiation-dependent gene expression of matrix components. *Experimental Cell Research*, 268, (2) 189-200

Battula, V.L., Bareiss, P.M., Treml, S., Conrad, S., Albert, I., Hojak, S., Abele, H., Schewe, B., Just, L., Skutella, T., & Bühring, H.-J. 2007. Human placenta and bone marrow derived MSC cultured in serum-free, b-FGF-containing medium express cell surface frizzled-9 and SSEA-4 and give rise to multilineage differentiation. *Differentiation*, 75, (4) 279-291

Battula, V.L., Treml, S., Abele, H., & Buhring, H.J. 2008. Prospective isolation and characterization of mesenchymal stem cells from human placenta using a frizzled-9-specific monoclonal antibody. *Differentiation*, 76, (4) 326-336

Bauer, N., Fonseca, A.V., Florek, M., Freund, D., Jaszai, J., Bornhauser, M., Fargeas, C.A., & Corbeil, D. 2008. New insights into the cell biology of haematopoietic progenitors by studying prominin-1 (CD133). *Cells Tissues Organs*, 188, (1-2) 127-138

Bhosale, A.M. & Richardson, J.B. 2008. Articular cartilage: structure, injuries and review of management. *British Medical Bulletin*, 87, (1) 77-95

Bianco, P., Riminucci, M., Gronthos, S., & Robey, P.G. 2001. Bone marrow stromal stem cells: Nature, biology, and potential applications. *Stem Cells*, 19, (3) 180-192

Bianco, P., Robey, P.G., & Simmons, P.J. 2008. Mesenchymal stem cells: Revisiting history, concepts, and assays. *Cell Stem Cell*, 2, (4) 313-319

Bieback, K., Kern, S., Kluter, H., & Eichler, H. 2004. Critical parameters for the isolation of mesenchymal stem cells from umbilical cord blood. *Stem Cells*, 22, (4) 625-634

Biswas, A. & Hutchins, R. 2007. Embryonic stem cells. *Stem Cells and Development*, 16, (2) 213-221

Bohm, A., Staiger, H., Hennige, A.M., Haas, C., Machicao, F., & Haring, H.U. 2008. Effect of insulin detemir, compared to human insulin, on 3T3-L1 adipogenesis. *Regulatory Peptides*, 151, (1-3) 160-163

Bonewald, L.F. 2011. The Amazing Osteocyte. *Journal of Bone and Mineral Research*, 26, (2) 229-238

Bonfield, T.L. 2010. Adult Mesenchymal Stem Cells: An Innovative Therapeutic for Lung Diseases. *Discovery Medicine*, 9, (47) 337-345

Boyle, W.J., Simonet, W.S., & Lacey, D.L. 2003. Osteoclast differentiation and activation. *Nature*, 423, (6937) 337-342

Brandl, F.P., Seitz, A.K., Tessmar, J.K.V., Blunk, T., & Gopferich, A.M. 2010. Enzymatically degradable poly(ethylene glycol) based hydrogels for adipose tissue engineering. *Biomaterials*, 31, (14) 3957-3966

Brittberg, M., Lindahl, A., Nilsson, A., Ohlsson, C., Isaksson, O., & Peterson, L. 1994. Treatment of Deep Cartilage Defects in the Knee with Autologous Chondrocyte Transplantation. *New England Journal of Medicine*, 331, (14) 889-895

Brittberg, M., Peterson, L., Sjogren-Jansson, E., Tallheden, T., & Lindahl, A. 2003. Articular cartilage engineering with autologous chondrocyte transplantation - A review of recent developments. *Journal of Bone and Joint Surgery-American Volume*, 85A, 109-115

Bruder, S.P., Ricalton, N.S., Boynton, R.E., Connolly, T.J., Jaiswal, N., Zala, J., & Barry, F.P. 1998. Mesenchymal stem cell surface antigen SB-10 corresponds to activated leukocyte cell adhesion molecule and is involved in osteogenic differentiation. *Journal of Bone and Mineral Research*, 13, (4) 655-663

Buckwalter, J.A., Glimcher, M.J., Cooper, R.R., & Becker, R. 1996. Bone biology part I: structure, blood supply, cells, matrix, and mineralization. *Instructional Course Lectures*, 45, 371-386

Buhring, H.J., Battula, V.L., Treml, S., Schewe, B., Kanz, L., & Vogel, W. 2007. Novel markers for the prospective isolation of human MSC. *Haematopoietic Stem Cells Vi*, 1106, 262-271

Bujia, J., Sittinger, M., Pitzke, P., Wilmes, E., & Hammer, C. 1993. Synthesis of Human Cartilage Using Organotypic Cell-Culture. *Orl-Journal for Oto-Rhino-Laryngology and Its Related Specialties*, 55, (6) 347-351

Campagnoli, C., Roberts, I.A.G., Kumar, S., Bennett, P.R., Bellantuono, I., & Fisk, N.M. 2001. Identification of mesenchymal stem/progenitor cells in human first-trimester fetal blood, liver, and bone marrow. *Blood*, 98, (8) 2396-2402

Caplan, A.I. 1991. Mesenchymal Stem-Cells. *Journal of Orthopaedic Research*, 9, (5) 641-650

Caplan, A.I. 2007. Adult mesenchymal stem cells for tissue engineering versus regenerative medicine. *Journal of Cellular Physiology*, 213, (2) 341-347

Carano, R.A.D. & Filvaroff, E.H. 2003. Angiogenesis and bone repair. *Drug Discovery Today*, 8, (21) 980-989

Chang, Y., Hsieh, P.H., & Chao, C.C. 2009. The efficiency of Percoll and Ficoll density gradient media in the isolation of marrow derived human mesenchymal stem cells with osteogenic potential. *Chang Gung Medical Journal*, 32, (3) 264-275

Chang, Y.L., Stanford, C.M., & Keller, J.C. 2000. Calcium and phosphate supplementation promotes bone cell mineralization: Implications for hydroxyapatite (HA)-enhanced bone formation. *Journal of Biomedical Materials Research*, 52, (2) 270-278

Chen, D., Zhao, M., & Mundy, G.R. 2004. Bone morphogenetic proteins. *Growth Factors*, 22, (4) 233-241

Chen, P., Feng, X.J., Du, W., & Liu, B.F. 2008. Microfluidic chips for cell sorting. *Frontiers in Bioscience*, 13, 2464-2483

Cheng, J., Sheldon, E.L., Wu, L., Heller, M.J., & O'Connell, J.P. 1998. Isolation of cultured cervical carcinoma cells mixed with peripheral blood cells on a bioelectronic chip. *Analytical Chemistry*, 70, (11) 2321-2326

Cheung, K., Gawad, S., & Renaud, P. 2005. Impedance spectroscopy flow cytometry: On-chip label-free cell differentiation. *Cytometry Part A*, 65A, (2) 124-132

Cho, H.J., Lee, C.S., Kwon, Y.W., Paek, J.S., Lee, S.H., Hur, J., Lee, E.J., Roh, T.Y., Chu, I.S., Leem, S.H., Kim, Y., Kang, H.J., Park, Y.B., & Kim, H.S. 2010. Induction of pluripotent stem cells from adult somatic cells by protein-based reprogramming without genetic manipulation. *Blood*, 116, (3) 386-395

Choi, K.Y., Kim, H.J., Lee, M.H., Kwon, T.G., Nah, H.D., Furuichi, T., Komori, T., Nam, S.H., Kim, Y.J., Kim, H.J., & Ryoo, H.M. 2005. Runx2 regulates FGF2-induced Bmp2 expression during cranial bone development. *Developmental Dynamics*, 233, (1) 115-121

Choi, Y.S., Im, M.W., Kim, C.S., Lee, M.H., Noh, S.E., Lim, S.M., Kim, S.L., Cho, C.G., & Kim, D.I. 2008. Chondrogenic differentiation of human umbilical cord blood-derived multilineage progenitor cells in atelocollagen. *Cytotherapy*, 10, (2) 165-173

Chomczynski, P. & Sacchi, N. 1987. Single-Step Method of Rna Isolation by Acid Guanidinium Thiocyanate Phenol Chloroform Extraction. *Analytical Biochemistry*, 162, (1) 156-159

Chung, B.G., Flanagan, L.A., Rhee, S.W., Schwartz, P.H., Lee, A.P., Monuki, E.S., & Jeon, N.L. 2005. Human neural stem cell growth and differentiation in a gradient-generating microfluidic device. *Lab on A Chip*, 5, (4) 401-406

Cohen, N.P., Foster, R.J., & Mow, V.C. 1998. Composition and dynamics of articular cartilage: Structure, function, and maintaining healthy state. *Journal of Orthopaedic & Sports Physical Therapy*, 28, (4) 203-215

Connolly, J., Guse, R., Lippiello, L., & Dehne, R. 1989. Development of An Osteogenic Bone-Marrow Preparation. *Journal of Bone and Joint Surgery-American Volume*, 71A, (5) 684-691

Covas, D.T., Panepucci, R.A., Fontes, A.M., Silva, W.A., Orellana, M.D., Freitas, M.C.C., Neder, L., Santos, A.R.D., Peres, L.C., Jamur, M.C., & Zago, M.A. 2008. Multipotent mesenchymal stromal cells obtained from diverse human tissues share functional properties and gene-expression profile with CD146(+) perivascular cells and fibroblasts. *Experimental Hematology*, 36, (5) 642-654

Croner, R.S., Lausen, B., Schellerer, V., Zeittraeger, I., Wein, A., Schildberg, C., Papadopoulos, T., Dimmler, A., Hahn, E.G., Hohenberger, W., & Brueckl, W.M. 2009. Comparability of Microarray Data between Amplified and Non Amplified RNA in Colorectal Carcinoma. *Journal of Biomedicine and Biotechnology*

Curl, W.W., Krome, J., Gordon, E.S., Rushing, J., Smith, B.P., & Poehling, G.G. 1997. Cartilage injuries: A review of 31,516 knee arthroscopies. *Arthroscopy*, 13, (4) 456-460

Davis, A.A., Bernstein, P.S., Bok, D., Turner, J., Nachtigal, M., & Hunt, R.C. 1995. A Human Retinal-Pigment Epithelial-Cell Line That Retains Epithelial Characteristics After Prolonged Culture. *Investigative Ophthalmology & Visual Science*, 36, (5) 955-964

De Bari, C., Dell'Accio, F., Vanlauwe, J., Eyckmans, J., Khan, Y.M., Archer, C.W., Jones, E.A., McGonagle, D., Mitsiadis, T.A., Pitzalis, C., & Luyten, F.P. 2006. Mesenchymal multipotency of adult human periosteal cells demonstrated by single-cell lineage analysis. *Arthritis and Rheumatism*, 54, (4) 1209-1221

de Haan, G. & Ploemacher, R. 2001. Haematopoietic Stem Cell Protocols: The Cobblestone-Area-Forming Cell Assay. *Methods in Molecular Medicine*, 63, 143-151

Deans, R.J. & Moseley, A.B. 2000. Mesenchymal stem cells: Biology and potential clinical uses. *Experimental Hematology*, 28, (8) 875-884

Delany, A.M., McMahon, D.J., Powell, J.S., Greenberg, D.A., & Kurland, E.S. 2007. Osteonectin/SPARC polymorphisms in Caucasian men with idiopathic osteoporosis. *Osteoporosis International,* 19, (7) 969-978

Delise, A.M., Fischer, L., & Tuan, R.S. 2000. Cellular interactions and signaling in cartilage development. *Osteoarthritis and Cartilage*, 8, (5) 309-334

Derfoul, A., Perkins, G.L., Hall, D.J., & Tuan, R.S. 2006. Glucocorticoids promote chondrogenic differentiation of adult human mesenchymal stem cells by enhancing expression of cartilage extracellular matrix genes. *Stem Cells*, 24, (6) 1487-1495

Deschaseaux, F., Selmani, Z., Falcoz, P.E., Mersin, N., Meneveau, N., Penfornis, A., Kleinclauss, C., Chocron, S., Etievent, J.P., Tiberghien, P., Kantelip, J.P., & Davani, S. 2007. Two types of circulating endothelial progenitor cells in patients receiving long term therapy by HMG-CoA reductase inhibitors. *European Journal of Pharmacology*, 562, (1-2) 111-118

Devine, S.M. 2002. Mesenchymal stem cells: Will they have a role in the clinic? *Journal of Cellular Biochemistry,* 73-79

Dominici, M., Le Blanc, K., Mueller, I., Slaper-Cortenbach, I., Marini, F.C., Krause, D.S., Deans, R.J., Keating, A., Prockop, D.J., & Horwitz, E.M. 2006. Minimal criteria for defining multipotent mesenchymal stromal cells. The International Society for Cellular Therapy position statement. *Cytotherapy*, 8, (4) 315-317

Dovey, O.M., Foster, C.T., & Cowley, S.M. 2010. Histone deacetylase 1 (HDAC1), but not HDAC2, controls embryonic stem cell differentiation. *Proceedings of the National Academy of Sciences of the United States of America*, 107, (18) 8242-8247

Downey, P.A. & Siegel, M.I. 2006. Bone biology and the clinical implications for osteoporosis. *Physical Therapy*, 86, (1) 77-91

Ducy, P., Schinke, T., & Karsenty, G. 2000. The osteoblast: A sophisticated fibroblast under central surveillance. *Science*, 289, (5484) 1501-1504

Egot-Lemaire, S., Pijanka, J., Sule-Suso, J., & Semenov, S. 2009. Dielectric spectroscopy of normal and malignant human lung cells at ultra-high frequencies. *Physics in Medicine and Biology*, 54, (8) 2341-2357

Ellis, M., Jarman-Smith, M., & Chaudhuri, J. B. 2005, "Bioreactors for tissue engineeering: a four-dimensional challenge," *In Bioreactors for tissue engineeering: principles, design and operation*, J. B. Chaudhuri & M. Al-Rubeai, eds., Springer, pp. 1-18.

Emmerson, B.C., Gortz, S., Jamali, A.A., Chung, C., Amiel, D., & Bugbee, W.D. 2007. Fresh osteochondral allografting in the treatment of osteochondritis dissecans of the femoral condyle. *American Journal of Sports Medicine*, 35, (6) 907-914

Erices, A., Conget, P., & Minguell, J.J. 2000. Mesenchymal progenitor cells in human umbilical cord blood. *British Journal of Haematology*, 109, (1) 235-242

Ermolina, I., Polevaya, Y., & Feldman, Y. 2001. Study of normal and malignant white blood cells by time domain dielectric spectroscopy. *Ieee Transactions on Dielectrics and Electrical Insulation*, 8, (2) 253-261

Evans, M.J. & Kaufman, M.H. 1981. Establishment in Culture of Pluripotential Cells from Mouse Embryos. *Nature*, 292, (5819) 154-156

Eyre, D. 2002. Collagen of articular cartilage. *Arthritis Research*, 4, (1) 30-35

Ferrera, D., Poggi, S., Biassoni, C., Dickson, G.R., Astigiano, S., Barbieri, O., Favre, A., Franzi, A.T., Strangio, A., Federici, A., & Manduca, P. 2002. Three-dimensional cultures of normal human osteoblasts: Proliferation and differentiation potential in vitro and upon ectopic implantation in nude mice. *Bone*, 30, (5) 718-725

Forte, G., Minieri, M., Cossa, P., Antenucci, D., Sala, M., Gnocchi, V., Fiaccavento, R., Carotenuto, F., De Vito, P., Baldini, P.M., Prat, M., & Di Nardo, P. 2006. Hepatocyte growth factor effects on mesenchymal stem cells: Proliferation, migration, and differentiation. *Stem Cells*, 24, (1) 23-33

Fraser, J.R.E., Laurent, T.C., & Laurent, U.B.G. 1997. Hyaluronan: Its nature, distribution, functions and turnover. *Journal of Internal Medicine*, 242, (1) 27-33

Frenkel, S.R., Saadeh, P.B., Mehrara, B.J., Chin, G.S., Steinbrech, D.S., Brent, B., Gittes, G.K., & Longker, M.T. 2000. Transforming growth factor beta superfamily members: Role in cartilage modeling. *Plastic and Reconstructive Surgery*, 105, (3) 980-990

Freshney, R.I. 2005. "Organotypic culture" *In Culture of Animal Cells*, 5th ed. Wiley-Blackwell, pp. 406-407

Friedenstein, A., Chailakhyan, R.K., & Lalykina, K.S. 1970. Development of Fibroblast Colonies in Monolayer Cultures of Guinea-Pig Bone Marrow and Spleen Cells. *Cell and Tissue Kinetics*, 3, (4) 393-403

Fuhr, G., Hagedorn, R., & Goring, H. 1985. Separation of Different Cell-Types by Rotating Electric-Fields. *Plant and Cell Physiology*, 26, (8) 1527-1531

Gage, F.H. 2000. Mammalian neural stem cells. *Science*, 287, (5457) 1433-1438

Gahwiler, B.H. 1981. Organotypic Monolayer-Cultures of Nervous-Tissue. *Journal of Neuroscience Methods*, 4, (4) 329-342

Garrett-Sinha, L.A., Eberspaecher, H., Seldin, M.F., & deCrombrugghe, B. 1996. A gene for a novel zinc-finger protein expressed in differentiated epithelial cells and transiently in certain mesenchymal cells. *Journal of Biological Chemistry*, 271, (49) 31384-31390

Gascoyne, P.R.C., Noshari, J., Anderson, T.J., & Becker, F.F. 2009. Isolation of rare cells from cell mixtures by dielectrophoresis. *Electrophoresis*, 30, (8) 1388-1398

Gawad, S., Cheung, K., Seger, U., Bertsch, A., & Renaud, P. 2004. Dielectric spectroscopy in a micromachined flow cytometer: theoretical and practical considerations. *Lab on A Chip*, 4, (3) 241-251

Gawad, S., Schild, L., & Renaud, P. 2001. Micromachined impedance spectroscopy flow cytometer for cell analysis and particle sizing. *Lab on A Chip*, 1, (1) 76-82

Gelse, K., Poschl, E., & Aigner, T. 2003. Collagens - structure, function, and biosynthesis. *Advanced Drug Delivery Reviews*, 55, (12) 1531-1546

Gilbert, S.F. 2000. "Neural Crest Cells and Axonal Specificity" *In Developmental Biology*, 6th ed. Sinauer Associates Inc., pp. 420-421

Glasser, H. & Fuhr, G. 1998. Cultivation of cells under strong ac-electric field - differentiation between heating and trans-membrane potential effects. *Bioelectrochemistry and Bioenergetics*, 47, (2) 301-310

Glowacki, J. & Mizuno, S. 2008. Collagen scaffolds for tissue engineering. *Biopolymers*, 89, (5) 338-344

Goessler, U.R., Bugert, P., Bieback, K., Deml, M., Sadick, H., Hormann, K., & Riedel, F. 2005. In-vitro analysis of the expression of TGFbeta-superfamily-members during chondrogenic differentiation of mesenchymal stem cells and chondrocytes during dedifferentiation in cell culture. *Cellular & Molecular Biology Letters*, 10, 345-362

Goldring, M.B., Tsuchimochi, K., & Ijiri, K. 2006. The control of chondrogenesis. *Journal of Cellular Biochemistry*, 97, (1) 33-44

Govender, S., Csimma, C., Genant, H.K., & Valentin-Opran, A. 2002. Recombinant human bone morphogenetic protein-2 for treatment of open tibial fractures - A prospective, controlled, randomized study of four hundred and fifty patients. *Journal of Bone and Joint Surgery-American Volume*, 84A, (12) 2123-2134

Grimaud, E., Heymann, D., & Redini, F. 2002. Recent advances in TGF-beta effects on chondrocyte metabolism - Potential therapeutic roles of TGF-beta in cartilage disorders. *Cytokine & Growth Factor Reviews*, 13, (3) 241-257

Gronthos, S., Graves, S.E., Ohta, S., & Simmons, P.J. 1994. The STRO-1(+) Fraction of Adult Human Bone-Marrow Contains the Osteogenic Precursors. *Blood*, 84, (12) 4164-4173

Gronthos, S., Zannettino, A.C.W., Hay, S.J., Shi, S.T., Graves, S.E., Kortesidis, A., & Simmons, P.J. 2003. Molecular and cellular characterisation of highly purified stromal stem cells derived from human bone marrow. *Journal of Cell Science*, 116, (9) 1827-1835

Grosse, C. & Schwan, H.P. 1992. Cellular Membrane-Potentials Induced by Alternating-Fields. *Biophysical Journal*, 63, (6) 1632-1642

Guillot, P.V., Gotherstrom, C., Chan, J., Kurata, H., & Fisk, N.M. 2007. Human first-trimester fetal MSC express pluripotency markers and grow faster and have longer telomeres than adult MSC. *Stem Cells*, 25, (3) 646-654

Guo, X.R., Gong, H.X., Gao, Y.Q., Fei, L., Ni, Y.H., & Chen, R.H. 2004. A mutation in signal peptide of rat resistin gene inhibits differentiation of 3T3-L1 preadipocytes. *Acta Pharmacologica Sinica*, 25, (12) 1705-1711

Guo, Z.K., Li, H., Li, X.S., Yu, X.D., Wang, H.X., Tang, P.H., & Mao, N. 2006. In vitro characteristics and in vivo immunosuppressive activity of compact bone-derived murine mesenchymal progenitor cells. *Stem Cells*, 24, (4) 992-1000

Habeler, W., Pouillot, S., Plancheron, A., Puceat, M., Peschanski, M., & Monville, C. 2009. An in vitro beating heart model for long-term assessment of experimental therapeutics. *Cardiovascular Research*, 81, (2) 253-259

Hadjidakis, D.J. & Androulakis, I.I. 2006. Bone Remodeling. *Annals of the New York Academy of Sciences*, 1092, 385-396

Hall, B.K. & Miyake, T. 1995. Divide, accumulate, differentiate: Cell condensation in skeletal development revisited. *International Journal of Developmental Biology*, 39, (6) 881-893

272

Henriksen, K., Neutzsky-Wulff, A.V., Bonewald, L.F., & Karsdal, M.A. 2009. Local communication on and within bone controls bone remodeling. *Bone*, 44, (6) 1026-1033

Hill, P.A. 1998. Bone remodelling. *J.Orthod*, 25, 101-107

Homminga, G.N., Bulstra, S.K., Bouwmeester, P.S., & van der Linden, A.J. 1990. Perichondral grafting for cartilage lesions of the knee. *Journal of Bone and Joint Surgery - British Volume*, 72-B, (6) 1003-1007

Hong, S.H., Gang, E.J., Jeong, J.A., Ahn, C.Y., Hwang, S.H., Yang, I.H., Park, H.K., Han, H., & Kim, H. 2005. In vitro differentiation of human umbilical cord blood-derived mesenchymal stem cells into hepatocyte-like cells. *Biochemical and Biophysical Research Communications*, 330, (4) 1153-1161

Hopkins, D.R., Keles, S., & Greenspan, D.S. 2007. The bone morphogenetic protein 1/Tolloid-like metalloproteinases. *Matrix Biology*, 26, (7) 508-523

Horwitz, E.M., Le Blanc, K., Dominici, M., Mueller, I., Slaper-Cortenbach, I., Marini, F.C., Deans, R.J., Krause, D.S., & Keating, A. 2005. Clarification of the nomenclature for MSC: The international society for cellular therapy position statement. *Cytotherapy*, 7, (5) 393-395

Howard, D., Partridge, K., Yang, X.B., Clarke, N.M.P., Okubo, Y., Bessho, K., Howdle, S.M., Shakesheff, K.M., & Oreffo, R.O.C. 2002. Immunoselection and adenoviral genetic modulation of human osteoprogenitors: in vivo bone formation on PLA scaffold. *Biochemical and Biophysical Research Communications*, 299, (2) 208-215

Huang, R., Barber, T.A., Schmidt, M.A., Tompkins, R.G., Toner, M., Bianchi, D.W., Kapur, R., & Flejter, W.L. 2008. A microfluidics approach for the isolation of nucleated red blood cells (NRBCs) from the peripheral blood of pregnant women. *Prenatal Diagnosis*, 28, (10) 892-899

Huang, W.C., Xie, Z.H., Konaka, H., Sodek, J., Zhau, H.E., & Chung, L.W.K. 2005. Human osteocalcin and bone sialoprotein mediating osteomimicry of prostate cancer cells: Role of cAMP-dependent protein kinase a signaling pathway. *Cancer Research*, 65, (6) 2303-2313

Huang, Y., Joo, S., Duhon, M., Heller, M., Wallace, B., & Xu, X. 2002. Dielectrophoretic cell separation and gene expression profiling on microelectronic chip arrays. *Analytical Chemistry*, 74, (14) 3362-3371

Hughes, M.P. 2002. Strategies for dielectrophoretic separation in laboratory-on-a-chip systems. *Electrophoresis*, 23, (16) 2569-2582

Hulmes, D.J.S. 2002. Building collagen molecules, fibrils, and suprafibrillar structures. *Journal of Structural Biology*, 137, (1-2) 2-10

Hung, P.J., Lee, P.J., Sabounchi, P., Aghdam, N., Lin, R., & Lee, L.P. 2005. A novel high aspect ratio microfluidic design to provide a stable and uniform microenvironment for cell growth in a high throughput mammalian cell culture array. *Lab on A Chip*, 5, (1) 44-48

Hung, S.C., Chen, N.J., Hsieh, S.L., Li, H., Ma, H.L., & Lo, W.H. 2002. Isolation and characterization of size-sieved stem cells from human bone marrow. *Stem Cells*, 20, (3) 249-258

Hutmacher, D.W. 2000. Scaffolds in tissue engineering bone and cartilage. *Biomaterials*, 21, (24) 2529-2543

Inglis, D.W., Riehn, R., Austin, R.H., & Sturm, J.C. 2004. Continuous microfluidic immunomagnetic cell separation. *Applied Physics Letters*, 85, (21) 5093-5095

Iozzo, R.V. 1998. Matrix proteoglycans: From molecular design to cellular function. *Annual Review of Biochemistry*, 67, 609-652

Ishimi, Y., Miyaura, C., Jin, C.H., Akatsu, T., Abe, E., Nakamura, Y., Yamaguchi, A., Yoshiki, S., Matsuda, T., Hirano, T., Kishimoto, T., & Suda, T. 1990. Il-6 Is Produced by Osteoblasts and Induces Bone-Resorption. *Journal of Immunology*, 145, (10) 3297-3303

Jahn, K., Richards, R.G., Archer, C.W., & Stoddart, M.J. 2010. Pellet Culture Model for Human Primary Osteoblasts. *European Cells & Materials*, 20, 149-161

Jakeway, S.C., de Mello, A.J., & Russell, E.L. 2000. Miniaturized total analysis systems for biological analysis. *Fresenius Journal of Analytical Chemistry*, 366, (6-7) 525-539

Janssens, K., ten Dijke, P., Janssens, S., & Van Hul, W. 2005. Transforming growth factor-beta 1 to the bone. *Endocrine Reviews*, 26, (6) 743-774

Jiang, Y.H., Vaessena, B., Lenvik, T., Blackstad, M., Reyes, M., & Verfaillie, C.M. 2002. Multipotent progenitor cells can be isolated from postnatal murine bone marrow, muscle, and brain. *Experimental Hematology*, 30, (8) 896-904

Jilka, R.L. 2003. Biology of the basic multicellular unit and the pathophysiology of osteoporosis. *Medical and Pediatric Oncology*, 41, (3) 182-185

Johann, R.M. 2006. Cell trapping in microfluidic chips. *Analytical and Bioanalytical Chemistry*, 385, (3) 408-412

Johansson, B.M. & Wiles, M.V. 1995. Evidence for Involvement of Activin-A and Bone Morphogenetic Protein-4 in Mammalian Mesoderm and Haematopoietic Development. *Molecular and Cellular Biology*, 15, (1) 141-151

Johnson, L.L. 2001. Arthroscopic abrasion arthroplasty: a review. *Clin.Orthop.Relat Res.* (391 Suppl) S306-S317

Jones, E.A., English, A., Kinsey, S.E., Straszynski, L., Emery, P., Ponchel, F., & McGonagle, D. 2006. Optimization of a flow cytometry-based protocol for detection and phenotypic characterization of multipotent mesenchymal stromal cells from human bone marrow. *Cytometry Part B-Clinical Cytometry*, 70B, (6) 391-399

Jorgensen, N.R., Henriksen, Z., Sorensen, O.H., & Civitelli, R. 2004. Dexamethasone, BMP-2, and 1,25-dihydroxyvitamin D enhance a more differentiated osteoblast phenotype: validation of an in vitro model for human bone marrow-derived primary osteoblasts. *Steroids*, 69, (4) 219-226

Kanczler, J.M., Mirmalek-Sani, S.H., Hanley, N.A., Ivanov, A.L., Barry, J.J.A., Upton, C., Shakesheff, K.M., Howdle, S.M., Antonov, E.N., Bagratashvili, V.N., Popov, V.K., & Oreffo, R.O.C. 2009. Biocompatibility and osteogenic potential of human fetal femur-derived cells on surface selective laser sintered scaffolds. *Acta Biomaterialia*, 5, (6) 2063-2071

Kang, Q., Song, W.X., Luo, Q., Tang, N., Luo, J.Y., Luo, X.J., Chen, J., Bi, Y., He, B.C., Park, J.K., Jiang, W., Tang, Y., Huang, J.Y., Su, Y.X., Zhu, G.H., He, Y., Yin, H., Hu, Z.M., Wang, Y., Chen, L., Zuo, G.W., Pan, X.C., Shen, J.K., Vokes, T., Reid, R.R., Haydon, R.C., Luu, H.H., & He, T.C. 2009. A Comprehensive Analysis of the Dual Roles of BMPs in Regulating Adipogenic and Osteogenic Differentiation of Mesenchymal Progenitor Cells. *Stem Cells and Development*, 18, (4) 545-U33

Kasper, J.C. & Mandelbaum, B.R. 2006. Articular cartilage repair - current and future treatments. *US Musculoskeletal review* 88-91

Kato, Y. 1992, "Roles of fibroblast growth factor and transforming growth factor-β in cartilage formation," *In Biological Regulation of the Chondrocytes*, M. Adolphe, ed., CRC Press, pp. 141-160.

Kaushik, R.S., Begg, A.A., Wilson, H.L., Aich, P., Abrahamsen, M.S., Potter, A., Babiuk, L.A., & Griebel, P. 2008. Establishment of fetal bovine intestinal epithelial cell cultures susceptible to bovine rotavirus infection. *Journal of Virological Methods*, 148, (1-2) 182-196

Khosla, S. 2001. Minireview: The OPG/RANKL/RANK system. *Endocrinology*, 142, (12) 5050-5055

Kim, D.-H., Haake, A., Sun, Y., Neild, A.P., Ihm, J.-E., Dual, J., Hubbell, J.A., Ju, B.-K., & Nelson, B.J. 2004. High-Throughput Cell Manipulation Using Ultrasonic Fields. *Proceedings of the 26th Annual International Conference of the IEEE EMBS* 2571-2574

Kim, M.S., Hwang, H., Choi, Y., & Park, J. 2008a. Microfluidic Micropillar Arrays for 3D Cell Culture. *The Open Biotechnology Journal*, 2, 224-228

Kim, U., Qian, J.R., Kenrick, S.A., Daugherty, P.S., & Soh, H.T. 2008b. Multitarget Dielectrophoresis Activated Cell Sorter. *Analytical Chemistry*, 80, (22) 8656-8661

Kimura, T., Sato, Y., Kimura, F., Iwasaka, M., & Ueno, S. 2005. Micropatterning of cells using modulated magnetic fields. *Langmuir*, 21, (3) 830-832

Kirton, J.P. & Xu, Q.B. 2010. Endothelial precursors in vascular repair. *Microvascular Research*, 79, (3) 193-199

Knudson, C.B. & Knudson, W. 2001. Cartilage proteoglycans. *Seminars in Cell & Developmental Biology*, 12, (2) 69-78

Kolf, C.M., Cho, E., & Tuan, R.S. 2007. Mesenchymal stromal cells - Biology of adult mesenchymal stem cells: regulation of niche, self-renewal and differentiation. *Arthritis Research & Therapy*, 9, (1)

Kriel, H., Rios, C., & Tyan, A. 2006. *Stem Cell Isolation using Acoustic Standing Waves in Microfluidic Channels.* The University of Texas, Austin, Inaugural BME B.Sc. Senior Design Thesis

Langer, R. & Vacanti, J.P. 1993. Tissue engineering. *Science*, 260, (5110) 920-926

Lanza, R., Langer, R., & Vacanti, J.P. 2007. "Tissue engineering and transplantation in the fetus" *In Principles of Tissue Engineering*, 3rd ed. Academic Press, pp. 377-386

Lapidot, T., Dar, A., & Kollet, O. 2005. How do stem cells find their way home? *Blood*, 106, (6) 1901-1910

Laurent, T.C. & Fraser, J.R.E. 1992. Hyaluronan. *Faseb Journal*, 6, (7) 2397-2404

Leclerc, E., David, B., Griscom, L., Lepioufle, B., Fujii, T., Layrolle, P., & Legallaisa, C. 2006. Study of osteoblastic cells in a microfluidic environment. *Biomaterials*, 27, (4) 586-595

Lee, C., Grad, S., Wimmer, M., & Alini, M. 2006. The Influence of Mechanical Stimuli on Articular Cartilage Tissue Engineering. *Topics in Tissue Engineering*, 2,

Lee, T.C., Staines, A., & Taylor, D. 2002. Bone adaptation to load: microdamage,as a stimulus for bone remodelling. *Journal of Anatomy*, 201, (6) 437-446

Lefebvre, V., Behringer, R.R., & de Crombrugghe, B. 2001. L-Sox5, Sox6 and Sox9 control essential steps of the chondrocyte differentiation pathway. *Osteoarthritis and Cartilage*, 9, S69-S75

Lieberman, J.R. & Friedlaender, G.E. 2005. "Fracture repair" & "Common molecular mechanisms regulating fetal bone formation and adult fracture repair" *In Bone regeneration and repair: biology and clinical applications.* Humana Press, pp 21-56

Ling, Y., Rubin, J., Deng, Y., Huang, C., Demirci, U., Karp, J.M., & Khademhosseini, A. 2007. A cell-laden microfluidic hydrogel. *Lab on A Chip*, 7, (6) 756-762

Linkhart, T.A., Mohan, S., & Baylink, D.J. 1996. Growth factors for bone growth and repair: IGF, TGF beta and BMP. *Bone*, 19, (1) S1-S12

Lodish, H., Berk, A., Kaiser, C.A., Krieger, M., Scott, M.P., Bretscher, A., Ploegh, H., & Matsudaira, P.T. 2007. *Molecular Cell Biology*, 6th ed. W.H.Freeman & Co Ltd.

Long, X.X., Olszewski, M., Huang, W., & Kletzel, M. 2005. Neural cell differentiation in vitro from adult human bone marrow mesenchymal stem cells. *Stem Cells and Development*, 14, (1) 65-69

Mackie, E.J., Ahmed, Y.A., Tatarczuch, L., Chen, K.S., & Mirams, M. 2008. Endochondral ossification: How cartilage is converted into bone in the developing skeleton. *International Journal of Biochemistry & Cell Biology*, 40, (1) 46-62

Manaresi, N., Romani, A., Medoro, G., Altomare, L., Leonardi, A., Tartagni, M., & Guerrieri, R. 2003. A CMOS chip for individual cell manipulation and detection. *Ieee Journal of Solid-State Circuits*, 38, (12) 2297-2305

Marcus, J.S., Anderson, W.F., & Quake, S.R. 2006. Microfluidic single-cell mRNA isolation and analysis. *Analytical Chemistry*, 78, (9) 3084-3089

Marcus, R., Feldman, D., Rosen, C.J., & Nelson, D. 2007. "Cytokines and Bone Remodelling" *In Osteoporosis, Volume 1*, 3rd ed. Academic Press, pp.503-509

Mark, D., Haeberle, S., Roth, G., von Stetten, F., & Zengerle, R. 2010. Microfluidic lab-on-a-chip platforms: requirements, characteristics and applications. *Chemical Society Reviews*, 39, (3) 1153-1182

Massague, J. 1990. The Transforming Growth-Factor-Beta Family. *Annual Review of Cell Biology*, 6, 597-641

Matsumoto, K., Kamiya, N., Suwan, K., Atsumi, F., Shimizu, K., Shinomura, T., Yamada, Y., Kimata, K., & Watanabe, H. 2006. Identification and characterization of versican/PG-M aggregates in cartilage. *Journal of Biological Chemistry*, 281, (26) 18257-18263

Mckibbin, B. 1978. Biology of Fracture Healing in Long Bones. *Journal of Bone and Joint Surgery-British Volume*, 60, (2) 150-162

Medoro, G., Nastruzzi, C., Guerrieri, R., Gambari, R., & Manaresi, N. 2007. Lab on a chip for live-cell manipulation. *Ieee Design & Test of Computers*, 24, (1) 26-36

Menachery, A. & Pethig, R. 2005. Controlling cell destruction using dielectrophoretic forces. *Ieee Proceedings-Nanobiotechnology*, 152, (4) 145-149

Metcalf, D. 2003. The unsolved enigmas of leukemia inhibitory factor. *Stem Cells*, 21, (1) 5-14

Meyerkort, D., Wood, D., & Zheng, M.-H. 2010. One-stage vs two-stage cartilage repair: a current review. *Orthopedic Research and Reviews*, 2, 95-106

Mikami, Y., Lee, M., Irie, S., & Honda, M.J. 2011. Dexamethasone Modulates Osteogenesis and Adipogenesis With Regulation of Osterix Expression in Rat Calvaria-Derived Cells. *Journal of Cellular Physiology*, 226, (3) 739-748

Miltenyi, S., Muller, W., Weichel, W., & Radbruch, A. 1990. High-Gradient Magnetic Cell-Separation with Macs. *Cytometry*, 11, (2) 231-238

Minguell, J.J., Erices, A., & Conget, P. 2001. Mesenchymal stem cells. *Experimental Biology and Medicine*, 226, (6) 507-520

Mirmalek-Sani, S.H., Stokes, P.J., Tare, R.S., Ralph, E.J., Inglis, S., Hanley, N.A., Houghton, F.D., & Oreffo, R.O.C. 2009. Derivation of a novel undifferentiated human foetal phenotype in serum-free cultures with BMP-2. *Journal of Cellular and Molecular Medicine*, 13, (9B) 3541-3555

Mirmalek-Sani, S.H., Tare, R.S., Morgan, S.M., Roach, H.I., Wilson, D.I., Hanley, N.A., & Oreffo, R.O.C. 2006. Characterization and multipotentiality of human fetal femur-derived cells: Implications for skeletal tissue regeneration. *Stem Cells*, 24, (4) 1042-1053

Mohan, N. & Nair, P.D. 2010. A Synthetic Scaffold Favoring Chondrogenic Phenotype over a Natural Scaffold. *Tissue Engineering Part A*, 16, (2) 373-384

Montjovent, M.O., Burri, N., Mark, S., Federici, E., Scaletta, C., Zambelli, P.Y., Hohlfeld, P., Leyvraz, P.F., Applegate, L.L., & Pioletti, D.P. 2004. Fetal bone cells for tissue engineering. *Bone*, 35, (6) 1323-1333

Mueller, M.B. & Tuan, R.S. 2008. Functional characterization of hypertrophy in chondrogenesis of human mesenchymal stem cells. *Arthritis and Rheumatism*, 58, (5) 1377-1388

Muir, H. 1995. The Chondrocyte, Architect of Cartilage - Biomechanics, Structure, Function and Molecular-Biology of Cartilage Matrix Macromolecules. *Bioessays*, 17, (12) 1039-1048

Mundy, G.R. 1999. "Bone remodelling" *In Bone remodeling and its disorders*, second ed. Taylor and Francis, pp. 1-11

Muraglia, A., Corsi, A., Riminucci, M., Mastrogiacomo, M., Cancedda, R., Bianco, P., & Quarto, R. 2003. Formation of a chondro-osseous rudiment in micromass cultures of human bone-marrow stromal cells. *Journal of Cell Science*, 116, (14) 2949-2955

Musina, R.A., Bekchanova, E.S., Belyavskii, A.V., Grinenko, T.S., & Sukhikh, G.T. 2007. Umbilical cord blood mesenchymal stem cells. *Bulletin of Experimental Biology and Medicine*, 143, (1) 127-131

Narsinh, K.H., Sun, N., Sanchez-Freire, V., Lee, A.S., Almeida, P., Hu, S.J., Jan, T., Wilson, K.D., Leong, D., Rosenberg, J., Yao, M., Robbins, R.C., & Wu, J.C. 2011. Single cell transcriptional profiling reveals heterogeneity of human induced pluripotent stem cells. *Journal of Clinical Investigation*, 121, (3) 1217-1221

Nicodemus, G.D. & Bryant, S.J. 2008. Cell encapsulation in biodegradable hydrogels for tissue engineering applications. *Tissue Engineering Part B-Reviews*, 14, (2) 149-165

Noble, B.S. & Reeve, J. 2000. Osteocyte function, osteocyte death and bone fracture resistance. *Molecular and Cellular Endocrinology*, 159, (1-2) 7-13

Noel, D., Gazit, D., Bouquet, C., Apparailly, F., Bony, C., Plence, P., Millet, V., Turgeman, G., Perricaudet, M., Sany, J., & Jorgensen, C. 2003. Short-term BMP-2 expression is sufficient for in vivo osteochondral differentiation of mesenchymal stem cells. *Stem Cells*, 22, (1) 74-85

Olsen, B.R., Reginato, A.M., & Wang, W.F. 2000. Bone development. *Annual Review of Cell and Developmental Biology*, 16, 191-220

Ong, S.M., Zhang, C., Toh, Y.C., Kim, S.H., Foo, H.L., Tan, C.H., van Noort, D., Park, S., & Yu, H. 2008. A gel-free 3D microfluidic cell culture system. *Biomaterials*, 29, (22) 3237-3244

Oreffo, R.O.C., Cooper, C., Mason, C., & Clements, M. 2005. Mesenchymal stem cells: Lineage, plasticity, and skeletal therapeutic potential. *Stem Cell Reviews*, 1, (2) 169-178

Oreffo, R.O.C., Driessens, F.C.M., Planell, J.A., & Triffitt, J.T. 1998. Growth and differentiation of human bone marrow osteoprogenitors on novel calcium phosphate cements. *Biomaterials*, 19, (20) 1845-1854

Oswald, J., Boxberger, S., Jorgensen, B., Feldmann, S., Ehninger, G., Bornhauser, M., & Werner, C. 2004. Mesenchymal stem cells can be differentiated into endothelial cells in vitro. *Stem Cells*, 22, (3) 377-384

Ottesen, E.A., Hong, J.W., Quake, S.R., & Leadbetter, J.R. 2006. Microfluidic digital PCR enables multigene analysis of individual environmental bacteria. *Science*, 314, (5804) 1464-1467

Outka, G. 2002. The ethics of human stem cell research. *Kennedy Institute of Ethics Journal*, 12, (2) 175-213

Ozkan, M., Wang, M., Ozkan, C., Flynn, R., Birkbeck, A., & Esener, S. 2003. Optical manipulation of objects and biological cells in microfluidic devices. *Biomedical Microdevices*, 5, (1) 61-67

Pan, Q.H., Yu, Y.C., Chen, Q.Y., Li, C.S., Wu, H., Wan, Y., Ma, J., & Sun, F.Y. 2008. Sox9, a key transcription factor of bone morphogenetic protein-2-induced chondrogenesis, is activated through BMP pathway and a CCAAT box in the proximal promoter. *Journal of Cellular Physiology*, 217, (1) 228-241

Parenteau, N.L., Bilbo, P., Nolte, C.J., Mason, V.S., & Rosenburg, M. 1992. The Organotypic Culture of Human Skin Keratinocytes and Fibroblasts to Achieve Form and Function. *Cytotechnology,* 9, (1-3) 163-171

Pavesio, A., Abatangelo, G., Borrione, A., Brocchetta, D., Hollander, A.P., Kon, E., Torasso, F., Zanasi, S., & Marcacci, M. 2003. Hyaluronan-based scaffolds (Hyalograft C) in the treatment of knee cartilage defects: preliminary clinical findings. *Novartis Foundation Symposium* (249) 203-217

Pelttari, K., Steck, E., & Richter, W. 2008. The use of mesenchymal stem cells for chondrogenesis. *Injury-International Journal of the Care of the Injured*, 39, S58-S65

Penick, K.J., Solchaga, L.A., & Welter, J.F. 2005. High-throughput aggregate culture system to assess the chondrogenic potential of mesenchymal stem cells. *Biotechniques*, 39, (5) 687-691

Pera, M.F., Reubinoff, B., & Trounson, A. 2000. Human embryonic stem cells. *Journal of Cell Science*, 113, (1) 5-10

Pittenger, M.F., Mackay, A.M., Beck, S.C., Jaiswal, R.K., Douglas, R., Mosca, J.D., Moorman, M.A., Simonetti, D.W., Craig, S., & Marshak, D.R. 1999. Multilineage potential of adult human mesenchymal stem cells. *Science*, 284, (5411) 143-147

Pittenger, M.F., Mosca, J.D., & McIntosh, K.R. 2000. Human mesenchymal stem cells: Progenitor cells for cartilage, bone, fat and stroma. *Lymphoid Organogenesis*, 251, 3-11

Pohl, H.A. 1978. *Dielectrophoresis the behavior of neutral matter in nonuniform electric fields.* Cambridge, Cambridge University Press.

Pound, J.C., Green, D.W., Chaudhuri, J.B., Mann, S., Roach, H.I., & Oreffo, R.O.C. 2006. Strategies to promote chondrogenesis and osteogenesis from human bone marrow cells and articular chondrocytes encapsulated in polysaccharide templates. *Tissue Engineering*, 12, (10) 2789-2799

Radbruch, A. 1999. *Flow Cytometry & Cell Sorting*, 2nd Revised Edition ed. Berlin, Springer-Verlag.

Raman, J.D., Mongan, N.P., Liu, L., Tickoo, S.K., Nanus, D.M., Scherr, D.S., & Gudas, L.J. 2006. Decreased expression of the human stem cell marker, *Rex-1 (zfp-42)*, in renal cell carcinoma. *Carcinogenesis*, 27, (3) 499-507

Redman, S.N., Oldfield, S.F., & Archer, C.W. 2005. Current strategies for articular cartilage repair. *European Cells & Materials*, 9, 23-32

Reece, J.B., Urry, L.A., Cain, M.L., Wasserman, S.A., Minorsky, P.V., & Jackson, R.B. 2010. *Campbell Biology*, 9th ed.

Reed, R.K., Lilja, K., & Laurent, T.C. 1988. Hyaluronan in the Rat with Special Reference to the Skin. *Acta Physiologica Scandinavica*, 134, (3) 405-411

Reger, R.L., Tucker, A.H., & Wolfe, M.R. 2008. Differentiation and Characterization of Human MSCs. *Methods in Molecular Biology*, 449, (2) 93-107

Ries, C., Egea, V., Karow, M., Kolb, H., Jochum, M., & Neth, P. 2007. MMP-2, MTI-MMP, and TMP-2 are essential for the invasive capacity of human mesenchymal stem cells: differential regulation by inflammatory cytokines. *Blood*, 109, (9) 4055-4063

Roodman, G.D. 1999. Cell biology of the osteoclast. *Experimental Hematology*, 27, (8) 1229-1241

Rosenthal, A. & Voldman, J. 2005. Dielectrophoretic traps for single-particle patterning. *Biophysical Journal*, 88, (3) 2193-2205

Salem, H.K. & Thiemermann, C. 2010. Mesenchymal Stromal Cells: Current Understanding and Clinical Status. *Stem Cells*, 28, (3) 585-596

Sanchez-Ramos, J., Song, S., Cardozo-Pelaez, F., Hazzi, C., Stedeford, T., Willing, A., Freeman, T.B., Saporta, S., Janssen, W., Patel, N., Cooper, D.R., & Sanberg, P.R. 2000. Adult bone marrow stromal cells differentiate into neural cells in vitro. *Experimental Neurology*, 164, (2) 247-256

Sandino, C., Planell, J.A., & Lacroix, D. 2008. A finite element study of mechanical stimuli in scaffolds for bone tissue engineering. *Journal of Biomechanics*, 41, (5) 1005-1014

Satomaa, T., Heiskanen, A., Mikkola, M., Olsson, C., Blomqvist, M., Tiittanen, M., Jaatinen, T., Aitio, O., Olonen, A., Helin, J., Hiltunen, J., Natunen, J., Tuuri, T., Otonkoski, T., Saarinen, J., & Laine, J. 2009. The N-glycome of human embryonic stem cells. *Bmc Cell Biology*, 10

Scharstuhl, A., Schewe, B., Benz, K., Gaissmaier, C., Buhring, H.J., & Stoop, R. 2007. Chondrogenic potential of human adult mesenchymal stem cells is independent of age or osteoarthritis etiology. *Stem Cells*, 25, (12) 3244-3251

Schindeler, A., McDonald, M.M., Bokko, P., & Little, D.G. 2008. Bone remodeling during fracture repair: The cellular picture. *Seminars in Cell & Developmental Biology*, 19, (5) 459-466

Schnelle, T., Hagedorn, R., Fuhr, G., Fiedler, S., & Muller, T. 1993. 3-Dimensional Electric-Field Traps for Manipulation of Cells - Calculation and Experimental-Verification. *Biochimica et Biophysica Acta*, 1157, (2) 127-140

Sengers, B.G., Dawson, J.I., & Oreffo, R.O.C. 2010. Characterisation of human bone marrow stromal cell heterogeneity for skeletal regeneration strategies using a two-stage colony assay and computational modelling. *Bone*, 46, (2) 496-503

Shafiee, H., Sano, M.B., Henslee, E.A., Caldwell, J.L., & Davalos, R.V. 2010. Selective isolation of live/dead cells using contactless dielectrophoresis (cDEP). *Lab on A Chip*, 10, (4) 438-445

Sharapova, N.E., Kotnova, A.P., Galushkina, Z.M., Poletaeva, N.N., Lavrova, N.V., Aksenova, E.I., Semikhin, A.S., Karyagina, A.S., & Lunin, V.G. 2009. Isolation and characterization of collagen-binding domains from human von Willebrand factor. *Molecular Genetics Microbiology and Virology*, 24, (3) 150-154

Shea, J.E. & Miller, S.C. 2005. Skeletal function and structure: Implications for tissue-targeted therapeutics. *Advanced Drug Delivery Reviews*, 57, (7) 945-957

Shen, G. 2005. The role of type X collagen in facilitating and regulating endochondral ossification of articular cartilage. *Orthodontics & Craniofacial Research*, 8, (1) 11-17

Shi, S. & Gronthos, S. 2003. Perivascular niche of postnatal mesenchymal stem cells in human bone marrow and dental pulp. *Journal of Bone and Mineral Research*, 18, (4) 696-704

Shivtiel, S., Kollet, O., Lapid, K., Schajnovitz, A., Goichberg, P., Kalinkovich, A., Shezen, E., Tesio, M., Netzer, N., Petit, I., Sharir, A., & Lapidot, T. 2008. CD45 regulates retention, motility, and numbers of haematopoietic progenitors, and affects osteoclast remodeling of metaphyseal trabecules. *Journal of Experimental Medicine*, 205, (10) 2381-2395

Simms, D., Cizdziel, P.E., & Chomczynski, P. 1993. TRIzol: a new reagent for optimal single-step isolation of RNA. *Focus*, 15, (4) 99-102

Sims, C. E. & Allbritton, N. L. 2008, "Microfabricated devices for cell sorting," *In Biological applications of microfluidics*, F. A. Gomez, ed., Wiley-Blackwell.

Soncini, M., Vertua, E., Gibelli, L., Zorzi, F., Denegri, M., Albertini, A., Wengler, G.S., & Parolini, O. 2007. Isolation and characterization of mesenchymal cells from human fetal membranes. *Journal of Tissue Engineering and Regenerative Medicine*, 1, (4) 296-305

Sonoda, E., Aoki, S., Uchihashi, K., Soejima, H., Kanaji, S., Izuhara, K., Satoh, S., Fujitani, N., Sugihara, H., & Toda, S. 2008. A new organotypic culture of adipose tissue fragments maintains viable mature adipocytes for a long term, together with development of immature adipocytes and mesenchymal stem cell-like cells. *Endocrinology,* 149, (10) 4794-4798

Sorrentino, A., Ferracin, M., Castelli, G., Biffoni, M., Tomaselli, G., Baiocchi, M., Fatica, A., Negrini, M., Peschle, C., & Valtieri, M. 2008. Isolation and characterization of CD146(+) multipotent mesenchymal stromal cells. *Experimental Hematology*, 36, (8) 1035-1046

Stadtfeld, M., Nagaya, M., Utikal, J., Weir, G., & Hochedlinger, K. 2008. Induced Pluripotent Stem Cells Generated Without Viral Integration. *Science*, 322, (5903) 945-949

Standal, T., Borset, M., & Sundan, A. 2004. Role of osteopontin in adhesion, migration, cell survival and bone remodeling. *Experimental Oncology*, 26, (3) 179-184

Stark, H.-J., Szabowski, A., Fusenig, N.E., & Maas-Szabowski, N. 2004. Organotypic cocultures as skin equivalents: A complex and sophisticated in vitro system. *Biological Procedures Online*, 6, (1) 55-60

Steadman, J.R., Rodkey, W.G., & Rodrigo, J.J. 2001. Microfracture: surgical technique and rehabilitation to treat chondral defects. *Clin.Orthop.Relat Res.* (391 Suppl) S362-S369

Stewart, A.A., Byron, C.R., Pondenis, H.C., & Stewart, M.C. 2008. Effect of dexamethasone supplementation on chondrogenesis of equine mesenchymal stem cells. *American Journal of Veterinary Research*, 69, (8) 1013-1021

Stewart, K., Monk, P., Walsh, S., Jefferiss, C.M., Letchford, J., & Beresford, J.N. 2003. Stro-1, Hop-26 (Cd63), Cd49A and Sb-10 (Cd166) As Markers of Primitive Human Marrow Stromal Cells and Their More Differentiated Progeny: A Comparative Investigation in Vitro. *Cell and Tissue Research*, 313, (3) 281-290
282

Stockwell, R.A. 1979. "Chondrocyte structure" *In Biology of Cartilage Cells*, 1st ed. Cambridge University Press, pp. 7-30

Stoppini, L., Buchs, P.A., & Muller, D. 1991. A Simple Method for Organotypic Cultures of Nervous-Tissue. *Journal of Neuroscience Methods*, 37, (2) 173-182

Suh, J.K.F. & Matthew, H.W.T. 2000. Application of chitosan-based polysaccharide biomaterials in cartilage tissue engineering: a review. *Biomaterials*, 21, (24) 2589-2598

Sundelacruz, S. & Kaplan, D.L. 2009. Stem cell- and scaffold-based tissue engineering approaches to osteochondral regenerative medicine. *Seminars in Cell & Developmental Biology*, 20, (6) 646-655

Taff, B.M. & Voldman, J. 2005. A scalable addressable positive-dielectrophoretic cell-sorting array. *Analytical Chemistry*, 77, (24) 7976-7983

Takahashi, K., Tanabe, K., Ohnuki, M., Narita, M., Ichisaka, T., Tomoda, K., & Yamanaka, S. 2007. Induction of pluripotent stem cells from adult human fibroblasts by defined factors. *Cell*, 131, (5) 861-872

Takahashi, K. & Yamanaka, S. 2006. Induction of pluripotent stem cells from mouse embryonic and adult fibroblast cultures by defined factors. *Cell*, 126, (4) 663-676

Talary, M.S., Mills, K.I., Hoy, T., Burnett, A.K., & Pethig, R. 1995. Dielectrophoretic Separation and Enrichment of Cd34+ Cell Subpopulation from Bone-Marrow and Peripheral-Blood Stem-Cells. *Medical & Biological Engineering & Computing*, 33, (2) 235-237

Talbot, N.C., Caperna, T.J., Edwards, J.L., Garrett, W., Wells, K.D., & Ealy, A.D. 2000. Bovine blastocyst-derived trophectoderm and endoderm cell cultures: Interferon tau and transferrin expression as respective in vitro markers. *Biology of Reproduction*, 62, (2) 235-247

Tan, H.P., Chu, C.R., Payne, K.A., & Marra, K.G. 2009. Injectable in situ forming biodegradable chitosan-hyaluronic acid based hydrogels for cartilage tissue engineering. *Biomaterials*, 30, (13) 2499-2506

Tang, Y., Wu, X., Lei, W., Pang, L., Wan, C., Shi, Z., Zhao, L., Nagy, T.R., Peng, X., Hu, J., Feng, X., Van Hul, W., Wan, M., & Cao, X. 2009. TGF-beta1-induced migration of bone mesenchymal stem cells couples bone resorption with formation. *Nature Medicine*, 15, 757-765

Tare, R.S., Howard, D., Pound, J.C., Roach, H.I., & Oreffo, R.O.C. 2005. Tissue engineering strategies for cartilage generation - Micromass and three dimensional cultures using human chondrocytes and a continuous cell line. *Biochemical and Biophysical Research Communications*, 333, (2) 609-621

Tare, R.S., Kanczler, J., Aarvold, A., Jones, A.M.H., Dunlop, D.G., & Oreffo, R.O.C. 2010. Skeletal stem cells and bone regeneration: translational strategies from bench to clinic. *Proceedings of the Institution of Mechanical Engineers Part H-Journal of Engineering in Medicine*, 224, (H12) 1455-1470

Taylor, M.R., Campbell, N.A., & Reece, J.B. 2001. "The genetic basis of development" *In Biology: Student Study Guide,* Sixth ed. Prentice Hall College Div, pp. 409

Teitelbaum, S.L. 2007. Osteoclasts: What do they do and how do they do it? *American Journal of Pathology*, 170, (2) 427-435

Temenoff, J.S. & Mikos, A.G. 2000. Review: tissue engineering for regeneration of articular cartilage. *Biomaterials*, 21, (5) 431-440

Termine, J.D., Kleinman, H.K., Whitson, S.W., Conn, K.M., Mcgarvey, M.L., & Martin, G.R. 1981. Osteonectin, A Bone-Specific Protein Linking Mineral to Collagen. *Cell*, 26, (1) 99-105

Thomas, R.S. 2006. *Electrokinetics for Microparticle Manipulation.* University of Southampton, MPhil thesis.

Thomas, R. S. 2007. Theory and uses of Dielectrophoresis, Personal Communication

Thomas, R.S. 2010. *Single particle dielectrophoretic sorting technologies.* University of Southampton, PhD thesis.

Thomas, R.S., Morgan, H., & Green, N.G. 2009. Negative DEP traps for single cell immobilisation. *Lab on A Chip*, 9, (11) 1534-1540

Thomas, R.S.W., Mitchell, P.D., Oreffo, R.O.C., & Morgan, H. 2010. Trapping single human osteoblast-like cells from a heterogeneous population using a dielectrophoretic microfluidic device. *Biomicrofluidics*, 4, (2)

Thomson, J.A., Itskovitz-Eldor, J., Shapiro, S.S., Waknitz, M.A., Swiergiel, J.J., Marshall, V.S., & Jones, J.M. 1998. Embryonic stem cell lines derived from human blastocysts. *Science*, 282, (5391) 1145-1147

Tickle, C. & Munsterberg, A. 2001. Vertebrate limb development - the early stages in chick and mouse. *Current Opinion in Genetics & Development*, 11, (4) 476-481

Togel, F., Lange, C., Zander, A.R., & Westenfelder, C. 2007. Regenerative Medicine with Adult Bone Marrow Derived Stem Cells. *Deutsches Ärzteblatt*, 104(23), 1663-1670

Tortelli, F. & Cancedda, R. 2009. Three-Dimensional Cultures of Osteogenic and Chondrogenic Cells: A Tissue Engineering Approach to Mimic Bone and Cartilage in Vitro. *European Cells & Materials*, 17, 1-14

Tuan, R.S. 2004. Biology of developmental and regenerative skeletogenesis. *Clinical Orthopaedics and Related Research* (427) S105-S117

Uccelli, A., Moretta, L., & Pistoia, V. 2008. Mesenchymal stem cells in health and disease. *Nature Reviews Immunology*, 8, (9) 726-736

Ulloa-Montoya, F., Verfaillie, C.M., & Hu, W.S. 2005. Culture systems for pluripotent stem cells. *Journal of Bioscience and Bioengineering*, 100, (1) 12-27

Vallier, L., Alexander, M., & Pedersen, R.A. 2005. Activin/Nodal and FGF pathways cooperate to maintain pluripotency of human embryonic stem cells. *Journal of Cell Science*, 118, (19) 4495-4509

Vallier, L., Mendjan, S., Brown, S., Chng, Z., Teo, A., Smithers, L.E., Trotter, M.W.B., Cho, C.H.H., Martinez, A., Rugg-Gunn, P., Brons, G., & Pedersen, R.A. 2009. Activin/Nodal signalling maintains pluripotency by controlling Nanog expression. *Development*, 136, (8) 1339-1349

Voldman, J., Toner, M., Gray, M.L., & Schmidt, M.A. 2003. Design and analysis of extruded quadrupolar dielectrophoretic traps. *Journal of Electrostatics*, 57, (1) 69-90

Wang, E., Miller, L.D., Ohnmacht, G.A., Liu, E.T., & Marincola, F.M. 2000. High-fidelity mRNA amplification for gene profiling. *Nature Biotechnology*, 18, (4) 457-459

Wang, M.M., Tu, E., Raymond, D.E., Yang, J.M., Zhang, H.C., Hagen, N., Dees, B., Mercer, E.M., Forster, A.H., Kariv, I., Marchand, P.J., & Butler, W.F. 2005. Microfluidic sorting of mammalian cells by optical force switching. *Nature Biotechnology*, 23, (1) 83-87

Wang, Y.D., Hu, Y., Zhang, L., & Sun, C.Y. 2008. Brain derived neurotrophic factor induces endothelial cells angiogenesis through AKT and ERK1/2 signal pathway. *Zhongguo Shi Yan Xue Ye Xue Za Zhi*, 16, (1) 175-180

Watanabe, H., Yamada, Y., & Kimata, K. 1998. Roles of aggrecan, a large chondroitin sulfate proteoglycan, in cartilage structure and function. *Journal of Biochemistry*, 124, (4) 687-693

Watt, F.M., Lo Celso, C., & Silva-Vargas, V. 2006. Epidermal stem cells: an update. *Current Opinion in Genetics & Development*, 16, (5) 518-524

Weiner, S. & Wagner, H.D. 1998. The material bone: Structure mechanical function relations. *Annual Review of Materials Science*, 28, 271-298

Wolff, A., Perch-Nielsen, I.R., Larsen, U.D., Friis, P., Goranovic, G., Poulsen, C.R., Kutter, J.P., & Telleman, P. 2003. Integrating advanced functionality in a microfabricated high-throughput fluorescent-activated cell sorter. *Lab on A Chip*, 3, (1) 22-27

Wozney, J.M., Rosen, V., Celeste, A.J., Mitsock, L.M., Whitters, M.J., Kriz, R.W., Hewick, R.M., & Wang, E.A. 1988. Novel Regulators of Bone-Formation - Molecular Clones and Activities. *Science*, 242, (4885) 1528-1534

Wu, H.W., Hsu, R.C., Lin, C.C., Hwang, S.M., & Lee, G.B. 2010. An integrated microfluidic system for isolation, counting, and sorting of haematopoietic stem cells. *Biomicrofluidics*, 4, (2)

Xiao, L., Yuan, X., & Sharkis, S.J. 2006. Activin A maintains self-renewal and regulates fibroblast growth factor, Wnt, and bone morphogenic protein pathways in human embryonic stem cells. *Stem Cells*, 24, (6) 1476-1486

Yamaguchi, Y., Arakawa, T., Takeda, N., Edagawa, Y., & Shoji, S. 2009. Development of a poly-dimethylsiloxane microfluidic device for single cell isolation and incubation. *Sensors and Actuators B-Chemical*, 136, (2) 555-561

Yamanouchi, K., Gotoh, Y., & Nagayama, M. 1997. Dexamethasone enhances differentiation of human osteoblastic cells in vitro. *Journal of Bone and Mineral Metabolism*, 15, (1) 23-29

Yeatts, A.B. & Fisher, J.P. 2011. Bone tissue engineering bioreactors: Dynamic culture and the influence of shear stress. *Bone*, 48, (2) 171-181

You, W.K. & McDonald, D.M. 2008. The hepatocyte growth factor/c-Met signaling pathway as a therapeutic target to inhibit angiogenesis. *Bmb Reports*, 41, (12) 833-839

Yu, J.Y., Vodyanik, M.A., Smuga-Otto, K., Antosiewicz-Bourget, J., Frane, J.L., Tian, S., Nie, J., Jonsdottir, G.A., Ruotti, V., Stewart, R., Slukvin, I.I., & Thomson, J.A. 2007. Induced pluripotent stem cell lines derived from human somatic cells. *Science*, 318, (5858) 1917-1920

Zaehres, H., Kim, J.B., & Schöler, H.R. 2010. Chapter 18 - Induced Pluripotent Stem Cells. *Methods in Enzymology*, 476, 309-325

Zeddou, M., Briquet, A., Relic, B., Josse, C., Malaise, M.G., Gothot, A., Lechanteur, C., & Beguin, Y. 2010. The umbilical cord matrix is a better source of mesenchymal stem cells (MSC) than the umbilical cord blood. *Cell Biology International*, 34, (7) 693-701

Zhang, L.M., Su, P.Q., Xu, C.X., Yang, J.L., Yu, W.H., & Huang, D.S. 2010. Chondrogenic differentiation of human mesenchymal stem cells: a comparison between micromass and pellet culture systems. *Biotechnology Letters*, 32, (9) 1339-1346

Zhang, Z.Y., Teoh, S.H., Chong, M.S.K., Schantz, J.T., Fisk, N.M., Choolani, M.A., & Chan, J. 2009. Superior Osteogenic Capacity for Bone Tissue Engineering of Fetal Compared with Perinatal and Adult Mesenchymal Stem Cells. *Stem Cells*, 27, (1) 126-137

Zhou, H., Wu, S., Joo, J.Y., Zhu, S., Han, D.W., Lin, T., Trauger, S., Bien, G., Yao, S., Zhu, Y., Siuzdak, G., Schöler, H.R., Duan, L., & Ding, S. 2009. Generation of Induced Pluripotent Stem Cells Using Recombinant Proteins. *Cell Stem Cell*, 4, (5) 381-384

Zhu, J.F., Zhang, Y.T., Alber, M.S., & Newman, S.A. 2010. Bare Bones Pattern Formation: A Core Regulatory Network in Varying Geometries Reproduces Major Features of Vertebrate Limb Development and Evolution. *Plos One*, 5, (5)